Single-pole switching schemes for EHV transmission systems

Alias, Qais M.

Award date:
1986

Awarding institution:
University of Bath

SINGLE-POLE SWITCHING SCHEMES FOR EHV TRANSMISSION SYSTEMS

submitted by

Qais M. Alias
B.Sc. , M.Sc.

for the degree of PhD

of

the University of Bath

1986

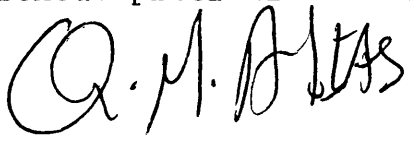

ProQuest LLC
789 East Eisenhower Parkway
P.O. Box 1346
Ann Arbor, MI 48106-1346

CONTENTS

SUMMARY

The increasing financial constraints that electric utilities face today require that new and innovative techniques must be utilized to minimize the installation of new power system facilities, while maintaining a high degree of reliability. Furthermore, the enactment of siting regulations for transmission lines makes it more difficult to install new transmission facilities in a timely manner. Recognizing that a high percentage of transmission line faults are single-phase to earth and temporary in nature, provides the impetus for considering single-pole switching as a means to enhance the reliability of EHV transmission systems. The effectiveness of single-pole switching schemes, is largely determined by the speed with which the secondary arcs extinguish, and hence allow system restoration. Simulation techniques that enable better prediction of the faulted system response are of obvious importance to the design and assessment of the various single-pole switching scheme applications. In this thesis, digital methods are developed to enable the faulted response of EHV systems to be simulated for a variety of different single-pole switching schemes. These include, conventional single-pole switching, the hybrid method of autoreclosure, the neutral switched reactor and the High Speed Grounding Switch implementations. The work is of importance to, system protection schemes design, prediction of system internal overvoltages and system stability studies. The thesis concludes by comprehensively illustrating and discussing the results of computational studies relating to typical 500kV transmission systems employing the above mentioned single-pole switching schemes.

ACKNOWLEDGEMENTS

The work presented in this thesis was carried out under the supervision of prof. A. T. Johns, formerly, director of P. G. studies, School of Electrical Engineering, University of Bath, presently with the School of Electrical Engineering and Applied Physics, the City University. I wish to thank prof. Johns for his constant guidance and encouragement throughout this work.

The provision of facilities by the School of Electrical Engineering, University of Bath is gratefully acknowledged.

The financial support of the CVCP (U.K.) and the University of Technology (IRAQ) are greatly appreciated.

Sincere thanks are due to Dr. R. K. Aggarwal, of the School of Electrical Engineering, University of Bath, for the constructive discussions on the computational aspects of this work.

Thanks are also due to the staff of the University of Bath Computer Centre for their assistance.

Finally, my gratitude is also due to the Redhead Family for their active and moral support.

LIST OF SYMBOLS

A_1, B_1, C_1, D_1, A_2, B_2, C_2, D_2 = Matrices defining the line sections linking the fault point to the sending and receiving ends respectively

A_L, B_L, C_L, D_L, A_R, B_R, C_R, D_R = Matrices defining the equivalent line/reactor combinations linking the fault point to the sending and receiving ends respectively

Alfa (α) = Frequency shift constant

B_{ch}, B_{cg} = Interphase and phase-to-earth capacitive susceptances of assumed ideally transposed line

B_{c1}, B_{co} = p.p.s. and z.p.s. line capacitive susceptances

B_{L1}, B_{Lo} = p.p.s. and z.p.s. inductive susceptances of a shunt reactor bank at power frequency

C_1, C_o = p.p.s. and z.p.s. capacitances of assumed ideally transposed line

C_{ab}, C_{bc}, C_{ca}, C_{ag}, C_{bg}, C_{cg} = Interphase and phase to earth capacitances of untransposed line

$\Delta\omega$ = Basic frequency step length

E_a, E_b, E_c = Normal phase-to-neutral voltages

$\bar{E}_T$ = Transform of the Thevenin voltage

$\bar{E}_{FK}$, $\bar{E}_{SK}$, $\bar{E}_{RK}$ = Transforms of voltages at the fault point, sending and receiving ends respectively

$\bar{E}_{SWK}$, $\bar{E}_{SgK}$, $\bar{E}_{RgK}$ = Transforms of voltages at the neutral switched reactor, HSGS at the sending and receiving ends respectively

h_1, h_o = Degrees of p.p.s. and z.p.s. shunt compensation

HSGS = High Speed Grounding Switch

h(t) = Unit step function

h(t - T) = Delayed unit step function
= 0 for $t < T$, and
= 1 for $t > T$

I_{sec} = Secondary arc current of phase-to-earth fault

$\bar{I}$ = Current Transform

i(t) = Current time variation

$\bar{I}_{SS}$, $\bar{I}_{RS}$ = Transform of pre-fault currents at the sending and receiving ends

$\bar{I}_{F}$, I_{SF}, $\bar{I}_{RF}$ = Transforms of superimposed currents at fault point, sending and receiving ends due to fault inception

$\bar{I}_{SK}$, $\bar{I}_{RK}$ = Transform of superimposed currents at the sending and receiving ends as a result of the Kth. switching event

$\bar{I}_{FSK}$, $\bar{I}_{FK}$, $\bar{I}_{FRK}$ = Transforms of the superimposed currents at the fault point

$\bar{I}_{SWK}$, $\bar{I}_{SgK}$, $\bar{I}_{RgK}$ = Transforms of the superimposed currents in the ideal neutral switch, sending and receiving end HSGS's

j = operator $j = (-1)^{\frac{1}{2}}$

k = Line capacitance ratio (C_o/C_1)

L_p, L_n = Phase and neutral inductance of a shunt reactor bank

L_1, L_o = p.p.s. and z.p.s. inductances of a shunt reactor bank

L_{ph}, L_{pg} = Mesh equivalent inductances of a shunt reactor bank

L = Length of a line section

n = Number of switching events

N = Number of frequency samples

Π = Truncation frequency

O = Zero matrix

p.p.s. = Positive phase sequence

Q = Quality factor = X/R

R_F = Primary arc fault resistance

R_p, R_n = Phase and neutral resistances of a shunt reactor bank

R_s = HSGS resistance

s.c.l. = Short-circuit level

θ = Line angle

T_{ob} = Observation time

t = Any time

τ = Convolution time variable

T_F = Fault inception time

T_{bi} = Main breaker poles operating times, i = 2, 13

T_{s1}, T_{s2} = Opening and closing times of the ideal neutral switch

T_{hc} = Closing time of the HSGS's

T_{ho1}, T_{ho2} = Opening times of the HSGS's

T_{o1}, T_{o2} = Arc transition times

T_{ext} = Arc extinction time

U = Unit matrix

V_{rp} = Steady-state phase recovery voltage

v(t) = Voltage time variation

$\bar{V}$ = Voltage Transform

$\bar{V}_{FS}$, $\bar{V}_{SS}$, $\bar{V}_{RS}$ = Transforms of the pre-fault voltages at point of fault, sending and receiving ends

v_{arc} = Arc voltage

$\bar{V}_{FK}$, $\bar{V}_{SK}$, $\bar{V}_{RK}$ = Transforms of the superimposed voltages at the fault point, sending and receiving ends

$\bar{V}_{nK}$ = Transform of the superimposed voltage across the neutral of a shunt reactor bank

ω_o = Nominal system angular frequency

x = Distance to fault from the sending end

X_p = Phase reactance of a shunt reactor bank

X_{ns}, X_{nr} = Neutral reactances of conventional 4-legged and neutrally switched reactor banks

z.p.s. = Zero phase sequence

Z_{SS}, Z_{SR} = Sending and receiving ends source matrices

Z_{sr} = Shunt reactor impedance sub-matrix

Z_p, Z_n = Phase and neutral impedances of a shunt reactor bank

Z_F = Fault resistance matrix

Z_g = HSGS resistance matrix

Z_{So}/Z_{Sl} = Ratio of z.p.s. to p.p.s. impedance of the source at power frequency

a.f. = After fault

Subscripts

S, R, F = Sending end, Receiving end, and Fault point

a, b, c = phases a,b,c

p = phase

n = Neutral

superscripts

T = Transpose of matrix

-1 = Inverse of matrix

CHAPTER 1

INTRODUCTION

1.1 Review

The world wide demand for electrical energy over the past few decades resulted in an appreciable rate of growth. For economical as well as ecological reasons, the efficiency, reliability, and performance of the different components integrated within a power system must be maximized.

Extra high voltage (EHV) transmission lines are vital components in any power transmission network, and due to their cost effectiveness, their performance in conjunction with other system components under different operational conditions is of current interest.

Three-phase switching was and still is being used by numerous utilities as a means of clearing any type of fault occuring on EHV transmission lines at different voltage levels. To some extent, this is justified by the benefits made on simple relaying schemes, conventional less complicated circuit breaker designs and the very high possibility of fast arc extinction to facilitate subsequent reclosure.

With the advancement in circuit breakers and selective relaying technologies, plus the fact that the majority of

faults encountered in EHV transmission lines are of transitory, single-phase-to-earth type, single-pole switching emerged as a feasibile technique for minimizing the subsequent system disturbances caused by such faults. Single-pole switching was first used in 1941, on an 80km , 138kV single-circuit transmission system[1]. Field experience, and documented analysis of systems equipped with single-pole switching schemes promoted the following in favour of such technique :-

a. A primary benefit of using single-pole switching, involves system reliability improvement in so far as the system transient stability is concerned[2,3].

b. Single-pole switching may eliminate the need for additional transmission circuit, and/or can be a benefit when stressed conditions are due to delay in planned facilities[4].

c. For lines terminating at a thermal power plant, single-pole switching may reduce turbine-generator shaft stresses arising from torsional oscillations[5,6].

d. Single-pole switching could reduce the need for overhead earth wires, or in marginal cases facilitate their elimination[3,7].

e. There are less obvious reliability reasons for applying single-pole switching to double-circuit lines, however, cases where two like phase conductors simultaneously flash-over are possible. In such cases, single-pole switching can be of advantage[8]

f. From the stand point of system switching overvoltages, single-pole switching produces surge levels that are generally less severe than comparable three-phase switching surge levels[4,9,10].

Single-pole switching does however intoduce some complications. From the design viewpoint, more complex protective relaying schemes and circuit breakers are required. In addition, the system unbalance during the dead-time (dead-time is defined here as, the period of time during which the faulted phase of it remains de-energised) causes zero and negative sequence currents to flow. The former could affect the performance of the ground relays in nearby installations, while the latter could cause generator-rotor body heating[11].

Long EHV transmission lines tend to bring a more pronounced state of secondary arcing, which must be cosidered in evaluating the single-pole switching performance of such lines. Hence, an essential pre-requisite for such applications, is the possibility and speed of final secondary arc extinction during suitably short dead-times. When a single-phase-to-earth fault is isolated by single-pole switching, the arc cannot be immediately extinguished. As a result of the capacitive and inductive coupling of the switched phase with the sound phases, a relatively low residual or secondary arc current is maintained through the primary highly ionized fault path. Upon temporal or final extinction of the secondary arc, the sound phases determine the restriking voltage transients, and the recovery voltage (the recovery voltage here defined as, the phase-earth voltage of the switched phase at the fault location subsequent to secondary arc extinctions). Ultimately, for successful reclosure, the switched phase has to withstand the transient overvoltages at the instant of reclosure.

1.2 The Arcing Process - Simulation Problem

For the analysis of systems equipped with single-pole switching techniques, the simulation of the high current

primary long arc as well as the low current secondary arc is of great importance. The primary arc current has its impact especially on the system transients which influence the insulation design and the protection equipment response. The secondary arc, mainly its extinction time, determines whether or not successful reclosure can be achieved within a suitably short dead-time.

Several authors have analysed the arcing phenomena and the factors which influence the arc extinction. Generally, arc extinction takes place when the energy supplied to the arc from the system is not sufficient to sustain ionization of the arc path. Relevant to long a.c. arcs in open air, extinction may result if the rate at which the arcing medium attain dielectric strength exceeds that of the recovery voltage across the arc[12]. Eaton et al[13] show that, in capacitive circuits, the maximum value as well as the rate of rise of the recovery voltage are equally important in determining the final arc extinction. Terase et al[14,15], in studies on the dielectric strength recovery characteristics for different types of 500kV transmission line insulators, concluded that the highest speed of medium recovery occurs with suspension insulator strings. Laboratory studies indicated that the recovery voltage across the arcing medium decreases with increasing arcing current[16,17]. In general, one can arrange the factors affecting the arc current and the process of its extinction in two broad interrelated categories. The first contains the system related factors. These determine the value and duration of the primary arc current. Also, they determine the value of the secondary arc current and the recovery voltage across the arc path upon intermediate or final extinction. The second category covers the arcing boundary factors. These are very much weather dependent

(e.g. wind speed, humidity, ... etc.), and to a large extent they control the build up of the dielectric strength of the arcing medium and the arc geometry.

Due to the amount and variety of factors affecting the arcing process in power systems, mathematical modelling of the long primary and secondary arcs posed a complex problem. Based on limited experimental results from investigations into the effect of primary arcing faults on system protection, Warrington[18] proposed the characteristic arc equation as, $V = 8750\, \ell_o\, I^{-0.4}$, where ℓ_o is the arc length in feet, and I is the fault current obtained from steady-state calculations. Storm[19], and Miakopar[20] have investigated the Volt-Ampere characteristics for arcs of 10 - 122 cm in length, set between electrodes and of 10 - 20000A current range. Maikopar proposed the use of th empirical formula $V = 75\, \ell_o\, I_p^{-0.4}$, where ℓ_o here, is the arc length in cm and I_p is the arc current in Ampere (peak). Using a digital computer, studies by Cornick et al[21] concluded that the primary arc path can be represented to a good degree of accuracy by a constant linear resistance in the range of 0.3 - 42Ω depending on the magnitude of the fault current. Using parameters derived from staged fault throwing tests[4], Balser et al[22] represented the primary arc path by a constant low resistance, and the secondary arc path by a linear time dependent resistance. Fakheri et al[23], recently proposed a resistive secondary arc model, which was derived from arc voltage and current waveforms of one cycle of the secondary arcing period recorded during a single-phase-to-earth fault test.

Based on extensive analysis of the available information about arcing phenomenon[24], Johns and Al-Rawi[25,26] proposed an elaborate secondary arc model. The model was incorporated in a digital computer program to study

conventional single-pole switched EHV transmission systems, under single-phase-to-earth fault conditions. Basically, the model is defined by simulating, a) the relationship between arc voltage and current, b) the arc path reignition voltage variation, and c) the arc length variation. These with the system Thevenin impedance and voltage seen across the arc terminals, were combined to obtain the secondary arc voltage and current waveforms throughout the dead-time interval.

1.3 System Requirements For Successful Single-Pole Switching And Solutions

The prime concern in utilizing single-pole switching in a particular EHV transmission network is the length of the dead-time interval. The dead-time depends mainly on how long the secondary arc takes to extinguish. Factors which determine the extinction time are, a) the steady-state value of the secondary arc current, b) the steady-value and rate of rise of the recovery voltage, and c) to some extent, the value and duration of the primary arc current. These are system dependent factors which can be controlled to a certain degree to achieve suitable short extinction time. The boundary dependent factors which affect the secondary arc extinction include, d) the length of the arc path, which in turn is very much dependent on, e) the weather conditions. Factors a and b above, were used frequently as a measure of the secondary arc extinction time[25,27], but hybrid and digital computer studies of shunt compensated EHV lines concluded that the transient recovery voltage component also affects the extinction process[22,26].

System voltage level, loading and line length among

other parameters, which to a large extent determine the secondary arc current and recovery voltage, are basic system design parameters. Therefore, to ensure a high probability of secondary arc extinction by lowering the above (a-c) factors, certain measures and/or methods should be adopted.

It is a well established fact that line transposition can reduce the secondary arc current and recovery voltage and therefore, produce a high probability of rapid arc extinction[11,22,26,28]. To achieve successful single-pole switching performance in long distance transmission networks, extra measures need to be considered to realize rapid arc extinction. Muller et al[29] discussed the use of salt solution jets to shunt the faulted phase on the French 220kV system. A modification of the above idea is the use of High Speed Grounding Switches (HSGS's), to replace the solution jets. Hasibar et al[30], reported the results of field test on a 196km, 500kV transposed, uncompensated line, which showed immediate extinction of the secondary arc after grounding the faulted phase. Jahn[31] has suggested the use of high conductivity earth wires to reduce the magnetically induced component of the secondary arc current and recovery voltage. In 1969, Peterson[32] suggested a method to nullify the sound phases to faulted phase capacitive coupling in a transposed line. In his method, he suggested the use of a capacitor slightly larger than $(C_1 - C_o)$, connected across the faulted phase breaker contacts at each line end, to reduce the recovery voltage at the middle of the line to zero.

The continuous increase in transmission voltage levels, line lengths, and number of conductors per bundle have emphasized the importance in EHV systems of the excess of line VAR's and of the associated voltage and reactive power controls. In the case of initial systems or in the case of

long lines energised through relatively weak sources, the adoption of shunt reactors to compensate a portion of the line charging VAR's is an indispensable method for controlling excessive voltage and the capacitive charging current flowing through the system[33,34].

In 1962, Knudsen[35], and independently Kimbark[36] in 1964, proposed a method for reducing the capacitively coupled component of the secondary arc current and recovery voltage for transposed shunt compensated lines. The basis of the method hinged upon using a fourth reactor (neutral reactor) connected between the star point of the main reactor and earth, which has a value so as to make the 4-legged shunt reactor X_o/X_1 greater than 1. Tuning of the neutral reactor can result theoretically in total elimination of, or in a specific reduction of the capacitive coupling between faulted and sound phases. Staged fault test results have been published for applications involving 4-legged shunt reactor compensated transposed lines, operating at different voltage levels[2,4,37,38,39,40]. The effect of transposition arrangements, degree of compensation, line length, loading, number and position of the reactors used and source parameters on the secondary arc extinction time and the recovery voltage, have been analysed by several authors[9,11,22,26,27,41,42,43].

Costs of effecting discrete conductor transposition, the increased probability of faults at the transposition towers, and the possibility of installing an intermediate switching station en-route in future system expansion, have led to the increasing preference in transmission system practice to avoid transposition in long distance EHV transmission applications. Untransposed long EHV lines are characterised by significant difference between the phase-to-phase capacitances. For example, in typical horizontal

line configurations, the capacitance between the outer phases often approaches one quarter of that between the inner and outer phases. It is, consequently not possible to fully compensate either the electrostatic or the electromagnetic component of the secondary arc current by using the balanced 4-legged reactor arrangement[26]. Few authors have discussed the feasibility of using such reactors to enhance single-pole switching performance in long untransposed line applications. Balser et al[44] reported the results of hybrid computer studies concerning the effect of a balanced and an unbalanced 4-legged shunt reactor on the transient recovery voltage. The authors concluded that, using a neutral reactance chosen on the basis that the line is transposed, in untransposed line application, can give rise to 3.5 times the transient recovery voltage encountered in a transposed line application, for a fault on the outer phase.

Johns et al[26] studied the effect of the balanced 4-legged reactor arrangement on the secondary arc extinction time in untransposed line applications. The authors concluded that, for an outer phase fault, limiting the secondary arc current and the first peak of the recovery voltage to less than approximately 25A (r.m.s) and 80kV (r.m.s) respectively, can engender satisfactory reclosure with a dead-time of approximately 0.5 sec, with a limiting line length of 200km at 500kV level. Kimbark[45] suggested balancing the line interphase capacitances, by connecting block capacitors between the outer phases, so that a balanced 4-legged reactor compensator can be used to achieve satisfactory single-pole switching performance.

A considerable amount of work has been done on developing alternative switched reactor arrangements that more adequately compensate the untransposed line capacitance

unbalance[46,47]. In the neutral switched reactor arrangement, four neutral switches are used, and their operation is coordinated with the circuit breakers. The switches are closed during normal operation, and assume a configuration that depends on which phase is faulted. The main objective of using the switched reactor arrangement, is to provide additional compensation required for the mid-to-outer phase capacitance, while the basic outer-to-outer phase compensation can be provided using a conventional 4-legged reactor bank. Relevant results of staged fault tests have been published in the description of the first practical application of the neutral switched reactor in conjunction with a conventional 4-legged reactor bank, in order to improve the single-pole switching performance of a 765kV 243km untransposed line[40,48,49]. These tests indicated that, secondary arc extinction times in the range of 0.16 sec were experienced for calculated steady-state secondary arc currents up to 40A (r.m.s.). It is worth mentioning here that most of the above mentioned tests were performed with the line fed from one end only. Recently, the results of a second series of single-pole switching tests of the same system, with the reactor parameters chosen to give higher secondary arc currents were reported[23]. In these tests, extinction times did not exceed 0.767 sec for steady-state values of secondary arc currents up to 58A (r.m.s.), and recovery voltage not in excess of 333kV (r.m.s.). The two sets of test results mentioned above, confirmed the importance of the rate of rise of the recovery voltage (rrrv) in assessing the single-pole switching performance of the system, and shows explicit dependence of the rrrv on the line and reactor parameters only.

In untransposed line applications, the use of HSGS's to facilitate fast secondary arc extinction can provide

a powerful method with less complexities apart from the additional cost of the HSGS's. No relevant simulation studies of such systems has been located in the literature.

In systems where the secondary arc current is comparatively high, and which can lead to prolonged arcing state, the possibility of involving the sound phases in the extinction process arises. For such systems and others whose stability criteria do not allow direct three-phase switching, a technique utilizing a suitable combination of single-pole and three-phase switching can be of advantage. In this technique, the two sound phases are tripped after fault clearance by single-pole switching. This followed by fast reclosure of all three phases. In the discussion of reference 5, Mittelstadt suggested the intention of BPA (Bonneville Power Administrartion) to implement such technique to allow natural arc extinction, especially in systems where very fast single-pole reclosure in not necessary. Recently, an IEEE report[3] discussed the transient stability aspect of adopting such technique (named "The hybrid method" in reference 3) in a double-circuit transmission system. Although the overall dead-time suggested in (3 & 5) is relatively long, there is some evidence which suggests that successful reclosure after 0.5 sec dead-time with the hybrid method of autoreclosure can be achieved. Concerning the secondary arc extinction process, as the arc length increases, and the dielectric strength of the medium builds up due to the factors mentioned in section 1.2. The arc consequently needs more energy from the system to persist. By de-energising the sound phases, the energy is no longer available, and fast arc extinction follows. The hybrid method of autoreclosure can be applied to systems with transposed as well as untransposed EHV lines, to achieve fast arc extinction and subsequent three-phase reclosure.

1.4 Power System Transients

Transients occur on power systems due to a variety of reasons. They may produce, 1) overvoltages, which mainly determines the system apparatus insulation design, 2) over-currents, which determine the interrupting duty of the circuit breakers, mechanical and thermal stresses within machines, transformers, ... etc., 3) abnormal current and voltage waveforms whose prediction and analysis is of importance to protection systems design and, 4) electro-mechanical transients. The traditional method of assessing the severity of power system transients is to use the transient network analyser (TNA) in modelling a scaled down version of the system. This method has the advantage of fast response for any particular study, and the main disadvantage is that the frequency dependence of the system parameters can not be represented exactly. For many years now digital computer methods have been used for the calculation of power system transients. The computational techniques used may be broadly classified into, Frequency-Domain methods based on the Fourier Transform, and time-domain methods using the travelling-wave approach[50]. Ideally, the method of calculation used should be capable of representing both lumped and distributed parameters of the various components of the system, and reproducing these parameter variations with frequency[51].

In this work, the modified Fourier Transform method is used to calculate the system response throughout fault, fault clearance, various switching operations and line restoration. The modified Fourier Transform in conjunction with the time-domain convolution is used to account for the non-linearity caused by the secondary arc.

1.5 Objectives of The Present Work

The first objective of the present work is to analyse in depth the use of the conventional 4-legged compensating reactor, and to quantify the effect of the neutral reactance on minimizing dead-times in EHV untransposed line applications. The results are compared with relevant transposed line, and examine the extent to which the secondary arc extinction is affected by deviations in the neutral reactance value from the optimum, in both transposed and untransposed line applications. The second objective is to develop methods of digitally simulating typical neutrally switched reactor compensated, long EHV untransposed line systems. The same is to be carried out for systems equipped with HSGS's, and systems employing the hybrid method of autoreclosure. In the modelling of such systems, a flexible computational method has to be adopted in the simulation, so as to incorporate different system conditions (e.g. similar, different, or no reactor compensation arrangement at one or both line ends). The effect of the system parameters on the secondary arc extinction time, the recovery voltage and the overvoltages arising at different points of the system are analysed for the above mentioned methods of single-pole switching. Finally, an over all estimation of the limits, practical implications and performance of the various single-pole switching schemes in clearing single-phase-to-earth faults on 500kV lines are quantified and compared.

1.6 Scope of The Present Work

Chapter 1 generally presents the background and up to date state of the art in single-pole switching. Chapter 2 describes the methods of calculating the steady-state value of the secondary arc current and

the recovery voltage for the various line and reactor applications. The source simulation, reactor and fault simulation are presented in the same chapter.

Chapter 3 describes the simulation of the main breaker opening and isolation of the fault. The procedures followed to simulate the hybrid method of autoreclosure, the opening of the ideal neutral switch, and the closing of the HSGS's are also presented.

The simulation of the system under secondary arcing conditions and the derivation of the Thevenin impedance and voltage algorithms for the different single-pole switching schemes are presented in chapter 4. The techniques developed to evaluate the currents and voltages at the relaying points of the system are also presented in the same chapter.

System restoration to normal operating conditions, procedures and digital formulation are presented in chapter 5, for all the single-pole switching schemes considered.

Details of the basic systems studied are presented in chapter 6. These include, line parameters, line construction, shunt reactor parameters, source and HSGS parameters. The modified Fourier Transform parameters used throughout this work are also presented in chapter 6.

Digital computer results of investigation of single-phase-to-earth faults and relevant conclusions are presented in chapters 7, 8, 9, and 10, for systems employing conventional single-pole switching, the hybrid method of autoreclosure, the neutrally switched reactor and the HSGS's implementations respectively.

General conclusions and suggestions for future work are presented in chapter 11.

CHAPTER 2

BASIC SYSTEM FORMULATION

2.1 Introduction

It is generally agreed that, estimation of the steady-state secondary arc current and the recovery voltage in single-pole switched systems can give an indication of the dead-time needed for arc extinction and system restoration. Based on numerous laboratory and field test results, the upper boundary for dead-time dependency on secondary arc current for uncompensated lines was estimated as,

$$t\ (\text{sec}) = 0.25(0.1\ I_{sec} + 1)$$

where, I_{sec} is the secondary arc current in Ampere r.m.s.[27]. However, published data suggests that reclosure at 0.5 sec, can be achieved if the steady-state secondary arc current and recovery voltage are up to 20A and 50kV r.m.s. respectively at 500kV level. Such limits can be enforced in transposed line applications by proper choice of the neutral reactance in the conventional 4-legged reactor compensator. In untransposed line applications, the effectiveness of such reactors is however seriously limited. Therefore, the use of a special reactor compensator equipped with neutral switches can be of advantage in reducing the secondary arc current and recovery voltage.

Predicting faulted system response is of considerable

importance for both system design and performance evaluation of its protection schemes. To achieve an acceptable degree of realism, detailed and accurate mathematical modelling of the faulted system is necessary[52,53]. Generally, the elements of an EHV transmission system may be divided into two types: first, those whose parameters are essentially lumped, such as generators, transformers,... etc. and secondly, overhead transmission lines, whose parameters are distributed in nature.

In this chapter, the steady-state component of the secondary arc current and recovery voltage for the different single-pole switching schemes application are formulated. General source and shunt reactor mathematical models are presented. The mathematical technique to incorporate the shunt reactor under steady-state and fault conditions are described, followed by the single line-to-ground fault simulation[54].

2.2 Steady-State Secondary Arc Current and Recovery Voltage

When one conductor of a 3-phase transmission line is de-energised at both ends in order to clear a phase-to-ground fault, the faulted conductor remains capacitively and inductively coupled to the sound phase conductors. The two sound phases are still energised at approximately normal circuit voltage and carrying load current. This coupling has two effects[36]:

1- Before arc extinction, it feeds current to the fault and maintains the arc.

2- After arc extinction(final or intermediate), the coupling causes a recovery voltage across the arc path. If the rate of rise of this voltage is too high, the arc is reignited.

It is obvious that for short lines and/or for faults midway between the line ends, the inductively induced component of the secondary arc current and recovery voltage can be ignored. However, for lines longer than 300km, the inductively induced component must be taken into consideration[35]. In this section, only the capacitively induced component of the secondary arc current and recovery voltage will be considered.

2.2.1 Ideally transposed line

Fig. 2.1 shows the general PI-section lumped parameter representation of a 3-phase transmission line, where the notations are self explanatory. Considering an ideally transposed line connected to an ideal source at one end, and neglecting all lossy and inductive elements, fig. 2.1 can be simplified to that of fig. 2.2. In fig. 2.2, the line is represented by its positive and zero phase sequence capacitances C_1 and C_o respectively for the line length under consideration. For a line-to-ground fault(represented by switch F in the closed position) on any particular phase, and the corresponding circuit-breaker(CB) pole is open to clear the fault, fig. 2.2 can be further simplified to that of fig. 2.3. With switch F closed, the induced secondary arc current(assuming zero arc resistance) and the faulted phase voltage as a reference, is given by:

$$I_{secp} = -jE_p\omega_o C_1 (1-k)/3 \qquad (2.1)$$

If switch F is open(secondary arc extinguished), the induced voltage on the faulted phase is:

$$V_{rp} = -E_p\left[(1 - k)/(2 + k)\right] \qquad (2.2)$$

where $k = C_o / C_1$, and p denotes the faulted phase.

The effect of the balanced 4-legged shunt reactor (fig. 2.4) on reducing the capacitive coupling between phases under fault condition can be deduced from analysing the system equivalent circuit of fig. 2.5. For the secondary arc current and recovery voltage calculation, fig. 2.5 can be further simplified to that of fig. 2.6. While the secondary arc current is present(switch F closed), it bypasses the lower arm(see fig. 2.6), and I_{secp} is then given[45]:

$$I_{secp} = -jE_p\,\omega_o C_1\left[(1 - h_1) - k(1 - h_o)\right]/3 \qquad (2.3)$$

And, upon arc extinction(switch F open), the faulted phase recovery voltage is given by,

$$V_{rp} = -E_p\left[\frac{(1 - h_1) - k(1 - h_o)}{2(1 - h_1) + k(1 - h_o)}\right] \qquad (2.4)$$

where $h_1 = 1/\omega_o^2 L_1 C_1$, $h_o = 1/\omega_o^2 L_o C_o$, $L_1 = L_p$ and

$$L_o = L_p + 3L_n$$

From eqns. 2.3 and 2.4, it is obvious that the condition to be met for total elimination of the capacitive component of I_{secp} and V_{rp} is, $(1 - h_1) = k(1 - h_o)$. Examination of eqns. 2.3 and 2.4 with $h_o = h_1/k$, gives I_{secp} equal to that in eqn. 2.1, while V_{rp} can be higher than that in eqn. 2.2 depending on the value of h_1.

2.2.2 Untransposed line

Modern EHV transmission lines are not usually transposed, and it follows that neither the self nor the inter-phase capacitances of such lines are equal. This is particularly the case for the inter-phase capacitances in

the horizontal line configuration, where the ratio of the inner-to-outer to outer-to-outer phase capacitances is in the range of 3-4. Following the same assumptions and procedures in section 2.2.1, fig. 2.7 shows the capacitance equivalent circuit of the untransposed line in the phase frame quantities. For a single line-to-ground fault, the secondary arc current and recovery voltage are easily found for each phase and are given as:

$$I_{seca} = j\omega_o(C_{ab}E_b + C_{ac}E_c) \tag{2.5a}$$

$$I_{secb} = j\omega_o(C_{ab}E_a + C_{bc}E_c) \tag{2.5b}$$

$$I_{secc} = j\omega_o(C_{ac}E_a + C_{bc}E_b) \tag{2.5c}$$

$$V_{ra} = (C_{ab}E_b + C_{ac}E_c)/(C_{ab} + C_{ac} + C_{ag}) \tag{2.6a}$$

$$V_{rb} = (C_{ab}E_a + C_{bc}E_c)/(C_{ab} + C_{bc} + C_{bg}) \tag{2.6b}$$

$$V_{rc} = (C_{ac}E_a + C_{bc}E_b)/(C_{ac} + C_{bc} + C_{cg}) \tag{2.6c}$$

The effect of utilizing a balanced 4-legged shunt reactor on the capacitive component of the secondary arc current and the recovery voltage can be found using the circuit of fig. 2.8. For such an application the expressions for I_{secp} and V_{rp} are:

$$I_{seca} = j\omega_o\left(C_{ab}E_b + C_{ac}E_c - \frac{E_b + E_c}{\omega_o^2 L_{ph}}\right) \tag{2.7a}$$

$$I_{secb} = j\omega_o\left(C_{ab}E_a + C_{bc}E_c - \frac{E_a + E_c}{\omega_o^2 L_{ph}}\right) \tag{2.7b}$$

$$I_{secc} = j\omega_o\left(C_{ac}E_a + C_{bc}E_b - \frac{E_a + E_b}{\omega_o^2 L_{ph}}\right) \tag{2.7c}$$

$$V_{ra} = \frac{E_b + E_c - \omega_o^2 L_{ph}(C_{ab}E_b + C_{ac}E_c)}{2 + (L_{ph}/L_{pg}) - \omega_o^2 L_{ph}(C_{ab} + C_{ac} + C_{ag})} \qquad (2.8a)$$

$$V_{rb} = \frac{E_a + E_c - \omega_o^2 L_{ph}(C_{ab}E_a + C_{bc}E_c)}{2 + (L_{ph}/L_{pg}) - \omega_o^2 L_{ph}(C_{ab} + C_{bc} + C_{bg})} \qquad (2.8b)$$

$$V_{rc} = \frac{E_a + E_b - \omega_o^2 L_{ph}(C_{ac}E_a + C_{bc}E_b)}{2 + (L_{ph}/L_{pg}) - \omega_o^2 L_{ph}(C_{ac} + C_{bc} + C_{cg})} \qquad (2.8c)$$

where $L_{ph} = (L_p/L_n)(L_p + 3L_n)$, and $L_{pg} = L_p + 3L_n$

It is clear from eqns. 2.7 that for balanced reactor phase inductances(L_p) (which have a value dictated by voltage regulation requirements), only one phase secondary arc current can be neutralized by proper choice of the neutral inductance(L_n). It is therefore apparent that the use of a balanced 4-legged shunt reactor in untransposed line applications is of limited benefit for single-pole switching purposes. Recently a CIGRE paper[55] reported investigations regarding the use of unbalanced shunt reactor for single-pole switching at 1100kV level. The authors concluded that the normal operation unbalances are negligible , and the secondary arc current and recovery voltage can be minimized to allow successful single-pole switching application.

2.2.2.1 Untransposed line compensated by balanced and neutral switched reactors

In 1978 the AEP(American Electric Power Service Coporation)[46] proposed the use of a neutral switched

reactor bank in conjunction with a conventional 4-legged reactor bank in untransposed line applications to improve single-pole switching performance. In principle, a balanced 4-legged reactor at one end of the line compensates the interphase capacitances by a value equal to the inner-to-outer conductor capacitance. The neutral switched reactor bank at the other end of the line, is arranged to compensate the difference between inner-to-outer and outer-to-outer conductor capacitances. Fig. 2.9 shows the simplified system diagram used to calculate the steady-state secondary arc current and recovery voltage. The neutral switches are closed during normal operation, but a specific pair operates when a particular faulted phase is identified. The operation of the neutral switches is coordinated with the line circuit breakers and is presented in fig. 2.9. For phase-"a" to ground fault(switch F closed, and the proper neutral switches open), the secondary arc current is given by eqn. 2.9. Upon arc extinction, the recovery voltage on the same phase is given by eqn. 2.10.

$$I_{seca} = (Y_{ab} + Y_{ls} + Y_{lr})E_b + (Y_{ac} + Y_{ls})E_c \qquad (2.9)$$

$$V_{ra} = I_{seca}/Y_{ta} \qquad (2.10)$$

where,

$$Y_{ta} = Y_{ab} + Y_{ac} + Y_{ag} + 2Y_{ls} + Y_{gs} + Y_{lr} + Y_{gr}$$

$$Y_{ls} = -j\left[1/X_p\left[3 + (X_p/X_{ns})\right]\right]$$

$$Y_{gs} = -j\left[1/X_{ns}\left[3 + (X_p/X_{ns})\right]\right]$$

$$Y_{lr} = -j\left[1/X_p\left[2 + (X_p/X_{nr})\right]\right]$$

$$Y_{gr} = -j\left[1/X_{nr}\left[2 + (X_p/X_{nr})\right]\right]$$

$$Y_{ab} = j\omega_o C_{ab} \; ; \; Y_{ac} = j\omega_o C_{ac} \; ; \; Y_{ag} = j\omega_o C_{ag}$$

For phase-"b" to ground fault, the secondary arc current and the recovery voltage are:

$$I_{secb} = (Y_{ab} + Y_{ls} + Y_{2r})E_a + (Y_{bc} + Y_{ls} + Y_{2r})E_c \qquad (2.11)$$

$$V_{rb} = I_{secb}/Y_{tb} \qquad (2.12)$$

where,

$$Y_{tb} = Y_{ab} + Y_{bc} + Y_{bg} + 2Y_{ls} + Y_{gs} + Y_{2r} + Y_{hr}$$

$$Y_{2r} = -j\left\{1/X_p\left[3 + (X_p/X_{nr})\right]\right\}$$

$$Y_{hr} = -j\left\{1/X_{nr}\left[3 + (X_p/X_{nr})\right]\right\}$$

$$Y_{bc} = j\omega_o C_{bc} \; ; \; Y_{bg} = j\omega_o C_{bg}$$

Similar expressions to those given by eqns. 2.9 and 2.10 can be derived for phase-"c" to ground fault. Examination of eqns. 2.9 and 2.11 with a certain value of X_p (particular degree or p.p.s. compensation), show that there is an infinite combination of sets of values for X_{ns} and X_{nr} to limit I_{seca} and I_{secb} to a certain value. Therefore, the final choice of the neutral reactances (X_{ns} and X_{nr}) are determined largely by economic considerations.

2.3 Source Simulation

In a power system, transmission lines are energised from source networks whose configurations and characteristics vary widely. Two extreme cases can be envisaged. First, that of a line energised from a bus-bar fed solely by generators or transformers. The second case is that of a line being energised from a bus-bar fed exclusively by other transmission lines and with no generators or

transformers connected directly to it. There is thus, in fact, no limit to the extent of such detailed source configurations. Where the source is a mixed network, difficulties may be experienced in fully representing such source because of storage limitations and computation times involved. Moreover, it is not always necessary to represent the entire source side network, since the travelling times to the distant points of such network and back, may exceed the time of interest in the particular study[56,62]. Therefore, there are advantages to be gained in the use of simple equivalent circuits, using lumped rather than distributed elements. An example of such equivalent circuit is shown in fig. 2.10, which represent the general source model used througout this work. In APPENDIX 2.1, a general source impedance matrix of the form given in eqn. 2.13 is derived, based upon any chosen short-circuit level at the terminating bus-bar .

$$Z_{SS} = \begin{bmatrix} Z_{S1} + Z_{n1} & Z_{n1} & Z_{n1} \\ Z_{n1} & Z_{S1} + Z_{n1} & Z_{n1} \\ Z_{n1} & Z_{n1} & Z_{S1} + Z_{n1} \end{bmatrix} \qquad (2.13)$$

2.4 Simulation of the Shunt Reactor Bank

For the purpose of VAR control in long EHV transmission systems, one or more banks of Y-connected shunt reactors with solidly grounded neutrals are commonly employed. The size of the reactor can be expressed in terms of, its VAR rating at rated voltage, its reactance per phase(X_p) or its degree of positive phase sequence compensation h_1. In single circuit transmission systems, where single-pole switching is desirable, shunt reactors have been used to wholly or partially supress the secondary arc current.

For such purpose, the neutral point of the Y-connected reactor bank is grounded through a fourth reactor[8] to form the balanced 4-legged reactor bank(fig. 2.11). APPENDIX 2.2 describes the formulation used to calculate the reactor phase impedances and the neutral impedance (if required).

To incorporate the shunt reactor bank(s) shown in fig. 2.11 in the general system model, the canonical form of the two-port or transfer matrix function defining the reactor as per eqn. 2.14 is particularly useful[54].

$$\begin{bmatrix} \bar{V}_1 \\ \bar{I}_1 \end{bmatrix} = \begin{bmatrix} U & O \\ Y_s & O \end{bmatrix} \begin{bmatrix} \bar{V}_2 \\ \bar{I}_2 \end{bmatrix} \qquad (2.14)$$

Where, "U" and "O" are a 3X3 unity and zero matrices respectively. The vector of the current difference$(\bar{I}_1 - \bar{I}_2)$ defines the current which flows in the reactor$(\bar{I}_s)$, and the latter is seen to be simply related to the impedance matrix $[Z_s] = [Y_s]^{-1}$ of the shunt reactor by eqn. 2.15.

$$\begin{bmatrix} \bar{V}_{2a} \\ \bar{V}_{2b} \\ \bar{V}_{2c} \end{bmatrix} = [Z_{sr}]\,\bar{I}_s = \begin{bmatrix} Z_p + Z_n & Z_n & Z_n \\ Z_n & Z_p + Z_n & Z_n \\ Z_n & Z_n & Z_p + Z_n \end{bmatrix} \bar{I}_s \qquad 2.15)$$

For the 4-legged shunt reactor arrangement of fig. 2.11, the sub-matrix $[Y_s] = [Z_{sr}]^{-1}$ which is used in the transfer matrix representation of the reactor is thus as given in eqn. 2.16.

$$Y_s = [Z_{sr}]^{-1} = \frac{1}{Z_p(Z_p + 3Z_n)} \begin{bmatrix} Z_p + 2Z_n & -Z_n & -Z_n \\ -Z_n & Z_p + 2Z_n & -Z_n \\ -Z_n & -Z_n & Z_p + 2Z_n \end{bmatrix} \tag{2.16}$$

For the reactor arrangement with solidly grounded neutral, the sub-matrix Y_s can be easily deduced from eqn. 2.16 by simply putting $Z_n = 0$.

For computational purposes, it is convenient to combine the line sections with the shunt reactors connected to them to form a line/reactor equivalent section. This is illustrated in fig. 2.12. The line transfer matrix equation linking the fault point and receiving end(see fig. 2.12), is of the form given by eqn. 2.17.

$$\begin{bmatrix} \bar{V}_F \\ \bar{V}_{FR} \end{bmatrix} = \begin{bmatrix} A_2 & B_2 \\ C_2 & D_2 \end{bmatrix} \begin{bmatrix} \bar{V}_{R1} \\ \bar{I}_{R1} \end{bmatrix} \tag{2.17}$$

Applying the previously developed eqn. 2.14 to the reactor bank at the receiving end gives:

$$\begin{bmatrix} \bar{V}_{R1} \\ \bar{I}_{R1} \end{bmatrix} = \begin{bmatrix} U & O \\ Y_s & U \end{bmatrix} \begin{bmatrix} \bar{V}_R \\ \bar{I}_R \end{bmatrix} \tag{2.18}$$

From eqns. 2.17 and 2.18, the over all line/reactor equivalent matrix equation can be formed and is given by:

$$\begin{bmatrix} \bar{V}_F \\ \bar{I}_{FR} \end{bmatrix} = \begin{bmatrix} A_R & B_R \\ C_R & D_R \end{bmatrix} \begin{bmatrix} \bar{V}_R \\ \bar{I}_R \end{bmatrix} \qquad (2.19)$$

Where,

$$A_R = A_2 + B_2 Y_s \; ; \; B_R = B_2 \; ; \; C_R = C_2 + D_2 Y_s \; ; \; D_R = D_2$$

It is likewise possible to obtain the over all line/reactor equivalent matrix equation for the section linking the fault point to the sending and it is given by eqn. 2.20.

$$\begin{bmatrix} \bar{V}_F \\ \bar{I}_{FS} \end{bmatrix} = \begin{bmatrix} A_L & B_L \\ C_L & D_L \end{bmatrix} \begin{bmatrix} \bar{V}_S \\ \bar{I}_S \end{bmatrix} \qquad (2.20)$$

Where,

$$A_L = A_1 + B_1 Y_s \; ; \; B_L = B_1 \; ; \; C_L = C_1 + D_1 Y_s \; ; \; D_L = D_1$$

A brief formulation of the line ABCD constants(A_1, B_1, C_1, D_1; A_2, B_2, C_2, D_2) is presented in APPENDIX 2.3.

2.5 Fault Simulation

The fundamental relationships developed in the previous sections have been deliberately formulated in such a way as to effectively enable any compensated or uncompensated line arrangements to be reduced to the faulted system model of fig. 2.12b. Details of the methods of digitally simulating a fault on such a model by using matrix functions and numerically evaluate Fourier Transforms are reported by Johns and Aggarwal[57]. The basis of the method hinges upon representing the voltage at the fault point by the sum of two voltages, $\bar{V}_{FS}$, $\bar{V}_{FF}$ as shown in fig. 2.13. $\bar{V}_{FS}$, is sinusoidal and is equal to the steady-state voltage at

the point of fault before the disturbance. $\bar{V}_{FF}$ is a suddenly applied voltage, which when added to $\bar{V}_{FS}$, represents the post fault voltage. A solution may thus be obtained by performing two separate calculations, in which the desired voltages and currents are evaluated when $\bar{V}_{FS}$ is applied to the energised system, and the superimposed voltage $\bar{V}_{FF}$ is applied to the system with all source voltages set at zero. The method is essentially one of superposition, and it should be noted that the steady-state voltage vector $\bar{V}_{FS}$ can be evaluated from knowledge of the pre-fault voltages and currents at the terminating bus-bars. As the pre-fault condition is a steady-state one, the fault point voltage and line end currents are calculated at power frequency (50Hz or 60Hz). For no fault condition, eqn. 2.21 holds for the currents at the fault point(see fig. 2.13).

$$\bar{I}_{FSS} + \bar{I}_{FRS} = 0 \tag{2.21}$$

Also, from fig. 2.13, the voltage-current matrix relationships for the two line sections are as follow:

$$\begin{bmatrix} \bar{V}_{FS} \\ \bar{I}_{FRS} \end{bmatrix} = \begin{bmatrix} A_R & B_R \\ C_R & D_R \end{bmatrix} \begin{bmatrix} \bar{V}_{RS} \\ \bar{I}_{RS} \end{bmatrix} \tag{2.22}$$

$$\begin{bmatrix} \bar{V}_{FS} \\ \bar{I}_{FSS} \end{bmatrix} = \begin{bmatrix} A_L & B_L \\ C_L & D_L \end{bmatrix} \begin{bmatrix} \bar{V}_{SS} \\ \bar{I}_{SS} \end{bmatrix} \tag{2.23}$$

From eqns. 2.21-2.23, the system general transfer matrix relation can be obtained and is given by eqn. 2.24.

$$\begin{bmatrix} \bar{V}_{SS} \\ \bar{I}_{SS} \end{bmatrix} = \begin{bmatrix} A & B \\ C & D \end{bmatrix} \begin{bmatrix} \bar{V}_{RS} \\ \bar{I}_{RS} \end{bmatrix} \tag{2.24}$$

where,

$$\begin{bmatrix} A & B \\ C & D \end{bmatrix} = \begin{bmatrix} A_L & B_L \\ -C_L & -D_L \end{bmatrix}^{-1} \begin{bmatrix} A_R & B_R \\ C_R & D_R \end{bmatrix}$$

From eqn. 2.24, the steady-state sending and receiving end currents, i.e. before fault initiation, are thus given by,

$$\bar{I}_{RS} = B^{-1}V_{SS} - B^{-1}A\bar{V}_{RS} \tag{2.25}$$

$$\bar{I}_{SS} = DB^{-1}V_{SS} + \left[C - DB^{-1}A\right]\bar{V}_{RS} \tag{2.26}$$

Solving for $\bar{V}_{FS}$ from eqns. 2.22 and 2.25 gives:

$$\bar{V}_{FS} = B_R B^{-1}\bar{V}_{SS} + \left[A_R - B_R B^{-1}A\right]\bar{V}_{RS} \tag{2.27}$$

Also, in systems equipped with the neutral switched reactor arrangement, the steady-state current flowing in the ideal neutral switch representing the two operative neutral switches(fig. 2.9) upon fault occurance on phases- "a", "b" and "c" is given by:

$$\bar{I}_{swa} = (\bar{V}_{ia} + \bar{V}_{ib})/Z_p \tag{2.28a}$$

$$\bar{I}_{swb} = (\bar{V}_{ia} + \bar{V}_{ib} + \bar{V}_{ic})/Z_p \tag{2.28b}$$

$$\bar{I}_{swc} = (\bar{V}_{ib} + \bar{V}_{ic})/Z_p \tag{2.28c}$$

respectively, where the suffix i designate the line end at which the reactor bank is connected(S for sending, R for receiving). The representation of the two operative switches by one ideal switch, is described in detail in section 3.5(CHAPTER 3).

The analysis for single phase-to-ground faults requires the calculation of the components due to the superimposed voltage $\bar{V}_{FF}$. These components should be added to the corresponding pre-fault steady-state variables to obtain the complete fault transient response. The formulation of the equations required for a complete solution is described in detail in APPENDIX 2.4.

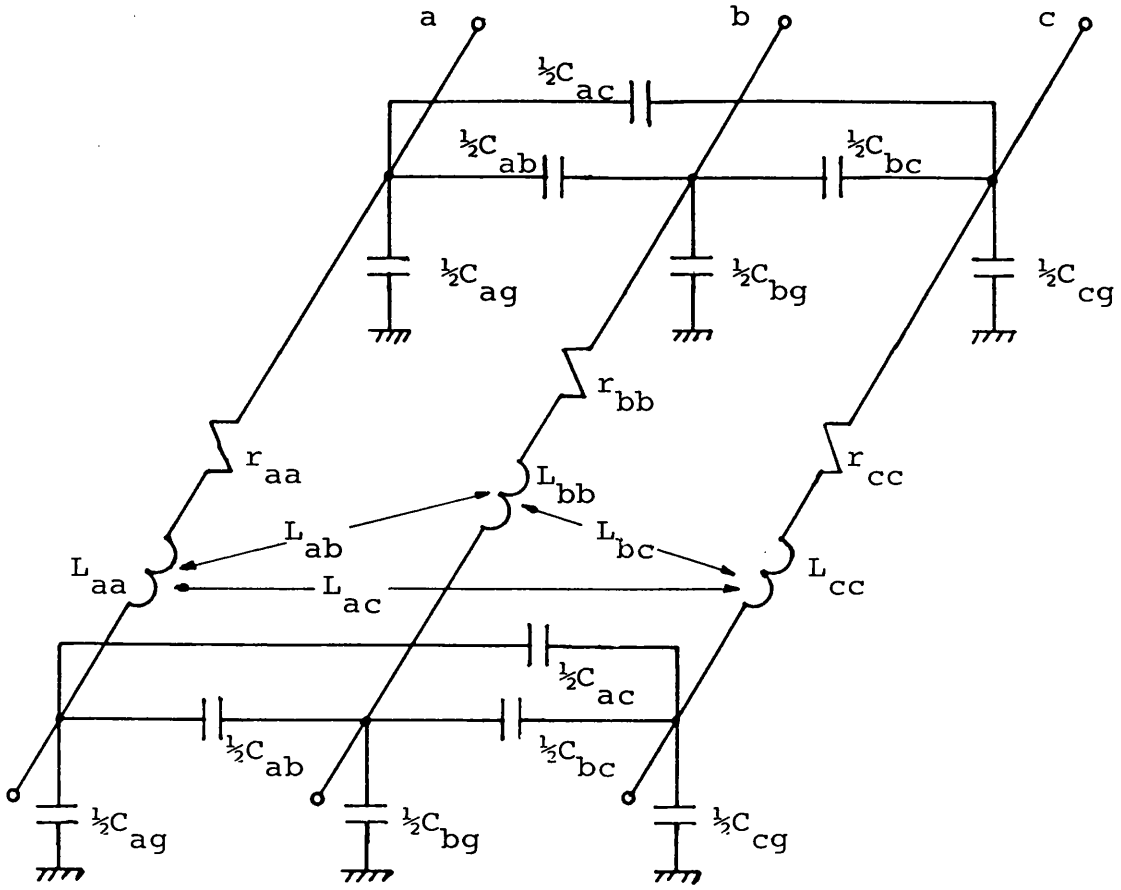

Fig. 2.1 Transmission line equivalent PI-section circuit

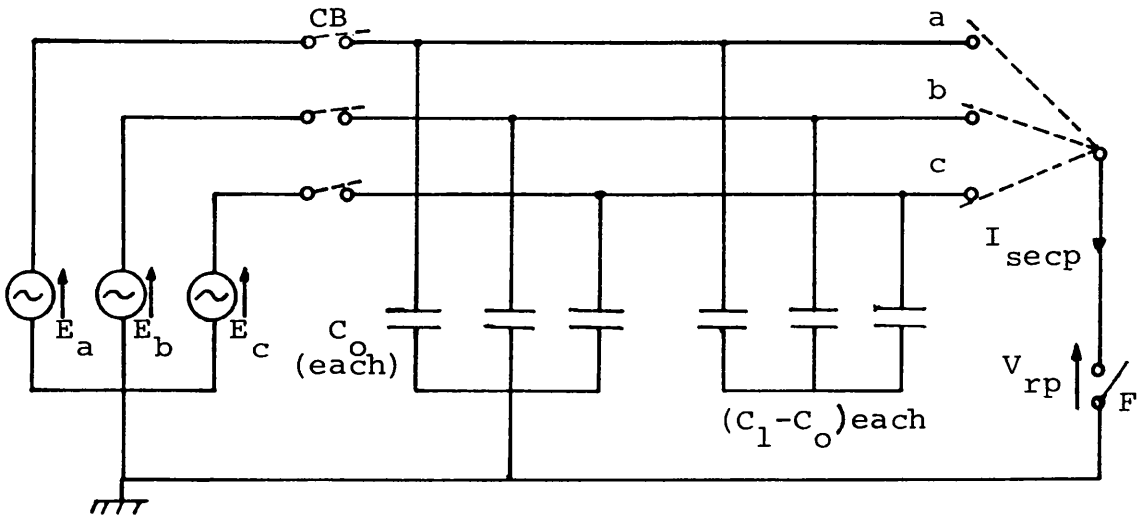

Fig. 2.2 Equivalent lumped capacitance three-phase system

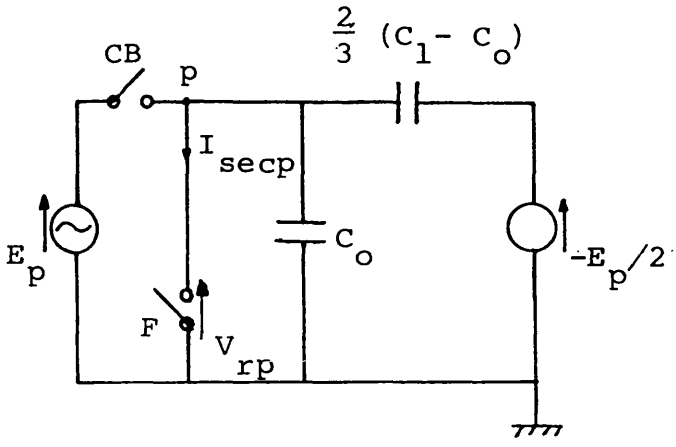

Fig. 2.3 Equivalent circuit of that of fig. 2.2

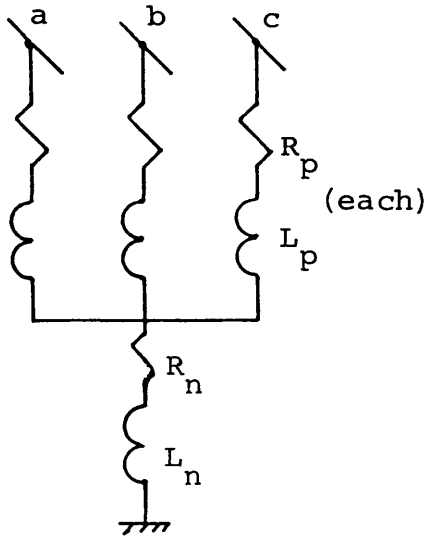

Fig. 2.4 Four-legged, balaced shunt reactor

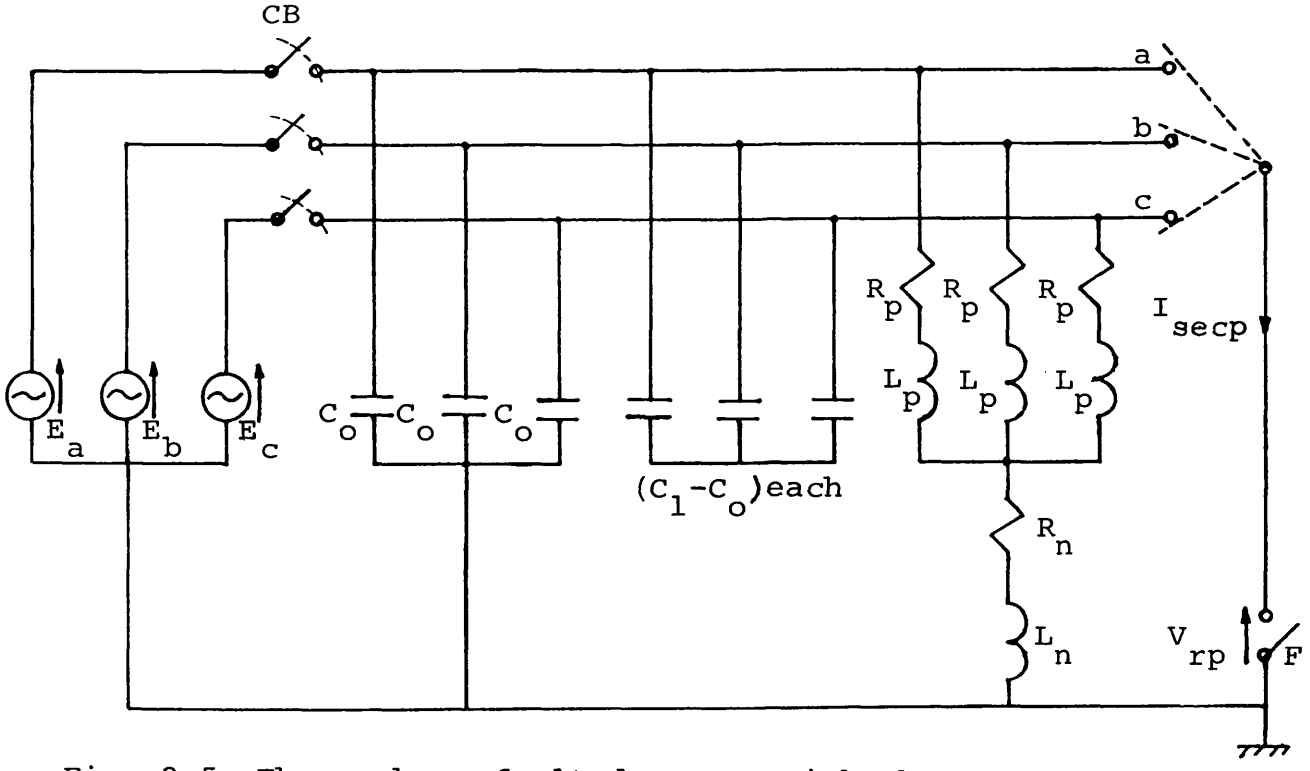

Fig. 2.5 Three phase faulted system with shunt compensation

Fig. 2.6
Circuit result from reduction of circuit of fig. 2.5

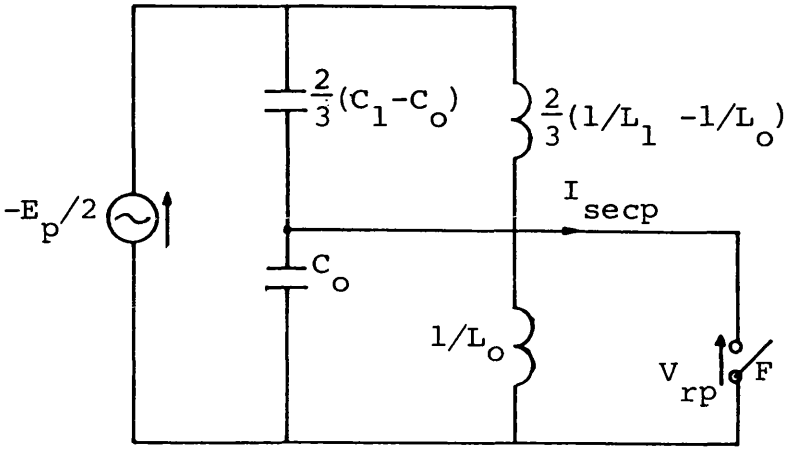

Fig. 2.7
Equivalent lumped capacitance, 3-phase system

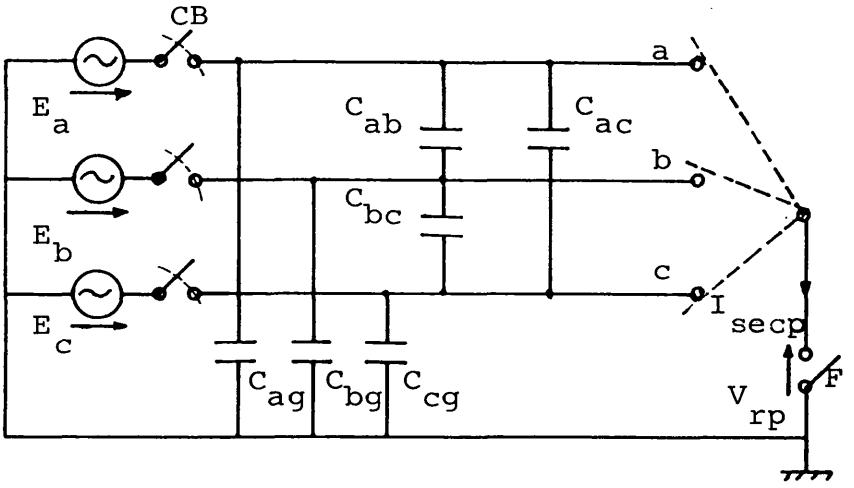

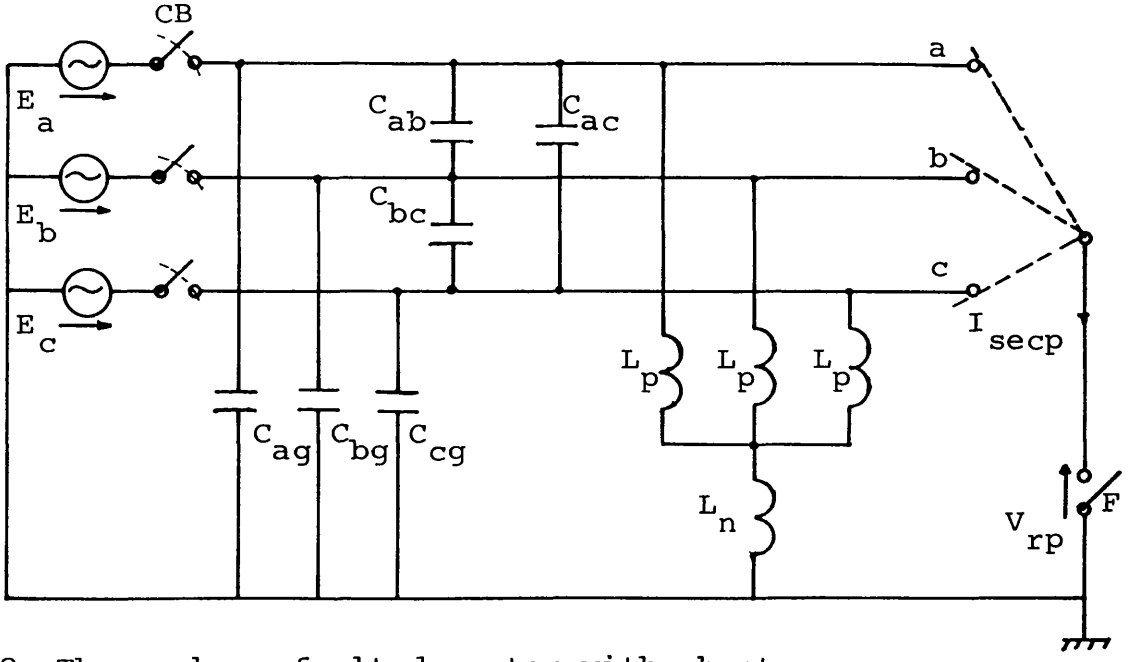

Fig. 2.8 Three phase faulted system with shunt compensation

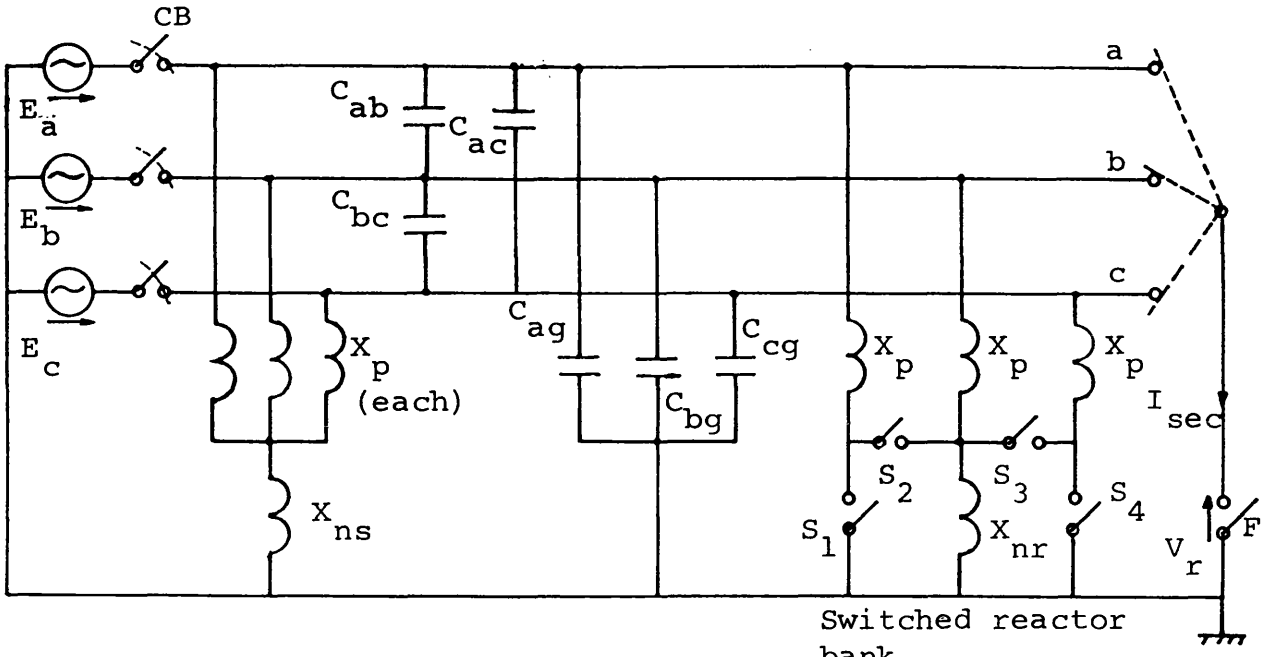

Fig. 2.9
System diagram with balanced and neutral switched reactor banks

Faulted phase	Switch states			
	S_1	S_2	S_3	S_4
a	O	C	O	C
b	O	C	C	O
c	C	O	C	O

"O"= Switch open

"C"= Switch close

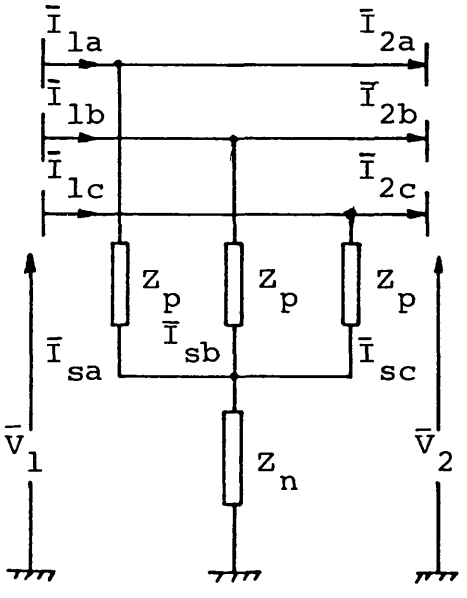

Fig. 2.11 Four-legged shunt reactor arrangement

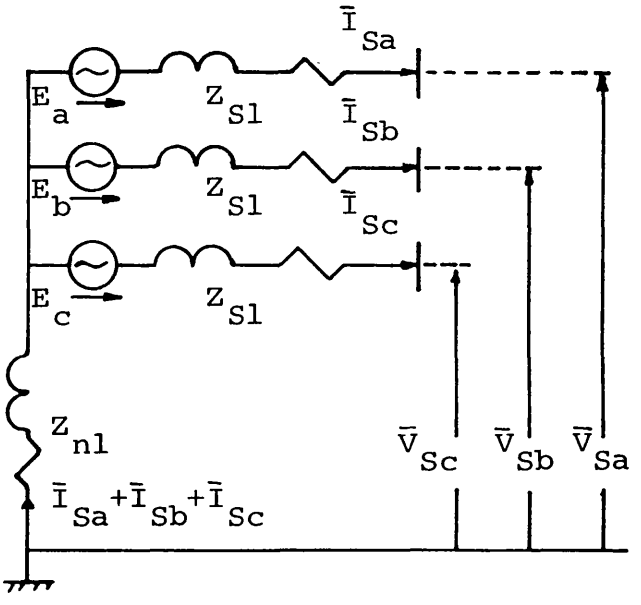

Fig. 2.10 Source network model

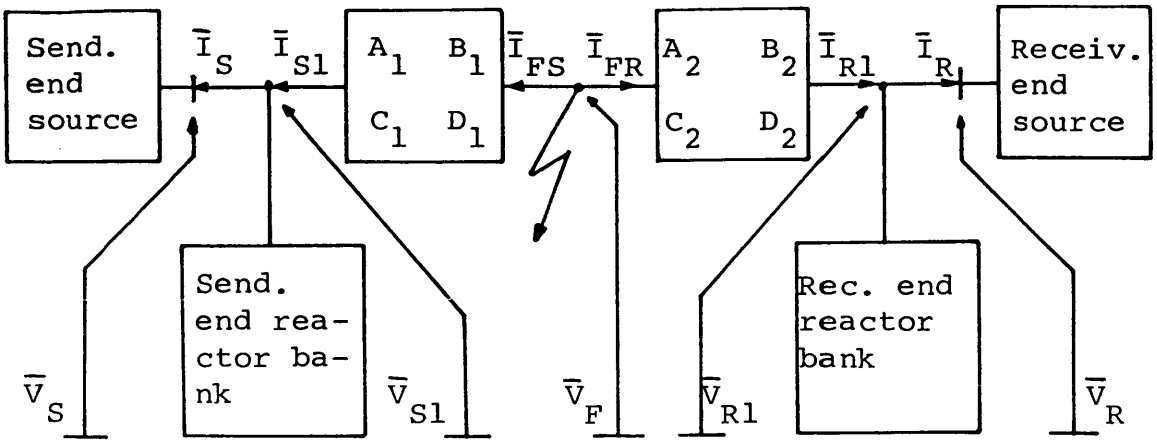

(a)

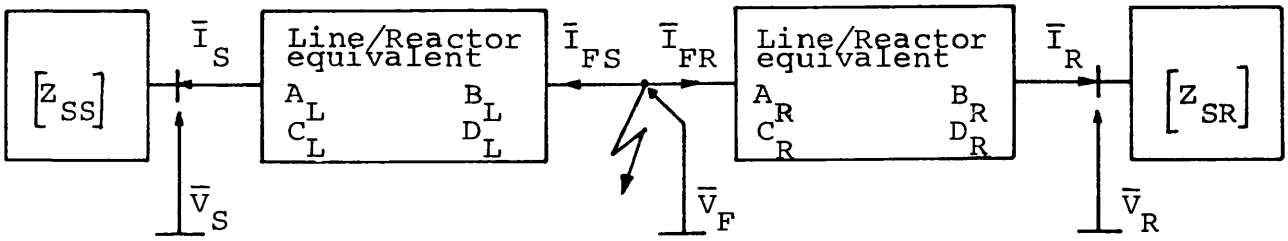

(b)

Fig. 2.12 Combination of line and shunt reactor bank(s)
(a) Actual model
(b) Equivalent arrangement

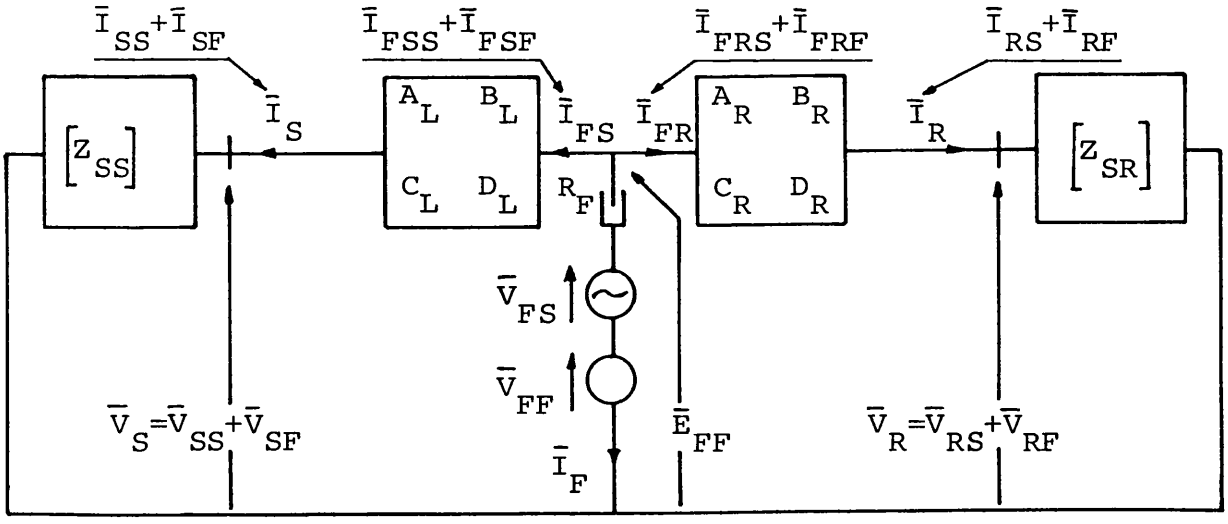

Fig. 2.13 Faulted system model
The steady-state components are: $\bar{V}_{SS}$, $\bar{V}_{RS}$, $\bar{V}_{FS}$, $\bar{I}_{FSS}$, $\bar{I}_{FRS}$, $\bar{I}_{SS}$, $\bar{I}_{RS}$

The transient components are: $\bar{V}_{SF}$, $\bar{V}_{RF}$, $\bar{V}_{FF}$, $\bar{I}_{FSF}$, $\bar{I}_{FRF}$, $\bar{I}_{SF}$, $\bar{I}_{RF}$

CHAPTER 3

SINGLE-POLE SWITCHING SIMULATION

3.1 Introduction

Ever since the earliest days of electricity supply, some form of switching operations have been needed to deal with the occurrence of faults. As a result of economic considerations, greater emphasis has been placed on high speed fault clearing strategies. The principal benefits of high speed fault clearing are the effective improvement of the power system transient stability and supply security. Other benefits are provided as a result of reduced fault clearing times, such as[63,64,65,66]:

1. Reduced damages to transmission system hardware (insulators, conductors,...etc.).

2. Reduced stresses on major terminal equipments (generators, turbines,...etc.).

3. Reduced possibility of evolving faults.

4. The possibility of faster reclosure due to less arc path ionization.

Generally, the overall fault -clearance time depends on the operating time of the protection scheme and, equally, on the speed of the circuit breakers. A considerable amount

of work has been done in both areas to realize, by present day standards, a relatively short fault-clearance times. As a result, recent years have seen the emergence of fast operating circuit breakers[63,64] (operating times of the order of ¾ - 1 cycle of power frequency), and the digitised travelling-wave based protection schemes[65,67,68,69] (response time in the order of several milliseconds). In single-pole switched systems, the fault clearing process is further complicated. The circuit breaker poles have to be equipped with separate tripping mechanisims, and the faulted phase selection is another feature to be incorporated with others in the protection scheme.

Although a power system is in a steady-state(or quasi steady-state) most of the time, it must be designed to withstand the worst possible stresses to which it may be subjected. Transient overvoltage resulting from switching operations are a form of such stresses. Field tests, and simulation studies of systems implementing single-pole switching show that the developed switching overvoltages are well within those corresponding to three-phase switching[27,48,70,71,72,73,74]. However, one of the prime requirements of design studies for single-pole switching schemes is the realistic knowledge of the transient phenomena involved. This is particularly the case for the performance evaluation of the protection schemes, which must, ideally operate selectively according to the type of fault. In order to fully assess such performance, a very realistic simulation of the transient phenomena is therefore essential over the total fault inception to system restoration period of time[75,76]. In general, the transient phenomena associated with system switching are very complex. System simulation from time of fault to that of system restoration, involves a large number of time discontinuties. The problem of such

nonlinearities has been solved using the lattice technique[51] and comparatively recently using the Modified Fourier Transform method[76,77].

In this chapter, the principles of a switch simulation are presented. Single line-to ground fault clearance along with the simulation of the hybrid method of autoreclosure are discussed. The development of the Frequency-Domain simulation techniques to incorporate the neutral switched reactor arrangement and the High Speed Grounding Switches (HSGS's) are also presented. Breaker pole, and/or any other switch operation(open or close) are simulated to take place at any instant of time after fault inception.

3.2 Switch Simulation-Basic Principles

Single-pole switching transient studies involve many discontinuities, which are mathematically modelled by the opening or closing of ideal switches(fig. 3.1a). In order to simplify the rather difficult problem of simulation, the analysis is split into several distinct stages[75,76]. This is done by simulating each switch and/or breaker pole with a parallel connection of n hypothetical current generators. Fig. 3.1 illustrates the method. The total current through the switch is given by the sum,

$$i_{s1} + i_{s2} + ... + i_{sn} = \sum_{K=1}^{n} i_{sK} ,$$

where n represent the total number of the system states, i.e., the total number of the switching events including fault inception. Generally, the individual components of current are arranged so that, for any period of time during which the switch is open, the summation is zero, i.e. $i_s = 0$. Conversely, during any period the switch is

closed, the summation $\sum i_{sk}$ is arranged such that $e_s = 0$. The transient response due to fault inception is thereby obtained(section 2.5) using the theory developed by Johns and Aggarwal[57,75]. The subsequent components of the response are then determined from a series of current and voltage injections at the switching points of the system, coupled with the principle of superposition.

3.3 Fault Clearance

Having obtained the fault transient response, the faulted phase current at both the sending and receiving ends are checked for zero crossing, to determine which pole opens first. The opening of the particular pole is simulated by injecting a current equal and opposite to that through the pole under consideration. This part of simulation is essentially one of superposition, and can be explained with reference to fig. 3.2, which shows the general system model for an "a"-phase to earth fault[53].

If the time after fault at which the first zero crossing of say the sending end phase-"a" current occurs is T_{b2}, then the Frequency Transform($\bar{I}_{S2a}$) of current which is injected as shown in fig. 3.3 to simulate the pole opening is given by :

$$\bar{I}_{S2a} = -\int_{T_{b2}}^{T_{ob}} i_{S2a} \exp\left[-j(\omega - j\alpha)t\right] dt \qquad (3.1)$$

where, $i_{S2a} = (i_{SOa} + i_{Sla})\ h(t-T_{b2})$

$(i_{SOa} + i_{Sla})$= total instantaneous faulted phase current at the sending end, which corresponds to$(i_{SSa}+i_{SFa})$ in chapter 2.

In fig. 3.3, $\bar{E}_{S2a}$ is the Frequency Transform of a voltage source which arises due to the injection of the current $\bar{I}_{S2a}$. The Transform of the voltage components $\bar{V}_{S2}$ and $\bar{V}_{R2}$ on the line side of the breaker are obtained by noting that[57],

$$\bar{V}_{S2} = Z_{SS}\,\bar{I}_{S2} - \bar{E}_{S2} \tag{3.2}$$

$$\bar{V}_{R2} = Z_{SR}\,\bar{I}_{R2} - \bar{E}_{R2} \tag{3.3}$$

Also, the variation of the relaying point voltage and current components are related to the fault point quantities by,

$$\begin{bmatrix} \bar{V}_{F2} \\ \bar{I}_{FR2} \end{bmatrix} = \begin{bmatrix} A_R & B_R \\ C_R & D_R \end{bmatrix} \begin{bmatrix} \bar{V}_{R2} \\ \bar{I}_{R2} \end{bmatrix} \tag{3.4}$$

and

$$\begin{bmatrix} \bar{V}_{F2} \\ \bar{I}_{FS2} \end{bmatrix} = \begin{bmatrix} A_L & B_L \\ C_L & D_L \end{bmatrix} \begin{bmatrix} \bar{V}_{S2} \\ \bar{I}_{S2} \end{bmatrix} \tag{3.5}$$

At the point of fault,

$$\bar{V}_{F2} = \bar{E}_{F2} + Z_F \left[-(\bar{I}_{FR2} + \bar{I}_{FS2}) \right] = \bar{E}_{F2} + Z_F\,\bar{I}_{F2} \tag{3.6}$$

If a 4-legged shunt reactor is connected at either or both ends of the line, the Transform of the voltage across the neutral reactance is given by:

$$\bar{V}_{n2} = (\bar{V}_{a2} + \bar{V}_{b2} + \bar{V}_{c2}) \left[Z_n / (Z_p + 3Z_n) \right] \qquad (3.7)$$

where $\left[\bar{V}_{a2} \ \bar{V}_{b2} \ \bar{V}_{c2} \right]^T$ is the voltage Transform vector of the line end bus at which the reactor is connected.

The foregoing relationships (3.2 to 3.6) effectively define a set of simultaneous equations , relating the superimposed circuit current Transforms to the associated voltage transforms across each hypothetical current generator, and they can be arranged in the alternative form of eqn. 3.8[76] .

$$\begin{bmatrix} \bar{I}_{F2} \\ \bar{I}_{S2} \\ \bar{I}_{R2} \end{bmatrix} = \begin{bmatrix} Y_{11} & Y_{12} & Y_{13} \\ Y_{21} & Y_{22} & Y_{23} \\ Y_{31} & Y_{32} & Y_{33} \end{bmatrix} \begin{bmatrix} \bar{E}_{F2} \\ \bar{E}_{S2} \\ \bar{E}_{R2} \end{bmatrix} \qquad (3.8)$$

Details of formulating the admittance matrix Y_{ij} of eqn. 3.8, are presented in APPENDIX 3.1. Each of the sub-matrices in Y_{ij} is defined in terms of the basic parameters (R_F, A_L, Z_{SS}, ... etc.) of the system at any spectral frequency of interest. It is important to note that each sub-matrix within Y_{ij} is a 3 x 3 matrix, and that each sub-vector (voltage or current) is a 3 x 1 column vector representing the voltage or current Transforms of the individual phase conductors.

To illustrate phase-"a" sending end breaker pole opening, consider fig. 3.3 with the suffix K=2. When the pole is open, there are eight known zero-valued Transforms, plus the Transform of the same pole current ($\bar{I}_{S2a}$). Therefore, eqn. 3.8 can be written in the following form.

$$\begin{bmatrix} \bar{I}_{F2a} \\ \bar{I}_{F2b} = 0 \\ \bar{I}_{F2c} = 0 \\ \bar{I}_{S2a} \\ \bar{I}_{S2b} \\ \bar{I}_{S2c} \\ \bar{I}_{R2a} \\ \bar{I}_{R2b} \\ \bar{I}_{R2c} \end{bmatrix} = \begin{bmatrix} & & \\ Y_{11} & Y_{12} & Y_{13} \\ & & \\ & & \\ Y_{21} & Y_{22} & Y_{23} \\ & & \\ & & \\ Y_{31} & Y_{32} & Y_{33} \\ & & \end{bmatrix} \begin{bmatrix} \bar{E}_{F2a} = 0 \\ \bar{E}_{F2b} \\ \bar{E}_{F2c} \\ \bar{E}_{S2a} \\ \bar{E}_{S2b} = 0 \\ \bar{E}_{S2c} = 0 \\ \bar{E}_{R2a} = 0 \\ \bar{E}_{R2b} = 0 \\ \bar{E}_{R2c} = 0 \end{bmatrix} \qquad (3.9)$$

Elimination of all rows and columns which correspond to zero-valued Transforms in the voltage vector of eqn. 3.9 produces the reduced matrix relationship of eqn. 3.10.

$$\begin{bmatrix} 0 \\ 0 \\ \bar{I}_{S2a} \end{bmatrix} = \begin{bmatrix} & \\ Y_2 & \\ & \end{bmatrix} \begin{bmatrix} \bar{E}_{F2b} \\ \bar{E}_{F2C} \\ \bar{E}_{S2a} \end{bmatrix} \qquad (3.10)$$

Now, $\bar{I}_{S2a}$ is a known current Transform (eqn. 3.1), which in turn enables the voltage vector in eqn. 3.10 to be calculated. Further substitution of the resulting known voltage vector $\left[\bar{E}_{F2b} \quad \bar{E}_{F2c} \quad \bar{E}_{S2a}\right]^T$ in the full matrix relation of eqn. 3.9, enables the remaining current Transform values $\left[\bar{I}_{F2a} \quad \bar{I}_{S2bc} \quad \bar{I}_{R2abc}\right]^T$ to be calculated. These quantities are then transformed back into the time-domain using the Fast Fourier Transform technique[57]. The total time-domain response at this stage, can be calculated by adding the three quantities, namely, 1) steady-state, 2) fault inception and 3) phase-"a" sending end

breaker pole opening. At the receiving end,

$$i_{RT}(t) = i_{RO}(t) + i_{R1}(t - T_F) + i_{R2}(t - T_{b2}) \qquad (3.11)$$

$$e_{RT}(t) = 0.0 \qquad (3.12)$$

$$v_{RT}(t) = v_{RO}(t) + v_{R1}(t - T_F) + v_{R2}(t - T_{b2}) \qquad (3.13)$$

and the voltage across the neutral of a 4-legged shunt reactor if present at the receiving end is,

$$v_{RnT}(t) = v_{Rn1}(t - T_F) + v_{Rn2}(t - T_{b2}) \qquad (3.14)$$

Similar equations can be written for the quantities at the fault point and the sending end.

The final process in the fault-clearance procedure, involves the opening of the receiving end phase-"a" breaker pole. The current concerned (eqn. 3.11) is checked for zero crossing, say to occur at a time T_{b3} after fault. Opening procedure, similar to that outlined for the sending end pole opening is performed to obtain the system superimposed components due to the receiving end pole opening. The total time-domain response, for example, of the fault path current at this stage would then be :-

$$i_{FT}(t) = i_{F1}(t - T_F) + i_{F2}(t - T_{b2}) + i_{F3}(t - T_{b3}) \qquad (3.15)$$

For $t > T_{b3}$, $i_{FT}(t)$ represent the secondary arc current assuming a constant fault path resistance(0.5Ω).

3.4 The Hybrid Method of Autoreclosure

The basis of the hybrid method, involves utilizing a properly timed combination of single-pole and three-phase

switching operations. In this method, the two sound phases are tripped after fault clearance by single-pole switching. Ultimately , this is followed by fast reclosure of all three phases. In order to conserve the benefits of single-pole switching, the tripping of the sound phases should be as late as possible within the overall selected reclose time. No relevant studies of implementing such method have been located in the literature, apart from transient stability studies reported in reference 3.

Upon fault clearance(section 3.3), the secondary arc characteristic[25] (discussed in chapter 4) are defined for the first period of secondary arcing. The first period here, is defined as the time interval from the instant of arc transition,i.e., faulted phase second pole opening time, to the instant of the first sound phase first pole opening. The opening of the sound phases, is then carried out in a similar successive fashion to that outlined in section 3.3, with the fault path represented by a small linear resistance. The time instant T_{b7} , when the last sound phase is cleared, is then considered as the transition time to the second period of secondary arcing, with the three phases de-energised.

3.5 Opening of The Reactor Switches

The standard superimposed circuit of the full system model (including the switched reactor bank) is represented in the Frequency-Domain by the circuit of fig. 3.4. The four neutral switches(S_1 .. S_4) are closed during normal system operation. The insets in fig. 3.4 show the pair of switches which operate in response to a particular phase-to-ground fault. Staged fault tests[48] , showed that, the

difference in the opening times of the neutral switches concerned is of the order of 0 to 8 milliseconds. Moreover, for any phase fault, the two operative switches appear in parallel across the neutral to earth impedance($R_{nr}+j\omega L_{nr}$). Therefore, it is adequate to represent the two operating switches by a single ideal neutral switch simulated in the superimposed circuit model. Fig. 3.5 shows the detailed representation of the neutral switched reactor bank including the ideal neutral switch for different phase faults. Consider fig. 3.4, at the sending end,

$$\bar{V}_{SK} = Z_{SS}\ \bar{I}_{SK} - \bar{E}_{SK} \tag{3.16}$$

At the point of fault,

$$\bar{V}_{FK} = \bar{E}_{FK} - Z_F(\bar{I}_{FSK} + \bar{I}_{FRK}) = \bar{E}_{FK} + Z_F\ \bar{I}_{FK} \tag{3.17}$$

At the receiving end,

$$\bar{V}_{RK} = Z_{SR}\ \bar{I}_{RK} - \bar{E}_{RK} \tag{3.18}$$

Also at the receiving end (see fig. 3.5),

$$\begin{bmatrix} \bar{V}_{RK} \\ \bar{E}_{SWK} \end{bmatrix} = \begin{bmatrix} & I & \end{bmatrix} \begin{bmatrix} \bar{I}_{mK} \\ \bar{I}_{SWK} \end{bmatrix} \tag{3.19}$$

Where,

$$[I] = \left[\begin{array}{c|c} I_1 & I_2 \\ \hline I_3 & I_4 \end{array}\right]$$

$I_4 = Z_{nR}$(single element)

$$[I_1] = \begin{bmatrix} Z_p + Z_{nR} & Z_{nR} & 0 \\ Z_{nR} & Z_p + Z_{nR} & 0 \\ 0 & 0 & Z_p \end{bmatrix} \qquad \text{for fault on phase-"a"}$$

$$[I_3] = [Z_{nR}\ Z_{nR}\ 0] = [I_2]^T$$

$$[I_1] = \begin{bmatrix} Z_p + Z_{nR} & Z_{nR} & Z_{nR} \\ Z_{nR} & Z_p + Z_{nR} & Z_{nR} \\ Z_{nR} & Z_{nR} & Z_p + Z_{nR} \end{bmatrix} \qquad \text{for fault on phase-"b"}$$

$$[I_3] = [Z_{nR}\ Z_{nR}\ Z_{nR}] = [I_2]^T$$

$$[I_1] = \begin{bmatrix} Z_p & 0 & 0 \\ 0 & Z_p + Z_{nR} & Z_{nR} \\ 0 & Z_{nR} & Z_p + Z_{nR} \end{bmatrix} \qquad \text{for fault on phase-"c"}$$

$$[I_3] = [0\ Z_{nR}\ Z_{nR}] = [I_2]^T$$

Furthermore, the variation of the line end voltages and currents are related to the fault point quantities by :

$$\begin{bmatrix} \bar{V}_{FK} \\ \bar{I}_{FRK} \end{bmatrix} = \begin{bmatrix} A_R & B_R \\ C_R & D_R \end{bmatrix} \begin{bmatrix} \bar{V}_{RK} \\ \bar{I}_{RK} + \bar{I}_{mK} \end{bmatrix} \qquad (3.20)$$

and,

$$\begin{bmatrix} \bar{V}_{FK} \\ \bar{I}_{FSK} \end{bmatrix} = \begin{bmatrix} A_L & B_L \\ C_L & D_L \end{bmatrix} \begin{bmatrix} \bar{V}_{SK} \\ \bar{I}_{SK} \end{bmatrix} \qquad (3.21)$$

The Transform of the voltage across the neutral of the 4-legged reactor bank at the sending end is given by :

$$\bar{V}_{SnK} = (\bar{V}_{SKa} + \bar{V}_{SKb} + \bar{V}_{SKc}) \; Z_{nS}/(Z_p + 3Z_{nS}) \qquad (3.22)$$

The foregoing relationships (3.16 to 3.21) effectively define a set of simultaneous equations relating Transforms of the Kth. superimposed circuit currents to the associated Transform voltages across each hypothetical current generator, and they can be arranged in the alternative form of eqn. 3.23.

$$\begin{bmatrix} \bar{I}_{FK} \\ \bar{I}_{SK} \\ \bar{I}_{RK} \\ \bar{I}_{SWK} \end{bmatrix} = \left[\begin{array}{ccc|c} Y_{11} & Y_{12} & Y_{13} & Y_{14} \\ Y_{21} & Y_{22} & Y_{23} & Y_{24} \\ Y_{31} & Y_{32} & Y_{33} & Y_{34} \\ \hline Y_{41} & Y_{42} & Y_{43} & Y_{44} \end{array}\right] \begin{bmatrix} \bar{E}_{FK} \\ \bar{E}_{SK} \\ \bar{E}_{RK} \\ \bar{E}_{SWK} \end{bmatrix} \qquad (3.23)$$

In the admittance matrix relationship of eqn. 3.23, each of the sub-matrices Y_{ij} , i= 1,3; j= 1,3, is a 3 x 3 matrix, and Y_{4i}, Y_{i4}, i= 1,3, are 1 x 3, 3 x 1 matrices respectively. Y_{44} is a single element, however, each element in the admittance matrix, is defined in terms of the basic system parameters(R_F, A_L, Z_{SS}, ... etc.) at any spectral frequency of interest. In APPENDIX 3.2, detailed derivation of the general admittance matrix of eqn. 3.23 is presented.

The system response up to the instant of the ideal neutral switch opening,is obtained by adding the components due to fault and fault clearance to those of the steady-state. It is worth mentioning that the faulted phase

clearance calculations, are carried out in a similar way to that outlined in section 3.3, using the relationship of eqn. 3.23. Opening of the ideal neutral switch can be simulated to take place either when its current(eqn. 3.24) waveform goes through zero, or randomly after a specified operating time.

$$i_{SWT}(t) = i_{SWO}(t) + i_{SW1}(t - T_F) + i_{SW2}(t - T_{b2}) + i_{SW3}(t - T_{b3}) \qquad (3.24)$$

Consider the opening of the ideal neutral switch to take place, say T_{sl} after fault, then the next stage of the computation involves finding the Frequency Spectrum ($\bar{I}_{SW4}$) of a current injected into the system as shown in fig. 3.5 and is given by :

$$\bar{I}_{SW4} = -\int_{T_{sl}}^{T_{ob}} i_{SWT}(t)\ \exp\left[\ -j(\omega - j\alpha)t\ \right] dt \qquad (3.25)$$

Assuming the fault occured on phase-"a", which then cleared by the corresponding breaker pole at the line ends, therefore there are nine known zero-valued Transforms associated with the ideal neutral switch current. Furthermore, the tenth known quantity, is the Frequency Transform of the superimposed current $\bar{I}_{SW4}$, so that eqn. 3.23 can therefore be written in the following form,

$$\begin{bmatrix} \bar{I}_{F4a} \\ \bar{I}_{F4b} = 0 \\ \bar{I}_{F4c} = 0 \\ \bar{I}_{S4a} = 0 \\ \bar{I}_{S4b} \\ \bar{I}_{S4C} \\ \bar{I}_{R4a} = 0 \\ \bar{I}_{R4b} \\ \bar{I}_{R4c} \\ \bar{I}_{SW4} \end{bmatrix} = \begin{bmatrix} \\ \\ Y_{ij} \\ \\ \\ \\ \\ \\ \\ \end{bmatrix} \begin{bmatrix} \bar{E}_{F4a} = 0 \\ \bar{E}_{F4b} \\ \bar{E}_{F4c} \\ \bar{E}_{S4a} \\ \bar{E}_{S4b} = 0 \\ \bar{E}_{S4c} = 0 \\ \bar{E}_{R4a} \\ \bar{E}_{R4b} = 0 \\ \bar{E}_{R4c} = 0 \\ \bar{E}_{SW4} \end{bmatrix} \qquad (3.26)$$

where, $i = 1,4$; $j = 1,4$

From eqn. 3.26, discarding all rows and columns that correspond to zero-valued voltage Transforms, produces the reduced matrix relationship of eqn.3.27.

$$\begin{bmatrix} 0 \\ 0 \\ 0 \\ 0 \\ \bar{I}_{SW4} \end{bmatrix} = \begin{bmatrix} \\ \\ Y_4 \\ \\ \end{bmatrix} \begin{bmatrix} \bar{E}_{F4b} \\ \bar{E}_{F4c} \\ \bar{E}_{S4a} \\ \bar{E}_{R4a} \\ \bar{E}_{SW4} \end{bmatrix} \qquad (3.27)$$

The known quantities in eqn. 3.27 are $\bar{I}_{SW4}$ and Y_4, which enables the calculation of $\bar{E}_{F4bc}$, $\bar{E}_{S4a}$, $\bar{E}_{R4a}$, and $\bar{E}_{SW4}$. Substituting these quantities in eqn. 3.26, the Transform

of the currents $\bar{I}_{F4}$, $\bar{I}_{S4}$, and $\bar{I}_{R4}$ can be obtained. Finally, $\bar{V}_{S4}$, $\bar{V}_{R4}$, and $\bar{V}_{F4}$ are calculated using eqns. 3.16 - 3.17. The Transform of the voltage across the neutral of the sending end reactor bank is calculated using eqn. 3.22. It is obvious that the Transform of the voltage across the receiving end reactor neutral is equal to $\bar{E}_{SW4}$, i.e.,

$$\bar{V}_{Rn4} = \bar{E}_{SW4} \tag{3.28}$$

The calculated superimposed components due to the ideal neutral switch opening, are then transformed back into the time-domain using the Fast Fourier Transform technique[57]. The total time-domain response at this stage is calculated by adding the five quantities, viz.(0) steady-state, (1) fault inception, (2) sending end pole opening, (3) receiving end pole opening, and (4) the ideal neutral switch opening. The total time-domain response, of say the fault path current would then be:

$$i_{FT}(t) = i_{F1}(t - T_F) + i_{F2}(t - T_{b2}) + i_{F3}(t - T_{b3}) + i_{F4}(t - T_{s1}) \tag{3.29}$$

For $t > T_{s1}$, $i_{FT}(t)$ represents the secondary arc current assuming a constant fault path resistance ($0.5\,\Omega$). The time T_{s1} in such system implementation, is considered to be the transition instant from the primary arcing state to the secondary arcing one.

3.6 Closing of The HSGS's

The primary advantage of grounding the faulted phase after the main circuit breakers interrupt the primary arc, is the reduction of the faulted phase recovery voltage to a very low value. This, coupled with the circulation of opposite loop currents in the fault path (i_1 and i_2, in fig. 3.6), which reduces the secondary arc current, can lead to a very fast extinction after the grounding at both ends. The sequence of operations which takes place after a single phase-to-ground fault, occurs on a transmission line equipped with HSGS's for single-pole switching are :-

1. The main circuit breakers clear the fault, interrupting the primary power arc.
2. Faulted phase HSGS close at both ends.
3. HSGS's open, followed by reclosure of the main circuit breakers.

Fig. 3.7 shows the standard superimposed circuit of the full system model represented in the Frequency-Domain. At the sending end,

$$\bar{V}_{SK} = Z_{SS}\ \bar{I}_{SK} - \bar{E}_{SK} \qquad (3.30)$$

Also at the sending end, $\bar{V}_{SK}$ is the voltage Transform across the HSGS, and is given by :

$$\bar{V}_{SK} = Z_g\ \bar{I}_{SgK} + \bar{E}_{SgK} \qquad (3.31)$$

where Z_g is a 3 x 3 diagonal matrix representing the HSGS

resistance. Moreover, with reference to fig. 3.7, at the sending end,

$$\bar{I}_{S1K} = \bar{I}_{SK} + \bar{I}_{SgK} \tag{3.32}$$

Similarly, at the receiving end,

$$\bar{V}_{RK} = Z_{SR}\ \bar{I}_{RK} - \bar{E}_{RK} \tag{3.33}$$

$$\bar{V}_{RK} = Z_{g}\ \bar{I}_{RgK} + \bar{E}_{RgK} \tag{3.34}$$

and

$$\bar{I}_{R1K} = \bar{I}_{RK} + \bar{I}_{RgK} \tag{3.35}$$

At the point of fault,

$$\bar{V}_{FK} = \bar{E}_{FK} + Z_{F}\ \bar{I}_{FK} = \bar{E}_{FK} - Z_{F}\ (\bar{I}_{FSK} + \bar{I}_{FRK}) \tag{3.36}$$

Also, the variation of the line ends voltage and current components, are related to the fault point quantities by :

$$\begin{bmatrix} \bar{V}_{FK} \\ \bar{I}_{FSK} \end{bmatrix} = \begin{bmatrix} A_L & B_L \\ C_L & D_L \end{bmatrix} \begin{bmatrix} \bar{V}_{SK} \\ \bar{I}_{S1K} \end{bmatrix} \tag{3.37}$$

$$\begin{bmatrix} \bar{V}_{FK} \\ \bar{I}_{FRK} \end{bmatrix} = \begin{bmatrix} A_R & B_R \\ C_R & D_R \end{bmatrix} \begin{bmatrix} \bar{V}_{RK} \\ \bar{I}_{R1K} \end{bmatrix} \tag{3.38}$$

Equations 3.30 to 3.38 can be arranged to define a set of simultaneous equations, relating superimposed circuit Transform currents to the associated Transform voltages across each hypothetical current generator. In APPENDIX 3.3, detailed formulation of such equations are presented, and

the result is given by the matrix relationship of eqn. 3.39.

$$\begin{bmatrix} \bar{I}_{FK} \\ \bar{I}_{SK} \\ \bar{I}_{RK} \\ \bar{I}_{SgK} \\ \bar{I}_{RgK} \end{bmatrix} = \begin{bmatrix} Y_{11} & Y_{12} & Y_{13} & Y_{14} & Y_{15} \\ Y_{21} & Y_{22} & Y_{23} & Y_{24} & Y_{25} \\ Y_{31} & Y_{32} & Y_{33} & Y_{34} & Y_{35} \\ Y_{41} & Y_{42} & Y_{43} & Y_{44} & Y_{45} \\ Y_{51} & Y_{52} & Y_{53} & Y_{54} & Y_{55} \end{bmatrix} \begin{bmatrix} \bar{E}_{FK} \\ \bar{E}_{SK} \\ \bar{E}_{RK} \\ \bar{E}_{SgK} \\ \bar{E}_{RgK} \end{bmatrix} \qquad (3.39)$$

Each of the sub-matrices in the admittance relationship of eqn. 3.39 is defined in terms of the basic parameters (R_F, R_S, A_L, ... etc.) of the system at any spectral frequency of interest. Moreover, each sub-matrix within the whole, is a 3 x 3 matrix.

The system response up to the time of fault-clearance is obtained following the procedure outlined in section 3.3. However, in utilizing the matrix relationship of eqn. 3.39, for each opening, there exist fourteen known zero-valued Transforms associated with the Transform of the current of the particular pole to open. The next step in the simulation, involves defining the secondary arc characteristics[25] (discussed in chapter 4) for the first period (the first period is defined here as the time interval from the instant of the arc first transition to the instant of closing the HSGS's).

In order to simulate the closure of the HSGS's, components of the faulted phase line end voltages to earth are first calculated for a fault branch that fails to conduct current, immediately following the second transition (hypothetical secondary arc extinction). This is done by

injecting the Transform of the secondary arc current in the opposite direction into the system, at the point of fault through 0.5Ω resistance. The voltage across the HSGS at each line end is then calculated as the sum of all its superimposed components up to this stage, i.e., steady-state, fault inception, fault clearance and the component corresponding to the hypothetical extinction of the secondary arc. Therefore, the total time-domain voltage response across the HSGS's, of phase-"a" for example, are given by :

$$e_{SgaT}(t) = v_{Sa0}(t) + v_{Sa1}(t - T_F) + v_{Sa2}(t - T_{b2}) + v_{Sa3}(t - T_{b3}) + v_{Sah}(t - T_{hc}) \quad (3.40)$$

at the sending end, and

$$e_{RgaT}(t) = v_{Ra0}(t) + v_{Ra1}(t - T_F) + v_{Ra2}(t - T_{b2}) + v_{Ra3}(t - T_{b3}) + v_{Rah}(t - T_{hc}) \quad (3.41)$$

at the receiving end.

In order to simplify the calculation procedure, and thereby reducing the computation time, the HSGS's at the line ends, are assumed to close simultaneously at a time equal to T_{hc} after fault inception. Considering the fault occured on phase-"a", the next stage in the computation, involves finding the Fourier Transforms $\bar{E}_{Sg4a}$, and $\bar{E}_{Rg4a}$ of the voltages e_{Sg4a}, and e_{Rg4a} respectively, i.e.,

$$\bar{E}_{Sg4a} = - \int_{T_{hc}}^{T_{ob}} e_{Sg4a} \exp\left[-j(\omega - j\alpha)t\right] dt \quad (3.42)$$

and

$$\bar{E}_{Rg4a} = - \int_{T_{hc}}^{T_{ob}} e_{Rg4a} \exp\left[-j(\omega - j\alpha)t\right] dt \quad (3.43)$$

Where, $e_{Sg4a} = e_{SgaT}\, h(t - T_{hc})$, and $e_{Rg4a} = e_{RgaT}\, h(t - T_{hc})$

With reference to fig. 3.7, $\bar{I}_{Sg4a}$ and $\bar{I}_{Rg4a}$ are the Frequency spectra of currents which flow in the HSGS at the sending and receiving end respectively, due to the injection of $\bar{E}_{Sg4a}$ and $\bar{E}_{Rg4a}$. When phase-"a" HSGS's at both ends are closed, there are thirteen known zero-valued Transforms associated with the superimposed voltage Transforms $\bar{E}_{Sg4a}$ and $\bar{E}_{Rg4a}$. Therefore, eqn. 3.39 can be written in the following form :

$$\begin{bmatrix} 0 \\ 0 \\ 0 \\ 0 \\ \bar{I}_{S4b} \\ \bar{I}_{S4c} \\ 0 \\ \bar{I}_{R4b} \\ \bar{I}_{R4c} \\ \bar{I}_{Sg4a} \\ 0 \\ 0 \\ \bar{I}_{Rg4a} \\ 0 \\ 0 \end{bmatrix} = \begin{bmatrix} \\ \\ \\ \\ \\ \\ \\ \\ \\ \\ \\ \\ \\ \\ \end{bmatrix} Y_{ij} \begin{bmatrix} \bar{E}_{F4a} \\ \bar{E}_{F4b} \\ \bar{E}_{F4c} \\ \bar{E}_{S4a} \\ 0 \\ 0 \\ \bar{E}_{R4a} \\ 0 \\ 0 \\ \bar{E}_{Sg4a} \\ \bar{E}_{Sg4b} \\ \bar{E}_{Sg4c} \\ \bar{E}_{Rg4a} \\ \bar{E}_{Rg4b} \\ \bar{E}_{Rg4c} \end{bmatrix} \qquad (3.44)$$

Where, i = 1,5 ; j = 1,5

In eqn. 3.44, discarding all rows and columns that correspond to zero-valued Transforms in the voltage vector, the reduced matrix relationship of eqn. 3.45 is obtained.

$$\begin{bmatrix} 0 \\ 0 \\ 0 \\ 0 \\ 0 \\ \bar{I}_{Sg4a} \\ 0 \\ 0 \\ \bar{I}_{Rg4a} \\ 0 \\ 0 \end{bmatrix} = \begin{bmatrix} & & Y_4 & & \end{bmatrix} \begin{bmatrix} \bar{E}_{F4a} \\ \bar{E}_{F4b} \\ \bar{E}_{F4c} \\ \bar{E}_{S4a} \\ \bar{E}_{R4a} \\ \bar{E}_{Sg4a} \\ \bar{E}_{Sg4b} \\ \bar{E}_{Sg4c} \\ \bar{E}_{Rg4a} \\ \bar{E}_{Rg4b} \\ \bar{E}_{Rg4c} \end{bmatrix} \qquad (3.45)$$

From eqn. 3.45,

$$\begin{bmatrix} \bar{E}_{F4a} \\ \bar{E}_{F4b} \\ \bar{E}_{F4c} \\ \bar{E}_{S4a} \\ \bar{E}_{R4a} \\ \bar{E}_{Sg4a} \\ \bar{E}_{Sg4b} \\ \bar{E}_{Sg4c} \\ \bar{E}_{Rg4a} \\ \bar{E}_{Rg4b} \\ \bar{E}_{Rg4c} \end{bmatrix} = \begin{bmatrix} & & Z_4 & & \end{bmatrix} \begin{bmatrix} 0 \\ 0 \\ 0 \\ 0 \\ 0 \\ \bar{I}_{Sg4a} \\ 0 \\ 0 \\ \bar{I}_{Rg4a} \\ 0 \\ 0 \end{bmatrix} \qquad (3.46)$$

Where $Z_4 = Y_4^{-1}$.

However, $\bar{E}_{Sg4a}$ and $\bar{E}_{Rg4a}$ are known voltage Transforms, hence, $\bar{I}_{Sg4a}$ and $\bar{I}_{Rg4a}$ can be obtained from eqn. 3.47.

$$\begin{bmatrix} \bar{I}_{Sg4a} \\ \bar{I}_{Rg4a} \end{bmatrix} = \begin{bmatrix} Z_4(6,6) & Z_4(6,9) \\ Z_4(9,6) & Z_4(9,9) \end{bmatrix}^{-1} \begin{bmatrix} \bar{E}_{Sg4a} \\ \bar{E}_{Rg4a} \end{bmatrix} \qquad (3.47)$$

Substituting for $\bar{I}_{Sg4a}$ and $\bar{I}_{Rg4a}$ in eqn. 3.46, the Transforms $\bar{E}_{F4abc}$, $\bar{E}_{S4a}$, $\bar{E}_{R4a}$, $\bar{E}_{Sg4bc}$ and $\bar{E}_{Rg4bc}$ are obtained. Further substitution of the resulting known voltage vector $\left[\bar{E}_{F4} \quad \bar{E}_{S4} \quad \bar{E}_{R4} \quad \bar{E}_{Sg4} \quad \bar{E}_{Rg4}\right]^T$ into eqn. 3.39 enables the remaining current Transform values to be calculated. Eqns. 3.30 to 3.36 are then used to calculate the superimposed voltage Transforms at the sending end, receiving end and the point of fault. These are then transformed back into the time-domain using the fast Fourier Transform technique[57]. The total time-domain response of say phase-"a" fault point voltage, would then be :

$$\begin{aligned} v_{FaT}(t) = {} & v_{Fa0}(t) + v_{Fa1}(t - T_F) + v_{Fa2}(t - T_{b2}) \\ & + v_{Fa3}(t - T_{b3}) + v_{Fah}(t - T_{hc}) \\ & + v_{Fa4}(t - T_{hc}) \end{aligned} \qquad (3.48)$$

For $t > T_{hc}$, $v_{FaT}(t)$ represents the Thevenin voltage across the fault terminals during the second period of secondary arcing, i.e., T_{hc} to T_{ob}.

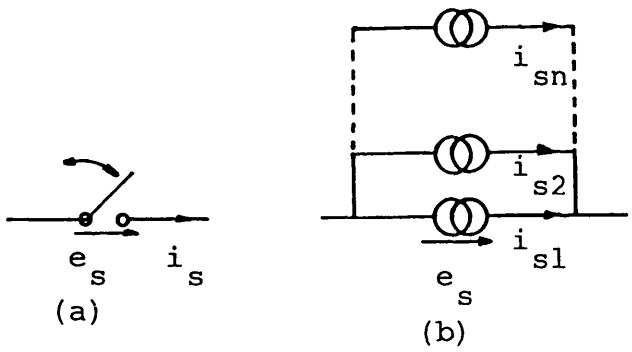

Fig. 3.1 Simulation of network time non-linearities

(a) Ideal switch

(b) Equivalent representation using parallel current generators

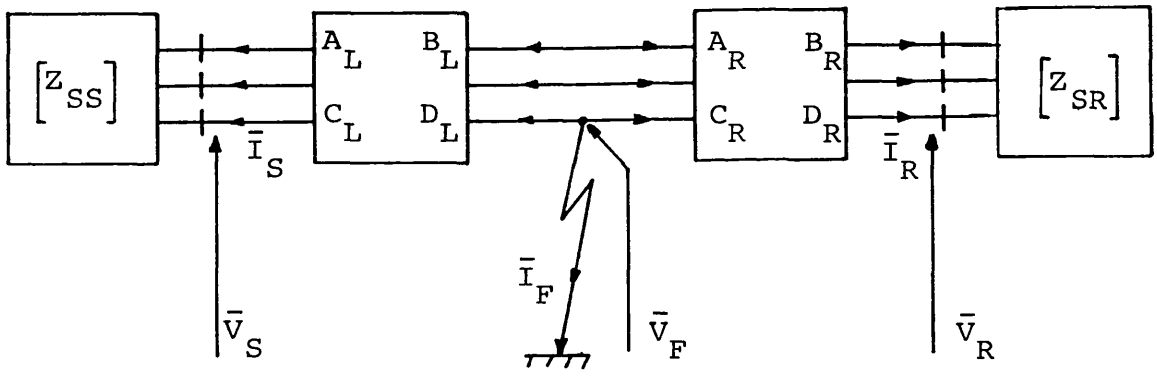

Fig. 3.2 Faulted system model

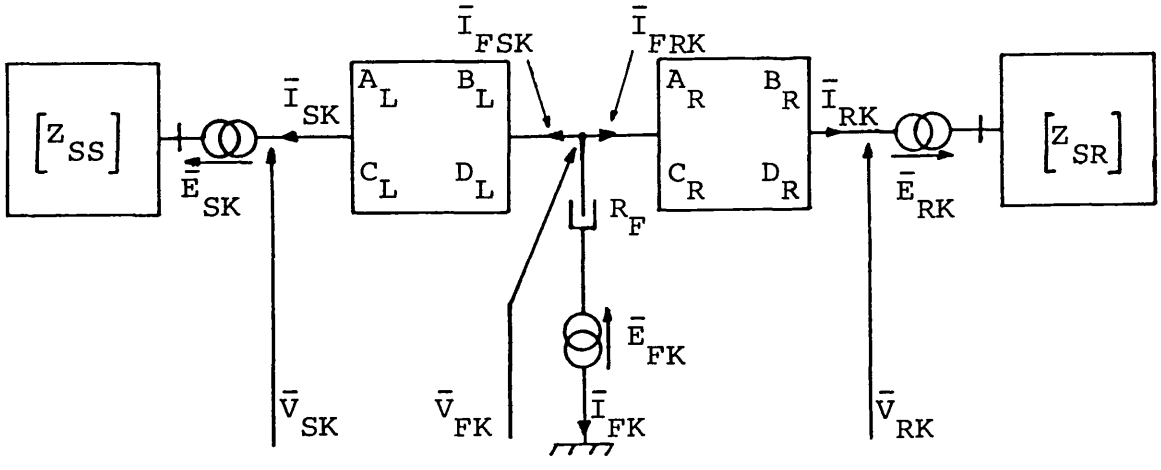

Fig. 3.3 Frequency domain superimposed system model

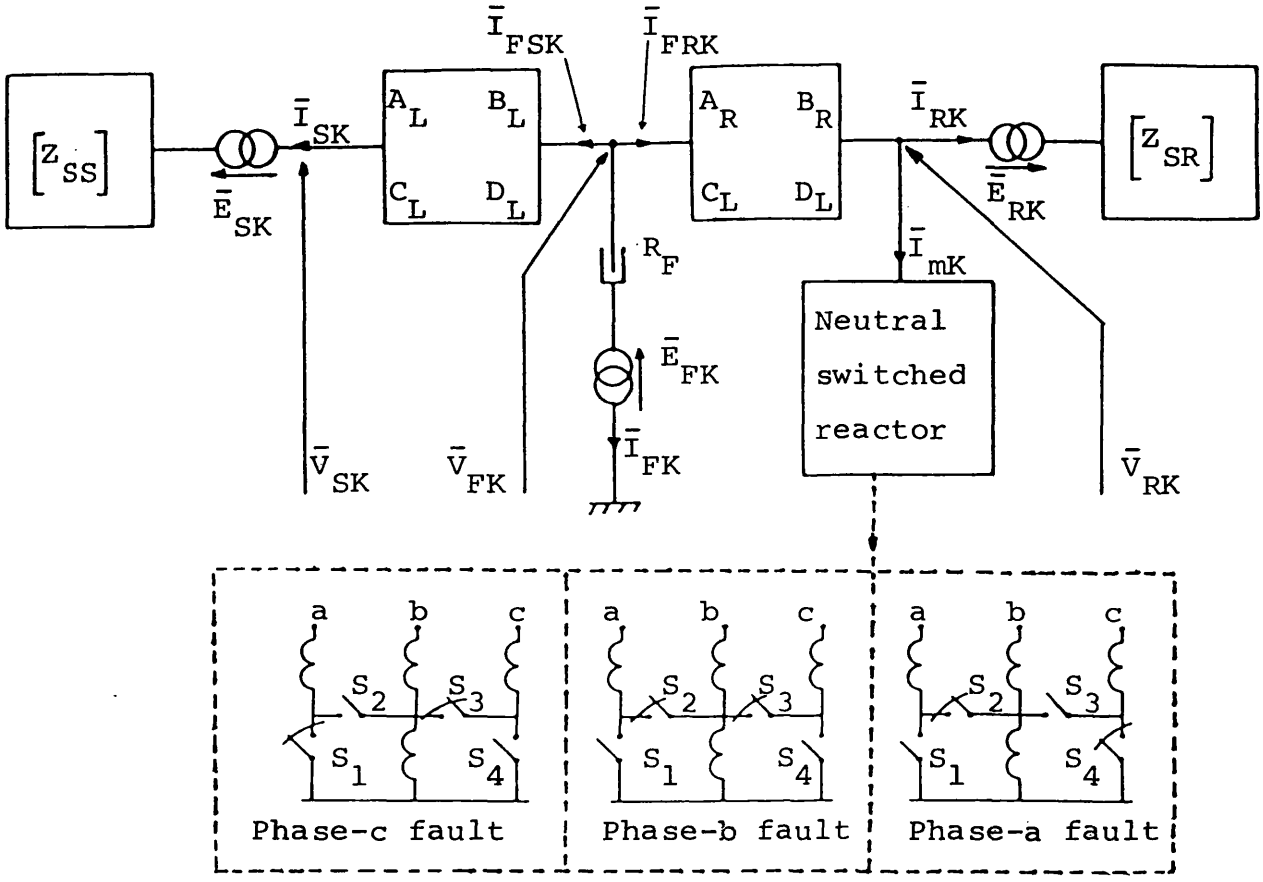

Fig. 3.4 Frequency domain superimposed system model

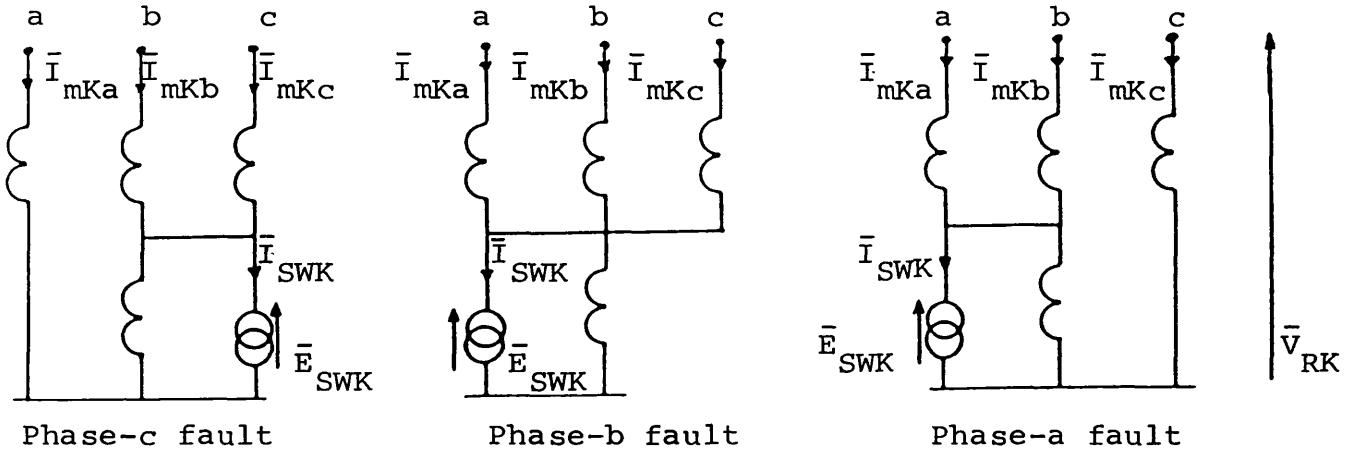

Fig. 3.5 Ideal neutral switch representation

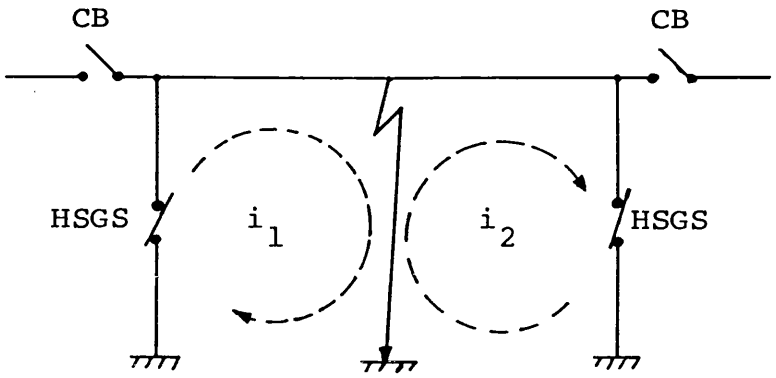

Fig. 3.6 Faulted phase during single pole switching, following HSGS closure
CB- Circuit breaker
HSGS- High speed grounding switch

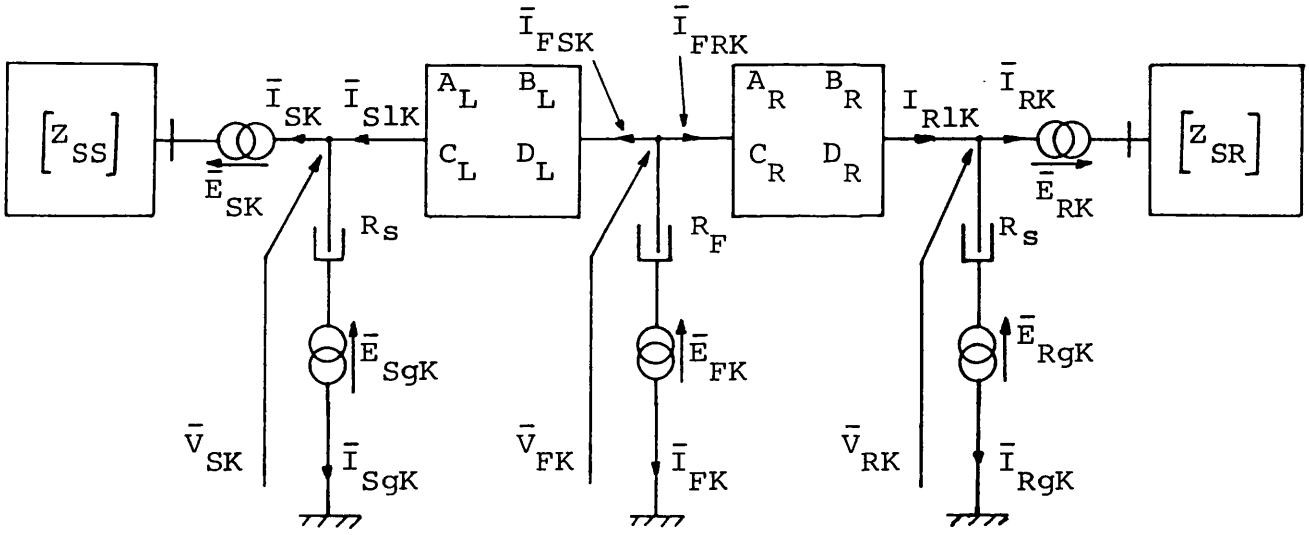

Fig. 3.7 Frequency domain superimposed system model

CHAPTER 4

THE SIMULATION OF THE SYSTEM UNDER SECONDARY ARCING CONDITION

4.1 Introduction

In EHV transmission systems equipped with single-pole switching, an accurate prediction of the likely time of extinction of the secondary arc and its transients are of great concern. This is particularly relevant to the development and testing of the modern digital and travelling-wave based protection equipments. Therefore, it is essential to reproduce the voltage and current waveforms at the protection point of a faulted system as realistically as possible. To obtain the necessary degree of accuracy, the fault path has to be represented during the dead-time in accurate detail.

Following fault clearance, the arc path undergoes a transition from relatively high primary arcing to low current secondary arcing, that is maintained by mutual coupling with the sound phases. The modelling of the secondary arc, and its incorporation into the general system simulation, represent a complex problem. This is due to the fact that with such a long unconstrained arc in air, neither, 1) the arc path geometry, 2) the arc

voltage and current non-linear relation, 3) the weather effects, nor 4) the arc reignition voltage characteristics, can be defined with precise degree of certainty. Consequently, when in the past it has been required to model the arc in system studies, a greatly simplified model, based upon limited experimental results has been used. In 1982, Johns et al[25] proposed a secondary arc model. Basically, the model simulation hinges upon defining the arc length variation, the arc hysteresis and the arc reignition voltage characteristics. The validity of the model was then confirmed by comparing computer studies to fault throwing test results of long compensated line , employing conventional single-pole switching[26,43]. The secondary arc model described in detail in refences 25, 26 and 43, is incorporated in the developed computer programs for the different single-pole switching schemes studied in this work.

In this chapter, the computational technique developed for simulating the faulted system response during the secondary arcing period is described. A brief description of the secondary arc model[25,26,43] used throughout this work is also presented, along with the calculation of the total system response.

4.2 Method of Simulation

Throughout the calculation of the system response undertaken in the previous chapter, the arc fault path was simply represented by a low constant resistance or open circuited.

For computational purposes, systems implementing the hybrid method of autoreclosure and the HSGS's, are considered to undergo two states of secondary arcing.

This is due to the change in the system configuration as a consequence of closing the HSGS's, or de-energising the two sound phases during the dead-time. Therefore, for both implementations, the first arc state transition is considered to take place at the instant of fault clearance (T_{b3}). The second transition in the arc state, for a system implementing HSGS's, is taken as the instant of the HSGS's closure (T_{hc}). However, the instant of the last sound phase clearance (T_{b7}) is considered in the hybrid method of autoreclosure as the time of the second transition. The instant of arc transition to secondary arcing state in the neutral switched reactor implementation, is taken as equal to that of the opening of the ideal neutral switch (T_{sl}).

At the instant of the first arc transition, the primary arc resistance is replaced by the non-linear secondary arc model (section 4.5), irrespective of the single-pole switching scheme under study. With reference to the HSGS's schemes, at the instant of the second transition, the fault path non-linear model is replaced by another. However, in the hybrid scheme, the nonlinear arc model is replaced by a constant resistance at the instant of the first sound phase first pole opening. An extensive series of studies have shown that the value of this constant resistance does not affect the arc extinction time. However, for ease of computation, a value of 0.5 has been used. At the instant of the second transition, again, the constant resistance is replaced by a non-linear arc model. It is worth mentioning that the method of simulation presented in this section, applies to either or both period(s) of secondary arcing.

Fig. 4.1a shows the double-end fed system following an "a"-phase to earth fault arc transition, i.e., conditions during the secondary arcing period(s). It must be noted that, with the exception of systems employing HSGS's, after the second transition, fig. 4.1a represents a general

system model, irrespective of the single-pole switching scheme. However, in order to determine the secondary arc response, it is necessary to first consider the Thevenin equivalent of the system, as viewed from the arc terminals[25]. This is shown in fig. 4.1b, from which, it is seen that the secondary arc forms a simple termination of the equivalent driving circuit. In fig. 4.1b, the Thevenin voltage $\bar{E}_T$ is essentially the Frequency spectrum of the fault point voltage, which develops as a result of arc extinction. Moreover, the Thevenin impedance Z_T is recognised as the impedance seen across the arc terminals, with the arc path open circuited, and the system sources represented by their short circuit impedances. As it is required to simulate the system response during the dead-time, and furthermore, to fulfil Thevenin's theorem requirements, the secondary arc is assumed to quench immediately following arc transition.

With reference to fig. 4.1b, it is evident that the arc voltage and current are related by the Frequency-Domain relationship of eqn. 4.1 :-

$$\bar{V}_{arc} = \bar{E}_T - I_{arc} Z_T \qquad (4.1)$$

However, the non-linear nature of the secondary arc requires that a solution during the secondary arcing period(s), be effected in the time-domain, and in order to achieve this, the Inverse Fourier Transform is applied to eqn. 4.1. Therefore,

$$v_{arc}(t) = e_T(t) - \frac{1}{2\pi} \int_{-\infty}^{\infty} \bar{I}_{arc} Z_T \exp(j\omega t) \, d\omega \qquad (4.2)$$

the Fourier integral term in eqn. 4.2 can be evaluated in the time-domain using the convolution theorem[25,43].

Therefore, the full time-domain solution is :-

$$v_{arc}(t) = e_T(t) - \int_{-\infty}^{\infty} Z_T(t-\tau)\, i_{arc}(\tau)\, d\tau \qquad (4.3)$$

where,

$$Z_T(t-\tau) = \frac{1}{2\pi} \int_{-\infty}^{\infty} Z_T \exp\left[j\omega(t-\tau)\right] d\omega \qquad (4.4)$$

The impedance function $Z_T(t-\tau)$, is obviously the voltage that would be developed across the Thevenin impedance if a unit impulse of current $\delta(t-\tau)$ were injected into Z_T[43]. In the process of simulation, this is evaluated numerically in discrete form by using a half range modified Fourier Transform integral[57]. As a result, the sequence involved in describing the function $Z_T(t-\tau)$ takes the form :-

$$Z_T(m\Delta T) = \frac{1}{2\pi} \int_{-\infty}^{\infty} Z_T \exp(j\omega m\Delta T)\, d\omega, \quad m=0,n \qquad (4.5)$$

For $t < \tau$, $\delta(t-\tau) = 0$, therefore, $Z_T(t-\tau) = 0$. Furthermore, if the time $t = 0$ is taken as the time of arc transition, then the Thevenin equivalent of fig. 4.1b is only applicable for a time $t > 0$, and $i_{arc}(t) = 0$ for $t \leq 0$. It follows that $i_{arc}(\tau) = 0$ for $\tau < 0$. With these conditions in mind, the limits of integration in eqn. 4.3 are modified :-

$$v_{arc}(t) = e_T(t) - \int_{0}^{t} Z_T(t-\tau)\, i_{arc}(\tau)\, d\tau \qquad (4.6)$$

Knowledge of the Thevenin impedance and voltage in discrete sampled data form, enables a recursive solution of eqn. 4.6 to be obtained[25,43], which is of the form :-

$$\begin{aligned} v_{arc}(n\Delta T) &\simeq e_T(n\Delta T) - Z_T(0)\, i_{arc}(n\Delta T)\, \Delta T/2 \text{ , for } n=1 \\ &\simeq e_T(n\Delta T) - Z_T(0)\, i_{arc}(n\Delta T)\, \Delta T/2 \\ &\quad - \sum_{k=1}^{n-1} Z_T\left[(n-k)\Delta T \right] i_{arc}(k\Delta T)\, \Delta T, \text{ for } n \geq 2 \end{aligned} \qquad (4.7)$$

The first of the above relations is solved using the value $e_T(\Delta T)$ to provide the secondary arc current at the first sample step ΔT after transition. Thereafter, the second relation of eqn. 4.7 is solved recursively by virtue of the summation term containing only past known history of the current.

4.3 The Thevenin Impedance - Digital Evaluation

The method of evaluating Z_T is based on reducing the system passive network, to a single-port equivalent as viewed from the fault terminals. In this section, the methods developed to calculate the Thevenin impedance digitally for the different single-pole switching schemes are presented, assuming that the single line-to-earth fault occured on phase-"a".

4.3.1 Conventional single-pole switching

With reference to fig. 4.1a, the Frequency-Domain relation of eqn. 4.8 applies to the system section linking the point of fault to the receiving end.

$$\begin{bmatrix} \bar{V}_F \\ \bar{I}_{FR} \end{bmatrix} = \begin{bmatrix} A_R & B_R \\ C_R & D_R \end{bmatrix} \begin{bmatrix} \bar{V}_{R2} \\ \bar{I}_{R2} \end{bmatrix} \qquad (4.8)$$

Also, at the receiving end,

$$\bar{V}_{R1} = Z_{SR}\, \bar{I}_{R1} \qquad (4.9)$$

Having cleared the fault, the current and voltage constraints at the receiving end breaker are :-

$$\bar{I}_{R1} = \bar{I}_{R2} = \left[\bar{I}_{R2a} = 0 \quad \bar{I}_{R2b} \quad \bar{I}_{R2c} \right]^T \qquad (4.10)$$

and,

$$\left[\bar{V}_{R1b} \quad \bar{V}_{R1c}\right]^T = \left[\bar{V}_{R2b} \quad \bar{V}_{R2c}\right]^T \tag{4.11}$$

From eqns. 4.9 to 4.11 the sound phase current and voltage relation of eqn. 4.12 can be obtained at the receiving end :-

$$\left[\bar{I}_{R2b} \quad \bar{I}_{R2c}\right]^T = \left[Y_{SR1}\right]\left[\bar{V}_{R2b} \quad \bar{V}_{R2c}\right]^T \tag{4.12}$$

where $Y_{SR1} = \left[Z_{SRs}\right]^{-1}$, and Z_{SRs} is a sub-matrix of Z_{SR} which can be obtained simply by discarding the row and column related to the faulted phase in Z_{SR} .

As $\bar{I}_{R2a} = 0$, then the matrix relation of eqn. 4.8 can be written in the separate form :-

$$\bar{V}_F = A_R \bar{V}_{R2} + B_{Rs}\left[\bar{I}_{R2b} \quad \bar{I}_{R2c}\right]^T \tag{4.13}$$

$$\bar{I}_{FR} = C_R \bar{V}_{R2} + D_{Rs}\left[\bar{I}_{R2b} \quad \bar{I}_{R2c}\right]^T \tag{4.14}$$

where, B_{Rs} and D_{Rs} are sub-matrices of B_R and D_R respectively.

Substituting eqn. 4.12 into eqns. 4.13 and 4.14 gives :

$$\bar{V}_F = A_{RM} \bar{V}_{R2} \tag{4.15}$$

$$\bar{I}_{FR} = C_{RM} \bar{V}_{R2} \tag{4.16}$$

where, A_{RM} and C_{RM} are modified matrices of A_R and C_R respectively, depending on the faulted phase. However, from eqns. 4.15 and 4.16,

$$\bar{I}_{FR} = C_{RM} A_{RM}^{-1} \bar{V}_F = Y_{Ra} \bar{V}_F \tag{4.17}$$

The part of the network linking the fault point to the sending end is likewise treated to obtain :-

$$\bar{I}_{FS} = C_{LM} A_{LM}^{-1} \bar{V}_F = Y_{Sa} \bar{V}_F \qquad (4.18)$$

Combining eqns. 4.17 and 4.18 , noting that (see fig. 4.1a) $\bar{I}_F = - (\bar{I}_{FS} + \bar{I}_{FR})$, yields :

$$\bar{I}_F = - (Y_{Sa} + Y_{Ra}) \bar{V}_F \qquad (4.19)$$

or,

$$\bar{V}_F = - Z_{TH} \bar{I}_F \qquad (4.20)$$

where, $Z_{TH} = \left[Y_{Sa} + Y_{Ra} \right]^{-1}$.

The fault point is constrained such that, $\bar{I}_{Fb} = \bar{I}_{Fc} = 0$, therefore, from eqn. 4.20,

$$\bar{V}_{Fa} = - Z_{TH}(a,a) \bar{I}_{Fa} \qquad (4.21)$$

According to the current directions assumed in fig. 4.1a, the Thevenin impedance Z_T is given by $- \bar{V}_{Fa} / \bar{I}_{Fa}$, which in turn is equal to $Z_{TH}(a,a)$. Z_T is thus computed and stored at all spectral frequencies of interest.

4.3.2 The hybrid method of autoreclosure

The evaluation of the Thevenin impedance Z_T during the first period of secondary arcing , is carried out in a similar way to that presented in section 4.3.1. However, to evaluate Z_T after de-energising the sound phases, fig. 4.1a can be used, with the circuit breaker at both ends open. The current constraints at the line ends are :-

$$\bar{I}_{R1} = \bar{I}_{R2} = \bar{I}_{S1} = \bar{I}_{S2} = 0 \qquad (4.22)$$

Using eqn. 4.8, with the constraints of eqn. 4.22, the following Frequency-Domain matrix relations can be obtained for the network section linking the fault point to the

receiving end :-

$$\bar{V}_F = A_R \bar{V}_{R2} \tag{4.23}$$

$$\bar{I}_{FR} = C_R \bar{V}_{R2} \tag{4.24}$$

From eqns. 4.23 and 4.24,

$$\bar{I}_{FR} = C_R A_R^{-1} \bar{V}_F = Y_R \bar{V}_F \tag{4.25}$$

Likewise, for the sending end section,

$$\bar{I}_{FS} = C_L A_L^{-1} \bar{V}_F = Y_S \bar{V}_F \tag{4.26}$$

Hereafter, similar steps to those described in 4.3.1 are followed to obtain the de-energised system Thevenin impedance.

4.3.3 Neutral switched reactor implementation

Fig. 4.2a shows the system state during the dead-time. Included, is the equivalent circuit of the neutral switched reactor after the opening of the proper neutral switches. In the passive network of fig. 4.2a, it is possible to combine the switched reactor arrangement with the line section linking the fault point to the receiving end. This is simply done by using the following Frequency- Domain matrix relationships (see fig. 4.2a).

$$\begin{bmatrix} \bar{V}_F \\ \bar{I}_{FR} \end{bmatrix} = \begin{bmatrix} A_R & B_R \\ C_R & D_R \end{bmatrix} \begin{bmatrix} \bar{V}_R \\ \bar{I}_{R3} \end{bmatrix} \tag{4.27}$$

$$\begin{bmatrix} \bar{V}_R \\ \bar{I}_{R3} \end{bmatrix} = \begin{bmatrix} U & O \\ Y_{Rs} & U \end{bmatrix} \begin{bmatrix} \bar{V}_R \\ \bar{I}_{R2} \end{bmatrix} \qquad (4.28)$$

where,

$$Y_{Rs} = \begin{bmatrix} Z_p + Z_{nr} & Z_{nr} & O \\ Z_{nr} & Z_p + Z_{nr} & O \\ O & O & Z_p \end{bmatrix}^{-1}$$ for an "a"-phase fault

Substituting eqn. 4.28 into eqn. 4.27 gives :-

$$\begin{bmatrix} \bar{V}_F \\ \bar{I}_{FR} \end{bmatrix} = \begin{bmatrix} A_R + B_R Y_{Rs} & B_R \\ C_R + D_R Y_{Rs} & D_R \end{bmatrix} \begin{bmatrix} \bar{V}_R \\ \bar{I}_{R2} \end{bmatrix} \qquad (4.29)$$

Here again, a similar procedure to that described in 4.3.1 is followed to obtain the system Thevenin impedance Z_T.

4.3.4 HSGS's implementation

The system Thevenin impedance , used throughout the first period of secondary arcing, is obtained in a similar manner to that given in 4.3.1. After the second transition, i.e., after the closing of the HSGS's at both ends, Fig. 4.2b is used in deriving the necessary procedure for evaluating Z_T. With reference to fig. 4.2b, at the receiving end,

$$\bar{V}_{R2} = Z_{RT}\ \bar{I}_{R2} \qquad (4.30)$$

where Z_{RT} for phase-"a" to earth fault is,

$$Z_{RT} = \begin{bmatrix} R_s & O & O \\ O & Z_{SR1} + Z_{nR1} & Z_{nR1} \\ O & Z_{nR1} & Z_{SR1} + Z_{nR1} \end{bmatrix}$$

Substituting for $\bar{V}_{R2}$ from eqn. 4.30 in eqn. 4.8 gives,

$$\bar{V}_F = \left[A_R\ Z_{RT} + B_R\right] \bar{I}_{R2} \tag{4.31}$$

$$\bar{I}_{FR} = \left[C_R\ Z_{RT} + D_R\right] \bar{I}_{R2} \tag{4.32}$$

From the above two equations,

$$\bar{I}_{FR} = \left[C_R\ Z_{RT} + D_R\right] \left[A_R\ Z_{RT} + B_R\right]^{-1} \bar{V}_F \tag{4.33}$$

Similar treatment to the sending end section gives :-

$$\bar{I}_{FS} = \left[C_L\ Z_{ST} + D_L\right] \left[A_L\ Z_{ST} + B_L\right]^{-1} \bar{V}_F \tag{4.34}$$

where Z_{ST} is an impedance matrix similar to that of Z_{RT}. The computation of Z_T then proceeds in a similar way to that given in 4.3.1.

4.4 Digital Evaluation of Thevenin Voltage

With reference to Thevenin's theorem, the voltage across the arc terminals has to be calculated with the arc current equal to zero. Consider fig. 4.3 at the point of fault. v_{Fo} is a voltage which is equal to zero for all time up to the instant of arc transition, which say, occurs at T_o. v_{Fo} is also a voltage which forces the total current $i_a(t)$ to zero immediately after arc transition. Therefore, the Thevenin voltage $e_T(t)$ can be calculated as equal to the fault point voltage $v_{Fl}(t)$ after time T_o, i.e.,

$$e_T(t) = v_{Fl}(t)\ h(t - T_o) \tag{4.35}$$

Also, in fig. 4.3, $i_a(t)$ is the total current flowing in the arc path. This is equal to the sum of the current

response due to , the fault inception, the switching events up to the time T_o and the application of v_{Fo} $(i_{ao}(t))$ to the system after transition. Consider fig. 4.4, which represents the driving circuit for the network equivalent after transition, and in which v_{Fo} is the only driving voltage source. From fig. 4.4, eqn. 4.36 holds in the Frequency-Domain.

$$\bar{V}_{Fo} = - \bar{I}_{ao}(Z_T + R_F) \tag{4.36}$$

As the total arc path current $i_a(t)$ is forced to zero after applying v_{Fo}, the current $i_{ao}(t)$ is equal and opposite to the fault path current for all time after transition, i.e.,

$$i_{ao}(t) = - i_{FT}(t)\ h(t - T_o) \tag{4.37}$$

In the Frequency-Domain,

$$\bar{I}_{ao} = - \int_{T_o}^{T_{ob}} i_{FT}(t)\ \exp\left[-j(\omega - j\alpha)t\right]\ dt \tag{4.38}$$

$\bar{V}_{Fo}$ can then be calculated using eqn. 4.36, and upon transforming this into the time-domain we obtain $v_{Fo}(t)$, which in turn provides for $e_T(t)$ to be calculated using eqn. 4.35.

4.5 The Secondary Arc Model

Based upon experimental studies relevant to long low current arcs in air[16,19,20,78], a mathematical model to simulate such arcs digitally, was developed by Johns and Al-Rawi[25]. The authors proposed the simulation of three

main characteristics of such arcs, namely ,

1. The relationship between the arc voltage ($v_{arc}(t)$) and current ($i_{arc}(t)$).
2. The arc path reignition voltage ($v_r(t)$) variation.
3. The arc length ($L_a(t)$) variation during the secondary arc period.

The first of the above characteristics is shown in its linearised form in fig. 4.5a. Assuming a bolted fault condition, the peak of the secondary arc current (I_p) is determined and considered constant throughout the secondary arc period. However, during the course of this work, the value of I_p is determined individually at each half cycle, and the arc cyclogram (fig. 4.5a) is therefore scaled accordingly. This of course includes a requirement for updating of the constant voltage region (V_p), which is adjusted to be equal to a value of $75I_p^{-0.4}$ V/cm. The arc cyclogram is traversed in the directions shown, and each time the current and voltage reaches zero, the current is held at zero until sufficient reignition voltage ($v_r(t)$) is developed to cause re-striking of the arc. Fig. 4.5a also shows how the effect of the reignition voltage is included in the cyclogram[43].

The variation of the arc reignition voltage was formulated as per eqn. 4.39 :-

$$v_r(t) = (5 + 50\,T_e)(t - T_e)\,h(t - T_e) \quad \text{kV/cm} \qquad (4.39)$$

where T_e is the time from arc transition to either temporary or final arc extinction. Graphically, eqn. 4.39 is plotted in fig. 4.5b, which shows the variation of the reignition voltage for several discrete times of extinction.

Comparatively recently, a modified empirical version of eqn. 4.39 was proposed[25,26] and is given by eqn. 4.40.

$$v_r(t) = \left[5 + 1620T_e/(2.15 + I_s) \right] (t - T_e)\, h(t - T_e) \qquad (4.40)$$

where I_s is the nominal steady-state secondary arc current (in r.m.s. values). In this work, the two above given equations of $v_r(t)$ have been used. The use of any particular one is governed by the level of the nominal steady-state secondary arc current and the particular single-pole switching scheme under study. Consequently, eqn. 4.39 is used whenever I_s is in the order of 30A (r.m.s.) and over, while eqn. 4.40 is used for the lower values.

In simulating the secondary arc length variation ($\ell_a(t)$), a linear arc length-time relation defined by eqn. 4.41 is used[25,26,43] :-

$$\ell_a(t) / \ell_o = \begin{cases} 1 & , \text{ for } t < 0.1 \text{ sec} \\ 10t & , \text{ for } t > 0.1 \text{ sec} \end{cases} \qquad (4.41)$$

where ℓ_o represents the arcing horns gap separation.

4.6 Evaluation of The Voltages And Currents at The Relaying Points

Having obtained the secondary arc current and voltage waveforms, the total fault point voltage throughout the pre-fault, primary and secondary arc periods are defined. If required, the total fault point voltage can then be used as a forcing function in the simulation of the system voltages and currents at any other point[25].

Fig. 4.6 shows the fault branch representation, where the

new superimposed voltage v_{FFn} is no longer equal and opposite to the steady-state voltage v_{FS}. The calculation of v_{FFn} is described thereinafter, which is then transformed into the Frequency-Domain using eqn. 4.42 :-

$$\bar{V}_{FFn} = \int_{0}^{T_{ob}} v_{FFn}(t) \exp\left[-j(\omega - j\alpha)t\right] \quad dt \qquad (4.42)$$

$\bar{V}_{FFn}$ is then injected into the system through the constant fault resistance R_F. Fault calculations and the subsequent switching operations are then repeated.

4.6.1 Conventional single-pole switching and the neutral switched reactor implementation

The equivalent time-domain representation of the system at the point of fault is shown in fig. 4.7, which also clarifies the process of transition to the secondary arcing period. If the time t = 0 is taken as the time of fault inception (T_F in chapters 2 and 3), then the total fault branch current $i_A(t)$ (see fig. 4.7), can be written :-

$$i_A(t) = i_{FT}(t)\, h(t) - i_{FT}(t)\, h(t - T_o) + i_{arc}(t)\, h(t - T_o) \qquad (4.43)$$

Also, from fig. 4.7, the voltage across the arc path for all time after the inception of the fault is given by :-

$$e_{FF}(t) = i_{FT}(t)\, R_F\, h(t) - i_{FT}(t)\, R_F\, h(t - T_o) + v_{arc}(t)\, h(t - T_o) \qquad (4.44)$$

From fig. 4.6,

$$v_{FFn}(t) = e_{FF}(t) - i_A(t)\ R_F - v_{FS}(t) \qquad (4.45)$$

Substitution for $i_A(t)$ and $e_{FF}(t)$ from eqns. 4.43 and 4.44 respectively, enables v_{FFn} to be calculated in the time-domain. It must be noted that the current $i_{FT}(t)$ is equal to that given by eqns. 3.15 and 3.29 (chapter 3) for coventional single-pole switching and neutral switched reactor implementation respectively.

4.6.2 The hybrid method of autoreclosure

With reference to fig. 4.8, the total fault branch current is :-

$$\begin{aligned} i_A(t) = {} & i_{FT}(t)\ h(t) - i_{FT}(t)\ h(t - T_{o1}) + i_{arc}(t)\ h(t - T_{o1}) \\ & - i_{arc1}(t)\ h(t - T_{b4}) + i_{FT}(t)\ h(t - T_{b4}) \\ & - i_{FT}(t)\ h(t - T_{o2}) + i_{arc2}(t)\ h(t - T_{o2}) \end{aligned} \qquad (4.46)$$

The voltage across the fault path terminals is :-

$$\begin{aligned} e_{FF}(t) = {} & i_{FT}(t)\ R_F\ h(t) - i_{FT}(t)\ R_F\ h(t - T_{o1}) \\ & + v_{arc1}(t)\ h(t - T_{o1}) - v_{arc1}(t)\ h(t - T_{b4}) \\ & + i_{FT}(t)\ R_F\ h(t - T_{b4}) - i_{FT}(t)\ R_F\ h(t - T_{o2}) \\ & + v_{arc2}(t)\ h(t - T_{o2}) \end{aligned} \qquad (4.47)$$

Where, T_{o1} and T_{o2} are the instants of the first and second transition respectively. Using eqns. 4.45, 4.46 and 4.47, the new superimposed voltage v_{FFn} can be calculated.

4.6.3 The HSGS's implementation

With reference to fig. 4.9, the fault path current for all time after the fault inception is given by eqn. 4.48.

$$i_A(t) = i_{FT}(t)\ h(t) - i_{FT}(t)\ h(t - T_{o1}) + i_{arc1}(t)\ h(t - T_{o1}) - i_{arc1}(t)\ h(t - T_{o2}) + i_{arc2}(t)\ h(t - T_{o2}) \quad (4.48)$$

Also,

$$e_{FF}(t) = i_{FT}(t)\ R_F\ h(t) - i_{FT}(t)\ R_F\ h(t - T_{o1}) + v_{arc1}(t)\ h(t - T_{o1}) - v_{arc1}(t)\ h(t - T_{o2}) + v_{arc2}(t)\ h(t - T_{o2}) \quad (4.49)$$

Substituting eqns. 4.48 and 4.49 into eqn. 4.45, enables the new superimposed voltage v_{FFn} to be calculated.

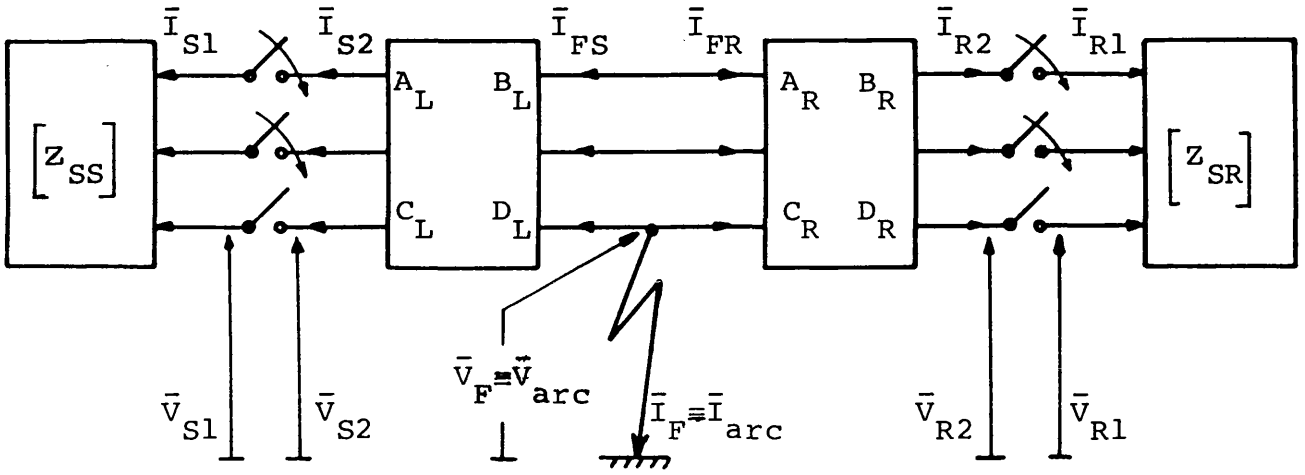

(a)

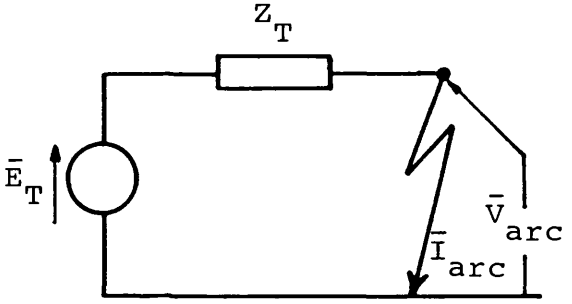

(b)

Fig. 4.1

(a) General netwok model, state during secondary arcing.

(b) Fault point Thevenin equivalent circuit.

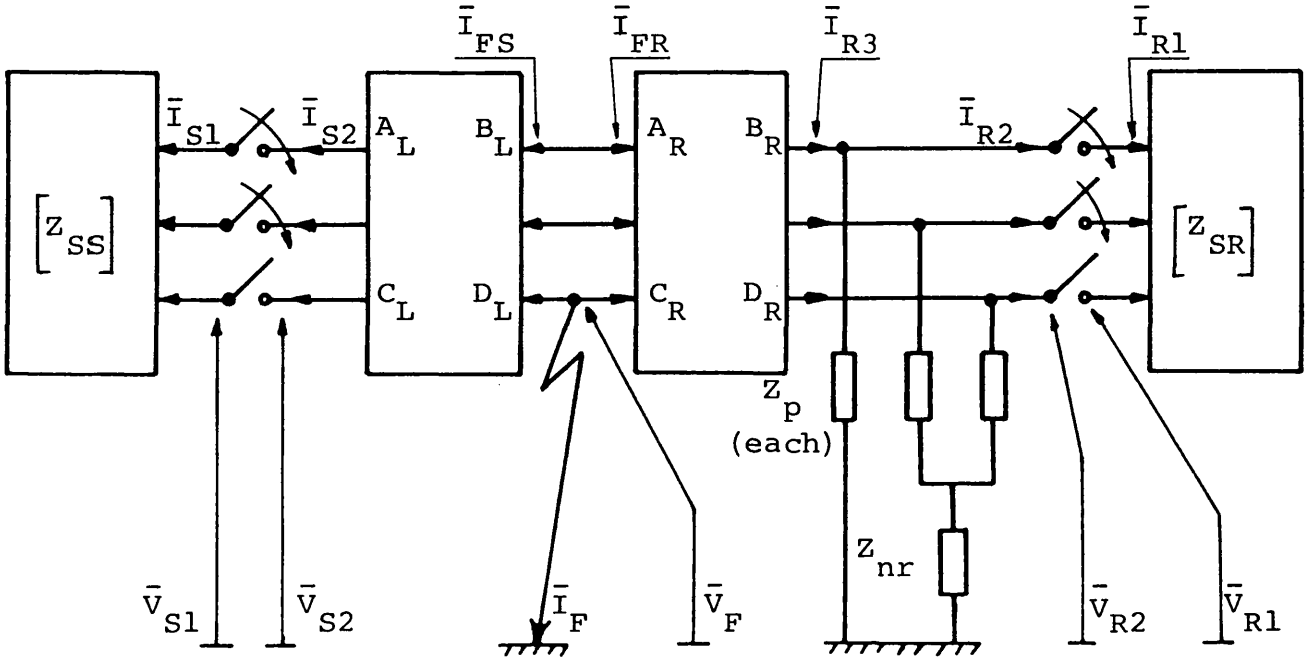

(a)

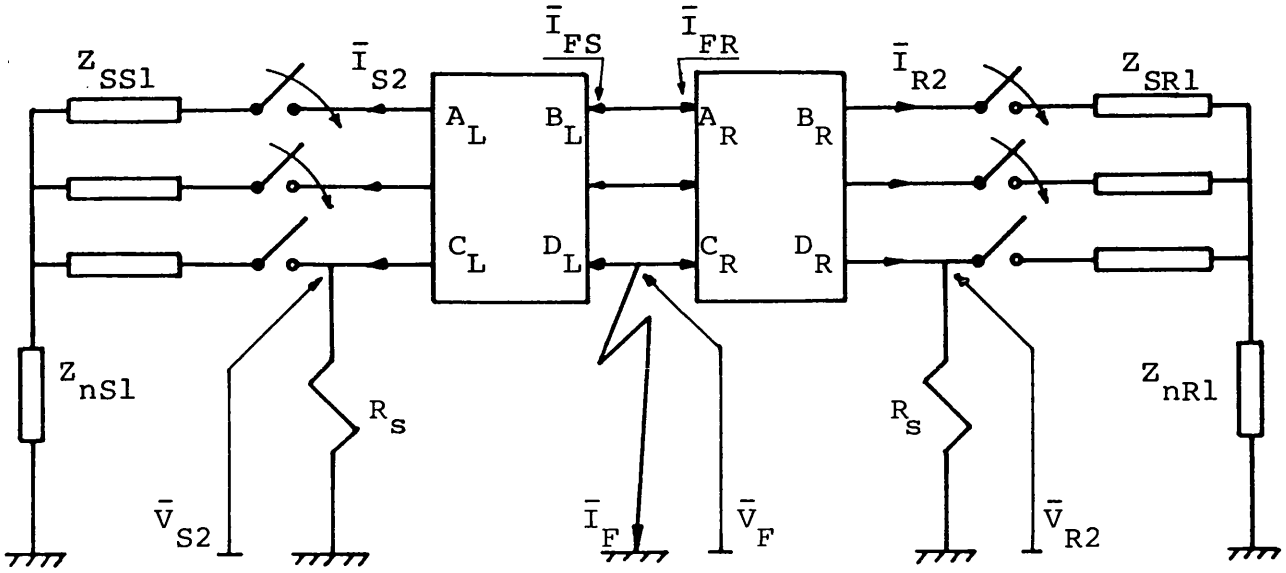

(b)

Fig. 4.2 Network state during secondary arcing,

(a) System with neutral swiched reactor bank

(b) System with HSGS's- after the second transition

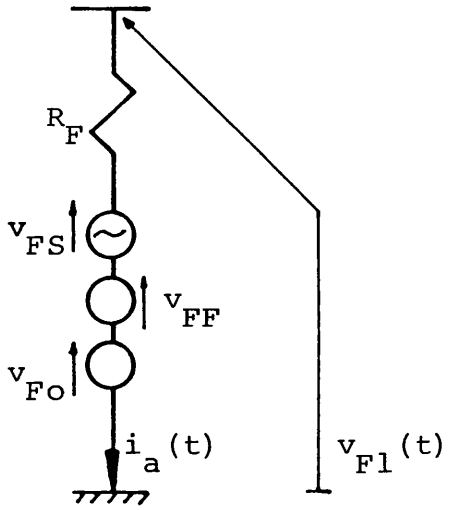

Fig. 4.3 Arc fault path repr-
esentation

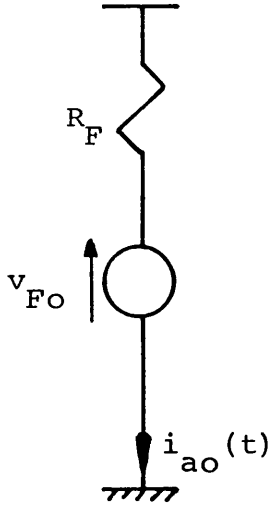

Fig. 4.4 Thevenin
equivalent circuit

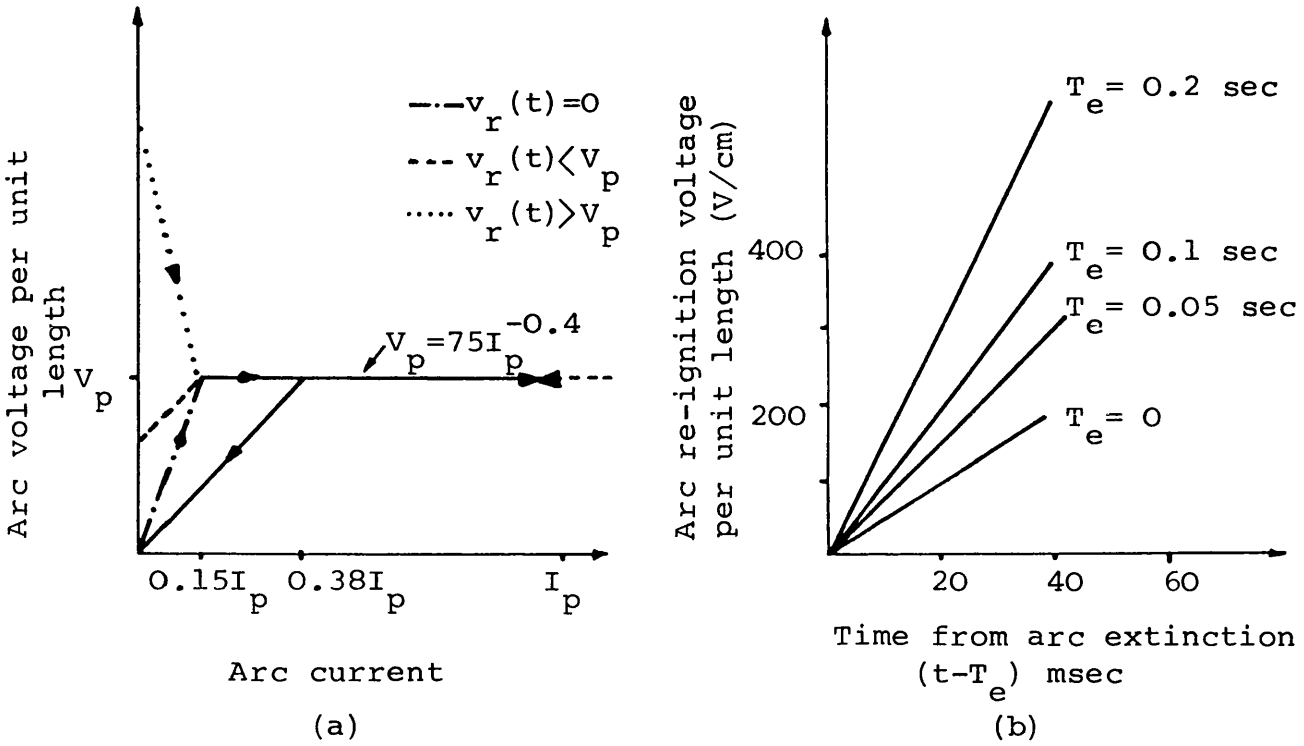

Fig. 4.5 Secondary arc chracteristics

(a) Piecewise linearised secondary arc cyclogram

(b) Simulated variation of arc re-ignition voltage

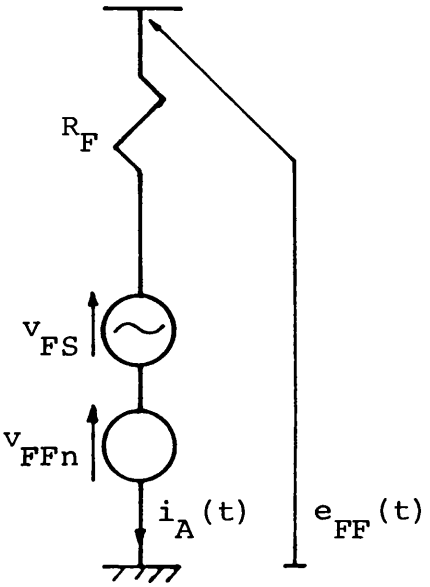

Fig. 4.6 General fault path representation

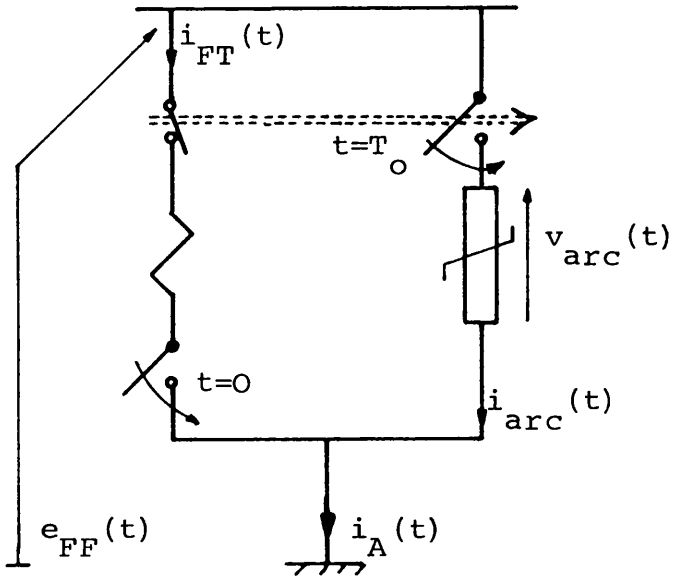

Fig. 4.7 Fault path non-liearities representation

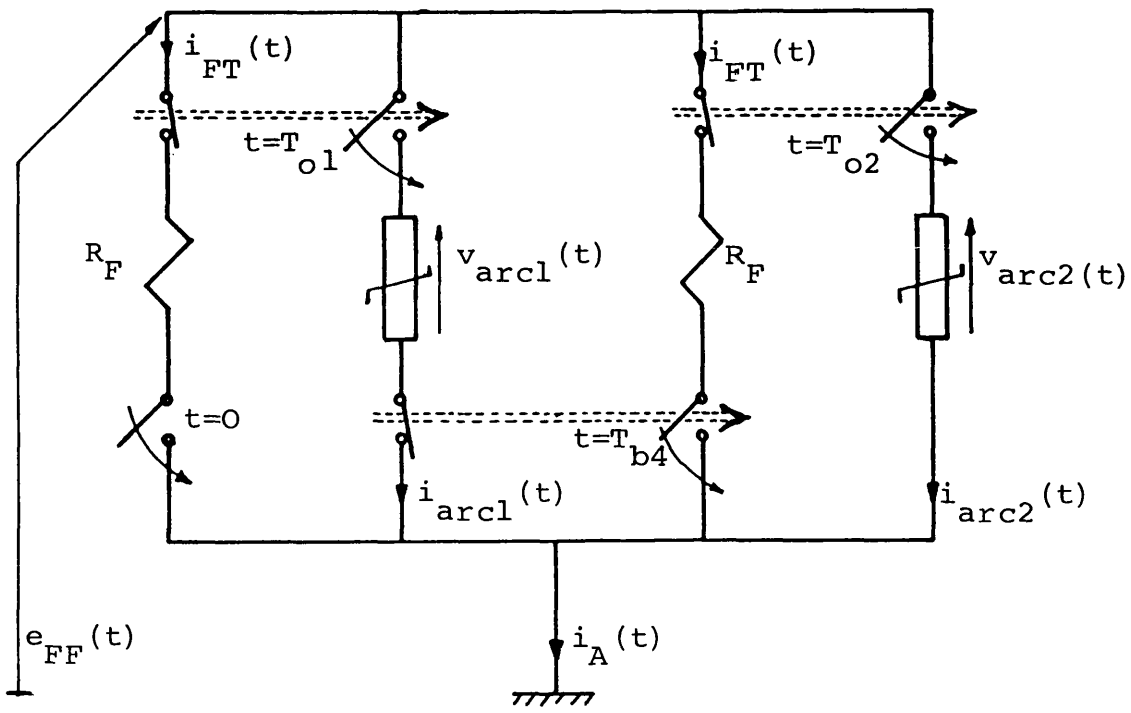

Fig. 4.8 Fault path non-linearities representation

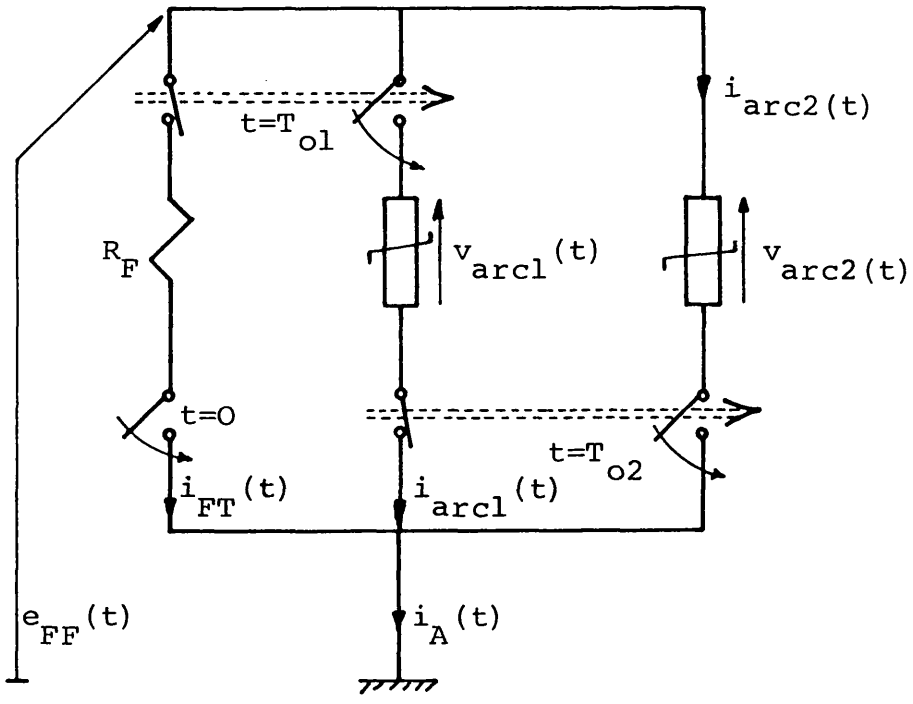

Fig. 4.9 Fault path non-linearities representation

CHAPTER 5

SYSTEM RESTORATION

5.1 Introduction

In transmission systems employing single-pole switching, fast reclosure is relatively less important to the system stability. This is due to the fact that during the dead-time, power is transmitted over the remaining two sound phases. Such power flow reduces the angular drift between the two ends of the line, and tends to maintain the stability of the system. However, this is not the case for systems implementing the hybrid method of autoreclosure, as fast reclosure after de-energising the two sound phases is necessary to maintain system stability. Therefore, the system reclose time is mainly governed by the extinction time of the secondary arc and equally importantly by the time after extinction for the arcing medium to recover its dielectric strength. Haubrich et al[27] suggested 0.25 sec as adequate time after extinction, for the medium to re-establish its dielectric strength. Staged fault tests on 230kV[80] and laboratory tests[79] on 400kV, and 765kV V-string insulators indicated that 2 cycles of power frequency, provide for the de-ionization of the arcing medium. Moreover, the results of tests on a 500kV suspension string showed that

the de-ionization time of the medium, depends on the secondary arc extinction time[16]. With the foregoing in mind, there are other relevant factors to be considered. These include the effect of the ground currents (which circulate during the dead-time) on the system ground relaying and generator-rotor body heating.

Single-pole switching schemes are attractive from the point of view of switching surges, as they are comparatively less than those associated with three-phase switching. However, single-pole switching transients can still exceed the voltage level necessary to effect an appreciable reduction in the system insulation level . This voltage level is often specified in the range 2.0 to 2.5 p.u. of the peak phase-to-neutral voltage of the system, and where energisation transients do not fall inherently below these, they must be restricted by other means. In general, the switching surges are dependent on the voltage across the circuit breaker contacts at the instant of closing, and reduced considerably if this voltage is zero. This forms the basis of the synchronous closing method for reducing energisation transients. The other well known method is to use circuit breakers equipped with closing resistors[81]. The critical tolerance on the breaker closing time, and the need for additional voltage measurements, makes the synchronous closing method unattractive. However, the combination of the two methods can be of advantage regarding the line energisation problem in EHV systems. This would make it possible to allow the breaker closing time to vary within certain limits, and yet have the transient overvoltages, limited to an acceptable level.

In this chapter, the methods used for simulating, the opening of the HSGS's, circuit breaker pole(s) closure,

and the closing of the ideal neutral switch, are described in the Frequency-Domain. The timing of any switching event can be controlled to take place at any time after fault inception.

5.2 Opening of The HSGS's

In simulating the opening of the HSGS's, the total time varying response of the current through an HSGS is transformed into the Frequency-Domain, which is then injected back into the system (fig. 5.1). The calculation is performed such that when any HSGS is open, its total currents sum to zero. In the developed computer program, the opening of the HSGS's is simulated to take place in succession, according to their current zero crossing sequence after a pre-specified time, after fault inception. At such time, say 0.4 sec, the faulted phase sending and receiving end HSGS currents are checked for zero crossing. The opening of the HSGS where current first passes through zero is simulated by injecting a current equal and opposite to that flowing through it. Fig. 5.1 shows the superimposed system model represented in the Frequency-Domain, for a line-to-earth fault on phase-"a", which is de-energised.

If the time after fault (allowing for the breaker opening time, first and second periods of arcing) at which the first current zero crossing occurs, is T_{hol} at the sending end HSGS, then the Frequency spectrum $\bar{I}_{Sg5a}$ of current which is injected as shown in fig. 5.1 to simulate the opening is given by :-

$$\bar{I}_{Sg5a} = - \int_{T_{hol}}^{T_{ob}} i_{Sga} \exp\left[-j(\omega - j\alpha)\ t\right] dt \qquad (5.1)$$

where, $i_{Sga} = i_{Sga}(t)\ h(t - T_{hol})$

In fig. 5.1, $\bar{E}_{Sg5}$, $\bar{E}_{F5}$, $\bar{E}_{Rg5}$, ... , $\bar{I}_{S5}$, $\bar{I}_{Rg5}$, ... , are the Frequency spectrum of voltages and currents, which arise due to the injection of $\bar{I}_{Sg5a}$.

The 15 x 15 admittance matrix of eqn. A3.3.23 is used at this stage of the simulation, to define the current and voltage relationship given by eqn. 5.2.

$$\begin{bmatrix} \bar{I}_{F5a} = 0 \\ \bar{I}_{F5b} = 0 \\ \bar{I}_{F5c} = 0 \\ \bar{I}_{S5a} = 0 \\ \bar{I}_{S5b} \\ \bar{I}_{S5c} \\ \bar{I}_{R5a} = 0 \\ \bar{I}_{R5b} \\ \bar{I}_{R5c} \\ \bar{I}_{Sg5a} \\ \bar{I}_{Sg5b} = 0 \\ \bar{I}_{Sg5c} = 0 \\ \bar{I}_{Rg5a} \\ \bar{I}_{Rg5b} = 0 \\ \bar{I}_{Rg5c} = 0 \end{bmatrix} = \begin{bmatrix} \\ \\ \\ \\ \\ \\ \\ \\ \\ \\ \\ \\ \\ \\ \\ \end{bmatrix} Y_{ij} \begin{bmatrix} \bar{E}_{F5a} \\ \bar{E}_{F5b} \\ \bar{E}_{F5c} \\ \bar{E}_{S5a} \\ \bar{E}_{S5b} = 0 \\ \bar{E}_{S5c} = 0 \\ \bar{E}_{R5a} \\ \bar{E}_{R5b} = 0 \\ \bar{E}_{R5c} = 0 \\ \bar{E}_{Sg5a} \\ \bar{E}_{Sg5b} \\ \bar{E}_{Sg5c} \\ \bar{E}_{Rg5a} = 0 \\ \bar{E}_{Rg5b} \\ \bar{E}_{Rg5c} \end{bmatrix} \qquad (5.2)$$

where, $i = 1,5$; $j = 1,5$

Eqn. 5.2 can be reduced to a matrix relation of the order of ten by discarding all rows and columns which correspond to zero-valued Transforms in the voltage vector, which upon inversion gives the reduced matrix relationship of eqn. 5.3 :-

$$\begin{bmatrix} \bar{E}_{F5a} \\ \bar{E}_{F5b} \\ \bar{E}_{F5c} \\ \bar{E}_{S5a} \\ \bar{E}_{R5a} \\ \bar{E}_{Sg5a} \\ \bar{E}_{Sg5b} \\ \bar{E}_{Sg5c} \\ \bar{E}_{Rg5b} \\ \bar{E}_{Rg5c} \end{bmatrix} = \begin{bmatrix} & & \\ & \bar{Y}_5 & \\ & & \end{bmatrix} \begin{bmatrix} 0 \\ 0 \\ 0 \\ 0 \\ 0 \\ \bar{I}_{Sg5a} \\ 0 \\ 0 \\ 0 \\ 0 \end{bmatrix} \qquad (5.3)$$

where, $\bar{Y}_5$ = the inverse of the reduced admittance matrix from eqn. 5.2.

Substituting for $\bar{I}_{Sg5a}$ in eqn. 5.3, the voltage vector in the same equation is obtained. Further substitution of the latter known voltage vector into the full admittance matrix relation of eqn. 5.2 enables the unknown current Transforms to be calculated. The Transform of the voltage superimposed component at, the sending end, the receiving end and the point of fault, are then calculated using eqns. A3.3.2, A3.3.5 and A3.3.7 respectively.

The voltage and current superimposed components are then transformed back into the time-domain using the Fourier Transform techniques. The total time-domain response, of say the current through the receiving end HSGS of phase-"a", at this stage would then be :-

$$i_{RgaT}(t) = i_{Rg4a}(t - T_{hc}) + i_{Rg5a}(t - T_{hol}) \qquad (5.4)$$

The receiving end HSGS current (eqn. 5.4) is then checked for zero-crossing, which occurs say at T_{ho2} after the fault. Following the same pattern of calculation as

that described above, the opening of the second HSGS is performed, and the system response is obtained. The total time-domain response of say the voltage across the sending end breaker (phase-"a") at this stage would then be as given in eqn. 5.5 :-

$$e_{Sa}(t) = e_{S2a}(t - T_{b2}) + e_{S3a}(t - T_{b3}) + e_{S4a}(t - T_{hc}) + e_{S5a}(t - T_{ho1}) + e_{S6a}(t - T_{ho2}) \qquad (5.5)$$

5.3 Closing of The Main Breaker

The closing of the line end main breaker poles is arranged to take place in a common fashion, whether conventional single-pole switching, the hybrid method of autoreclosure, the HSGS's, or the neutral switched reactor arrangement is employed. Having obtained the total time varying voltage response across the sending and receiving end circuit breakers, it is possible to inject an equal and opposite voltage to the latter, such that at breaker closure at a time say T_{bk}, the total voltage across it sums to zero.

Adopting the method of synchronous closing, the reclose instant is controlled to take place when the voltage across the specific pole is zero or minimum. At a certain time, say 0.5 sec after fault inception, the voltage across the sending and receiving end circuit breaker poles are checked for a zero crossing, to determine the first pole to close. Thereafter, an equal and opposite voltage to that across the particular pole is injected into the system to simulate its closing. This part of simulation is essentially one of superposition[76], and forms the final stage in obtaining the response for systems

where, conventional single-pole switching, the hybrid method of autoreclosure, or the HSGS's is implemented. In this section, it is assumed that a fault occured on phase-"a" which is then cleared by the main breakers, followed by the switching events according to the scheme employed. Moreover, it is considered that the secondary arc has extinguished well before reclosure to allow for the recovery of the fault path dielectric strength.

5.3.1 System implementing conventional single-pole switching

The procedure of closing a main breaker pole can be explained with reference to fig. 5.2a, which shows the system state prior to the first pole to close. The total voltage across the sending and receiving end breaker poles are $e_{Sa}(t)$ and $e_{Ra}(t)$ respectively , and are given :-

$$e_{Sa}(t) = 0 \quad \text{for } t < T_{b2}$$

$$e_{Ra}(t) = 0 \quad \text{for } t < T_{b3}$$

If the voltage across the sending end breaker pole passes through zero first at time say T_{b4} , then the Frequency spectrum $\bar{E}_{S4a}$ of voltage which is injected as shown in fig. 5.2b to simulate the pole closure, is given by ;-

$$\bar{E}_{S4a} = - \int_{T_{b4}}^{T_{ob}} e_{Sa} \exp\left[-j(\omega - j\alpha) \quad t\right] dt \qquad (5.6)$$

At this stage, it is known that,

$$\bar{E}_{S4b,c} = \bar{E}_{R4b,c} = \bar{I}_{R4a} = \bar{I}_{F4a,b,c} = 0$$

and eqn. A3.1.12 can be used here :-

$$\begin{bmatrix} 0 \\ 0 \\ 0 \\ \bar{I}_{S4a} \\ \bar{I}_{S4b} \\ \bar{I}_{S4c} \\ 0 \\ \bar{I}_{R4b} \\ \bar{I}_{R4c} \end{bmatrix} = \begin{bmatrix} \\ \\ \\ \\ \\ \\ \\ \\ \end{bmatrix} Y_{ij} \begin{bmatrix} \\ \\ \\ \\ \\ \\ \\ \\ \end{bmatrix} \begin{bmatrix} \bar{E}_{F4a} \\ \bar{E}_{F4b} \\ \bar{E}_{F4c} \\ \bar{E}_{S4a} \\ 0 \\ 0 \\ \bar{E}_{R4a} \\ 0 \\ 0 \end{bmatrix} \qquad (5.7)$$

where, $i = 1,3 \;\; ; \;\; j = 1,3$

In eqn. 5.7, discarding all rows and columns that correspond to zero-valued Transforms in the voltage vector, the reduced matrix relationship of eqn. 5.8 is obtained :-

$$\begin{bmatrix} 0 \\ 0 \\ 0 \\ \bar{I}_{S4a} \\ 0 \end{bmatrix} = \begin{bmatrix} \\ \\ \\ \\ \\ \end{bmatrix} Y_4 \begin{bmatrix} \\ \\ \\ \\ \\ \end{bmatrix} \begin{bmatrix} \bar{E}_{F4a} \\ \bar{E}_{F4b} \\ \bar{E}_{F4c} \\ \bar{E}_{S4a} \\ \bar{E}_{R4a} \end{bmatrix} \qquad (5.8)$$

The known quantities in eqn. 5.8 are $\bar{E}_{S4a}$ and Y_4 which enables the calculation of $\bar{I}_{S4a}$:-

$$\bar{I}_{S4a} = \bar{E}_{S4a} \; / \; \bar{Y}_4(4,4) \qquad (5.9)$$

where, $\bar{Y}_4 = \left[Y_4 \right]^{-1}$

From eqn. 5.9 and the inverse of eqn. 5.8, the unknown

voltage Transform vector $\left[\bar{E}_{F4a} \quad \bar{E}_{F4b} \quad \bar{E}_{F4c} \quad \bar{E}_{R4a}\right]^T$ can be obtained. Substituting the latter known voltage vector in eqn. 5.7 enables the sound phases current Transforms to be calculated.

The voltage and current Transforms resulting from the sending end breaker pole closure are then transformed back into the time-domain using the Fourier Transform technique. The total time-domain response of say the voltage across the receiving end breaker pole at this stage would then be :-

$$e_{Ra}(t) = e_{R3a}(t - T_{b3}) + e_{R4a}(t - T_{b4}) \qquad (5.10)$$

The above procedure is then repeated for the closing of the receiving end breaker pole, and the total overall response is obtained.

5.3.2 System implementing the hybrid method of autoreclosure

Upon reclosure, the voltage across the breaker poles at both line ends are checked for zero crossing. A voltage equal and opposite to that across the first pole to close is injected into the system as shown in fig. 5.2b to simulate its closure. Assuming phase-"a" sending end breaker pole is to be closed first, the voltage to be injected $\bar{E}_{S8a}$ is given by :-

$$\bar{E}_{S8a} = - \int_{T_{b8}}^{T_{ob}} e_{Sa} \exp\left[-j(\omega - j\alpha)\ t\right] dt \qquad (5.11)$$

where, $e_{Sa}(t) = \sum_i e_{Sia}(t - T_{bi})$, $i = 2,7$

$\bar{I}_{S8a}$ (fig. 5.2b) is the Frequency spectrum of a current

source which arises due to the injection of voltage $\bar{E}_{S8a}$. Eqn. A3.1.12 can be used here also, to define the super-imposed circuit current voltage relations, and can be written as per eqn. 5.12.

$$\begin{bmatrix} 0 \\ 0 \\ 0 \\ \bar{I}_{S8a} \\ 0 \\ 0 \\ 0 \\ 0 \\ 0 \end{bmatrix} = \begin{bmatrix} \\ \\ \\ \\ Y_{ij} \\ \\ \\ \\ \\ \end{bmatrix} \begin{bmatrix} \bar{E}_{F8a} \\ \bar{E}_{F8b} \\ \bar{E}_{F8c} \\ \bar{E}_{S8a} \\ \bar{E}_{S8b} \\ \bar{E}_{S8c} \\ \bar{E}_{R8a} \\ \bar{E}_{R8b} \\ \bar{E}_{R8c} \end{bmatrix} \qquad (5.12)$$

where, $i = 1,3$; $j = 1,3$

From eqn. 5.11 and eqn. 5.12, the voltage Transform vector, namely, $\left[\bar{E}_{F8a,b,c} \quad \bar{E}_{S8b,c} \quad \bar{E}_{R8a,b,c}\right]^T$ is obtained, and the voltage component of the fault point, the sending and receiving ends are then calculated using eqns. A3.1.5, A3.1.1 and A3.1.2 respectively.

These components are then transformed back into the time-domain and added to their respective quantities. The whole process is then repeated for the remaining poles to determine the total overall system response.

5.3.3 System implementing HSGS's

Generally, a similar procedure to that outlined in section 5.3.1 is used here to re-energise the open phase.

Upon the first breaker pole to close, say at the sending end, the known zero-valued transforms at this stage (see fig. 5.1) are, $\bar{E}_{S7b,c}$, $\bar{E}_{R7b,c}$, $\bar{I}_{Sg7a,b,c}$, $\bar{I}_{Rg7a,b,c}$ and $\bar{I}_{F7a,b,c}$. Moreover, the fifteenth known Transform is $\bar{E}_{S7a}$ which is given by :-

$$\bar{E}_{S7a} = - \int_{T_{b7}}^{T_{ob}} e_{Sa} \exp\left[-j(\omega - j\alpha) \quad t\right] dt \qquad (5.13)$$

where, e_{Sa} = the voltage given by eqn. 5.5

Substituting the above known Transforms in the matrix relationship of eqn. A3.3.23, gives the reduced form of eqn. 5.14 :-

$$\begin{bmatrix} 0 \\ 0 \\ 0 \\ \bar{I}_{S7a} \\ 0 \\ 0 \\ 0 \\ 0 \\ 0 \\ 0 \\ 0 \\ 0 \end{bmatrix} = \begin{bmatrix} \\ \\ \\ \\ Y_7 \\ \\ \\ \\ \\ \\ \\ \end{bmatrix} \begin{bmatrix} \bar{E}_{F7a} \\ \bar{E}_{F7b} \\ \bar{E}_{F7c} \\ \bar{E}_{S7a} \\ \bar{E}_{R7a} \\ \bar{E}_{Sg7a} \\ \bar{E}_{Sg7b} \\ \bar{E}_{Sg7c} \\ \bar{E}_{Rg7a} \\ \bar{E}_{Rg7b} \\ \bar{E}_{Rg7c} \end{bmatrix} \qquad (5.14)$$

Hereafter, similar steps to those in section 5.3.1 are followed to obtain the total overall system response.

5.3.4 System implementing neutral switched reactor arrangement

Assuming that the voltage across the sending end breaker pole passes through zero first, at a time T_{b5}, then the Transform of voltage $\bar{E}_{S5a}$ injected into the system as shown in fig. 5.3 to simulate the pole closure is given by :-

$$\bar{E}_{S5a} = - \int_{T_{b5}}^{T_{ob}} e_{Sa} \exp\left[-j(\omega - j\alpha) \quad t \right] dt \qquad (5.15)$$

where, $e_{Sa} = e_{S2a}(t - T_{b2}) + e_{S3a}(t - T_{b3}) + e_{S4a}(t - T_{s1})$

At this stage of simulation, $\bar{E}_{S5b,c}$, $\bar{E}_{R5b,c}$, $\bar{I}_{F5a,b,c}$, $\bar{I}_{R5a}$, and $\bar{I}_{SW5}$ are known zero-valued Transforms. Therefore, using eqn. A3.2.18 with the above known quantities, the reduced matrix relationship of eqn. 5.16 is obtained.

$$\begin{bmatrix} 0 \\ 0 \\ 0 \\ \bar{I}_{S5a} \\ 0 \\ 0 \end{bmatrix} = \begin{bmatrix} \\ \\ Y_5 \\ \\ \\ \\ \end{bmatrix} \begin{bmatrix} \bar{E}_{F5a} \\ \bar{E}_{F5b} \\ \bar{E}_{F5c} \\ \bar{E}_{S5a} \\ \bar{E}_{R5a} \\ \bar{E}_{SW5} \end{bmatrix} \qquad (5.16)$$

Following the same procedure as that described in section 5.3.1, the total time-domain system responses are obtained. For example, the voltage across the ideal neutral switch at this stage would be :-

$$e_{SW}(t) = e_{SW4}(t - T_{s1}) + e_{SW5}(t - T_{b5}) + e_{SW6}(t - T_{b6}) \qquad (5.17)$$

5.4 Closing The Ideal Neutral Switch

Having obtained the total time varying voltage response across the ideal neutral switch (eqn. 5.17), the injection of a voltage equal and opposite into the system, would simulate the closure. In the developed program, the closing of the ideal neutral switch can be simulated to take place at any time after fault inception, after or before the closing of the main breakers. However, staged fault test results[48], show that the closing time of the neutral switches is in the order of 0.5 to 0.56 sec after fault inception, when a dead-time of 0.5 sec is used. The closing of the ideal neutral switch can be arranged to take place when the voltage across it is zero, minimum, or randomly at a pre-set time.

If the closure of the ideal neutral switch takes place at a time T_{s2} after fault, the Frequency spectrum $\bar{E}_{SW7}$ of voltage which is injected into the system as shown in fig. 5.3 (for a fault on phase-"a") is given by,

$$\bar{E}_{SW7} = - \int_{T_{s2}}^{T_{ob}} e_{SW} \exp \left[-j(\omega - j\alpha) \quad t \right] dt \qquad (5.18)$$

where, e_{SW} = the voltage given by eqn. 5.17.

Here again, the 10 x 10 admittance matrix of eqn. A3.2.18 is used to define the system currents and voltages relationship, which is given by eqn. 5.19 (see fig. 5.3).

$$\begin{bmatrix} \bar{I}_{F7a} = 0 \\ \bar{I}_{F7b} = 0 \\ \bar{I}_{F7c} = 0 \\ \bar{I}_{S7a} \\ \bar{I}_{S7b} \\ \bar{I}_{S7c} \\ \bar{I}_{R7a} \\ \bar{I}_{R7b} \\ \bar{I}_{R7c} \\ \bar{I}_{SW7} \end{bmatrix} = \begin{bmatrix} \\ \\ \\ \\ \\ \\ \\ \\ \\ \\ \end{bmatrix} Y_{ij} \begin{bmatrix} \bar{E}_{F7a} \\ \bar{E}_{F7b} \\ \bar{E}_{F7c} \\ \bar{E}_{S7a} = 0 \\ \bar{E}_{S7b} = 0 \\ \bar{E}_{S7c} = 0 \\ \bar{E}_{R7a} = 0 \\ \bar{E}_{R7b} = 0 \\ \bar{E}_{R7c} = 0 \\ \bar{E}_{SW7} \end{bmatrix} \qquad (5.19)$$

where, $i = 1,4$; $j = 1,4$

Upon reducing eqn. 5.19 by discarding all rows and columns that correspond to zero-valued Transforms in the voltage vector and inverting, eqn. 5.20 is obtained :-

$$\begin{bmatrix} \bar{E}_{F7a} \\ \bar{E}_{F7b} \\ \bar{E}_{F7c} \\ \bar{E}_{SW7} \end{bmatrix} = \begin{bmatrix} \\ \\ \\ \\ \end{bmatrix} \bar{Y}_7 \begin{bmatrix} 0 \\ 0 \\ 0 \\ \bar{I}_{SW7} \end{bmatrix} \qquad (5.20)$$

where $\bar{Y}_7$ is the inverse of the reduced matrix obtained from that in eqn. 5.19. In eqn. 5.20, $\bar{E}_{SW7}$ and $\bar{Y}_7$ are known. Therefore, the current Transform $\bar{I}_{SW7}$ which arises due to the injection of $\bar{E}_{SW7}$ is obtained , and given by :-

$$\bar{I}_{SW7} = \bar{E}_{SW7} \; / \; \bar{Y}_7(4,4) \qquad (5.21)$$

Substituting for $\bar{I}_{SW7}$ in eqn. 5.20, the voltage Transforms $\bar{E}_{F7a,b,c}$ are obtained. Further substitution of the now known voltage vector $\left[\bar{E}_{F7a,b,c} \quad \bar{E}_{SW7}\right]^T$ in eqn. 5.19 enables the remaining current Transform values to be calculated.

The above calculated voltage and current components are finally transformed back into time-domain, and the total overall system response is calculated using superposition principles.

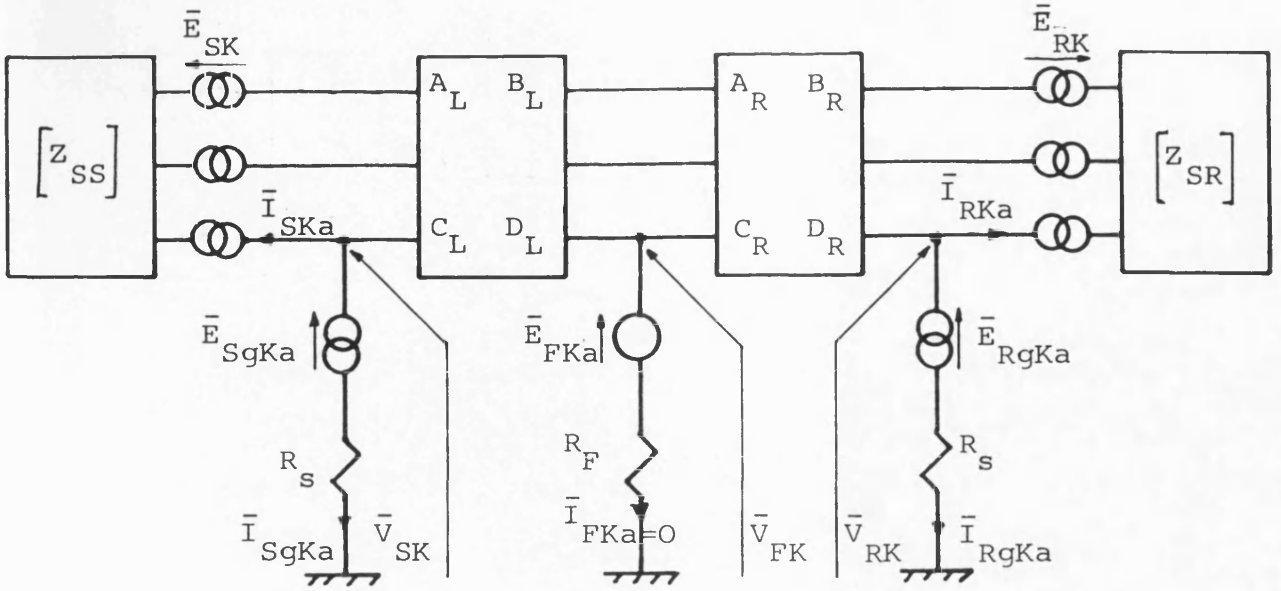

Fig. 5.1 Frequency domain superimposed system model

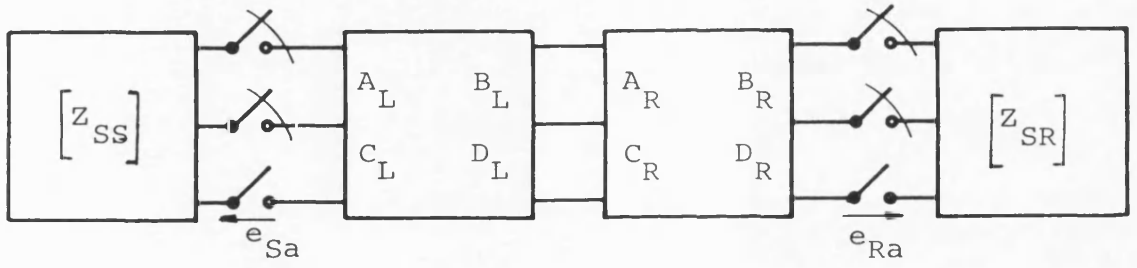

(a)

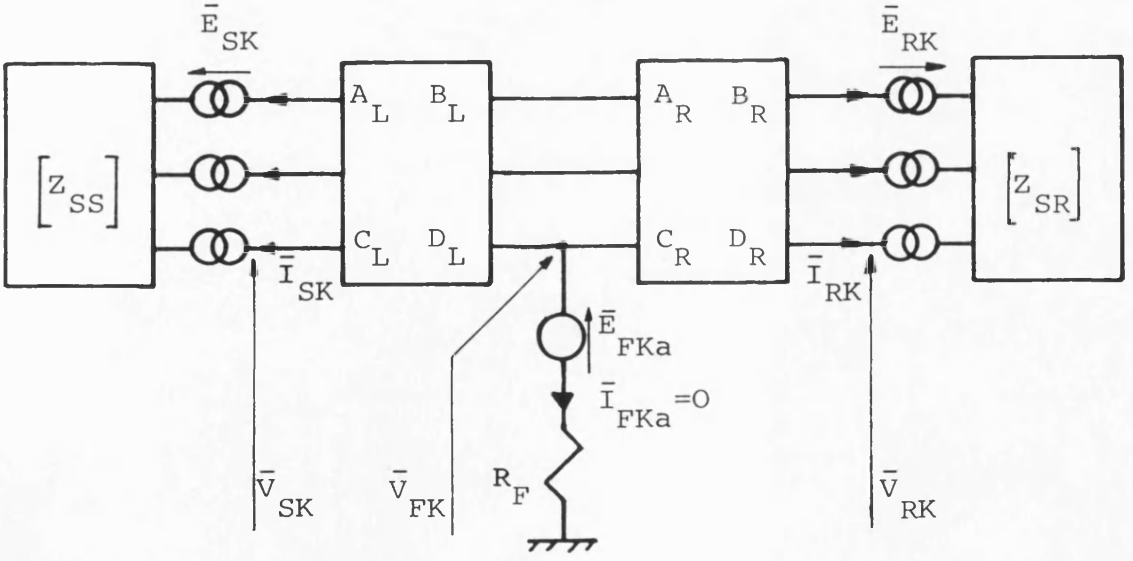

(b)

Fig. 5.2

(a) Basic system model

(b) Frequency domain superimposed system model

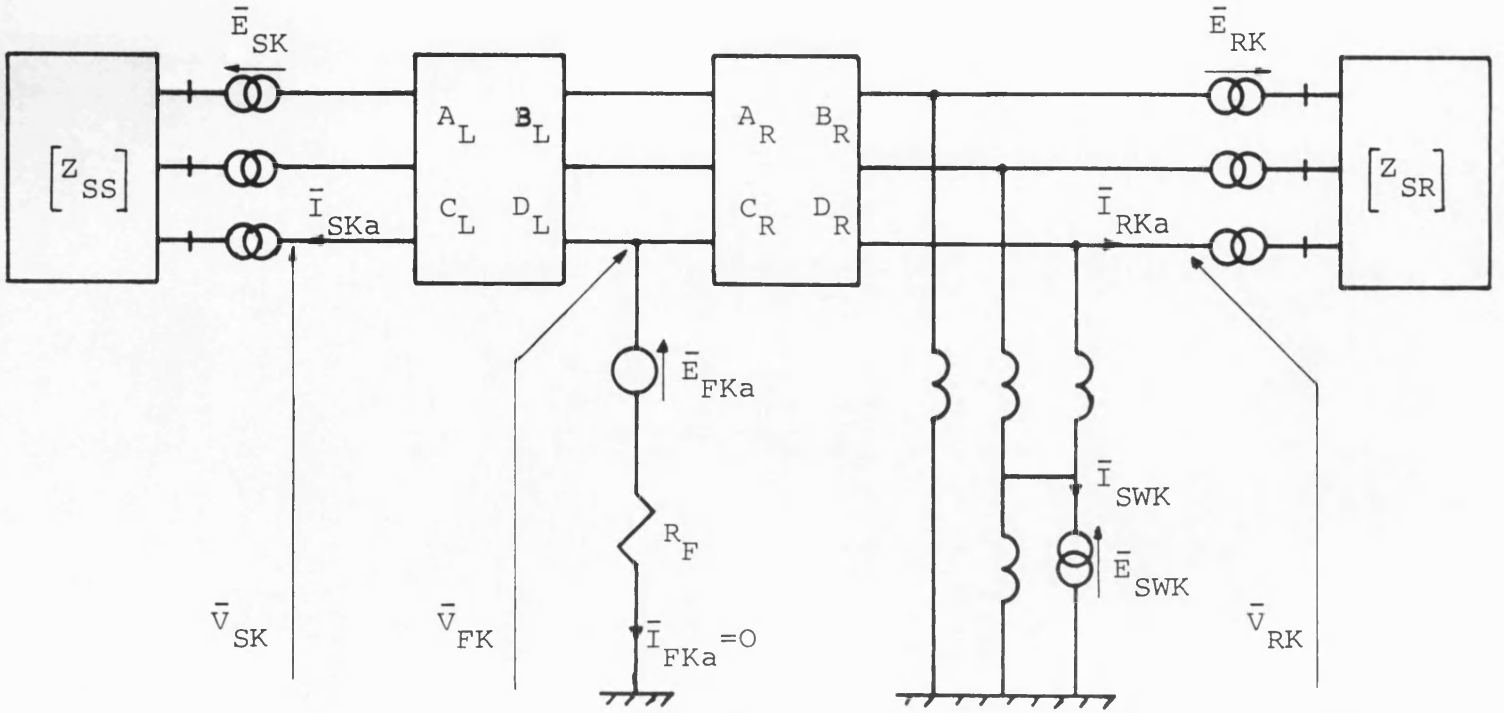

Fig. 5.3 Frequency domain superimposed system model

CHAPTER 6

BASIC SYSTEM PARAMETERS

6.1 Introduction

The computational results presented in this work (chapter 7 - 10) are for a 500kV, single-circuit transmission line systems. The transmission line can be either discretely transposed at L/3 intervals or untransposed, compensated at both or either end or uncompensated. For the different single-pole switching schemes discussed in chapters 1-5, the transmission line is considered to be fed at its remote ends by sources of short circuit capacities of S.C.1 and S.C.2.

In this chapter, the parameters of, the transmission line, the shunt reactor(s), the line end source, the HSGS and that used in the Fourier Transform routine are presented.

6.2 Transmission Line Parameters

6.2.1 Line construction

Fig. 6.1a shows the typical quad-conductor 500kV line configuration considered. The position of the conductors illustrated correspond to the position over the whole line length in non-transposed line application. However, in a transposed line application, the conductors position shown

in fig. 6.1a correspond to those over the first one third of the line length from the sending end (fig. 6.1b). The data for the line is:-

i) Phase conductors- 4x477 MCM Al alloy, 2.15mm over all equivalent, 242mm^2 Al equivalent, 19/4.3mm stranding.

ii) Earth shield wires- 7/35mm Alumoweld.

iii) Earth resistivity- 100 Ωm.

iv) Conductor resistance- 0.0217512 Ω/km (at 50Hz).

v) Earth wire resistance- 1.0916841 Ω/km (at 50Hz).

vi) Conductor reactance- 0.00380647 Ω/km (at 50Hz).

vii) Earth wire reactance- 0.3877944 Ω/km (at 50Hz).

viii) Line length varies according to study (commonly 300km).

ix) Distance between arcing horns- 4.05m.

6.2.2 Computed basic parameters

The basic line parameter matrices are the series impedance matrix $[Z]$ and the shunt admittance matrix $[Y]$ which are uniformly distributed along its length (APPENDIX 2.3). For a multiconductor line, the basic line parameter matrices have been formulated for realistic transient studies, and are reported elsewhere[60]. For the horizontally constructed line considered, the line $[Z]$ and $[Y]$ matrices at power frequency(50Hz) are:-

$$[Z] = \begin{bmatrix} 1.019+j5.011 & 0.791+j1.856 & 0.813+j2.273 \\ 0.791+j1.856 & 1.019+j5.011 & 0.813+j2.273 \\ 0.813+j2.273 & 0.813+j2.273 & 1.049+j4.98 \end{bmatrix} \times 10^{-4} \ \Omega/m \quad (6.1)$$

$$[Y] = j \begin{bmatrix} 0.3443485 & -0.01972752 & -0.0643521 \\ -0.01972752 & 0.3443486 & -0.0643521 \\ -0.0643521 & -0.0643521 & 0.3586486 \end{bmatrix} \times 10^{-8} \ \mho/m \quad (6.2)$$

From the $[Z]$ and $[Y]$ matrices, the propagation constant matrix $[\gamma]$, the surge impedance matrix $[Z_o]$, and the corresponding surge admittance matrix $[Y_o]$ are calculated.

With the line considered ideally transposed, its zero and positive sequence capacitances (C_o, C_1) are calculated from the average of the sum of all conductors self and mutual capacitances per unit length. Using the admittance values given in eqn. 6.2, C_o and C_1 can be found as follow.

$$C_o = 0.79628 \times 10^{-11} \text{ F/m}$$

$$C_1 = 1.26875 \times 10^{-11} \text{ F/m}$$

The line capacitance ratio k is:

$$k = C_o / C_1 = 0.62761$$

The peak steady-state secondary arc current assuming zero arc resistance, and the steady-state recovery voltage[35,36] can be calculated using eqns. 2.1 and 2.2 and are:-

$$I_{secp} = 2.02 \times 10^{-4} \text{ A/m (peak)}$$

$$V_{rp} = -57858 \text{ Volt (peak)}$$

It must be noted that the above two values represent the capacitively induced components only.

6.3 Shunt Reactor Parameters

The parameters of the shunt reactor bank(s) are determined assuming ideal transposition of the line. A typical Q-factor of 250 is assumed for the phase and neutral reactors at power frequency(50Hz). In practice, the normal service loading levels on long compensated lines are typically between 50-100% of the surge impedance loading of the line. Therefore, a typical p.p.s. degree of shunt compensation(h_1) required is approximately 0.75. In the course of this work, $h_1 = 0.75$ is

used whenever a compensated application is considered (unless otherwise stated). When the shunt reactor is arranged to compensate one half of the line length, its phase reactance can be calculated using eqn. A2.2.7. For a 300km line, this reactance is :-

$$X_p = 2230.1\ \Omega \text{ (at 50Hz)}$$

In cases where a 4-legged shunt reactor bank is used to limit the secondary arc current to a certain value, the z.p.s. degree of shunt compensation(h_o) has to be defined, and eqn. A2.2.8 is then used to calculate the neutral reactance. As an example, for the line under study, to limit the capacitive component of the steady-state secondary arc current to -j20A (r.m.s.), the value of h_o required is:

$$h_o = 0.8787121$$

which dictates a value for $X_n = 267.5\ \Omega$ (at 50Hz) for $h_1 = 0.75$.

For the nontransposed line compensated by a conventional 4-legged reactor bank at one end and a neutral switched reactor bank at the other, an extensive series of studies were performed to determine an optimum value for the neutral reactances(Chapter 9.2). At $h_1 = 0.75$, these were found to be:

$$X_{ns} = 400\ \Omega \text{ (at 50Hz)}$$

$$X_{nr} = 800\ \Omega \text{ (at 50Hz)}$$

6.4 Source Parameters

The impedance matrix of each line end source has been formulated from a knowledge of the short circuit level, the ratio of z.p.s. to p.p.s. impedance and the X/R ratio of the source as derived in APPENDIX 2.1. The following source parameters were considered throughout the present work.

i) Sending end source short circuit level(S.C.1),
S.C.1 = 5 - 10 GVA

ii) Receiving end source short circuit level(S.C.2),
S.C.2 = 5 - 10 GVA

iii) Source X/R ratio at 50Hz = 100

iv) Source Z_{So}/Z_{S1} = 0.5 - 1.0

6.5 HSGS Parameters

In the majority of the studies performed with the line equipped with HSGS's, the following parameters were used:

i) HSGS closing time = 10 cycles after fault inception (based on 50Hz)

ii) HSGS opening time = 20 cycles after fault inception

iii) HSGS resistance = 0.5 - 10 Ω

6.6 Modified Fourier Transform Parameters

It is a well known fact that fault occurrence on a line and the subsequent switching operations, causes voltage and current components to propagate through different paths along the transmission system. These form a series of travelling-waves which are ultimately damped by the system. Under such conditions, the elements of the transmission system are subjected to voltages and currents having a wide range of frequency variations, which are associated with frequency variant parameters[51,76]. Therefore it is necessary to evaluate the system response over the whole frequency spectrum of importance. In practice, nearly all protection devices employ prefiltering arrangements, which limit the band-width of information processed to below

typically 2kHz. In these circumstances, spectral components above the latter frequency do not significantly affect relay performance, and it is sufficient to compute the system responses over this limited frequency range[76]. Moreover, it has been found that the effect of considering higher frequency range on the secondary arc extinction time is negligible.

The Modified Fourier Transform method is used to determine the time variation of any voltage v(t) or current i(t) from the corresponding Frequency spectrum $\bar{V}(\omega)$, $\bar{I}(\omega)$ respectively. However, in implementing the Modified Fourier Transform method digitally, the basic frequency $(\Delta\omega)$, the maximum number of samples (N) and the frequency shift constant (α) can affect the system response. Therefore, appropriate values for these quantities must be used[82,83]. In the present work, the Modified Fourier Transform parameters are taken as follows :

Observation time "T_{ob}" = 0.8192 sec

Frequency shift constant "α" = 7.67

Number of samples "N" = 4096

Truncation frequency "Π" = 2.5kHz

Defining T_{ob} and the number of samples, α and Π are calculated on the following basis:

$$\alpha = 2\pi / T_{ob}$$

$$\Pi = N/2T_{ob}$$

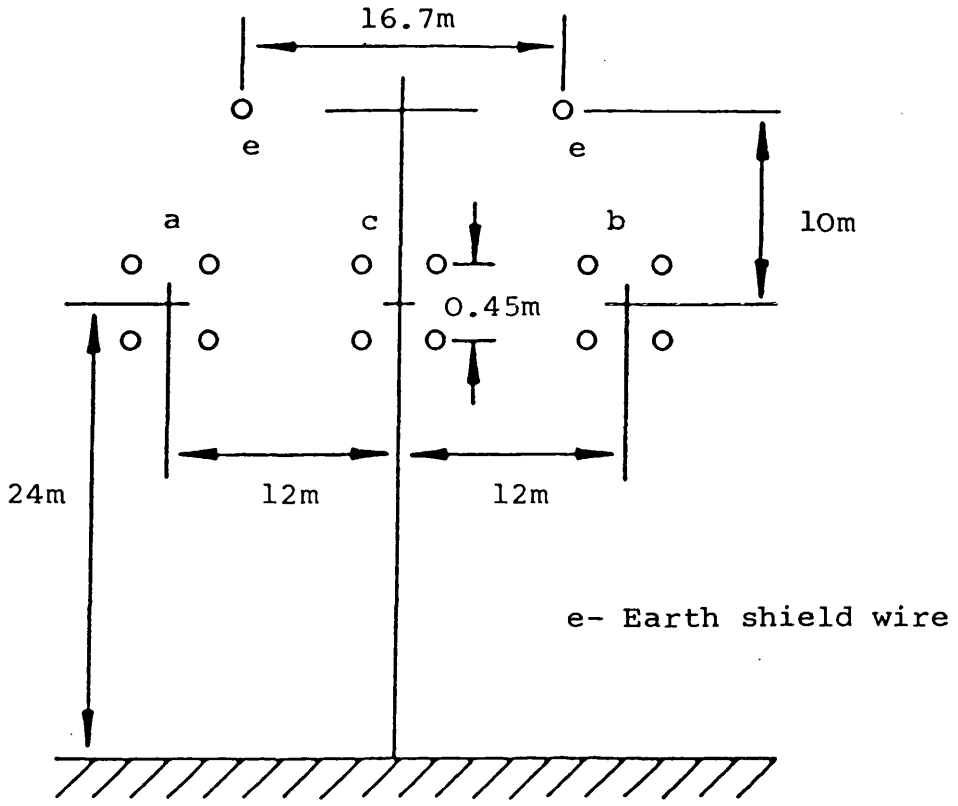

(a)

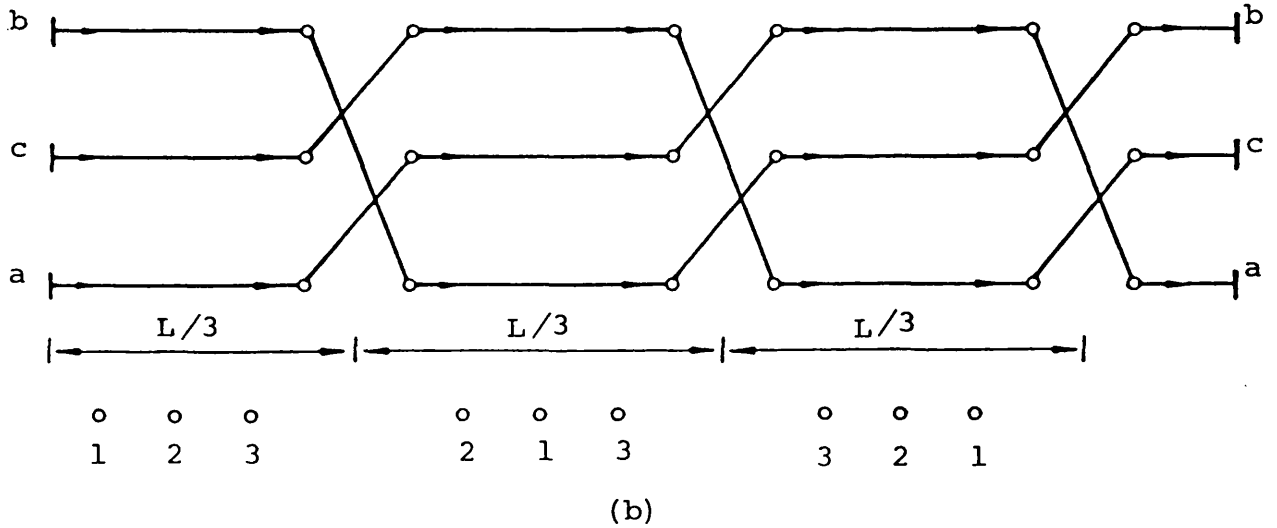

(b)

Fig. 6.1

(a) 500 kV horizontal line construction

(b) Schematic diagram of a transmission line with a complete cycle of transposition

CHAPTER 7

SYSTEM STUDIES: CONVENTIONAL SINGLE-POLE SWITCHING

7.1 Introduction

The electrical characteristics of a 300km, 500kV transmission system throughout conventional single-pole switching events are simulated using a digital computer. The non-linear secondary arc model is used in the present digital studies to quantify the effects of the various system parameters on the secondary arc extinction time. Although thorough results for the untransposed line applications are presented, some relevant ones to transposed line applications are also mentioned for comparison. Moreover, the results set forth should serve as a basis for the applicability of the various single-pole switching schemes discussed in the previous chapters, and whose analysis results are presented in chapters 8-10.

The secondary arc extinction time, and consequently the required single-pole switching dead-time, increases with the secondary arc current and recovery voltage. Higher system voltage and long EHV transmission lines result in increased secondary arc currents. Moreover, in long line applications, the addition of the shunt reactors raises the recovery voltage. Line conductors transposition is

one tool for reducing the above mentioned two quantities. However, line transposition can be economically unattractive if it is justified on the grounds of single-pole switching performance only. The use of the balanced 4-legged shunt reactor in transposed line applications in aid of single-pole switching is very well documented in the literature. However, the trend in modern power systems towards EHV lines non-transposition, has focused the need for establishing the limitations of adopting the above mentioned reactor arrangement in effecting acceptable single-pole switching performance in untransposed line applications.

In this chapter, discrete transposition at 100km intervals along the 300km length of the line is considered whenever a system with transposed line is under study. Moreover, a line of 200km length, untransposed is thoroughly investigated along with the 300km line in evaluating the effect of the shunt reactor neutral reactance on the secondary arc extinction time. The case of using one balanced 4-legged reactor bank at one end of the line is also highlighted.

The relevant common features of the systems investigated in this chapter are :-

1. Line length :200km and 300km.

2. The capacitive component of the secondary arc current for the uncompensated line is , 61.5A (peak) for the 300km transposed; 69.9A and 78.8A (peak) for the untransposed line with the fault on outer and inner phase respectively.

3. Faults are simulated on phase-"a" for the transposed line applications, and on phases-"a","c" (outer and inner respectively) for the untransposed line applications.

4. Breaker opening and closing time occurs when its current, and the voltage across it is zero or minimum.

5. The capacity of each line end source is 5GVA.

6. The initiation of the fault is at the maximum point on wave.

7. Degree of p.p.s. compensation $h_1 = 0.75$, unless otherwise stated.

7.2 Effect of The Neutral Reactance

In assessing the effect of the balanced 4-legged shunt reactor on the secondary arc parameters, two 500kV transmission systems are considered. The first contains a 300km line, while the second contains a 200km line, For the first system, the effect of the neutral reactance (X_n) on the peak of the secondary arc current and its extinction time in transposed and untransposed line applications is considered. However, for the second system, the effect of X_n on arc extinction time and the first peak of the recovery voltage under various loading conditions with untransposed line applications are discussed. In all the studies here, two balanced 4-legged shunt reactors are considered to be connected at the remote ends of the line. Moreover, all faults are considered to occur at the sending end of the system.

With a degree of p.p.s. compensation of 0.75, a value of $X_n = 733\,\Omega$ can be evaluated using the format in APPENDIX 2.2 as the optimum . Theoretically, such a value of X_n should give zero secondary arc current for the 300km line, with ideally balanced conditions. Examination of fig. 7.1b with such a value of X_n shows that for the

transposed line application, a secondary arc current of few Amperes (peak) is still flowing. This is more likely due to the inductive coupling with the two sound phases and the line series impedance. However, even with the optimum value of X_n , practically, the effect of the fault location with regard to the discrete transposition, would contibute to the level of the secondary arc current.

For the same line application, with such low level of secondary arc current, extinction time of 70 msec is evident from fig. 7.1a. Also, fig. 7.1a shows clearly the effectiveness of the line transposition as regard to secondary arc extinction time. Moreover, from fig. 7.1a it can be seen that much lower value of X_n can be adopted to provide for arc extinction and reclosure in the 0.5 sec dead-time.

In transmission systems where the line unbalance do not cause operational problems, economic advantage can be achieved with no transposition of the line. However, with the increased interest in applying single-pole switching techniques to such systems, it is felt necessary to investigate to what extent conventional measures can be used to advantage in promoting such techniques.

For the 300km transmission system, with the line untransposed, the minimum arc extinction time for a fault on the outer phase is of the order of 0.4 sec (see fig. 7.1a). For the inner phase fault, the variation of the arc extinction time with the neutral reactance approaches that of a transposed line application, for values of $X_n > 1000$. It is interesting to note that, for $0 < X_n < 150$, the peak secondary arc current and concomitant exinction time for an inner phase fault is higher than that for an outer phase fault. This is mainly due to the fact that , with such

values of X_n, the effectiveness of the shunt reactor in compensating the capacitive component of the secondary arc current is insignificant. This is enhanced by the higher capacitive coupling of the inner phase to the two sound outer phases. For higher values of X_n, the picture is different, and lower arc extinction times are clearly evident in fig. 7.1a for inner phase faults. This is attributed to the fact that the symmetry of the inner phase with respect to the two outers, makes the balanced reactor with such values of X_n, more correctly compensate the capacitive component of the secondary arc current. For such line length, it can be concluded that, in order to achieve successful single-pole switching performance, dead-time in the order of 0.55 - 0.65 sec is required , with the system compensated by the 4-legged reactor banks. However, with Y-connected shunt reactor at both ends, a dead-time in excess of 0.8 sec is required. Finally, it is worth noting from fig. 7.1a that the minimum extinction time of approximately 0.4 sec occurs for outer phase fault at $X_n = 625\,\Omega$.

7.2.1 Untransposed line - 200km length

With the aforementioned in mind, it is necessary to consider a shorter length of untransposed line in order to fully estimate the impact of employing conventional single-pole switching with the shortest practical dead-time. In 1984, Johns et al[26] reported results of studies concerning such line applications. In their paper, the authors studied the effect of the fault position and system loading on the secondary arc parameters, with the neutral reactance fixed at the optimum value (for the 200km line $X_{n(optimum)} = 1099\,\Omega$). Addition to the results presented in the above mentioned paper, fig. 7.2 shows the variation of the arc extinction

time and the first peak of the recovery voltage with respect to the neutral reactance. The effect of the pre-fault system loading is also presented. For outer phase fault, it is evident from fig. 7.2a that the arc extinction time is almost constant in the region of $350\Omega < X_n < 1200\Omega$. Therefore, a value of $X_n = 360\Omega$ is still sufficient to achieve extinction times in the order of 0.3 - 0.33 sec. On the assumption of ideal transposition, $X_n = 360\Omega$ represent a degree of z.p.s. compensation of 0.903355. Moreover, at this value of X_n, the difference between inner and outer phase fault arc extinction times is insignificant. From fig. 7.2a and 7.2b, the effect of the system pre-fault loading which is approximately 1262MW, and its direction of flow is more marked for faults on an outer phase. This is mainly due to the unbalance introduced by virtue of the line being untransposed. Although the two end sources are identical, higher arc extinction times and first peak of the recovery voltage for outer phase faults are evident at the importing end of the line, and the exporting end for inner phase faults (see fig. 7.2a,b). Finally, the effect of the line length on arc extinction time can be seen clearly by comparing fig. 7.1a and fig.7.2a. In conclusion, for such line length, balanced 4-legged shunt reactor can be used to achieve successful single-pole switching performance with reclosure at 0.5 sec. However, dead-times of the order of 0.7 sec are necessary if a Y-connected shunt reactor is employed.

7.3 Effect of Fault Position

The 300km transmission system is considered with transposed and untransposed line applications. Simulation cases were run for different fault positions along the line. The effect of compensating the line with a Y-connected shunt reactor ($h_1 = 0.75$) at both ends is also considered.

Fig. 7.3 shows the results of the studies for the system under no-load condition. From fig. 7.3, it can be seen that the extinction time is nearly constant for the line with no compensation. Although the installment of the shunt reactor does not affect the level of the steady-state secondary arc current, their use however increases the faulted phase recovery voltage. This is evident from the higher arc extinction times as shown in fig. 7.3 for the compensated system application. Moreover, lowest arc extinction times are evident for faults at the middle of the line. This is mainly due to the symmetry of the system on the two sides of the fault, which thereby result in total cancellation of the low inductively induced component of both the secondary arc current and the recovery voltage. Finally, the results of fig. 7.3 prove the uneffectiveness of conventional single-pole switching, particularly if 0.5 sec dead-time is required with such a system.

7.4 Effect of The Pre-Fault System Loading

In long line applications, appreciable power load flow does affect, both the secondary arc current and the faulted phase recovery voltage. Under such conditions, the higher sound phase currents induce a much more significant longitudinal voltage in the faulted phase during the dead-time, and thereby contribute to the secondary arc current and recovery voltage[35,22,9,25,28]. Studies on operational systems have shown that the steady-state and transient components of these longitudinal voltages depend heavily on fault position and point on wave initiation[22,25].

As the line end sources are considered identical, a fault at the sending end of the system is mainly investigated. The case where the line is considered to be uncompensated is also studied. However, where the line is

compensated by the 4-legged reactor banks, a value of $X_n = 625\Omega$ is used for the neutral reactance.

7.4.1 No-load condition

The effectiveness of the 4-legged shunt reactor in the transposed line application is evident from fig. 7.4b, which shows a very low recovery voltage of 12.4kV (peak). This, in addition to the very low steady-state secondary arc current in the order of few Amperes, accounts for the fast arc extinction at approximately 90 msec (see fig. 7.4a). In comparison, for the same phase fault (outer phase-"a") with the line being untransposed, the arc extinction time is significantly longer as shown in fig. 7.5a. However, for an inner phase fault (phase-"c"), the arc extinction time is approximately 71 msec longer than that for a transposed line application as seen in fig. 7.6a. In general, these differences in the arc extinction time are largely caused by the higher levels of the secondary arc current and recovery voltage in the untransposed line as compared to the transposed line application. Also, in figs. 7.4b, 7.5b and 7.6b, the beating nature of the recovery voltage is evident. This is due to the fact that in compensated lines, the recovery voltage contains a sinusoidal power frequency voltage and a relatively lower damped sinusoidal voltage component of a natural frequency dictated by the line/reactor combination[38,42,76].

7.4.2 Power transfer from sending to receiving end

Figs. 7.7, 7.8 and 7.9, illustrate the results of studies of a complete single-phase-to-earth fault clearance and reclosure sequence for a fault at the sending end, with a pre-fault power transfer from the sending to the recieving ($V_S/V_R = 1 \angle 25.73^\circ$) of 1262MW.

A comparison of fig. 7.7a and fig. 7.4a, shows that the arc extinction time for the transposed line application is almost four times that under no-load condition. Significant increase in the post-extinction recovery voltage is evident from fig. 7.7b. A maximum value of approximately 260kV is reached by the fault point voltage in 2.75 cycles after arc extinction, which is compared to 12.4kV under no-load condition. Thus, it can be concluded that the recovery voltage rises rapidly after arc extinction, which in addition to higher level of arc current, accounts for the longer extinction time. Fig. 7.7c,d, shows the faulted phase voltage to earth at the sending and receiving ends respectively. It is of interest to note that the voltage at the remote end from the fault is almost constant during the dead-time, apart from the first 1½ cycle after fault clearance, and is significantly higher than that at the fault point. This is essentially due to the phasor relation between the induced voltage components at the receiving end. From fig. 7.7d, the highest overvoltage of 647.3kV or 1.586 p.u. (based on phase-"a" to earth voltage) occurs at the receiving end. Upon fault clearance at the sending end, the drop in the sending end current to zero at time T_{b2} is evident from fig. 7.7e. The offset of the sending end current, particularly during the interval $T_{b4} - T_{b5}$ is also evident in fig. 7.7e. It is of interest to note that the voltage across the neutral reactance attains a constant level of 61.8kV during the secondary arc interval $T_{b3} - T_{ext}$. This is evident in fig. 7.7f, however, similar beating nature to that of the line end voltage is also clear in the neutral reactor voltage waveform after arc extinction.

For the untransposed line application, fig. 7.8 shows several features of the system response under such loading condition. It is interesting to note that the extinction

time in this case is 24 msec shorter than that with the line being transposed, despite the fact that higher steady-state secondary arc current and recovery voltage are evident in this case. However, careful examination of fig. 7.8b in comparison to fig. 7.7b reveals that, the first peak and rate of rise of the recovery voltage in this case is lower, which is more likely accounts for the lower arc extinction time. Faulted phase voltage beat is also evident in this case as shown in fig. 7.8c,d after arc extinction. However, the receiving end voltage decreases as approaching arc extinction, but is still relatively higher compared to the sending end voltage. This is primarily due to line non-transposition in as far as electromagnetic induction is concerned. Similar to the transposed line case, the highest overvoltage occurs at the receiving end, and of a value of 731.7kV or 1.79 p.u. (see fig. 7.8d). No significant difference in the line current is detected from that of the transposed line case (fig. 7.7e and fig. 7.8e). Although the general voltage profile across the neutral reactance as seen in fig. 7.8f is similar to that of the transposed line case (fig. 7.7f), its value, particularly during the secondary arcing interval, is rather lower. This is mainly due to the line unbalance enhanced by the different coupling effects.

Fig. 7.9 illustrates the system response for the inner phase fault with the line being untransposed. It is of interest to note that the secondary arc extinction time in this case is approximately 111 msec and 77 msec shorter than that of the outer phase fault in transposed and un-transposed line cases respectively. However, a study of an inner phase fault in a transposed line application under similar conditions, showed no significant difference in the arc extinction time to that seen in fig. 7.9a. Comparison

of the post-extinction recovery voltage waveforms of fig. 7.7, fig. 7.8 and fig. 7.9, shows that the first peak and the rate of rise of the recovery voltage in this case are lower than those in the two previous cases. This, in conjunction with low secondary arc current of 19.8A (r.m.s.) account for the shorter arc extinction time. However, in comparison to the no-load case, the arc extinction time here is 86 msec longer, which is obviously due to the electromagnetic coupling effect. From fig.7.9d, the receiving end voltage shows a decreasing feature as time approaching extinction, though still significantly higher than that of the sending end (fig. 7.9c). Lower overvoltage upon reclosing is evident in this case (fig. 7.9d) at the receiving end, compared to that with an outer phase fault. Similar to the case of the transposed line, the voltage across the neutral reactor (fig. 7.9f) is generally higher than that for an outer phase fault

Finally, several investigations for different fault locations along the line have indicated that the maximum arc extinction times occur at the line ends.

7.4.3 Power transfer from receiving to the sending end

The effect of reverse power flow to that considered in section 7.4.2 is discussed here in relation to the secondary arc parameters and line terminal voltage.

Fig. 7.10 illustrates the system behaviour when the pre-fault power transfer from the receiving to the sending end is approximately 1262MW, and the line being transposed. A comparison with fig. 7.4 and fig. 7.7 show that the arc extinction time is approximately 33 msec longer than that under no-load condition, and 235 msec shorter than that with the power exported from the sending end. It can

be noticed from fig. 7.10b that the first peak of the recovery voltage is 32.3kV. In this case, 18.2A (peak) is detected for the steady-state secondary arc current, compared to 29.4A under the opposite power flow direction. This reflects the major role of the electromagnetic component of the secondary arc current, which consequently affects its extinction time. As far as the line terminal voltage is concerned, no significant difference is noticed (see fig. 7.7 and fig. 7.10), apart from slightly lower overvoltage peak at the receiving end of 1.55 p.u..

Under the same fault conditions, fig. 7.11 illustrates the system response for the untransposed line application. A comparison with fig. 7.5 and fig. 7.8, shows that the secondary arc extinction time in this case is significantly longer. Moreover, a higher first peak, rate of rise and maximum values of the recovery voltage are evident in this case (see fig. 7.11b). After arc extinction, the breakers were forced to reclose after approximately half a cycle in an attempt to investigate the order of the overvoltages in the system. As a result, the highest overvoltage occurs at the receiving end, and of a value of 1.5 p.u., as seen in fig. 7.11d. From the same figure, the voltage shows a slight increase as the arc proceeds towards extinction. This indicates that the electromagnetically induced voltage component is in phase with the arc path voltage component.

Fig. 7.12 illustrates the system response for an inner phase fault in untransposed line application, under the same loading condition. A comparison with fig. 7.9 shows that the extinction time is 13 msec shorter in this case. This is despite the fact that the steady-state peak secondary arc current is higher in this case. However, slightly lower rate of rise of the recovery voltage in this case accounts for the shorter extinction time. Also, from

fig. 7.12a, it is interesting to note that the secondary arc current was almost extinguished at approximately 212 msec after transition, but a fast rise in the recovery voltage (fig. 7.12b) caused a restrike to take place. Moreover, it can be noticed that the recovery voltage variation is similar to that under opposite power flow direction (see fig. 7.12b and fig. 7.9b). In fig. 7.12d, the receiving end voltage exhibits a similar increasing trend as with an outer phase fault. However, comparison with fig. 7.9d shows clearly the inphase and antiphase nature of the electromagnetically induced voltage component at the receiving end. Here again, the highest overvoltage occurs at the receiving end and of a value of 1.6 p.u..

7.4.4 Uncompensated line application

Although a high percentage of long power transmission systems practically need compensation, especially under no or light load conditions, cases of no compensation may arise in practice. The effect of the pre-fault power transfer on the arc extinction time for uncompensated 300km line is here presented. Briefly, the results of investigations of a transposed and untransposed line applications under various loading conditions are given in Table 7.1. The results are for a fault at the sending end of the system.

Table 7.1 Highest secondary arc extinction time

Power Flow	No-load			$V_S/V_R=1\angle 25.73^o$			$V_S/V_R=1\angle -25.73^o$		
Line and Phase	Transposed "a"	Untransposed "a"	Untransposed "b"	Transposed "a"	Untransposed "a"	Untransposed "b"	Transposed "a"	Untransposed "a"	Untransposed "b"
Ext. Time (msec)	482.8	534.8	602.8	649.6	561.6	698.8	416.4	657.6	625.6

It is clear from Table 7.1 that with such application, the 0.5 sec dead-time is of no practical relevance as extinction times as high as approximately 0.7 sec are expected with untransposed line applications.

7.5 Line Compensated By One Reactor Bank

The effect of using one shunt reactor bank with a neutral reactance adjusted to limit the steady-state capacitive component of the secondary arc current to -j20A (r.m.s.) is investigated. The reactor bank is considered to be connected at the receiving end of the line. Studies for outer phase faults in a transposed line application and both outer and inner phase faults in untransposed line application are discussed. The results are of particular relevance to unidirectional (power flow) transmission systems, where one reactor bank may be needed at the system load end. The cases investigated here are for single-phase-to-earth fault at both ends of the system under no-load condition. The main purpose of these investigations are, 1) to have quantitative information about the arc extinction time involved in such application, and 2) to obtain some information on the possible line overvoltages during the full sequence of events. Such investigations have not been reported in the literature with regard to the secondary arc extinction time.

7.5.1 Transposed line application

Fig. 7.13 shows the system response for a fault at the sending and receiving end of the 300km line. To limit the capacitive component of the secondary arc current to -j20A, neutral reactance of 267Ω is required if two reactor banks are to be used. Examination of fig. 7.1a with such value of X_n gives an arc extinction time of 235 msec. From

fig. 7.13a,e, arc extinction times of 241 and 231 msec are evident for a fault at the sending and receiving ends of the system respectively, hence comparable to those with two reactor application. In fig. 7.13, for both fault positions, the secondary arc current waveforms show slight offset in the first few cycles after transition. This is due to the exponential decay of the faulted phase trapped charge through the fault path. In comparison to the case of the line with two reactor banks, the first peak and the rate of rise of the recovery voltage are slightly lower in this case. Also, higher overvoltages are evident from fig. 7.13c,g with a maximum for the receiving end fault. As far as the voltage across the neutral reactor is concerned (fig. 7.13d), no significant differences from that with two reactor application were found. Several simulation studies revealed insignificant dependency of, the arc extinction time and the closing overvoltages on the fault position.

7.5.2 Untransposed line application

Fig. 7.14 shows the results of investigation for an outer phase fault, with the line being untransposed. It is of interest to note that the arc extinction time for the two fault positions considered here (fig. 7.14a,e) are almost the same. Compared to studies with two reactor banks, the arc extinction times are in the order of 15 - 30 msec less in this case, depending on fault position. A comparison with fig. 7.13, higher line terminal overvoltages, and higher voltage across the neutral reactanc are evident in this case (see fig. 7.13d,h and fig. 7.14d,h).

Fig. 7.15 shows the results of similar study with the fault cosidered to occur on the inner phase. Substantially shorter extinction time from that experienced with the two reactor banks application, for a fault at the sending end

is evident from fig. 7.15a and fig. 7.1a. For the two reactor application, from fig. 7.1a, arc extinction time of 380 msec is observed compared to approximately 161 msec in this case (see fig. 7.15a). This is mainly due to the lower peak secondary arc current and lower first peak and rate of rise of the recovery voltage in this case. A comparison of fig. 7.15 with fig. 7.14 shows that, lower overvoltages occur in this case, however, similar voltage levels are evident across the neutral reactance.

Finally, extensive series of studies of such systems, concerning different fault positions along the line, revealed that, slightly shorter (several milliseconds) extinction times occurs for faults near the middle of the line.

7.6 Summary

The results presented in this chapter demonstrated the close dependency of the arc extinction time on the level of the secondary arc current and the recovery voltage features. These are namely, the first peak, the rate of rise and the maximum value of the recovery voltage. Also, the results clearly indicate that the arc extinction times becomes longer with an increase in the first peak of the recovery voltage. The amount of power transfer and its direction significantly affects the arc extinction time in the transposed line applications, and to a lesser extent in the untransposed line applications. The results also indicated that one 4-legged reactor bank can be used with the transposed line application to affect successful reclosure at 0.5 sec. However, even under no-load condition, such application with untransposed line system is of doubtful use, unless higher dead-time is considered.

Finally, for such line length, dead-time of 0.5 sec

can be adopted only if the line is transposed and compensated by a 4-legged shunt reactor bank(s). However, much longer dead-time is required if the line (transposed or untransposed) is to be compensated by a solidly grounded neutral Y-connected reactor or uncompensated.

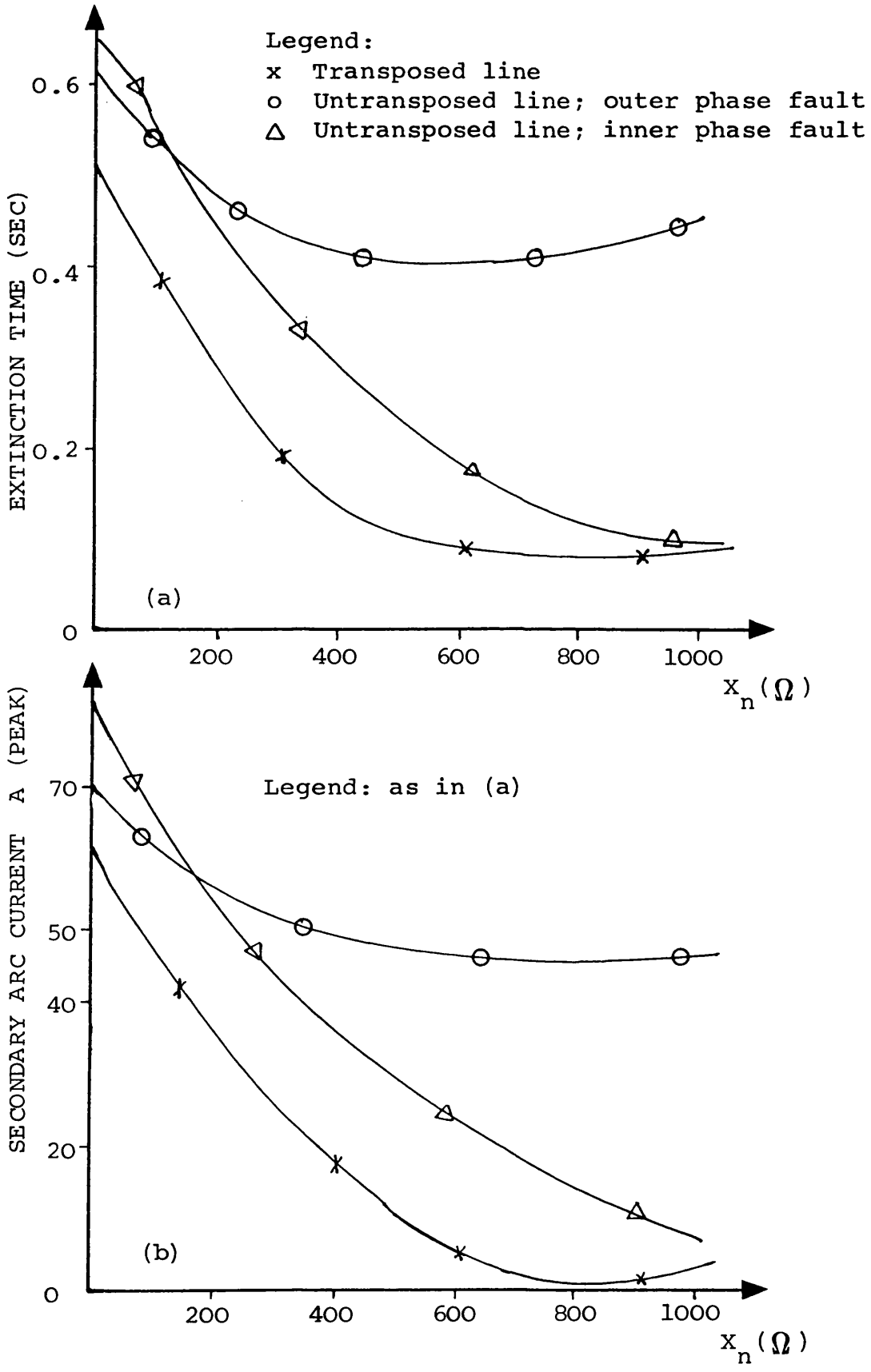

Fig. 7.1 Variation of the secondary arc parameters with X_n

300km line, h_I = 0.75, fault at sending end.

(a) Extinction time

(b) Peak secondary arc current (steady-state)

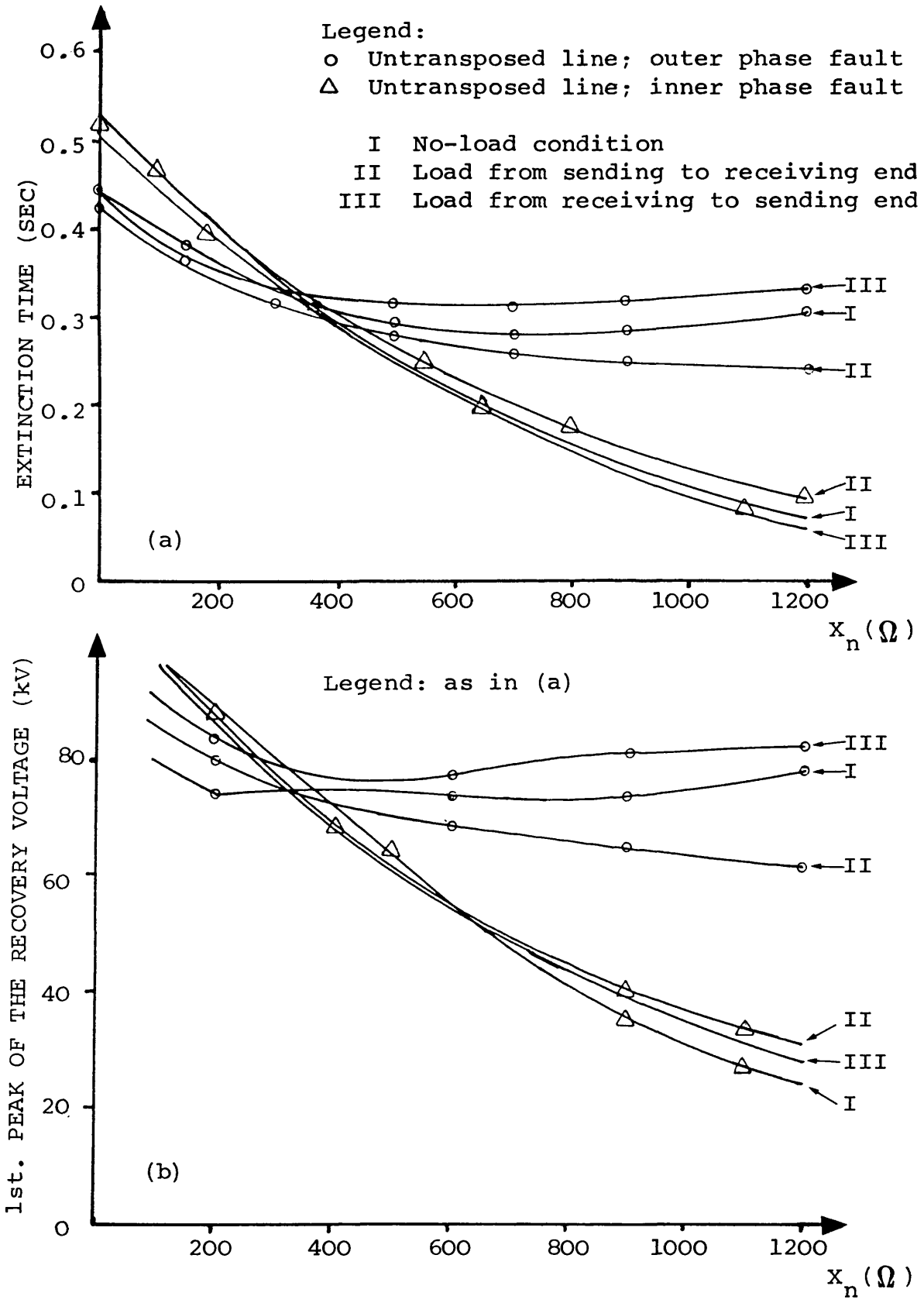

Fig. 7.2 Variation of the arc extinction time and the first peak of the recovery voltage with X_n

200km line, $h_1 = 0.75$, fault at sending end.

(a) Extinction time

(b) First peak of the recovery voltage

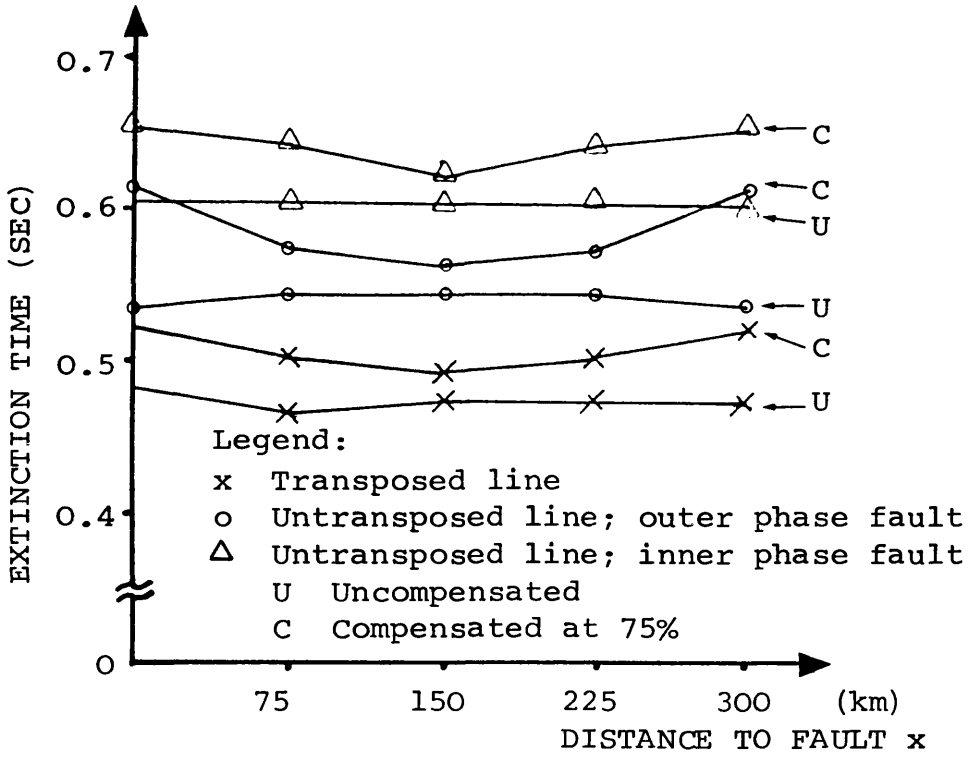

Fig. 7.3 Variation of the arc extinction time with fault position

300km line, no-load condition

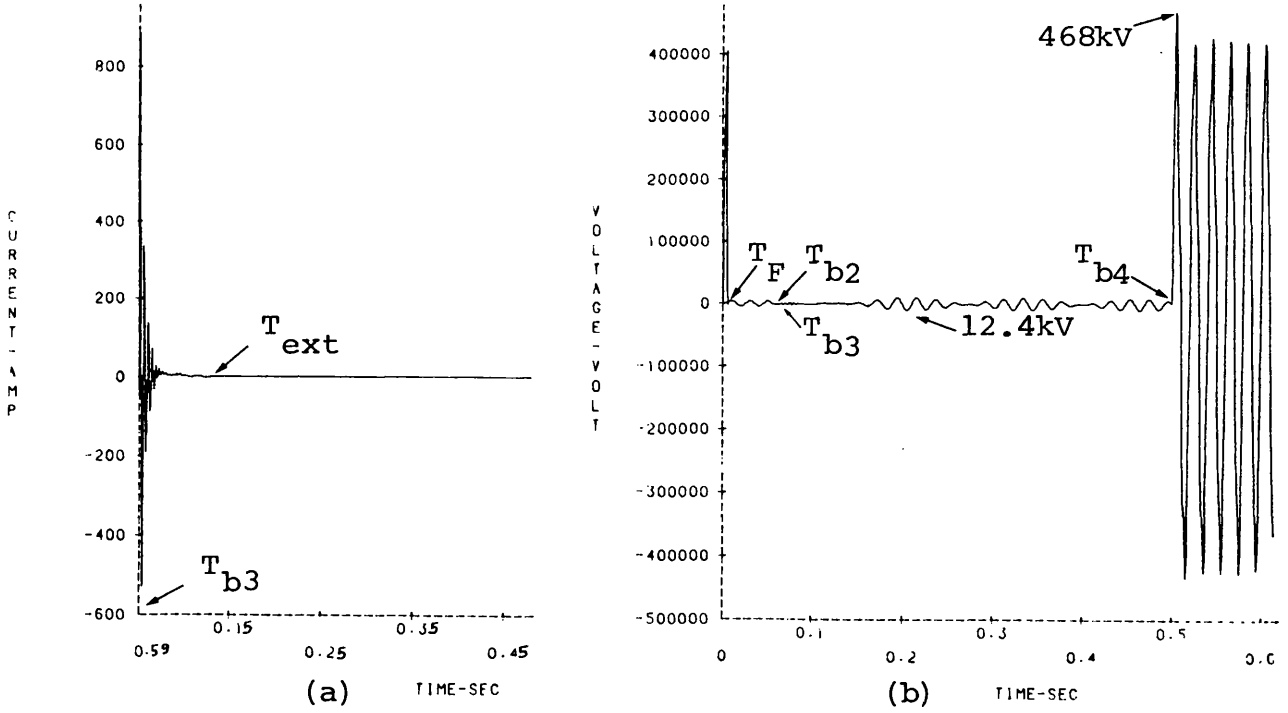

Fig. 7.4 Fault point variables: Transposed line application

L = 300km, fault at sending end, $V_S/V_R = 1\angle 0^o$

T_F = 5 msec, T_{b2} = 50 msec (a.f.), T_{b3} = 59.6 msec (a.f.), T_{ext} = 90.04 msec, T_{b4} = 495.2 msec (a.f.)

(a) Secondary arc current

(b) Fault point voltage to earth

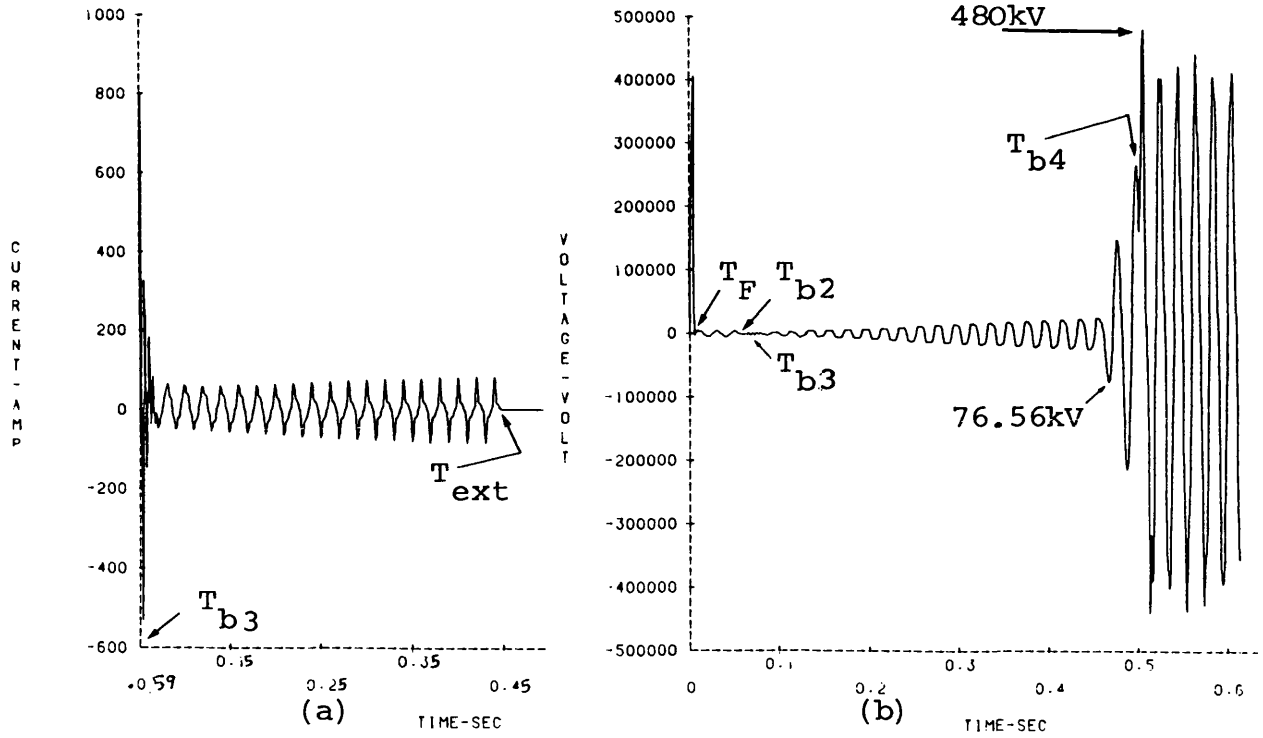

Fig. 7.5 Fault point variables: Untransposed line

L = 300km, fault on outer phase-"a" at sending end, $h_1 = 0.75$, $V_S/V_R = 1\angle 0^o$, $T_F = 5$ msec, $T_{b2} = 50$ msec (a.f.), $T_{b3} = 59.6$ msec (a.f.), $T_{ext} = 396.8$ msec

(a) Secondary arc current
(b) Fault point voltage to earth

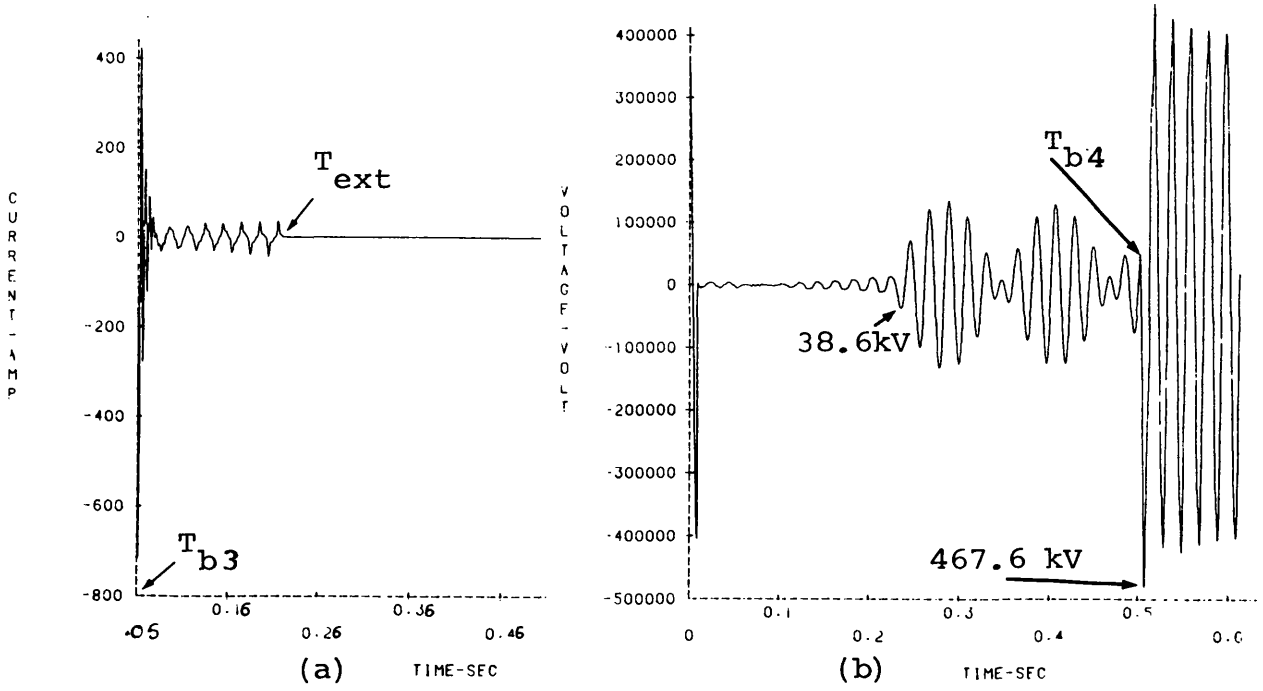

Fig. 7.6 Fault point variables: Untransposed line

L = 300km, fault on inner phase-"c" at sending end, $h_1 = 0.75$, $V_S/V_R = 1\angle 0^o$, $T_{b3} = 60$ msec (a.f.), $T_{ext} = 161.2$ msec, $T_{b4} = 494$ msec (a.f.)

(a) Secondary arc current
(b) Fault point voltage to earth

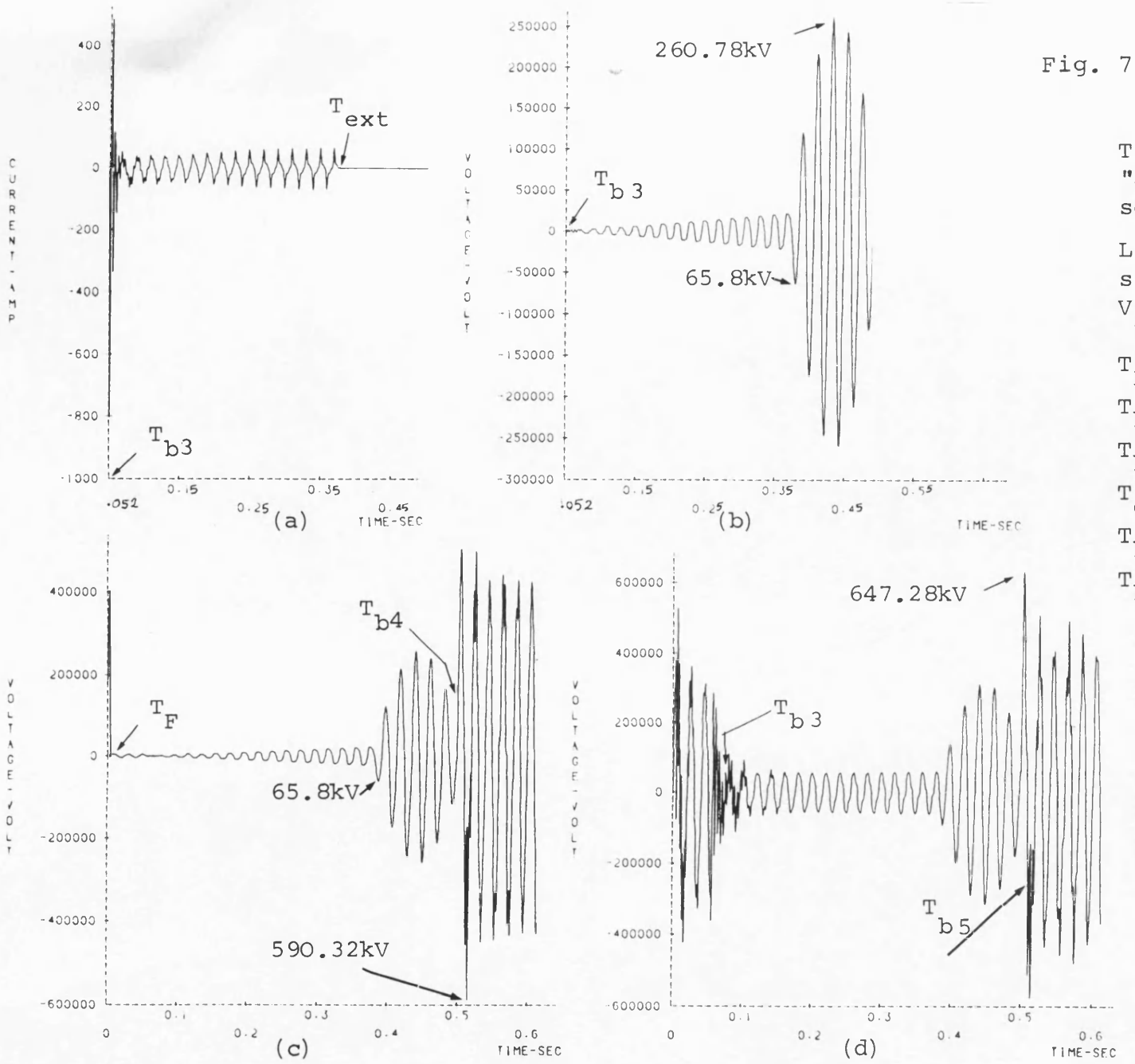

Fig. 7.7 Effect of pre-fault loading

Transposed line application, "a"-phase to earth fault at sending end.

L = 300km, h_1 = 0.75,
s.c.1 = s.c.2 = 5GVA,
$V_S/V_R = 1\underline{/25.73^{o}}$.

T_F = 5 msec,
T_{b2} = 49.2 msec (a.f.),
T_{b3} = 52.4 msec (a.f.),
T_{ext} = 358.8 msec,
T_{b4} = 494.8 msec (a.f.),
T_{b5} = 507.2 msec (a.f.).

(a) Secondary arc current
(b) Secondary arc voltage
(c) "a"-earth voltage at sending end
(d) "a"-earth voltage at receiving end
(e) Phase-"a" current at sending end
(f) Voltage across the neutral reactance at the receiving end

Fig. 7.7 (continued)

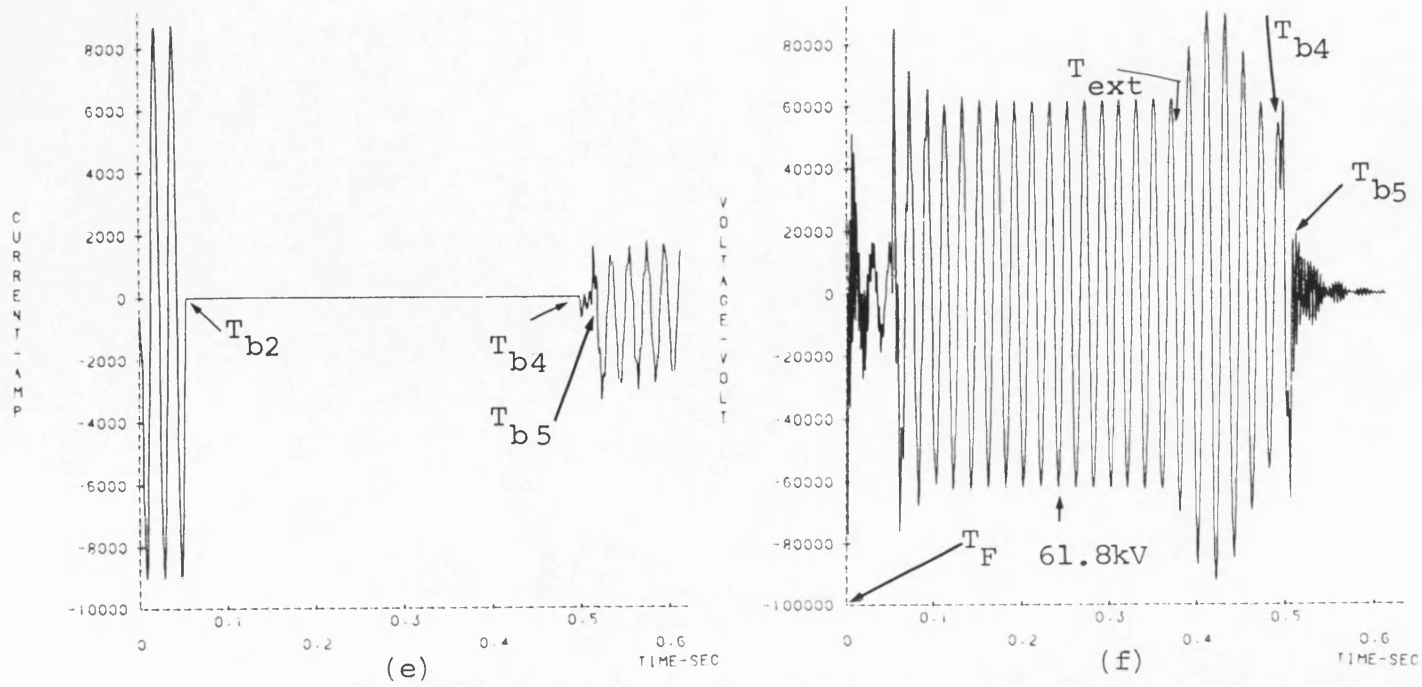

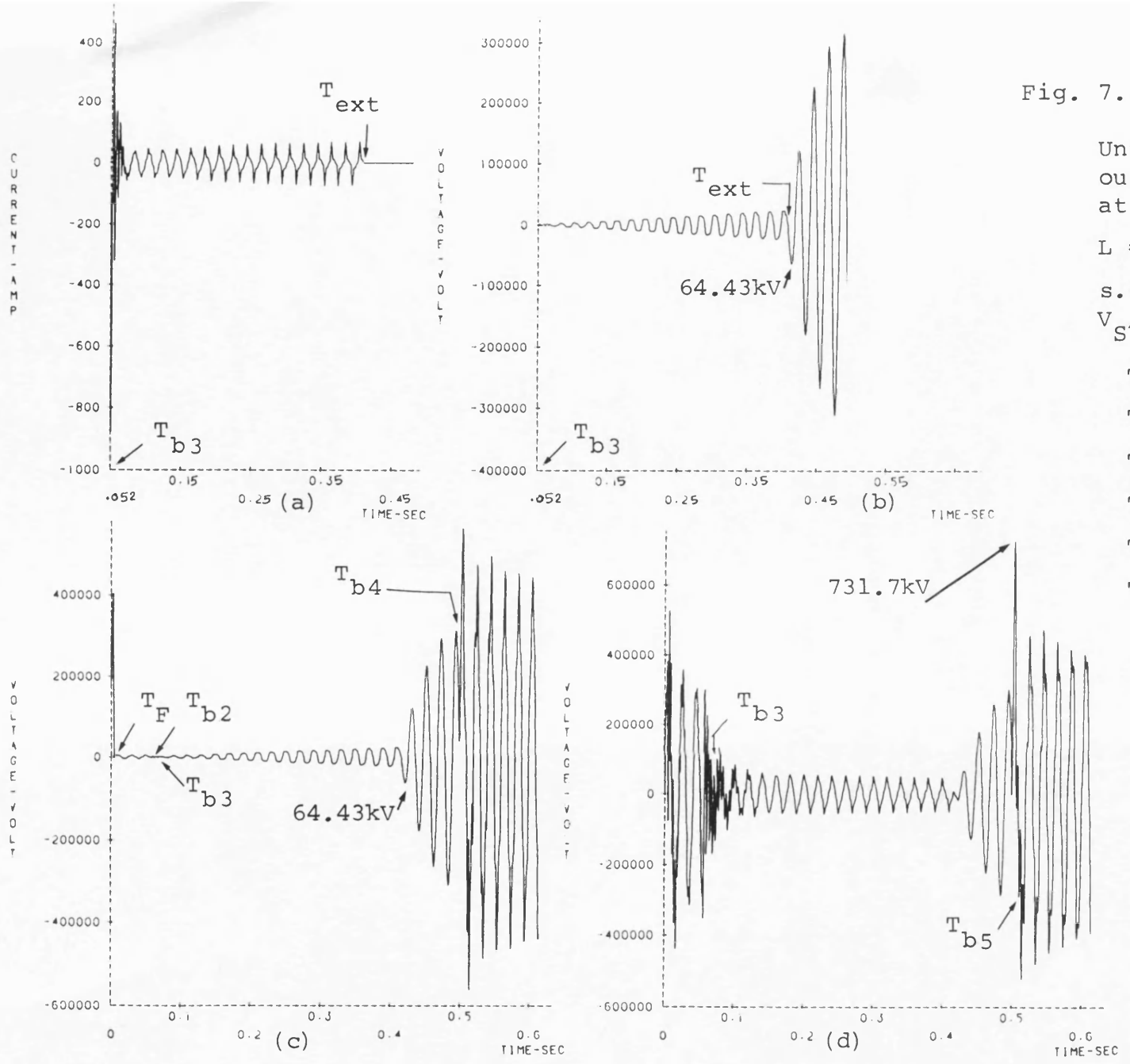

Fig. 7.8 Effect of pre-fault loading

Untransposed line application, outer phase-"a" to earth fault at the sending end.

L = 300km, h_1 = 0.75,

s.c.1 = s.c.2 = 5GVA,

$V_S/V_R = 1\angle 25.73^{o}$.

T_F = 5 msec,

T_{b2} = 49.6 msec (a.f.),

T_{b3} = 52.4 msec (a.f.) ,

T_{ext} = 324.8 msec,

T_{b4} = 494.4 msec (a.f.),

T_{b5} = 508 msec (a.f.).

(a) Secondary arc current
(b) Secondary arc voltage
(c) "a"-earth voltage at sending end
(d) "a"-earth voltage at receiving end
(e) Phase-"a" current at sending end
(f) Voltage across the neutral reactance at receiving end

Fig. 7.8 (continued)

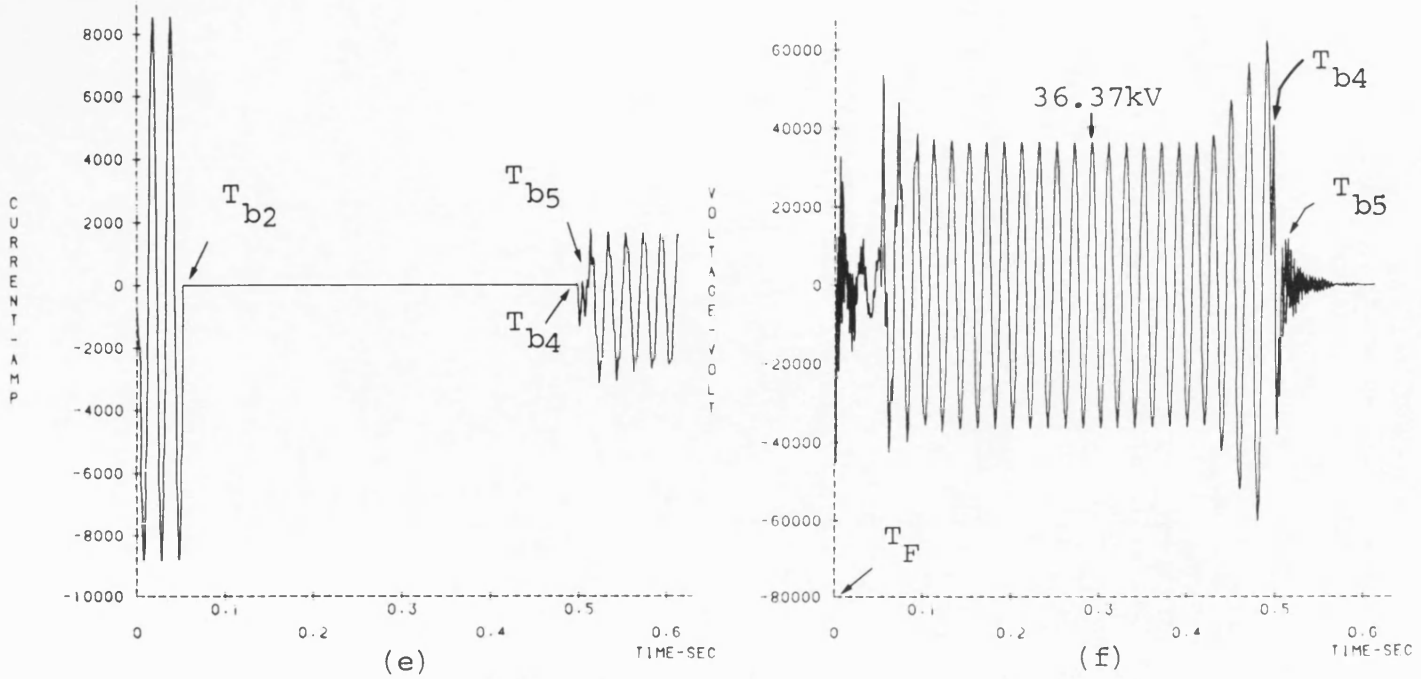

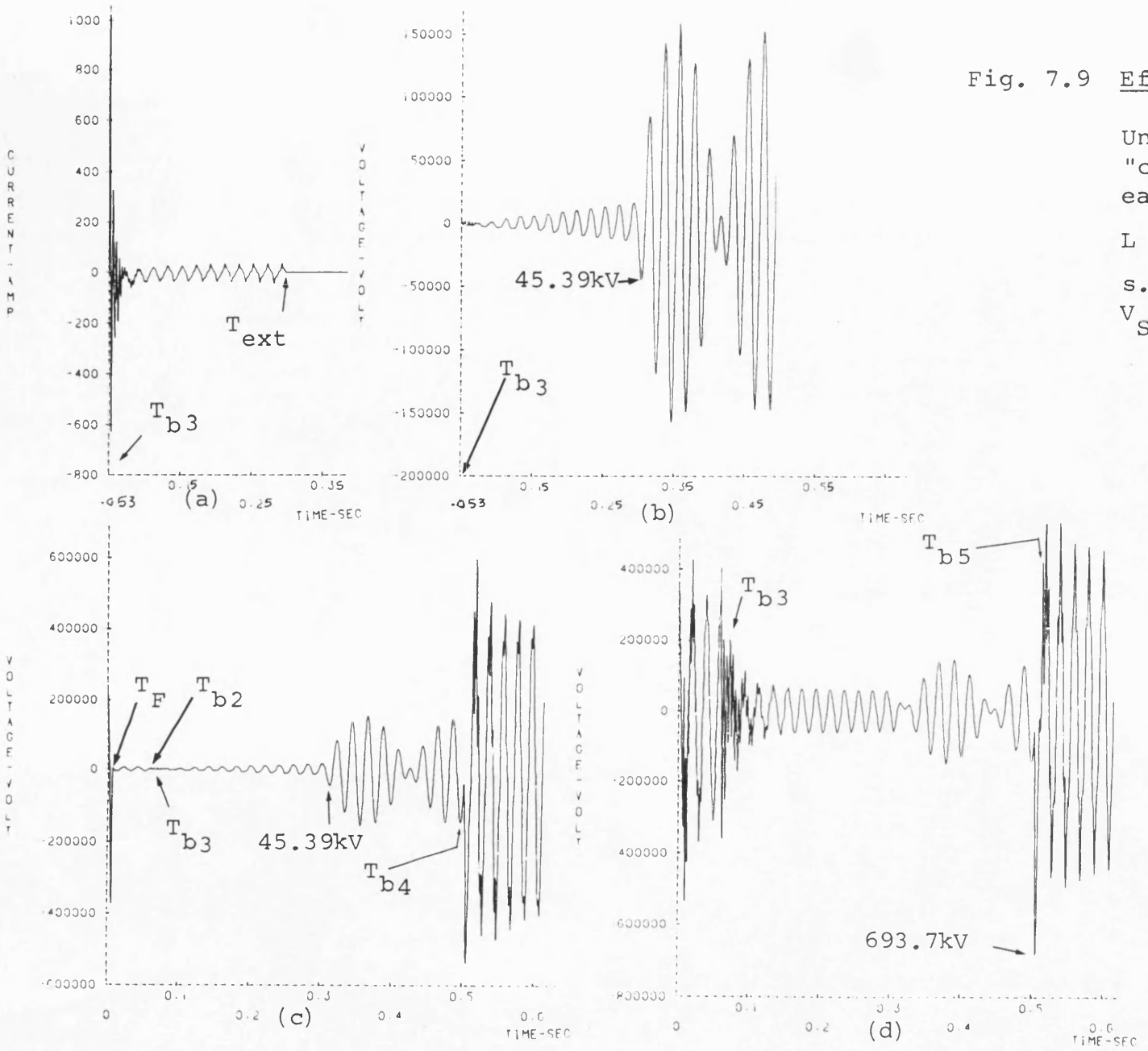

Fig. 7.9 Effect of pre-fault loading

Untransposed line application, "c"-phase (inner phase) to earth fault at sending end.

L = 300km, h_1 = 0.75,

s.c.1 = s.c.2 = 5GVA,

$V_S/V_R = 1/\underline{25.73^\circ}$.

T_F = 5 msec,

T_{b2} = 50.8 msec (a.f.),

T_{b3} = 53.6 msec (a.f.),

T_{ext} = 247.2 msec,

T_{b4} = 495.6 msec (a.f.),

T_{b5} = 508.4 msec (a.f.).

(a) Secondary arc current
(b) Secondary arc voltage
(c) "c"-earth voltage at sending end
(d) "c"-earth voltage at receiving end
(e) Phase-"c" current at sending end
(f) Voltage across the neutral reactance at receiving end

Fig. 7.9 (continued)

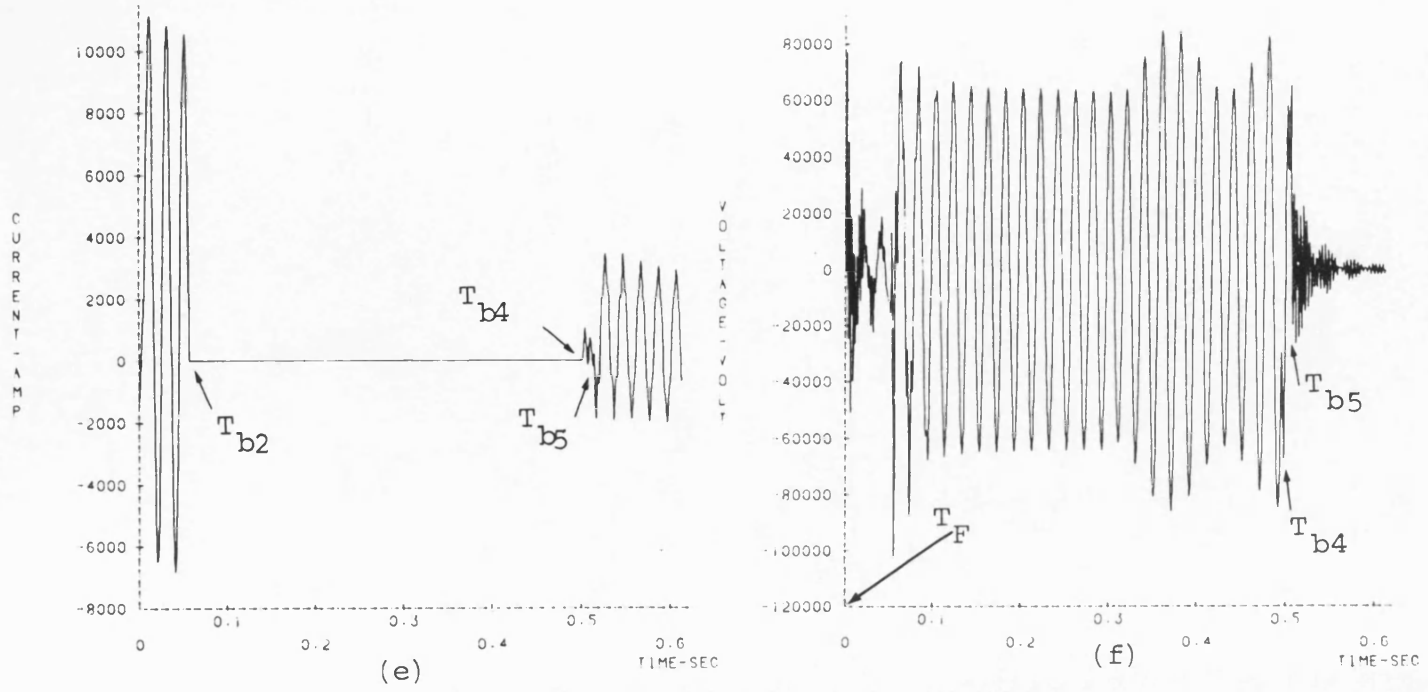

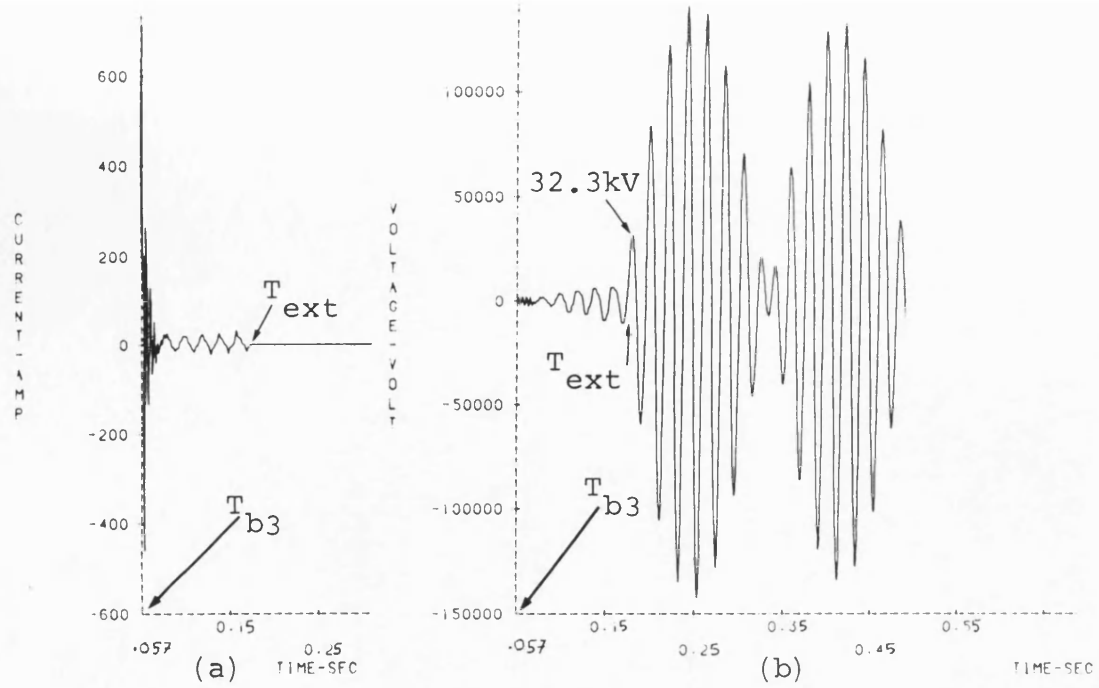

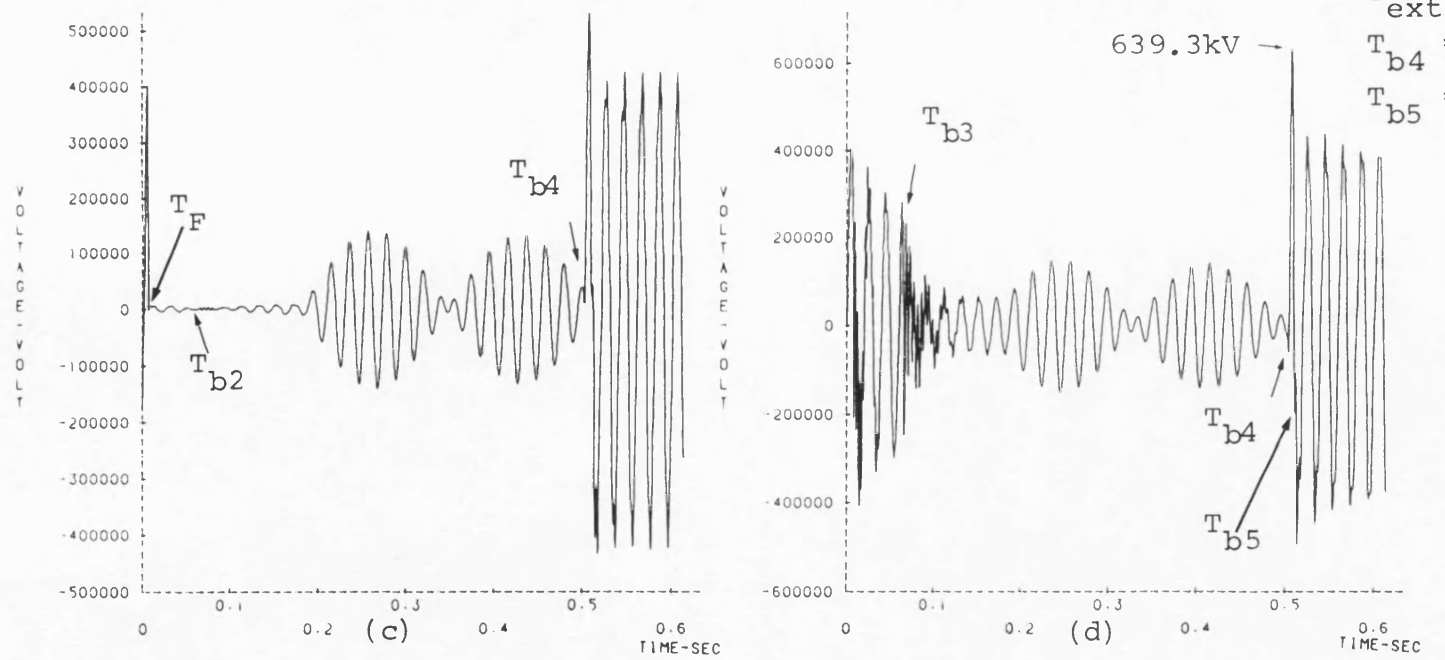

Fig. 7.10 Effect of power transfer direction

Transposed line application, "a"-phase to earth fault at the sending end.

L = 300km, h_1 = 0.75,

$V_S/V_R = 1\angle -25.73^{o}$,

s.c.1 = s.c.2 = 5GVA.

T_F = 5 msec,

T_{b2} = 40.8 msec (a.f.),

T_{b3} = 57.6 msec (a.f.),

T_{ext} = 123.2 msec,

T_{b4} = 496 msec (a.f.),

T_{b5} = 502.8 msec (a.f.).

(a) Secondary arc current
(b) Secondary arc voltage
(c) "a"-earth voltage at sending end
(d) "a"-earth voltage at receiving end

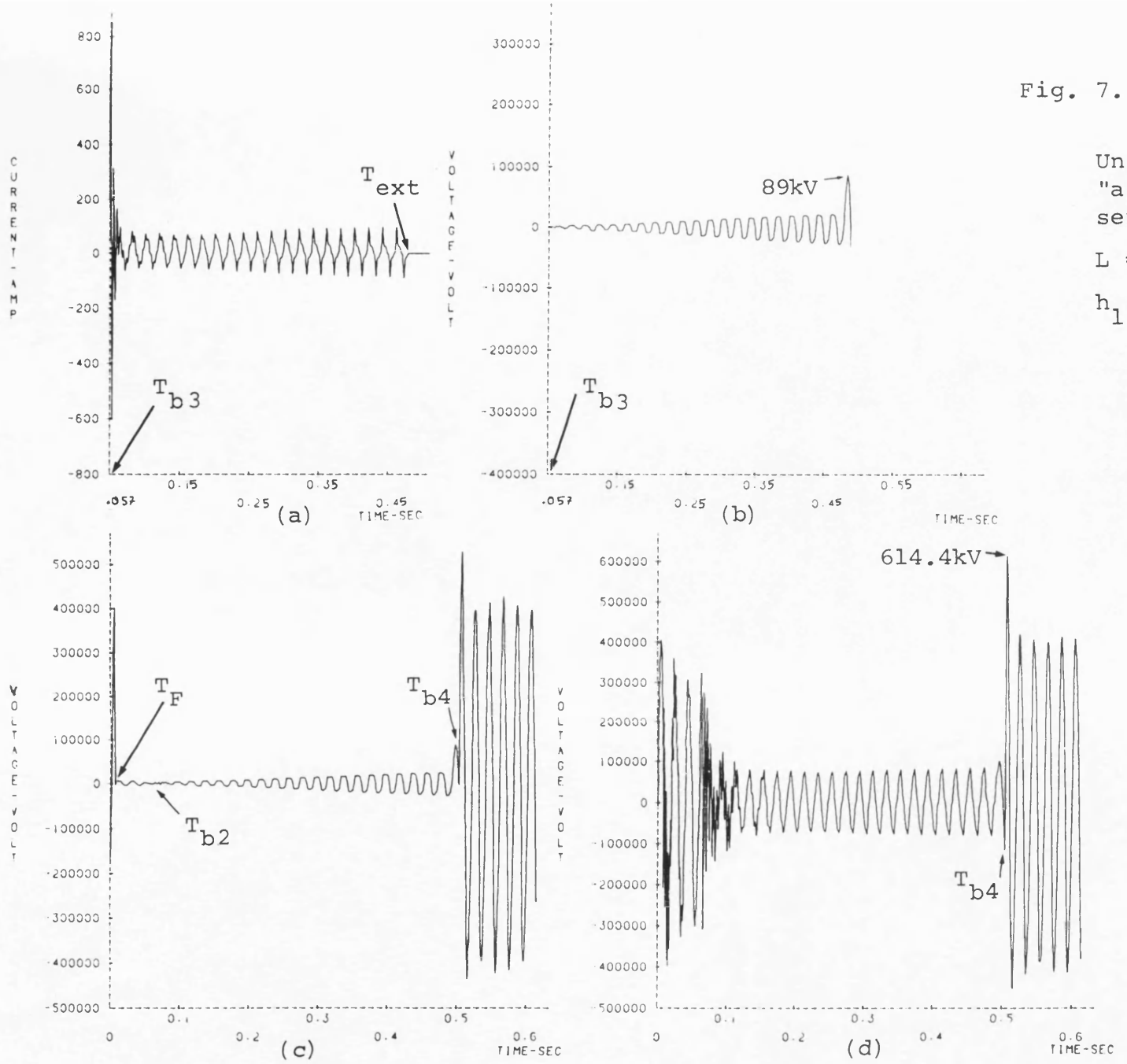

Fig. 7.11 Effect of power transfer direction

Untransposed line application, "a"-phase to earth fault at sending end.

L = 300km, $V_S/V_R = 1\angle -25.73^{o}$,

h_1 = 0.75, s.c.1=s.c.2= 5GVA .

T_F = 5 msec,

T_{b2} = 40.8 msec (a.f.),

T_{b3} = 57.6 msec (a.f.),

T_{ext} = 428.4 msec,

T_{b4} = 496 msec (a.f.),

T_{b5} = 504 msec (a.f.).

(a) Secondary arc current
(b) Secondary arc voltage
(c) "a"-earth voltage at sending end
(d) "a"-earth voltage at receiving end

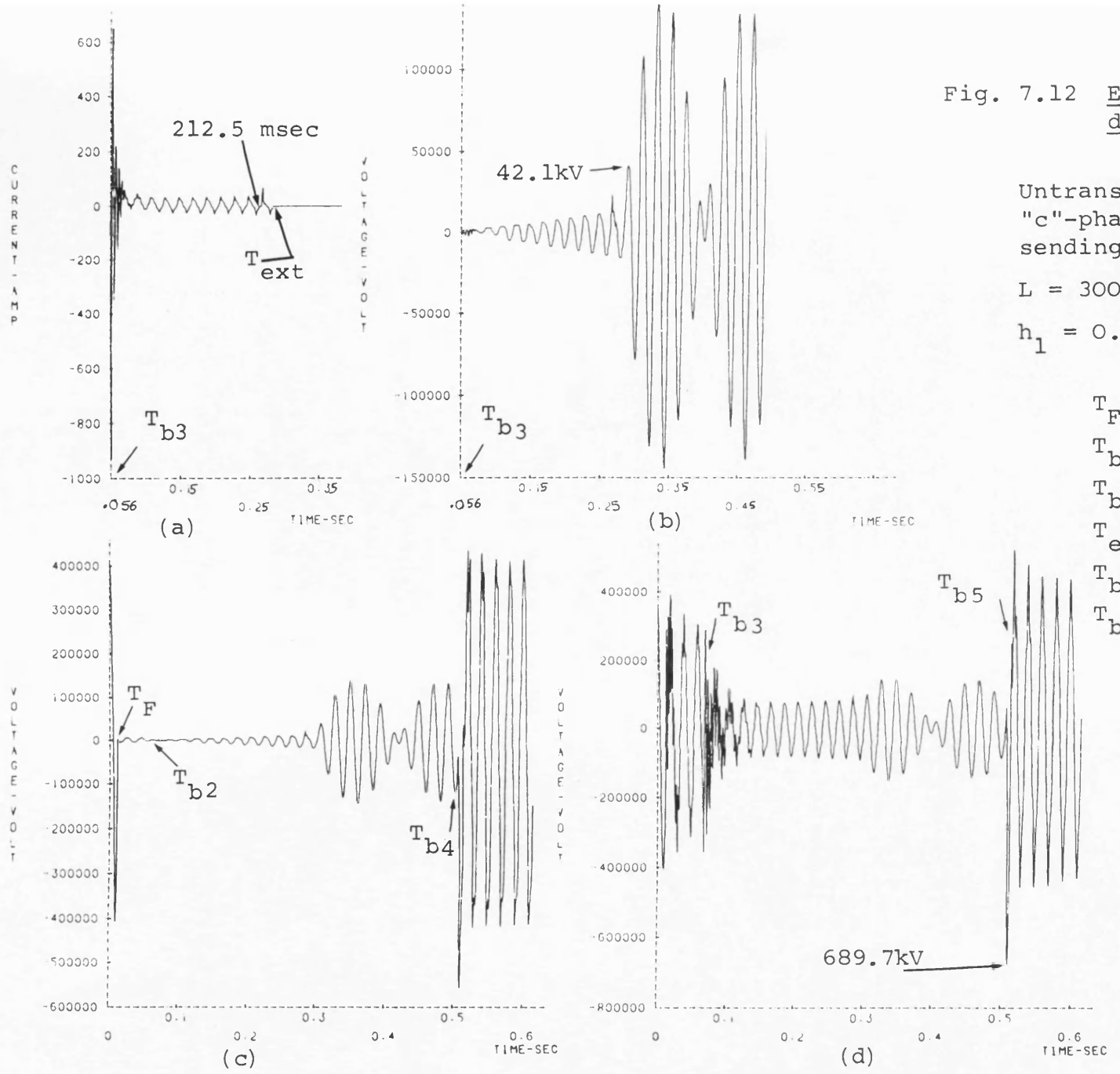

Fig. 7.12 Effect of power transfer direction

Untransposed line application, "c"-phase to earth fault at sending end.

L = 300km, $V_S/V_R = 1\angle -25.73^\circ$,

h_1 = 0.75, s.c.1 = s.c.2 = 5GVA.

T_F = 5 msec,

T_{b2} = 40.4 msec (a.f.),

T_{b3} = 56.4 msec (a.f.),

T_{ext} = 234 msec,

T_{b4} = 495.2 msec (a.f.),

T_{b5} = 502 msec (a.f.),

(a) Secondary arc current
(b) Secondary arc voltage
(c) "c"-earth voltage at sending end
(d) "c"-earth voltage at receiving end

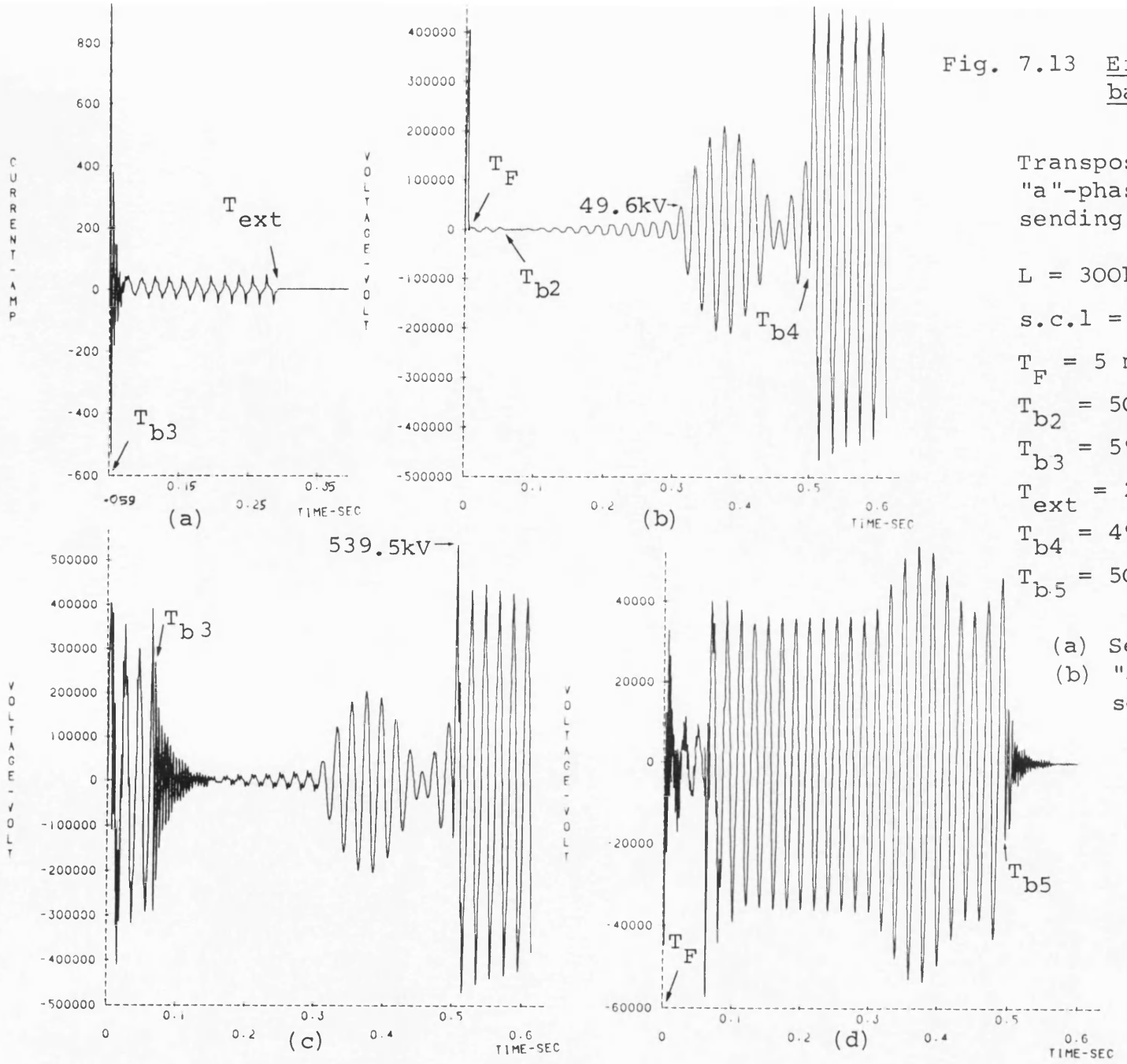

Fig. 7.13 Effect of using one reactor bank

Transposed line application, "a"-phase to earth fault at sending end.

L = 300km, $V_S/V_R = 1\angle 0^\circ$, $h_1 = 0.75$, s.c.1 = s.c.2 = 5GVA.

T_F = 5 msec,

T_{b2} = 50 msec (a.f.),

T_{b3} = 59.6 msec (a.f.),

T_{ext} = 241.6 msec,

T_{b4} = 494.4 msec (a.f.),

T_{b5} = 504.8 msec (a.f.).

(a) Secondary arc current
(b) "a"-earth voltage at sending end
(c) "a"-earth voltage at receiving end
(d) Voltage across the neutral reactance

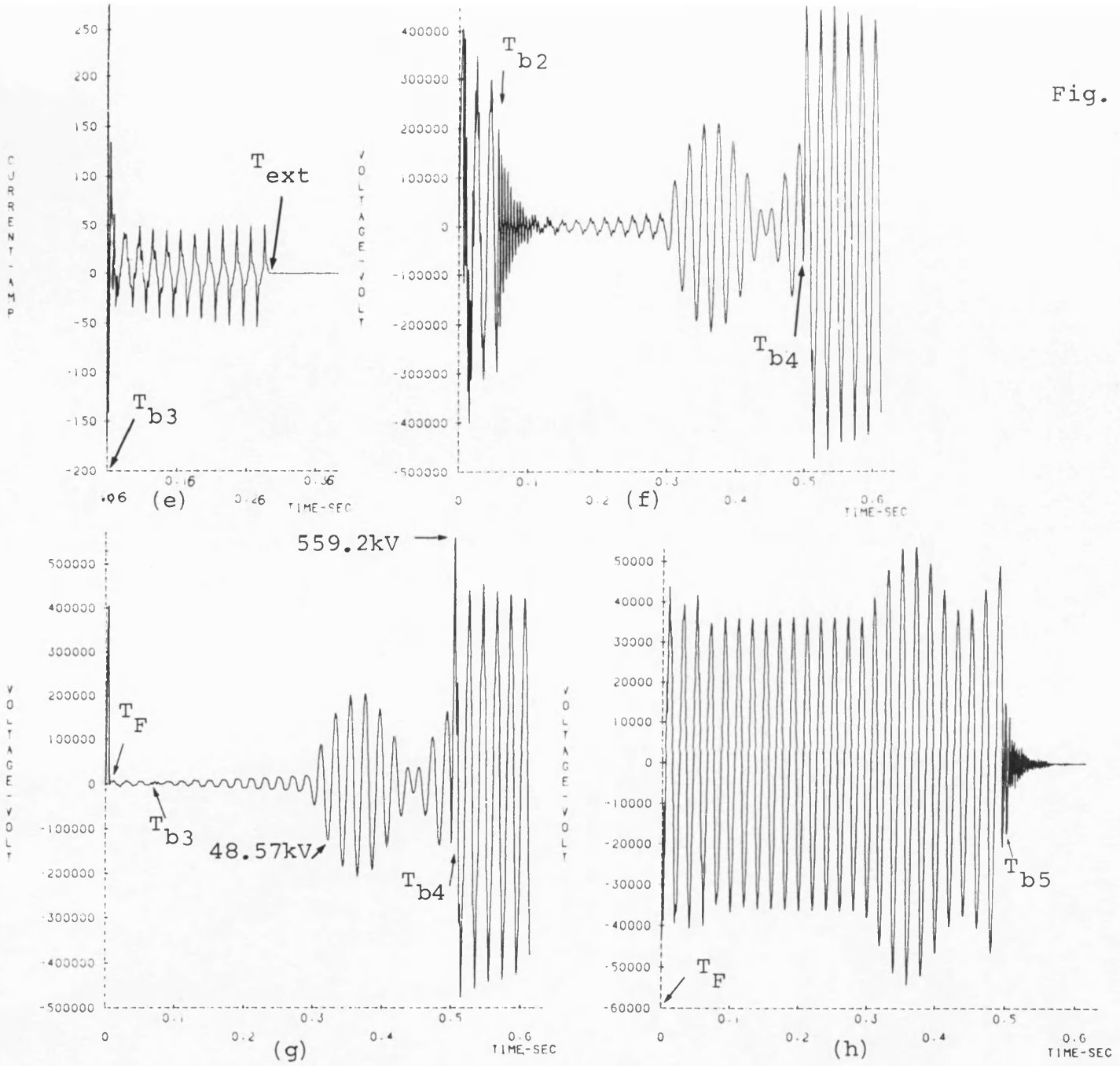

Fig. 7.13 (continued)

Fault at the receiving end

T_{b2} = 49.6 msec (a.f.),
T_{b3} = 60 msec (a.f.),
T_{ext} = 231 msec,
T_{b4} = 494.4 msec (a.f.),
T_{b5} = 504.8 msec (a.f.).

(e) Secondary arc current
(f) "a"-earth voltage at sending end
(g) "a"-earth voltage at receiving end
(h) Voltage across the neutral reactance

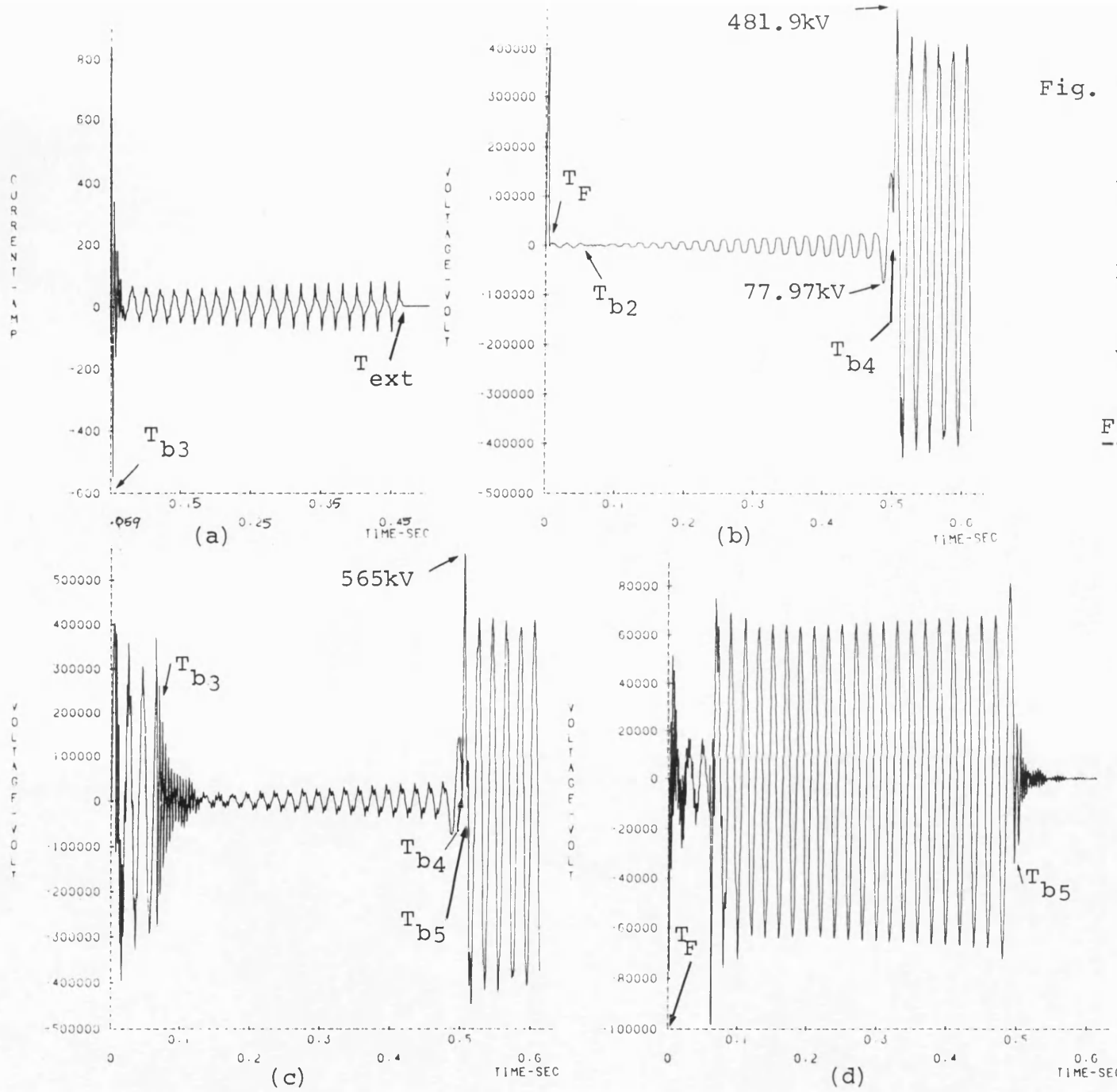

Fig. 7.14 Effect of using one reactor bank

Untransposed line application, "a"-phase to earth fault.

L = 300km, h_1 = 0.75, T_F = 5 msec

s.c.1 = s.c.2 = 5GVA,

$V_S/V_R = 1\angle 0^\circ$.

Fault at sending end

T_{b2} = 50 msec (a.f.),
T_{b3} = 59.6 msec (a.f.),
T_{ext} = 416.8 msec,
T_{b4} = 495.6 msec (a.f.),
T_{b5} = 506 msec (a.f.).

(a) Secondary arc current
(b) "a"-earth voltage at sending end
(c) "a"-earth voltage at receiving end
(d) Voltage across the neutral reactance

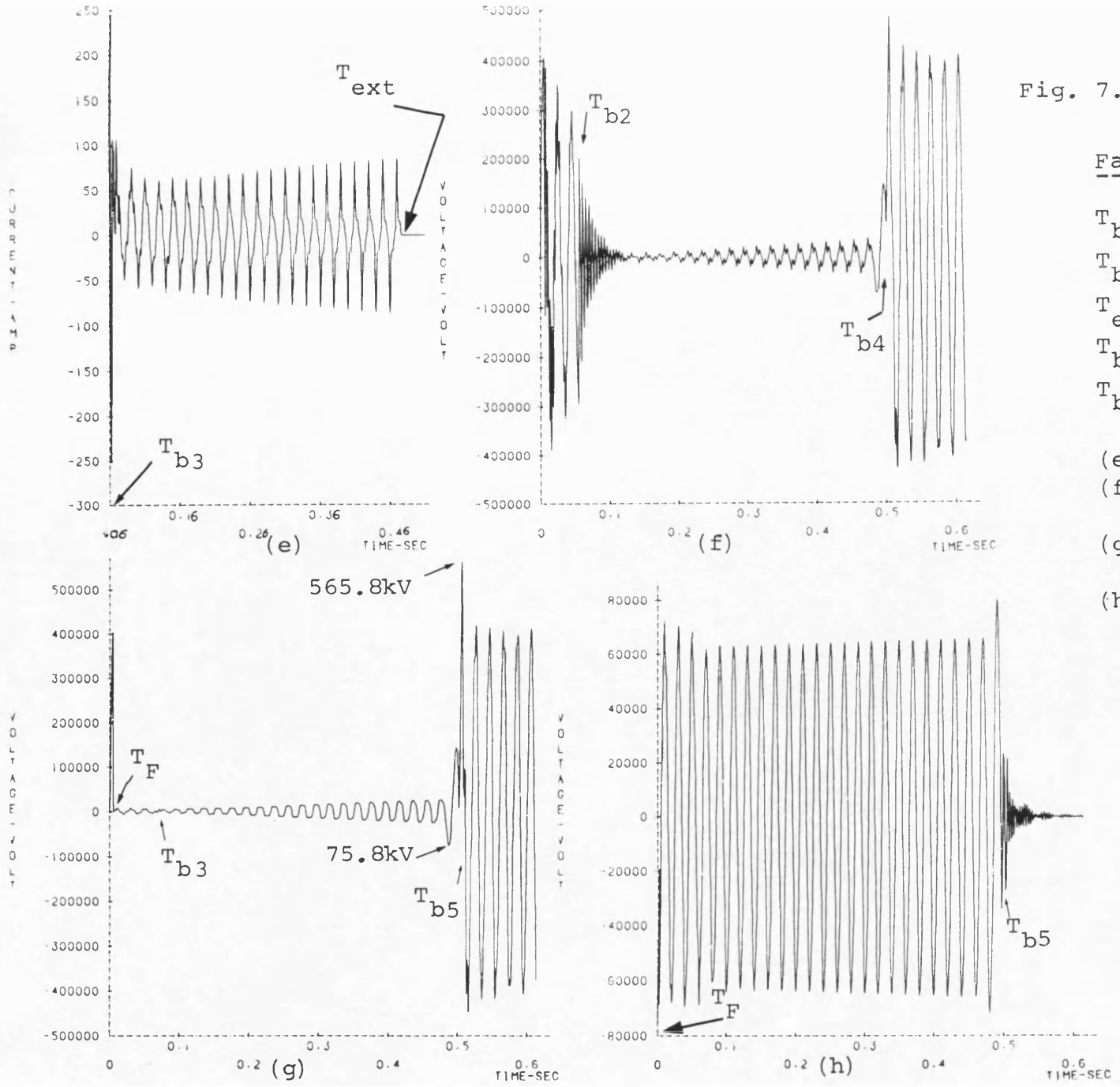

Fig. 7.14 (continued)

Fault at the receiving end

T_{b2} = 49.6 msec (a.f.),
T_{b3} = 60 msec (a.f.),
T_{ext} = 416.4 msec,
T_{b4} = 495.6 msec (a.f.),
T_{b5} = 506 msec (a.f.).

(e) Secondary arc current
(f) "a"-earth voltage at sending end
(g) "a"-earth voltage at receiving end
(h) Voltage across the neutral reactance

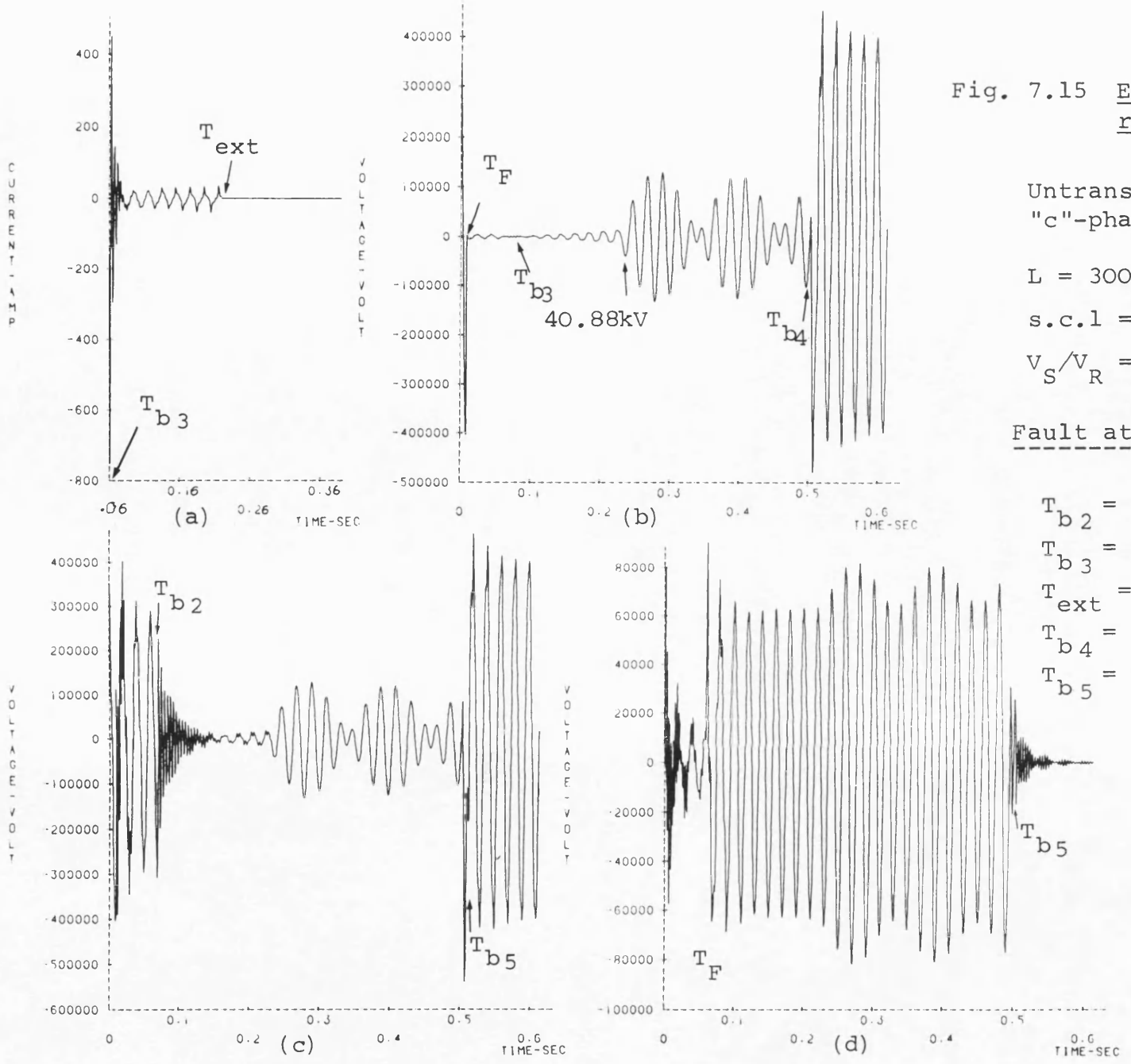

Fig. 7.15 Effect of using one reactor bank

Untransposed line application, "c"-phase to earth fault.

L = 300km, h_1 = 0.75, T_F = 5 msec,

s.c.1 = s.c.2 = 5GVA,

$V_S/V_R = 1\angle 0^o$.

Fault at sending end

T_{b2} = 50 msec (a.f.),

T_{b3} = 60 msec (a.f.),

T_{ext} = 161.2 msec,

T_{b4} = 494.8 msec (a.f.),

T_{b5} = 505.2 msec (a.f.).

(a) Secondary arc current
(b) "c"-earth voltage at sending end
(c) "c"-earth voltage at receiving end
(d) Voltage across the neutral reactance

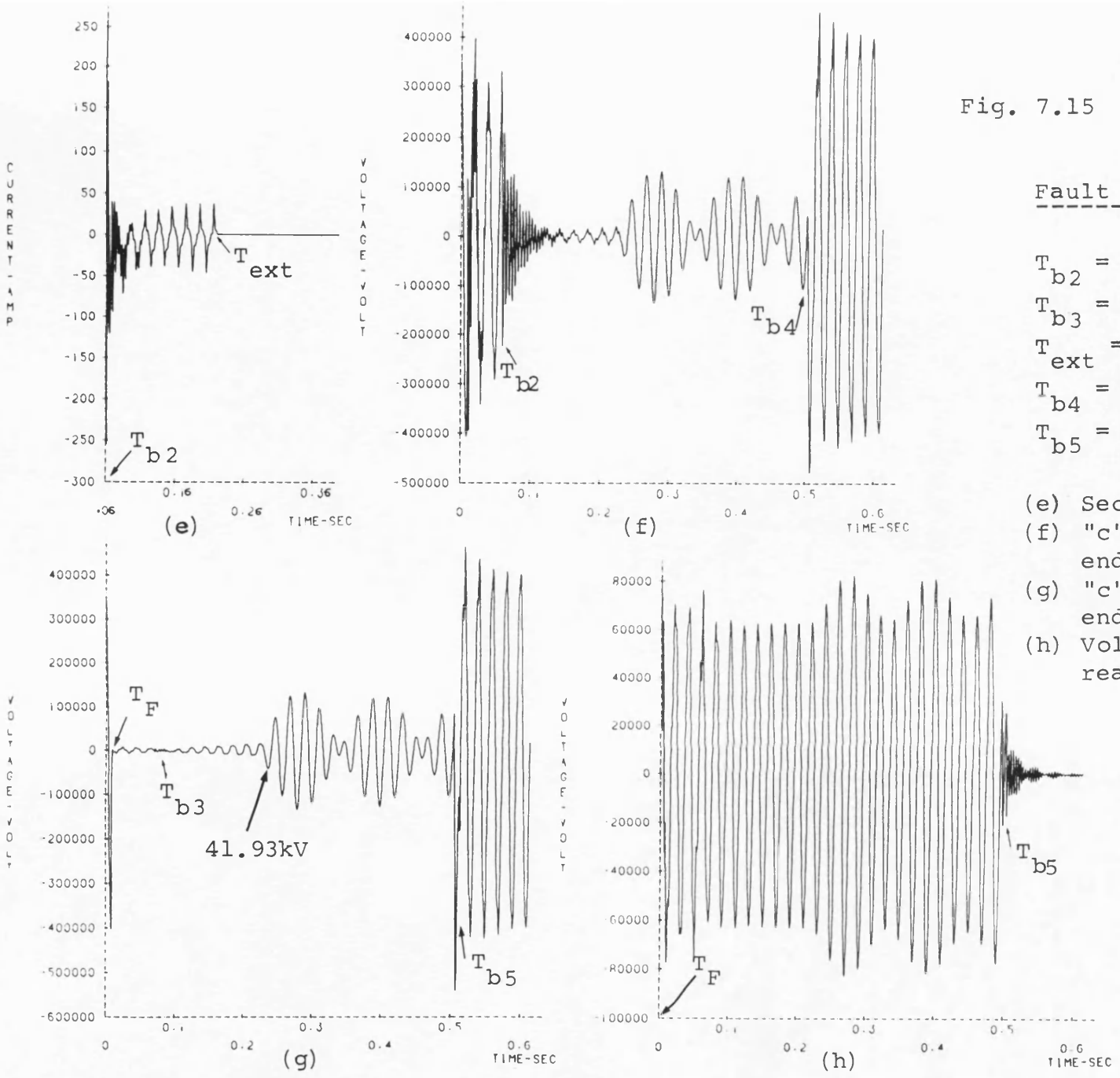

Fig. 7.15 (continued)

Fault at the receiving end

T_{b2} = 49.6 msec (a.f.),
T_{b3} = 60 msec (a.f.),
T_{ext} = 161.2 msec,
T_{b4} = 494.8 msec (a.f.),
T_{b5} = 505.2 msec (a.f.).

(e) Secondary arc current
(f) "c"-earth voltage at sending end
(g) "c"-earth voltage at receiving end
(h) Voltage across the neutral reactance

CHAPTER 8

SYSTEM STUDIES: THE HYBRID METHOD OF AUTORECLOSURE

8.1 Introduction

The hybrid method of autoreclosure[3] is based upon clearing the fault by conventional single-pole switching followed by de-energisation of the sound phases. Three-phase reclosure at a later time is used to return the transmission system to normal operation. By de-energising the sound phases, the secondary arc current and the recovery voltage at the fault point are decreased to low values, resulting in fast arc extinction. The advantage of implementing such a method is clear, though depending on the system stability limits, the timing of de-energising the sound phases can be of importance in securing fast reclosure. Moreover, there are advantages to be gained in implementing such a method over the conventional single-pole switching with slow reclosure, especially when the pre-fault power transfer is high.

The mathematical representation of the system during the whole sequence of events as developed in chapters 2 to 5, is used to obtain the system response. Mainly a 300km untransposed transmission line system is investigated. The line is considered to be compensated by two Y-connected with solidly grounded neutrals reactor banks , at the line

remote ends. In section 8.7, the possibility of implementing the hybrid method in a system with one reactor bank is investigated. The line terminal source at each end is considered of 5GVA capacity, and of $Z_{So}/Z_{Sl} = 1$. A degree of p.p.s compensation of 0.75 is used throughout the studies presented in this chapter. The pre-fault power transfer is considered either zero or approximately 1262MW ($V_S/V_R = 1 \angle \pm 25.73^{o}$). A fault on either outer or inner phase conductors is investigated. The effect of different factors on the secondary arc extinction time and the system reclose overvoltages are here investigated. These include:-

1. The transmission distance.
2. The de-energisation time of the sound phases.
3. The shunt reactor parameters.
4. The pre-fault power transfer and fault position.
5. The line source parameters.
6. The line transposition.

There is practically no reference in the literature to the effect of implementing the hybrid method of auto-reclosure on the secondary arcing process and consequently on the arc extinction time. Therefore, the studies presented in this chapter are mainly directed towards its assessment. Also, the results obtained here can be used as guidelines for stability studies of such system implementation.

8.2 Effect of The Transmission Distance

It is a known fact that the secondary arc current increases almost linearly with the transmission distance, and consequently also its extinction time. It is therefore felt necessary to examine the arc extinction time for different line lengths in a system implementing the hybrid method of autoreclosure. Fig. 8.1 shows the variation of

the arc extinction time with the line length, for an outer phase fault at the sending end of the system. The studies were performed with zero pre-fault power transfer. The results of investigation for transposed and untransposed line applications in systems implementing conventional single-pole switching are also incorporated in fig. 8.1 for comparison. From fig. 8.1, it is clear that with the hybrid method of autoreclosure, the arc extinction time is almost constant, i.e., unaffected by the line length. This is compared to a significant increase in the arc extinction time with line length in the conventional single-pole switching implementations. Also from fig. 8.1, it can be concluded that, for lines over 300km in length, the requirements for 0.5 sec dead-time can still be met with the hybrid method of autoreclosure.

8.3 Effect of Sound Phase De-Energising Time

The effect of the sound phase de-energising time is investigated for the 300km untransposed line application. The fault is considered to occur at the sending end of the system on the outer phase. The de-energising time is varied at about 50 msec intervals and the overall arc extinction time is obtained. The results are shown in fig. 8.2, which represent the overall arc extinction time T_{ext} and also the time difference T_x between the sound phase de-energising and arc extinction. It is evident from fig. 8.2 that T_x decreases with an increase in the sound phase de-energising time. However, in all, arc extinction occurs within 17 - 27 msec after de-energisation. It is worth noting that, although arc extinction occurs quickly after de-energisation, switching may endanger the system stability. Therefore, it is necessary to delay the sound phase de-energisation as late as possible within the specified dead-time.

Based on the above argument, and the results shown in fig. 8.2, the de-energising time of the sound phases is

specified to occur 18 cycles (based on 50Hz) after fault clearance. Such a time setting is adopted throughout the studies to be presented in the following sections. Similar investigations to those above were performed for an inner phase fault. The results were in close agreement with those shown in fig. 8.2.

8.4 Effect of The Shunt Reactor Parameters

In addition to the fault path arc, the Y-connected shunt reactor at the line remote ends are the leakage mean of the line remnant charge. Therefore, it is felt necessary to investigate the effect of the reactor parameters namely, the degree of p.p.s. compensation (h_1) and the quality-factor (Q).

Extensive series of studies on the 300km untransposed line transmission system is performed. The Q-factor was varied in the range of 50 - 350 and h_1 variation was in the range of 0.5 - 1.25. From the results obtained, the following are realised :-

a. For an outer phase fault, the arc extinction time was found to be constant for the different values of the Q-factor. However, a small variation was observed (few milliseconds) with varying h_1.

b. For an inner phase fault, a slight increase in the arc extinction time with increasing Q-factor and increasing h_1 was observed.

The above mentioned variations in the arc extinction time for outer and inner phase faults, are probably caused by the different resonating frequencies of the line capacitances and reactor inductance. No correlation could be drawn from the results concerning the de-energisation

instant of the sound phases and the arc extinction time in these studies.

8.5 Effect of The Pre-Fault Loading And Fault Position

8.5.1 Fault at the sending end: no-load condition

The behaviour of the fault arc path is exemplified in fig. 8.3. Fig. 8.3a displays clearly the reduction of the primary arc current following clearance at the sending end at time T_{b2}. The first transition to a secondary arcing state is also evident. However, the secondary arc current is relatively so small and the details in the period $T_{b3} - T_{ext}$. have to be appreciated from fig. 8.3b. The final arc extinction occurs 18 msec after the last sound phase breaker pole clearance. This gives an overall arc extinction time of approximately 373 msec as seen in fig. 8.3b. Although the secondary arc current waveform is distorted, the reduction in the peak value is evident after de-energising the sound phases. The steady-state secondary arc current waveform after de-energisation, is shown in fig. 8.3c. This waveform is based upon a constant arc resistance of $0.5\,\Omega$. It is of interest to note that the peak current reaches a maximum of around 90A, and rings down in a beating manner. The beat frequency is obviously dictated by the shunt reactor and line parameters. Such high peaks are most likely caused by the high beating voltage in the sound phases after de-energisation (see fig. 8.5). The arc path voltage after the first arc transition up to T_{ob} is shown in fig. 8.3d. It is evident that the arc voltage waveform builds up in a beating manner to values up to 400kV peaks after arc extinction. Also clear from fig. 8.3d is the presence of more than two frequencies, which is a characteristic of the compensated untransposed line, particularly for the outer phase[33].

Fig. 8.4 illustrates the faulted phase response at the sending and receiving ends. It can be seen from fig. 8.4b that the voltage at the receiving end (remote from fault) exhibits the usual high frequency travelling-wave induced distortion during the primary arc period[57]. Considerable high frequency distortion also occurs subsequent to clearance at the receiving end at time T_{b3}. Similar effects are also observed after de-energising the sound phases (see fig. 8.4b). It is of interest to note that comparable reclosing over-voltage at both ends of approximately 1.2 p.u. are evident. Fig. 8.4c and fig. 8.4d show the variation of the faulted phase current at the sending and receiving end respectively. It is evident that the non-simultaneous closure of the breaker pole at both ends, cause the high frequency distortion and unidirectional current variation at the sending end for over 5 cycles. This compares to about one cycle for the receiving end current waveform.

Fig. 8.5 shows the sound phase voltages at each end. Fig. 8.5b shows that the middle phase, fault point voltage exhibits higher values than the rest during the primary arc period. The beating ring down of the voltage at both ends is marked clearly after de-energising the sound phases (see fig. 8.5). Successful reclosure is achieved at times $T_{b7} - T_{b13}$. The sending end breaker closes first, starting with phase-"c" pole followed by phase-"a", "b", then the receiving end breaker in the "a"-"b"-"c" sequence. The highest overvoltage occurs on phase-"b" remote from fault and of a value of 1.637 p.u..

A series of studies have been carried out to determine the effect of the fault location on the arc extinction time, The results indicated no difference from those presented, bearing in mind the different sequence and clearance time of the breaker poles.

8.5.2 Fault at the sending end : Power transfer from sending to receiving end ($V_S/V_R = 1\angle 25.73^o$)

Fig. 8.6 illustrates the secondary arc behaviour following a fault at the sending end when the pre-fault power transfer imported to the receiving end is approximately 1262MW. Extinction of the secondary arc occur at 31 msec after de-energising the last sound phase. Compared to the no-load case (taking into account the instant the last pole clears), it is evident that the extinction time in this case is approximately 9 msec longer. It is of interest to note that the de-energisation of the sound phases causes a high frequency distortion in the arc voltage waveform (fig. 8.6b), compared to none in the no-load case (fig. 8.3d). The most probable cause of such extinction time difference is the different voltage profile along the line coupled with the different pole opening sequence. It is worth mentioning that the highly coupled phase (inner) to the faulted phase opens last in this case. From fig. 8.6b, the first peak of the recovery voltage is approximately 52kV compared to 40.6kV in the no-load case. With reference to fig. 8.5c, high frequency distortion is evident in the steady-state secondary arc current. This is caused by the different clearance sequence of the sound phases, in conjunction with the power transfer effect. It is clear from fig. 8.6c that current peaks, comparable to those under no-load condition, are evident.

The faulted phase voltage and current response at the line remote ends are shown in fig. 8.7. It is obvious from fig. 8.7a,b that up to the first sound phase pole opening, the sending and receiving end voltage waveform are identical to those of a system with conventional single-pole switching (see fig. 7.8, chapter 7). However, more high frequency

distortion is evident in the receiving end voltage waveform upon de-energisation in comparison to that under no-load condition. The sending end voltage exhibits comparatively less distortion during the same interval. The faulted phase overvoltage in this case is higher than that under no-load condition, and also occurs at the end remote from fault. As seen in fig. 8.7b, this has a value of 1.47 p.u.. The effect of non-simultaneous closure of the line breaker is evident in fig. 8.7c,d and fig. 8.8. This is particularly shown in the current waveforms at the sending end, where the breaker closes first. The closure sequence in this case starts at the sending end as "b"-"a"-"c", followed by "c"-"a"-"b" at the receiving end. The sound phase energisation overvoltages attain comparable values to those observed in the no-load case.

8.5.3 Fault at the receiving end : Power transfer from sending to receiving end ($V_S/V_R = 1\angle 25.73^{o}$)

For a fault at the importing end of the line, fig. 8.9 illustrates some of the system response. In an effort to lessen the effect of different breaker opening times to those in the previous case (section 8.5.3), the sending end breaker is controlled to open first. This is delibrately fixed to quantify only the effect of the pre-fault power transfer direction and fault position. From fig. 8.9a, it is clear that arc extinction occurs at 26 msec after de-energising the sound phases, hence approximately 5 msec less than that for a fault at the sending end, and 8 msec higher than that under no-load condition. This discrepancy is slightly caused by the different peak of the secondary arc current and recovery voltage, as can be appreciated, for example, from fig. 8.9a and fig. 8.6a. Also, the secondary arc current waveform is offset for the first 3½ cycles, which is,

as mentioned in chapter 7, caused by the interaction of the sound phase current and the unbalance by virtue of the line non-transposition. From fig. 8.9b, the first peak of the recovery voltage has a value of 12.5kV, compared to 52kV for a fault at the sending end (fig. 8.6b). The difference is attributed to the different de-energisation sequence and timing. The inner phase de-energisation occurs first in this case.

The voltage at the remote end from the fault exhibits similar frequency distortion upon de-energisation to that observed in the previous case. This is evident from fig.8.9c and fig. 8.9d, which also shows comparable reclosing overvoltages to those under no-load condition. However, the breaker pole closure sequence of "b"-"a"-"c" at the sending end, followed by "c"-"b"-"a" at the receiving end is observed in this case.

8.5.4 Fault at the sending end : Power transfer from receiving to sending end ($V_S/V_R = 1/-25.73^{o}$)

Fig. 8.10 shows the behaviour of the secondary arc path and the faulted phase terminal voltage for a fault at the sending end. The load in this case is exported from the receiving end. A comparison of fig. 8.10 with fig.8.6 shows that the arc extinction time is approximately 10 msec less in this case. Also evident is the significantly lower first peak of the recovery voltage, 26.4kV in this case compared to 52kV for the reverse power transfer (section 8.5.2). This accounts for the shorter time required for the final arc extinction. The faulted phase terminal overvoltages subsequent to reclosure as shown in fig. 8.10c and fig. 8.10d, are comparable to those in section 8.5.2 (fig. 8.7a,b). The effect of the power transfer direction

is clearly marked on the receiving end voltage waveform during the period T_{b3} - T_{b7}, i.e., up to the second arc transition. This can be appreciated from fig. 8.10b and fig. 8.7b.

From these results (section 8.5), it can be concluded that under heavy load conditions, the arc extinction time varies within 1½ cycle of power frequency for different fault positions and power transfer direction. Similar investigations involving a fault on the inner phase have shown identical results to those presented here. However, longer (0 - 2 cycles) arc extinction times were observed. This is caused by, 1) different de-energising sequence and timing, 2) different secondary arc current values, and 3) different rate of rise of the recovery voltage by virtue of the different resonant frequencies from those for an outer phase.

8.6 Effect of Line Transposition

In a study to investigate the effect of line transposition on the arc extinction time, the 300km line is simulated to be transposed at L/3 intervals along its length. The arc behaviour for a fault at the sending end on the outer and inner phases is shown in fig. 8.11. In comparison to fig. 8.3, it is interesting to note that the arc extinction time is approximately 37 msec longer in this case, which is caused by the higher rate of rise of the recovery voltage. Also, for the same phase fault, the first peak of the recovery voltage in this case is 64.4kV compared to 40.6kV in the untransposed line case. The results of fig. 8.11 shows the identical arc behaviour for the inner and outer phase faults. However, a higher first peak of the recovery voltage is observed for a fault on the inner phase (see

fig. 8.11d). Moreover, in comparison to the untransposed line case, the maximum peak of the recovery voltage is lower by almost half in this case.

8.7 Effect of Using One Reactor Bank

It has been indicated in the previous chapter (section 7.5) that,in the case of a transposed line application, one shunt reactor bank can be used with satisfactory single-pole switching performance. However, although the hybrid method of autoreclosure is not promoted here as an alternative to line transposition, its implementation, with the line being untransposed and compensated by one reactor bank is discussed. The shunt reactor is considered to be connected at the receiving end of the line, and tuned to compensate the line at $h_1 = 0.75$. The fault is assumed to occur on the inner phase, and the system is under no-load condition. Fig. 8.12 shows the secondary arc behaviour and the faulted phase terminal voltage for a fault at the sending end. Final extinction of the secondary arc occurs at 395 msec after fault clearance, hence at about 57 msec after the sound phase de-energisation, as evident from fig. 8.12a. In comparison with the line compensated equally at both ends, the arc extinction time is almost one cycle longer in this case. Upon reclosure, the faulted phase terminal overvoltage in this case is comparable to that with two banks. The highest overvoltage occurs at the remote end from the fault, and as seen in fig. 8.12d, it has a value of approximately 1.37 p.u..

For a fault at the shunt reactor terminal (receiving end), fig. 8.13a shows that arc extinction occurs at 384 msec after fault clearance, or at 47 msec after de-energisation. A comparison of fig. 8.13 and fig. 8.12 shows that the arc extinction time is approximately ½ cycle less

in this case. Moreover, the arc recovery voltage peaks are lower than those for a fault at the sending end (fig. 8.13b, fig. 8.12b). The reclosing overvoltage, also occurs at the remote end from the fault, and has a value of 1.54 p.u.. However, as seen in fig. 8.13d, the fault point overvoltage is comparable to that with a fault at the sending end.

8.8 Summary

The effectiveness of the hybrid method of autoreclosure has been assessed with the use of a computer program capable of modelling the multiconductor transmission line, the switching events, and the arc path behaviour. The de-energisation of the sound phases proved to be effective in ensuring fast arc extinction. The results presented in this chapter, and these of numerous studies indicated the following :-

a. The timing and sequence of de-energising the sound phases, affect the final arc extinction time.

b. The transmission line length has little effect on the arc extinction time.

c. Higher arc extinction times are observed for an inner phase fault than those for an outer phase fault .

d. The pre-fault power transfer and fault position, affects (to a small degree) the arc extinction time.

e. In the untransposed line application, the amplitude of the recovery voltage depends on the particular phase conductor position (inner or outer). However, in a transposed line application, insignificant difference is observed.

f. Overvoltages of the order of 1.7 p.u. are to be

expected upon reclosing.

g. The source side parameters have negligible effect on the arc extinction time.

Finally, it can be suggested that to implement the hybrid method of autoreclosure, a thorough investigation is required for the particular system. Based on the results and the system stability studies, the sound phase de-energisation time and the overall dead-time can be specified.

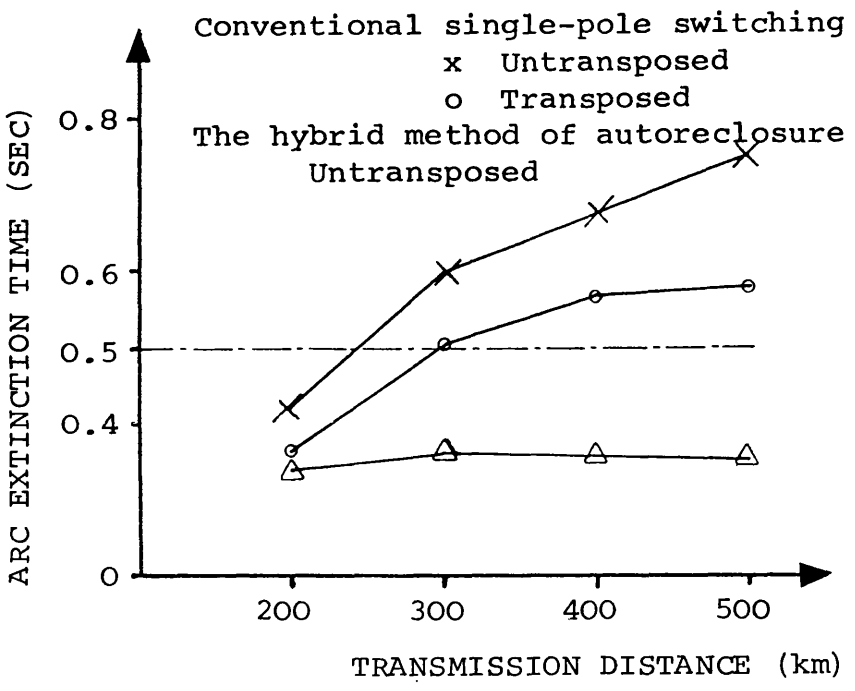

Fig. 8.1 Effect of the transmission distance on the secondary arc extinction time

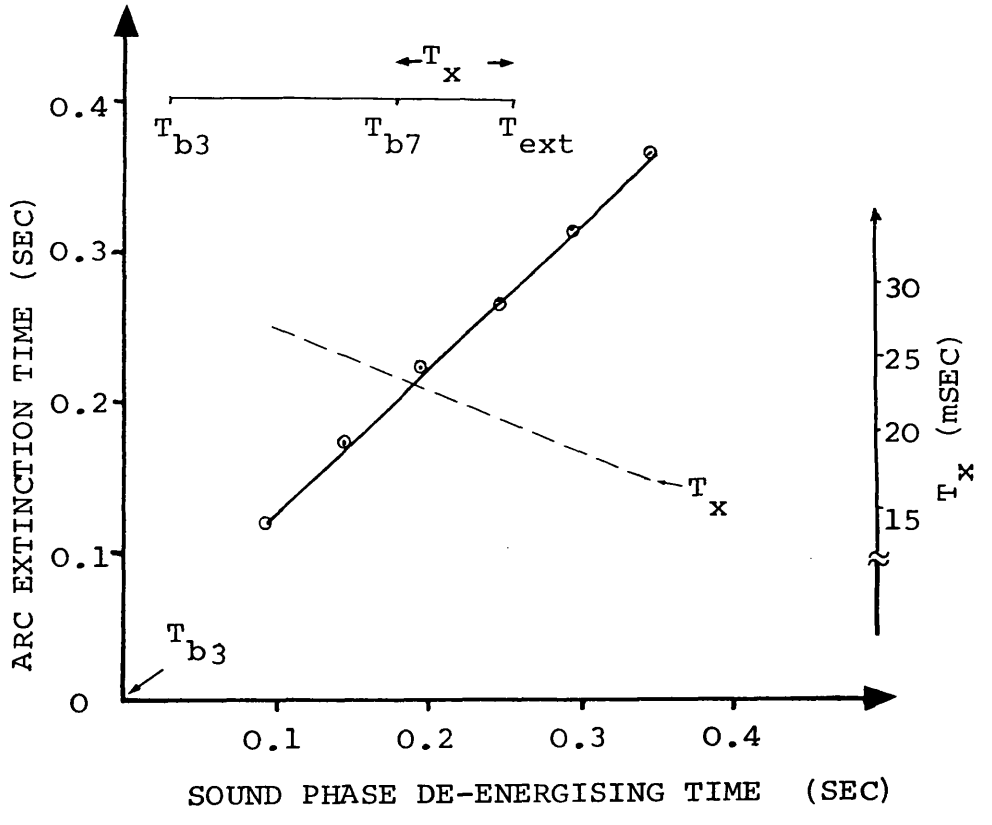

Fig. 8.2 Variation of the secondary arc extinction time with the sound phase de-energising time

T_{b3} Primary fault arc clearance (first arc transition)

T_{b7} Sound phase last pole clearance (second arc transition)

T_{ext} Secondary arc extinction

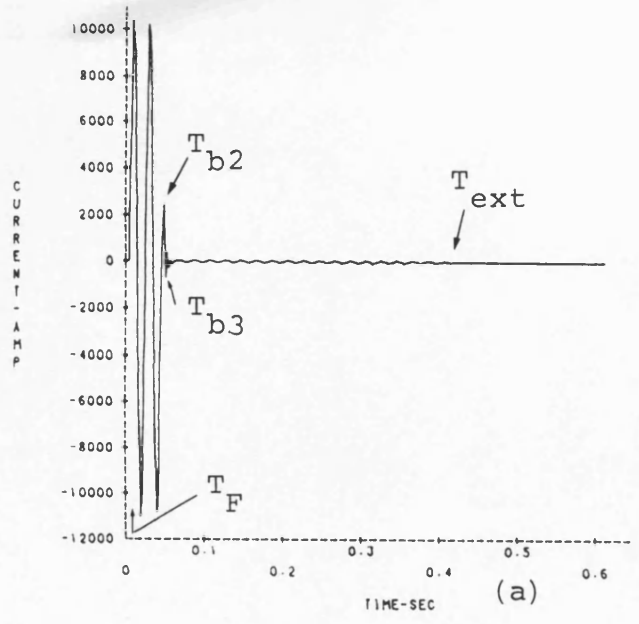

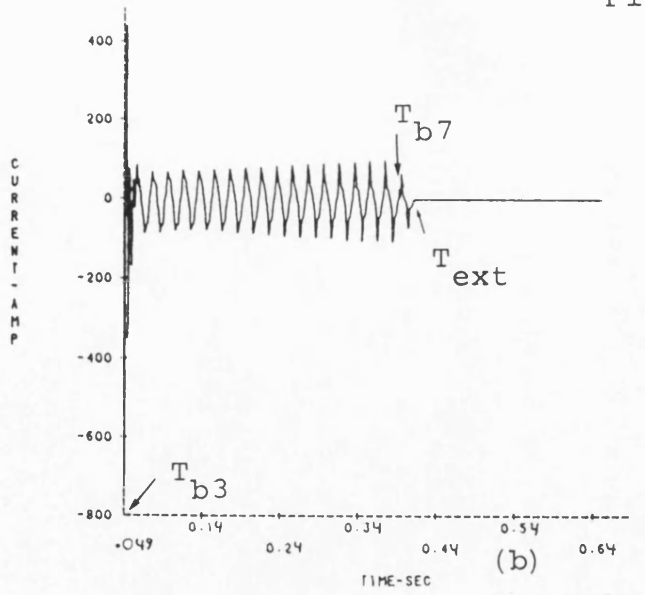

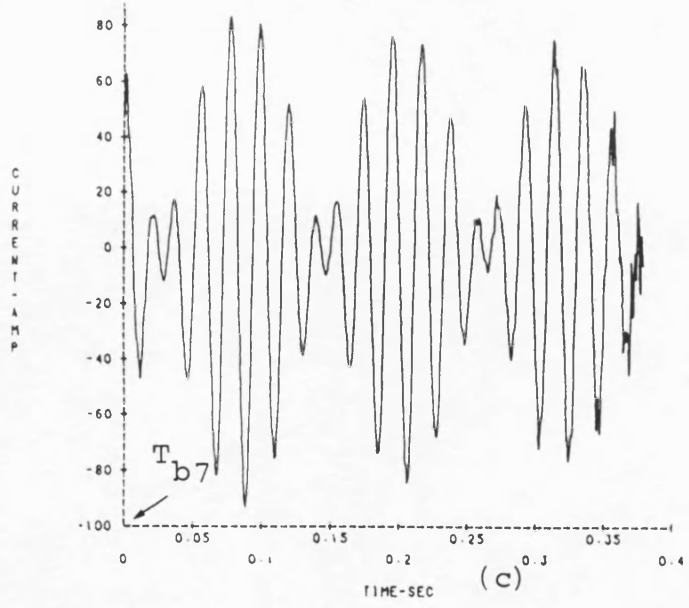

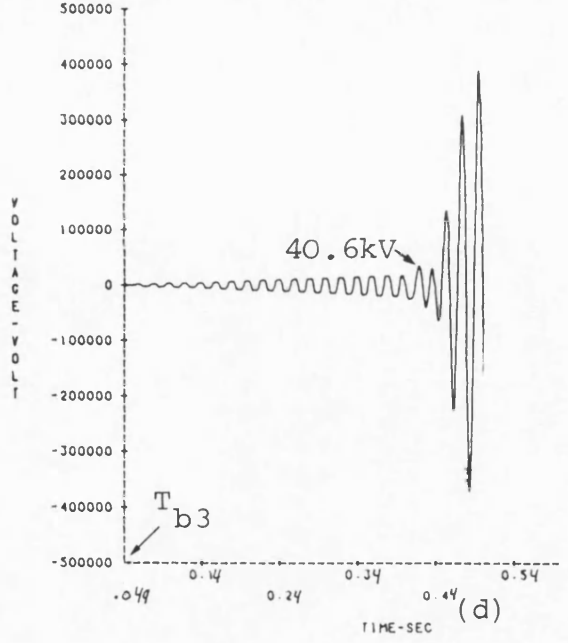

Fig. 8.3 Fault path arc behaviour

"a"-phase to earth fault at the sending end.

L = 300km, h_1 = 0.75,

$V_S/V_R = 1\angle 0^o$,

s.c.1 = s.c.2 = 5GVA.

T_F = 5 msec,

T_{b2} = 40 msec (a.f.),

T_{b3} = 49.6 msec (a.f.),

T_{b4} = 394.8 msec (a.f.),

T_{b5} = 395.2 msec (a.f.),

T_{b6} = 404.8 msec (a.f.),

T_{b7} = 405.2 msec (a.f.),

T_{ext} = 373.6 msec.

(a) Fault path current
(b) Secondary arc current
(c) secondary arc current ($R_F = 0.5\Omega$)
(d) Secondary arc voltage

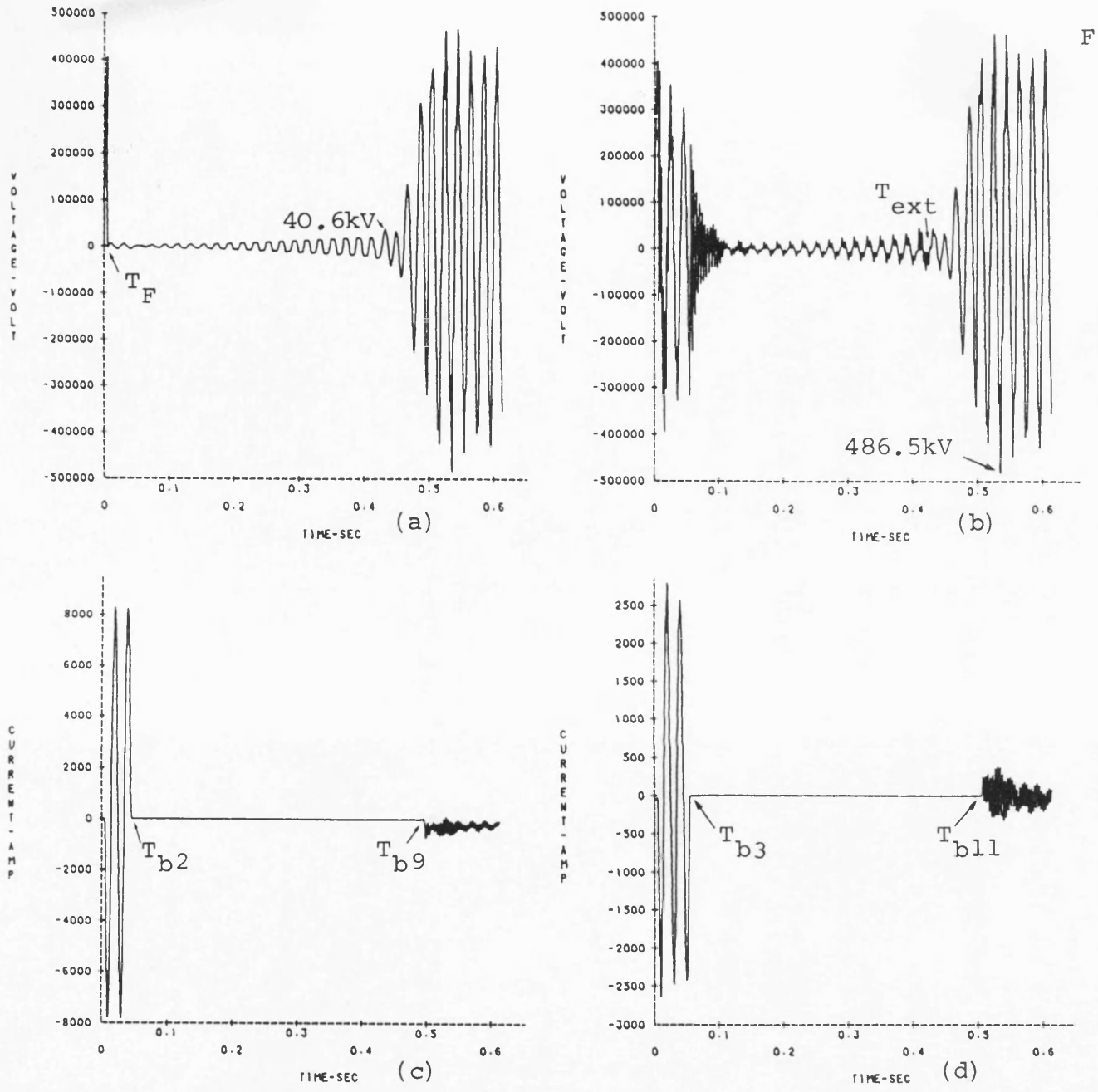

Fig. 8.4 Faulted phase voltage and current

Fault conditions as in fig. 8.3.

T_{b9} = 492 msec (a.f.),
T_{b11} = 502 msec (a.f.).

(a) "a"-earth voltage at sending end
(b) "a"-earth voltage at receiving end
(c) "a"-phase current at sending end
(d) "a"-phase current at receiving end

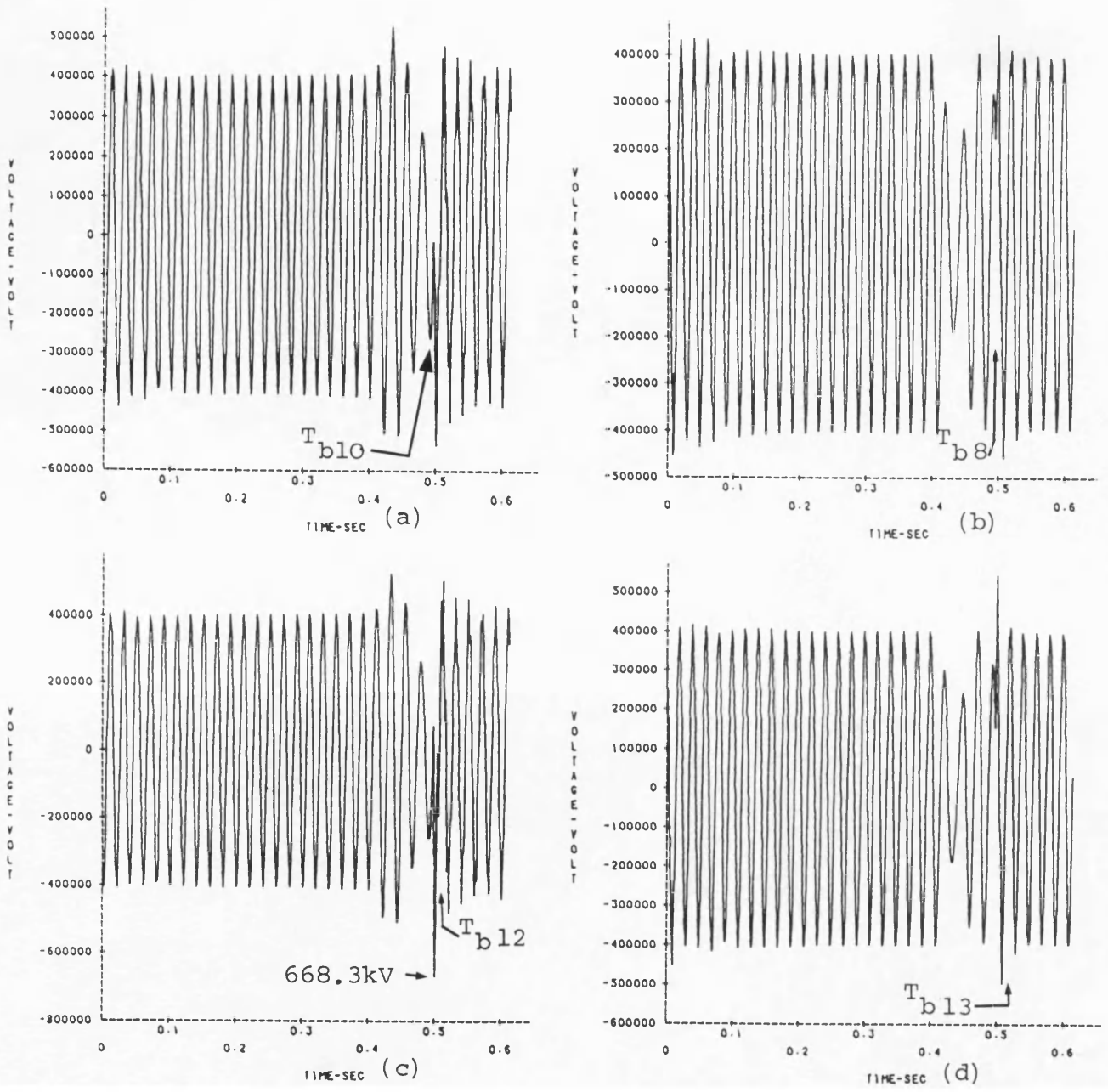

Fig. 8.5 Sound phase voltage

Fault conditions as in fig. 8.3

T_{b8} = 490.4 msec (a.f.),
T_{b10} = 492 msec (a.f.),
T_{b12} = 502.8 msec (a.f.),
T_{b13} = 508.8 msec (a.f.).

(a) "b"-earth voltage at sending end
(b) "c"-earth voltage at sending end
(c) "b"-earth voltage at receiving end
(d) "c"-earth voltage at receiving end

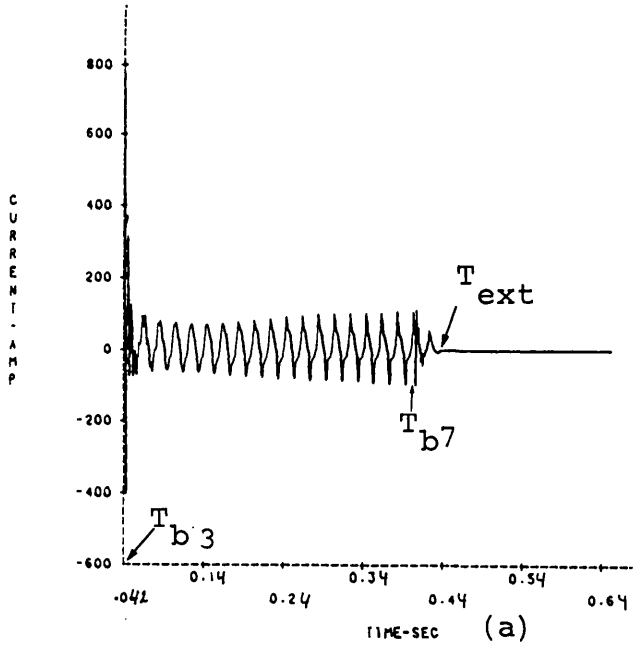

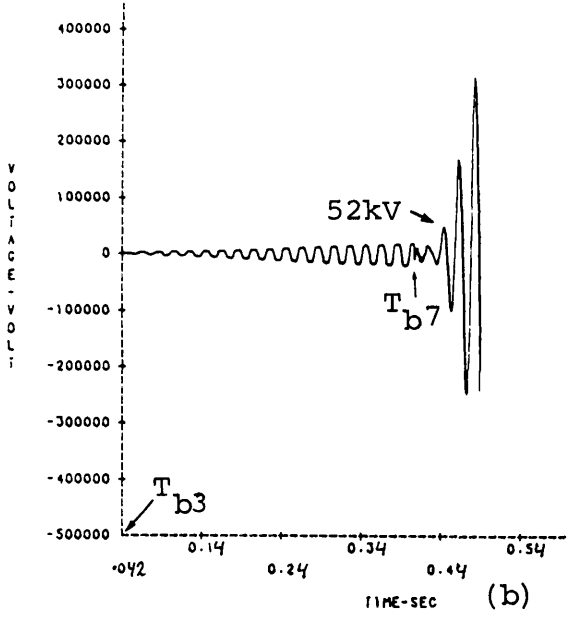

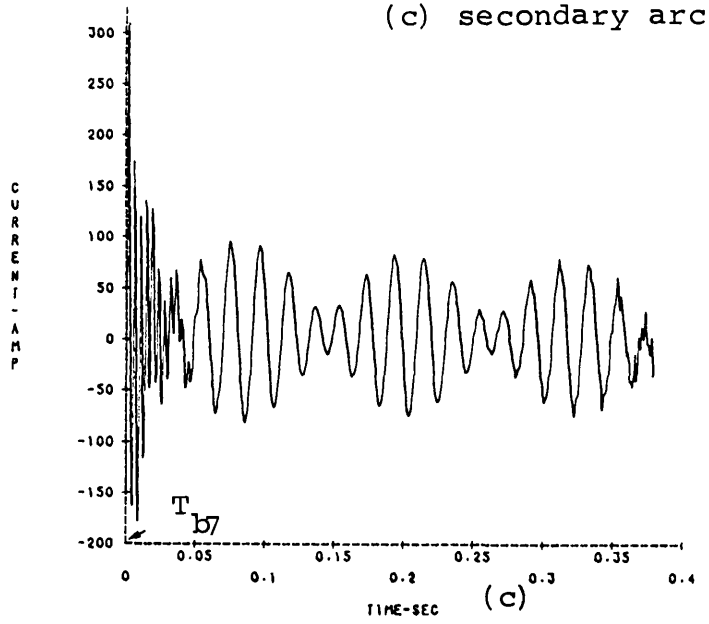

Fig. 8.6 Effect of pre-fault loading

"a"-phase to earth fault at sending end
1262MW power transfer from sending to receiving end, $V_S/V_R = 1\angle 25.73^o$.

$h_1 = 0.75$, L = 300km, s.c.1 = s.c.2 = 5GVA.

T_F = 5 msec, T_{b2} = 39.2 msec (a.f.),
T_{b3} = 42.4 msec (a.f.), T_{b4} = 391.6 msec (a.f.),
T_{b5} = 399.2 msec (a.f.), T_{b6} = 401.6 msec (a.f.),
T_{b7} = 409.6 msec (a.f.), T_{ext} = 398.8 msec.

(a) Secondary arc current
(b) Secondary arc voltage
(c) secondary arc current ($R_F = 0.5\,\Omega$)

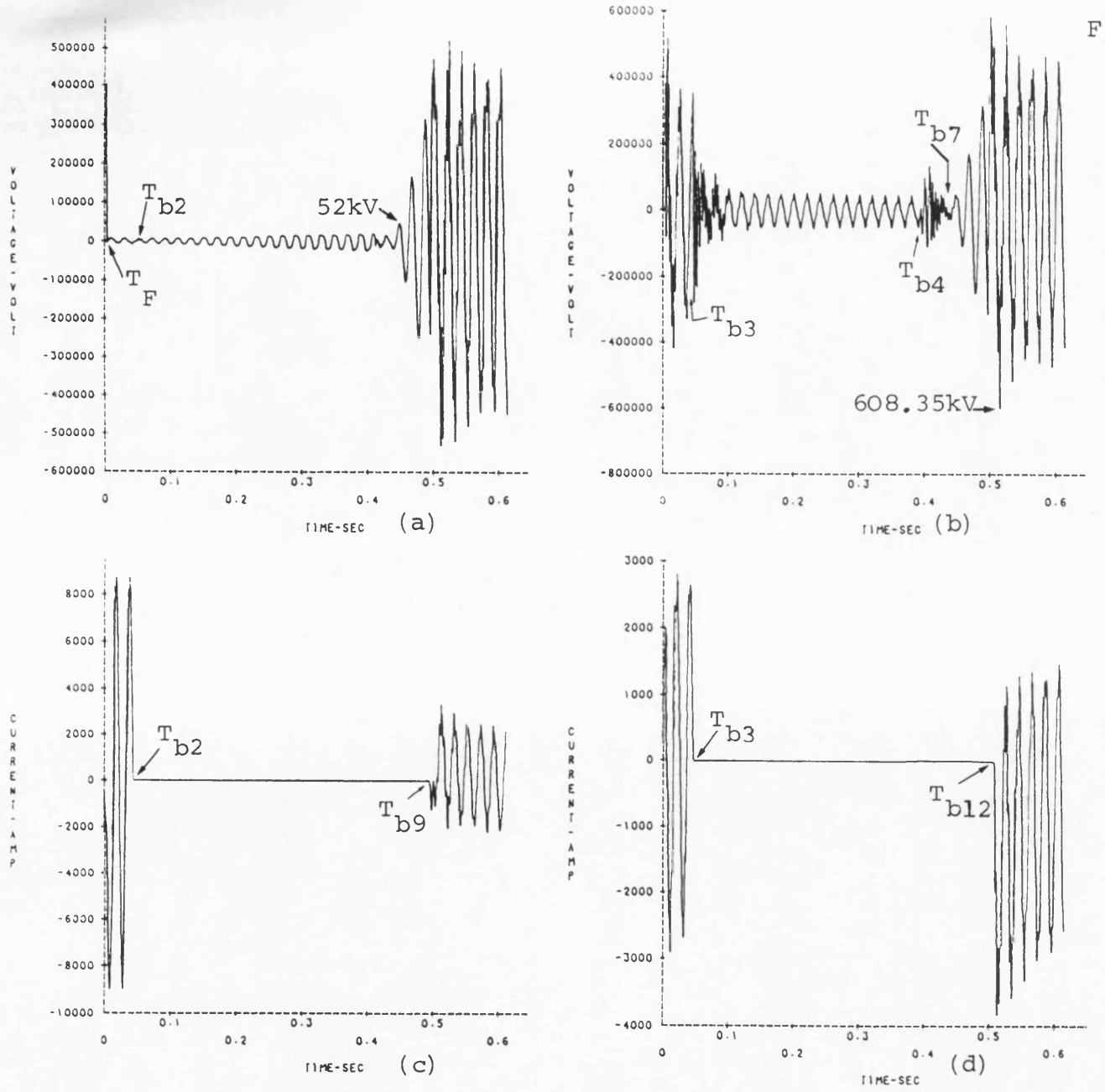

Fig. 8.7 Faulted phase voltage and current: Power transfer from sending to receiving end

Fault conditions as in fig. 8.6

T_{b9} = 492.8 msec (a.f.),

T_{b12} = 504.8 msec (a.f.),

(a) "a"-earth voltage at sending end
(b) "a"-earth voltage at receiving end
(c) "a"-phase current at sending end
(d) "a"-phase current at receiving end

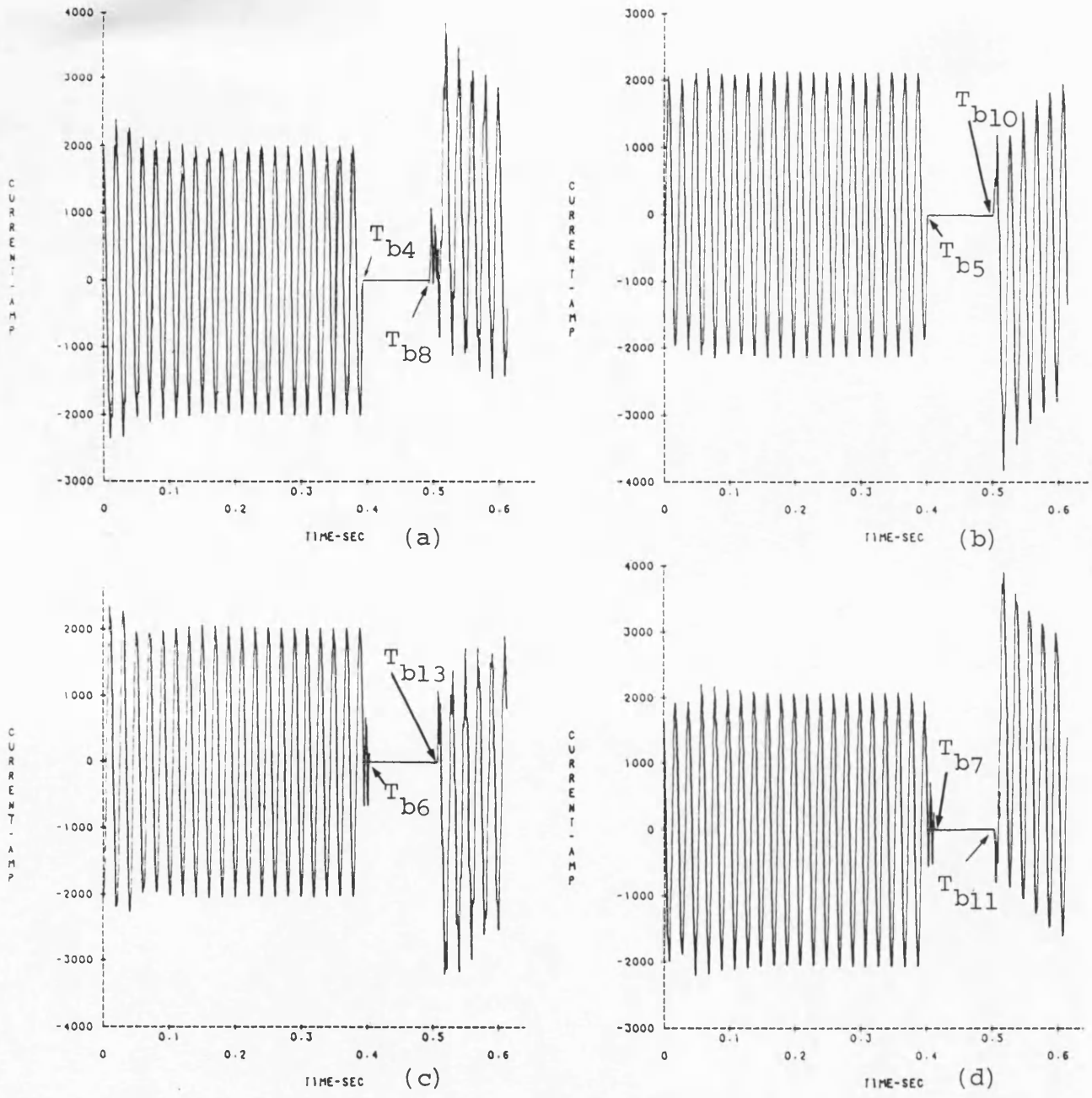

Fig. 8.8 Sound phase current: Power transfer from Sending to receiving end

Fault conditions as in fig. 8.6

T_{b8} = 492 msec (a.f.),
T_{b10} = 498.8 msec (a.f.),
T_{b11} = 502 msec (a.f.),
T_{b13} = 504.8 msec (a.f.).

(a) "b"-phase current at sending end
(b) "c"-phase current at sending end
(c) "b"-phase current at receiving end
(d) "c"-phase current at receiving end

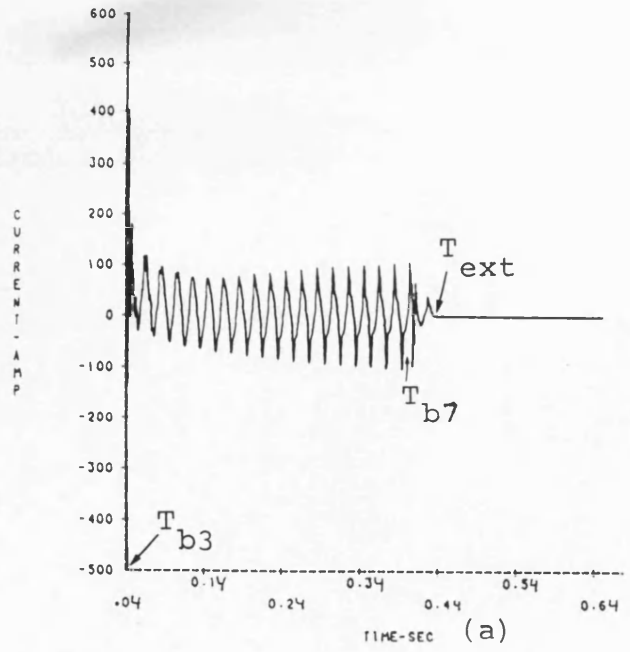

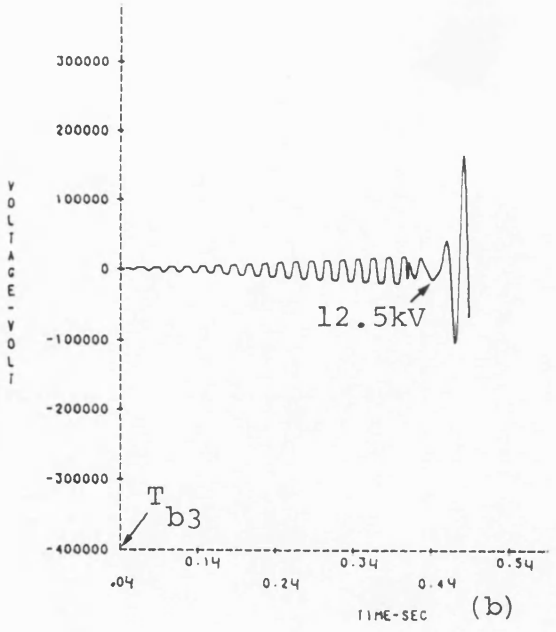

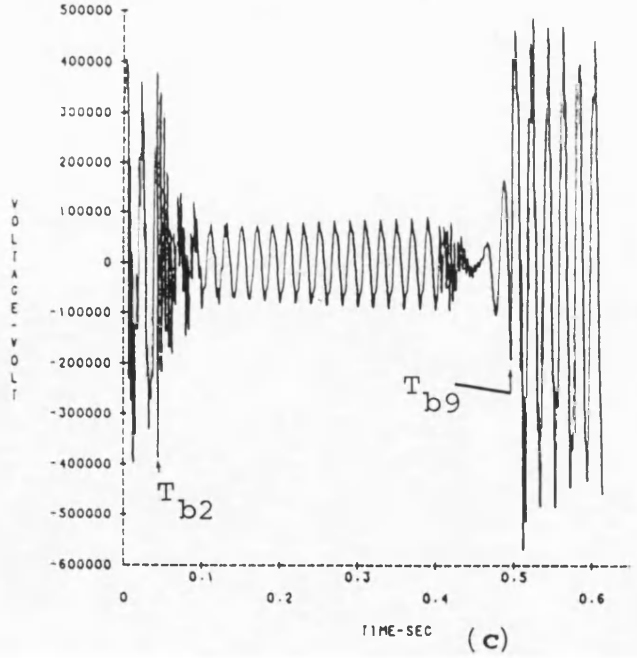

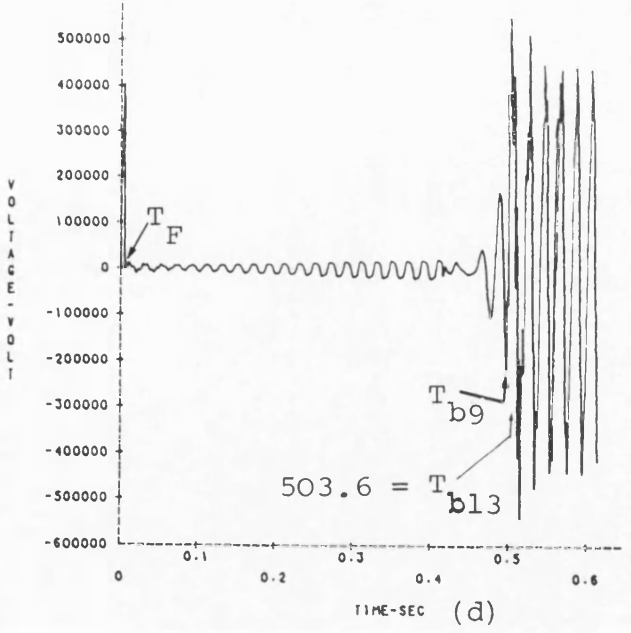

Fig. 8.9 Effect of pre-fault loading and fault position

"a"-phase to earth fault at the receiving end, power transfer from sending to receiving end.

$L = 300km$, $h_1 = 0.75$,

s.c.1 = s.c.2 = 5GVA,

$V_S/V_R = 1\angle 25.73^{o}$.

T_F = 5 msec,

T_{b2} = 37.2 msec (a.f.),

T_{b3} = 40.8 msec (a.f.),

T_{b4} = 397.6 msec (a.f.),

T_{b5} = 400 msec (a.f.),

T_{b6} = 408 msec (a.f.),

T_{b7} = 410 msec (a.f.),

T_{ext} = 395.6 msec,

(a) Secondary arc current
(b) Secondary arc voltage
(c) "a"-earth voltage at sending end
(d) "a"-earth voltage at receiving end

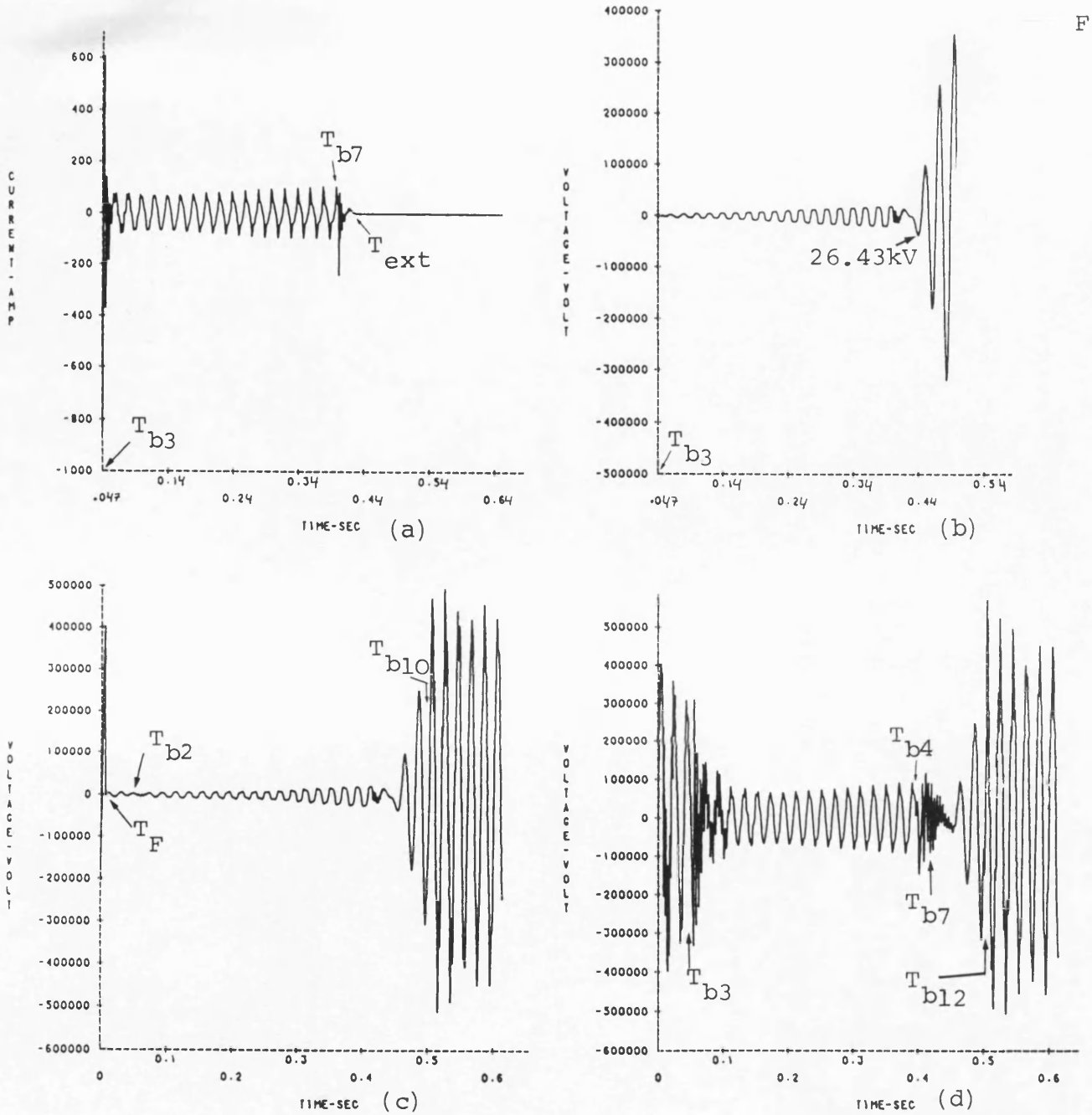

Fig. 8.10 Effect of power transfer direction

"a"-phase to earth fault at sending end, power transfer from receiving to sending end.

L = 300km, $V_S/V_R = 1/-25.73^{\circ}$,
s.c.1 = s.c.2 = 5GVA, h_1=0.75 .

T_F = 5 msec,
T_{b2} = 31.2 msec (a.f.),
T_{b3} = 47.6 msec (a.f.),
T_{b4} = 390.4 msec (a.f.),
T_{b5} = 398 msec (a.f.),
T_{b6} = 408 msec (a.f.),
T_{b7} = 410 msec (a.f.),
T_{ext} = 388.4 msec,
T_{b10} = 494.4 msec (a.f.),
T_{b12} = 500.8 msec (a.f.).

(a) Secondary arc current
(b) secondary arc voltage
(c) "a"-earth voltage at sending end
(d) "a"-earth voltage at receiving end

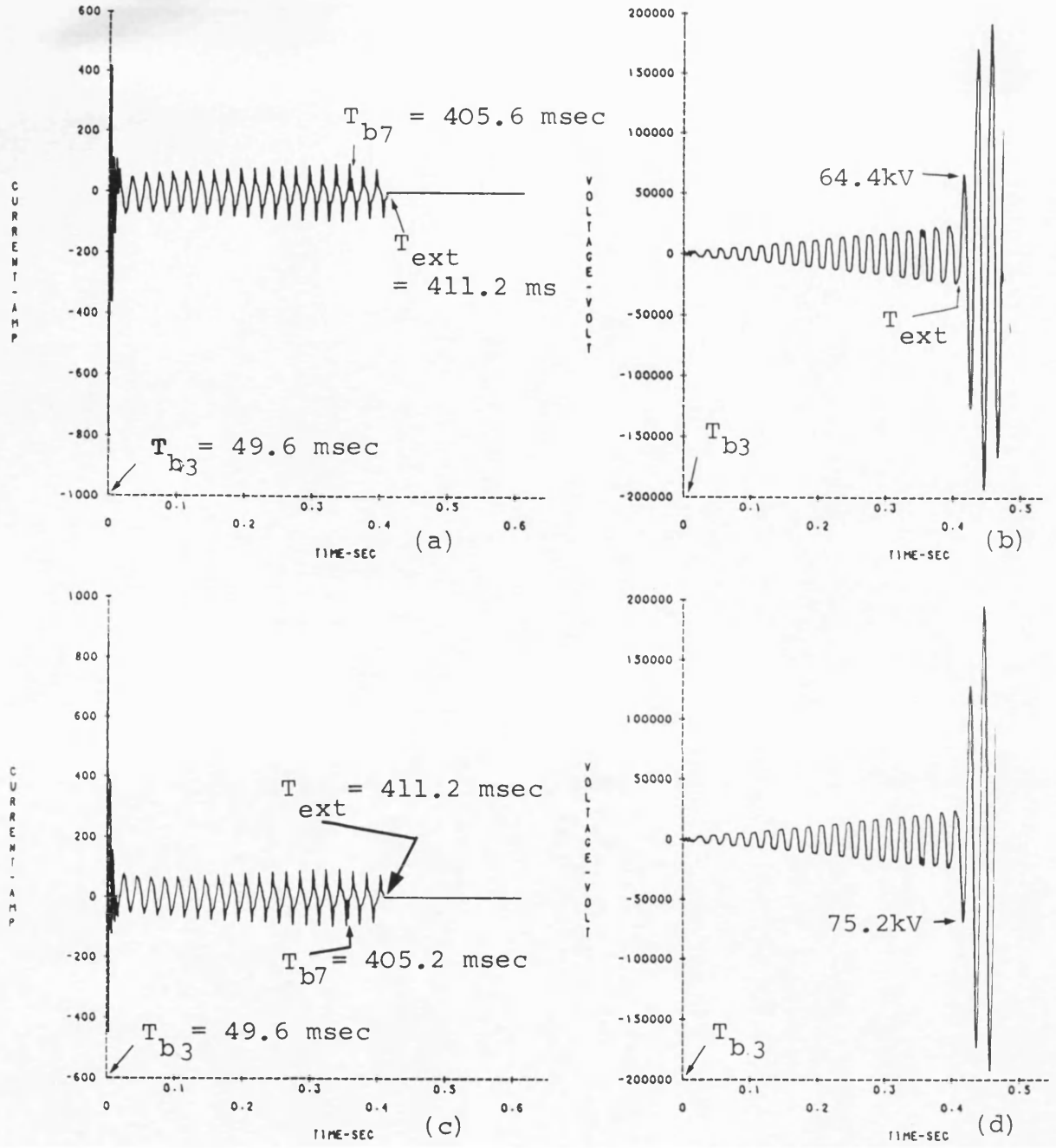

Fig. 8.11 Effect of line transposition

No-load condition,

$V_S/V_R = 1\angle 0^\circ$, $h_1 = 0.75$,
line transposed at L/3 intervals, fault at sending end.
L= 300km, s.c.l.=s.c.2= 5GVA.

Outer phase-"a" fault

(a) Secondary arc current
(b) Secondary arc voltage

Inner phase-"c" fault

(c) Secondary arc current
(d) Secondary arc voltage

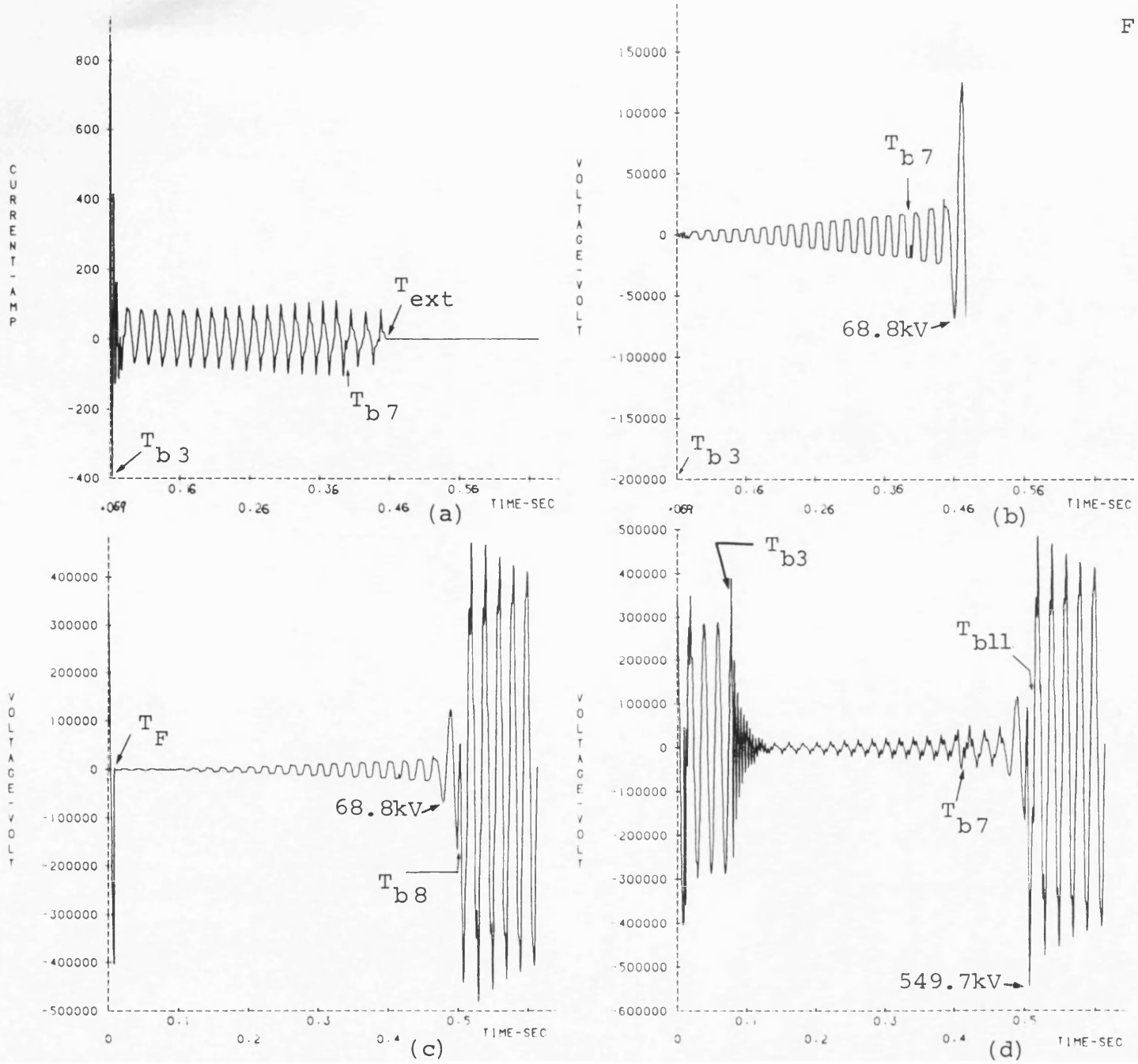

Fig. 8.12 Effect of using one reactor bank

Untransposed line, fault on phase-"c" at the sending end, no-load condition.

L= 300km, h_1 = 0.75,

s.c.1 = s.c.2 = 5GVA,

$V_S/V_R = 1\angle\delta^\circ$.

T_F = 5 msec,

T_{b3} = 69.6 msec (a.f.),

T_{b7} = 407.2 msec (a.f.),

T_{ext} = 395.2 msec,

T_{b8} = 490.4 msec (a.f.),

T_{b11} = 501.2 msec (a.f.).

(a) Secondary arc current
(b) Secondary arc voltage
(c) "c"-earth voltage at sending end
(d) "c"-earth voltage at receiving end

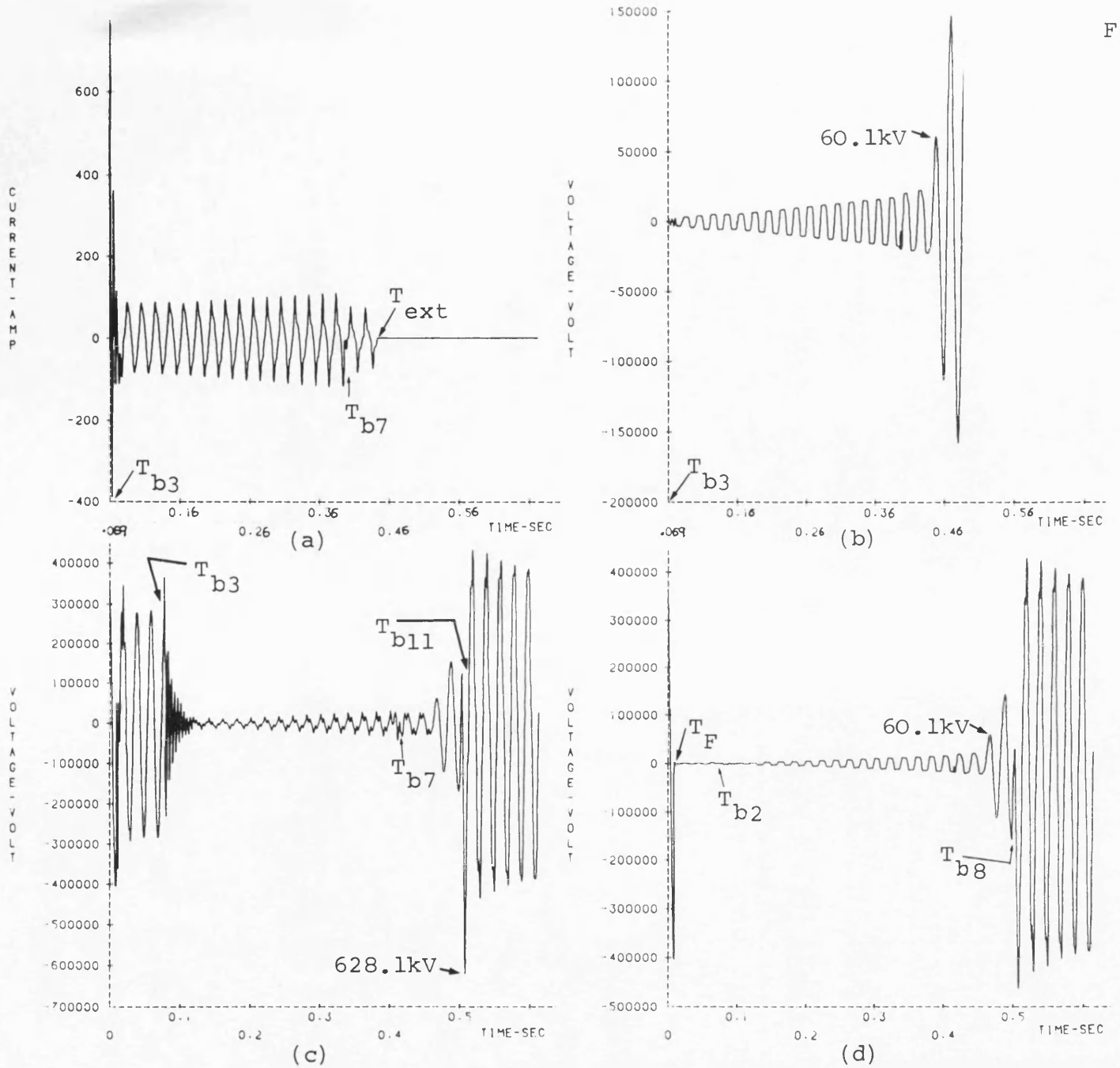

Fig. 8.13 Effect of using one reactor bank

Untransposed line, fault on phase-"c" at receiving end, no-load condition.

$L = 300km$, $h_1 = 0.75$,

s.c.1 = s.c.2 = 5GVA,

$V_S/V_R = 1\angle 0^\circ$.

$T_F = 5$ msec,

$T_{b2} = 60$ msec (a.f.),

$T_{b3} = 69.6$ msec (a.f.),

$T_{b7} = 406.4$ msec (a.f.),

$T_{ext} = 384$ msec,

$T_{b8} = 490.8$ msec (a.f.),

$T_{b11} = 501.2$ msec (a.f.).

(a) Secondary arc current
(b) Secondary arc voltage
(c) "c"-earth voltage at sending end
(d) "c"-earth voltage at receiving end

CHAPTER 9

SYSTEM STUDIES : NEUTRAL SWITCHED REACTOR IMPLEMENTATION

9.1 Introduction

The main purpose of a single-pole switching compensation scheme is to reduce the magnitude of the secondary arc current, thereby ensuring arc extinction during a specified dead-time. In the case of transposed transmission lines, where the interphase capacitances are approximately equal, conventional 4-legged reactor banks have been used to reduce the secondary arc current. With untransposed lines however, the interphase capacitances are significantly different. For example, the horizontal line configuration considered throughout this work, results in the inner-to-outer phase capacitance being 3.262 times larger than outer-to-outer phase capacitance. This, in conjunction with the system performance (refer to chapter 7), proved the noneffectiveness of the balanced 4-legged reactor compensation arrangement in securing fast arc extinction. In 1978, a modified or neutral switched 4-legged reactor arrangement was proposed for use with a balanced reactor for single-pole switching in untransposed line applications[46]. In principle, a balanced 4-legged reactor bank at one end of the line compensates the interphase capacitances by a value equal to the outer-to-outer phase capacitance. The neutral switched reactor bank at

the other end of the line is switched to compensate the unbalance capacitances, i.e., to compensate for the difference between outer-to-inner and outer-to-outer phase capacitances. Although two series of single-pole switching field test results were reported[23,49], full transient studies of such system implementation have not been located in the literature. Therefore, it was felt necessary to determine the effectiveness of such compensation arrangement, and to investigate the conditions of the secondary arc current , its extinction time and the recovery voltage for successful single-pole switching.

The simulation procedure of such systems is presented in chapter 2 to 5, and is used in evaluating and assessing the effect of certain factors on the secondary arcing process and the system reclosing overvoltages. These include, fault location, line loading, and the parameters of the terminal station. In all the studies presented in this chapter, the balanced reactor and the neutral switched reactor bank is considered to be connected at the sending and receiving ends respectively. Although any sequence of opening and closing can be catered for in the developed computer program, in all the studies performed, the ideal neutral switch was considered to open and close after fault clearance and re-energisation at both ends respectively. Moreover, the 300km untransposed line is considered to be compensated at 75% p.p.s.

9.2 Determination of The Neutral Reactance

According to the steady-state solution of the system, given in section 2.2.2.1, it is evident that there are indefinite sets of values of the neutral reactance X_{ns} and X_{nr}, which limit the secondary arc current to a certain

value. This, in addition to the fact that different values are required whether the outer or the inner phase is faulted, makes the determination of X_{ns} and X_{nr} optimum values complicated.

Avoiding any simplifying assumptions in a steady-state evaluation of the optimum X_{ns} and X_{nr}, a more realistic approach is adopted. This involves monitoring the steady-state secondary arc current and the arc extinction time for faults at different locations, and pre-fault system loading. Faults on both outer and inner phases at, the sending end, mid point and the receiving end of the line are considered. For each fault condition mentioned above, no-load and full load power transfer in both directions are accounted for. The neutral reactance of the balanced reactor bank (X_{ns}) is considered to vary in 100 Ω steps between 300 Ω and 600 Ω . The aim of such a comprehensive approach, is to establish the limits of the secondary arc current and accordingly its extinction time with respect to the neutral reactance of the switched bank (X_{nr}). From the results, the neutral reactance value for each bank can be specified.

The boundaries of the secondary arc current, and the arc extinction time for the fault conditions mentioned above, are shown in fig. 9.1 and fig. 9.2 respectively. For both outer and inner phase faults, the shown upper limit in figs. 9.1 and 9.2 corresponds to the lower value of X_{ns}. The correlation between the secondary arc current and its extinction time is evident. Also evident from fig. 9.1 and fig. 9.2, is the higher magnitude of the secondary arc current for faults on the inner phase. This is due to the fact that the inner phase exhibits stronger coupling to the two sound outer phases. It is clear from fig. 9.1b that, values of $X_{nr} < 800$ give rise to steady-state secondary

arc currents in excess of 20A (r.m.s). Accordingly, and bearing in mind the cost factor, X_{nr} = 800 Ω is chosen as optimum for the system considered. An optimum value of 400 Ω is chosen for X_{ns}, as lower values can give rise to secondary arc currents greater than 20A (r.m.s.) with X_{nr} = 800 Ω . Finally, the foregoing value of X_{ns} and X_{nr} are used throughout the studies presented in this chapter.

9.3 Effect of Fault Position - Unloaded Line

With zero pre-fault power transfer, three fault locations are considered. These are the sending end, mid point and the receiving end. The 300km , untransposed line is considered terminating at a 5GVA capacity station at both ends. Fig. 9.3 shows the fault path current and the arc voltage for a single-line-to-earth fault on the outer phase-"a", at the sending end. Fault clearance at both ends is evident from fig. 9.3a. The transition to secondary arcing state and the final arc extinction are illustrated clearly in fig. 9.3b. Arc extinction takes place at approximately 180 msec after the switching of the neutral reactance into the system. Analysing the secondary arc current waveform, one can notice two distinct periods. The first, the initial transient period which is characterised by high current spikes and contains a DC offset. This is caused by the sudden changes in the arc path current due to the breaker and the neutral switch operation. The second, which figuratively resembles a steady-state period, is characterised by different positive and negative half cycles as the arc progresses toward extinction. These two features of the secondary arc current have been noticed in field test results of the system reported in reference 23.

The secondary arc current waveform, assuming a constant arc resistance (0.5 Ω) is shown in fig. 9.3d. It is clear

from this figure that the steady-state peak value of the current is approximately 17.6A. This is compared to approximately 25A from the steady-state formulation of the system given in section 2.2.2.1. The difference is mainly caused by the distributed parameters of the line in conjunction with the line charging currents.

The beating nature of the arc recovery voltage after extinction is shown in fig. 9.3c. This shows an envelope frequency of approximately one sixth of the power frequency (50Hz). Also in fig. 9.3c, the first peak immediately after arc extinction is 32.5kV rising to a maximum of 114.8kV in two cycles.

The faulted phase response at the sending and receiving ends is shown in fig. 9.4. Comparison of fig. 9.4a with fig. 9.4b shows that the highest overvoltage of 1.344 p.u. occurs at the switched reactor terminal. It is evident from fig. 9.4d that the receiving end current is totally offset, compared to that at the sending end (fig. 9.4c). Also from figs. 9.4c,d, it is clear that the closure of the neutral switches cause a high frequency variation in the faulted phase current at both ends.

Fig. 9.5 shows the voltage across the neutral reactance at the sending end (X_{ns}) and the receiving end (X_{nr}) reactor bank. The effect of fault initiation and arc extinction is evident on both voltage waveforms. The higher voltage across X_{nr} (fig. 9.5b) in comparison to that across X_{ns} (fig. 9.5a), is obviously caused by the higher impedance value and the unbalance caused by the neutral switch operation. The ideal switch current, which represents the resultant current of both operative neutral switches, is shown in fig. 9.6. It is evident that fault initiation causes this current to decay slightly until fault clearance

at the receiving end. This is followed by a current rise up to approximately 200A peak. It is evident from fig. 9.6 that upon closure, the ideal neutral switch current is fully offset.

Fig. 9.7 illustrates the system response for a fault on the inner phase-"c" at the sending end. It is evident from fig. 9.7a that the arc extinction time in this case is 40 msec longer than that for an outer phase fault. This is mainly due to the higher secondary arc current (26.67A peak) in this case. A comparison of fig. 9.7b with fig. 9.3c shows that the arc recovery voltage is higher in this case. The voltage across the switched reactor neutral (fig. 9.7c) is similar to that with an outer phase fault. However, lower beating peaks after arc extinction are observed in this case. The dependency of the neutral switch current on the faulted phase, is evident from fig. 9.7d in comparison to fig. 9.6. It is clear that lower neutral switch current occurs with inner phase fault conditions.

For a fault at the middle of the line, fig. 9.8 shows the secondary arc current and fault point voltage. Arc extinction time of 150 msec is evident from fig. 9.8a for a fault on the outer phase. This is approximately 31 msec less than that for a fault at the sending end. Moreover, the DC offset observed here is negligible. The arc extinction time for an inner phase fault is approximately 10 msec less than that for the same phase fault at the sending end (see fig. 9.8c and fig. 9.7a). It is of interest to note that, the arc first attempts to extinguish at 172 msec after transition, but the rise of the recovery voltage to approximately 33kV causes its reignition. Similar to a fault at the sending end, high frequency distortion in the secondary arc current waveform is more predominant for outer phase faults than for an inner phase fault. The fault point

overvoltages are comparable for both fault conditions as can be seen from fig. 9.8b and fig. 9.8d.

Fig. 9.9 illustrates the secondary arc current and the fault point voltage for a fault at the receiving end. For a fault on the outer phase, it is evident from fig. 9.9a that final arc extinction takes place at 180 msec after transition. This is compared to arc extinction time of 231 msec for a fault on the inner phase as seen in fig. 9.9c. Close examination of fig. 9.9d and fig. 9.4b shows that, slightly higher arc recovery voltage is evident in this case which accounts for the approximately 10 msec longer extinction. A comparison of fig. 9.9b and fig. 9.9d shows that higher reclose overvoltage occurs for a fault on the inner phase. This has a value of 1.478 p.u..

9.4 Effect of Pre-Fault Loading And Fault Position

To estimate the effect of the pre-fault power transfer and its direction on the arc extinction time and reclosing overvoltage, twelve fault conditions are considered. These include faults on the outer and inner phase at, the sending end, mid point and the receiving end of the line. Moreover, in order to compare the simulation results to that of a practical field test reported in reference 49, two fault conditions are considered with the system energised from the receiving end only.

9.4.1 Fault at the sending end : Power transfer from sending to receiving end ($V_S/V_R = 1\angle 25.73^o$)

Fig. 9.10a,b illustrates the secondary arc behaviour following the outer phase-"a" to earth fault at the sending end. The pre-fault power transfer from sending to receiving

end is approximately 1262MW. A comparison with fig. 9.3 shows that the arc extinction time is 4 msec less for the loaded case. Also, it is evident from fig. 9.10b and fig. 9.3b that the first peak of the recovery voltage is approximately 10kV higher in this case than that under no-load condition. The effect of pre-fault loading is evident on the receiving end voltage as seen in fig. 9.10d. A comparison of the line terminal voltage of fig. 9.10c and fig. 9.10d shows that the highest overvoltage of 1.575 p.u. occurs at the receiving end. The switched reactor neutral voltage and the ideal switch current waveforms, are shown in fig. 9.10e and fig. 9.10f respectively. It is interesting to note that the neutral voltage is slightly higher in this case compared to the no-load case (fig. 9.5b). Moreover, a neutral overvoltage of 0.407 p.u. occurs, following the faulted phase energisation at the sending end. It is clear from fig. 9.10f that the ideal switch current during the fault period is comparable to that under no-load condition (fig. 9.6). However, higher current peaks are evident in this case after fault clearance. This is obviously related to the longitudinally induced voltage component in the faulted phase.

Fig. 9.11 shows the secondary arc current and the line terminal voltage, for a fault on the inner phase-"c". In comparison to fig. 9.7, it is clear that, despite the fact that the steady-state arc current is approximately the same, and the arc recovery voltage is higher in this case, the arc extinction time is 4 msec less in this case. The effect of the pre-fault power transfer on the secondary arc current waveform and the faulted phase voltage is evident, as seen in fig. 9.11a and fig. 9.11c respectively. The highest overvoltage occurs at the neutral switched reactor terminal, and has a value of 1.683 p.u. .

9.4.2 Fault at the sending end : Power transfer from receiving to sending end ($V_S/V_R = 1\angle -25.73^o$)

Fig. 9.12 illustrates a few features of the response of the system with a fault on the outer phase-"a" when the power exported from the receiving end is approximately 1262MW. In fig. 9.12a, the final arc extinction takes place at approximately 240 msec after transition. In comparison to the reverse power flow and no-load cases, the arc extinction time is 27 msec and 23 msec longer respectively. The effect of the power transfer direction is evident in fig. 9.12. This is marked on the secondary arc current waveform (fig. 9.12a), as it is offset for the first few cycles in comparison to that of fig. 9.10a. Also, it is marked on the receiving end voltage (fig. 9.12c) compared to that of fig. 9.10d.

Fig. 9.13 shows the secondary arc current and the line terminal voltage for a fault on the inner phase-"c". It is worth mentioning that the steady-state secondary arc current for such a fault condition is approximately 20A (r.m.s.). Final arc extinction occurs at 264 msec after transition. This is 43 msec and 37 msec longer than that under no-load and reverse power flow conditions respectively. Comparable terminal overvoltages to those under reverse power flow condition (fig. 9.11) are evident in figs. 9.13b,c.

9.4.3 Mid point fault : Power transfer from sending to receiving end ($V_S/V_R = 1\angle 25.73^o$)

Fig. 9.14 and fig.9.15 shows the system response for a fault on the outer phase-"a" and inner phase-"c" respectively. For the outer phase fault, the arc extinction time is approximately 8 msec longer than that under no-load

condition, as is evident from fig. 9.14a and fig. 9.8a. However, for the inner phase fault, it is 30 msec shorter (see fig. 9.15a and fig. 9.8c). The fault point voltage waveforms (fig. 9.14b and fig. 9.15b) shows slightly higher overvoltages as compared to those under no-load condition (fig. 9.8b,d). Considerable differences between the sending and receiving end voltages during the dead-time are evident from fig. 9.14 and fig. 9.15. This is primarily due to the phase difference between the induced electromagnetic and electrostatic voltage components along the faulted phase. Also contributing, is the different termination of the faulted phase, with respect to the shunt reactor circuit. For both phase faults, the maximum reclose overvoltage occurs at the receiving end as seen in fig. 9.14d and fig. 9.15d.

9.4.4 Fault at the receiving end : Power transfer from sending to receiving end ($V_S/V_R = 1\angle 25.73^{\circ}$)

Fig. 9.16 and fig. 9.17 shows several features of the system response for a fault on the outer and inner phases respectively, at the neutral switched reactor terminal. The power transfer from the sending end is approximately 1262MW. In comparison to the no-load case (fig. 9.9a,c) it is evident from fig. 9.16 and fig. 9.17, that the arc extinction time is 20 msec and 10 msec longer in this case for the outer and inner phase faults respectively. Moreover, a comparison with fig. 9.9b,d shows that the first peak of the recovery voltage is 10kV higher and 1.5kV lower for the outer and inner phase faults respectively. It is evident from fig. 9.16b,c and fig. 9.17b,c that the maximum overvoltage occurs at the receiving end for both faults.

9.4.5 Fault at the receiving end : Power transfer from receiving to sending end ($V_S/V_R = 1\angle -25.73^o$)

For the case where the power is imported into the sending end, fig. 9.18 and fig. 9.19 shows the system response for outer and inner phase faults respectively at the receiving end. It is of interest to note that the arc extinction time is significantly reduced in comparison to that under no-load and reverse power flow conditions. This is particularly so for the outer phase fault. Also evident in the above mentioned figures, is the lower level of reclosing overvoltage at the line ends. However, the maximum overvoltage occurs at the conventional reactor terminal (sending end) in this case.

From the results presented in section 9.3 and 9.4, Table 9.1 summarises the secondary arc parameters. Examination of Table 9.1, shows a general tendency for longer arc extinction time when a fault occurs on the inner phase. Also evident , longer arc extinction times are exhibited by faults at the importing terminal of the line. It can be appreciated from Table 9.1 that, in spite of the relatively wide range of the steady-state secondary arc current, the arc extinction time is independent of the current magnitude. This similarly holds in so far as the faulted phase recovery voltage is concerned. The peak secondary arc current values given in Table 9.1 confirms the choice of the neutral reactances. Finally, from the above studies, it has been noticed that the pre-fault power flow has negligible effect on the reactor neutral voltage.

		Fault at send. end (conventional reactor bank terminal)		Fault at mid point		Fault at recv. end (switched reactor bank terminal)	
		Outer phase	Inner phase	Outer phase	Inner phase	Outer phase	Inner phase
No-load	Peak current (A)	17.6	26.67	18.37	26.76	17.96	26.73
	1st. peak recovery voltage (kV)	32.5	43	33.7	45.6	33.6	43.3
	Extinc. time (msec)	180.8	221.6	150	211.2	180.4	231.2
Load from sending to receiv. end	Peak current (A)	22.43	26.3	17.79	16.79	21.3	19.22
	1st. peak recovery voltage (kV)	42.4	51.7	43.4	46.9	43.6	41.8
	Extinc. time (msec)	177.2	217.6	158.4	179.2	200.4	241.2
Load from receiving to Sending end	Peak current (A)	22.4	28.9	-----	-----	10.44	27.8
	1st. peak recovery voltage (kV)	38.9	46.2	-----	-----	15.9	46.6
	Extinc. time (msec)	204.4	264.8	-----	-----	130.8	201.2

Table 9.1 Secondary Arc Parameters

9.4.6 Fault at the sending end : Line energised from the receiving end only

In order to simulate fault throwing tests on a practical system[49], the 300km, 500kV line is simulated with the sending end breaker open. Despite the differences between the system of reference 49 and that considered here, the results obtained are in good agreement. Fig. 9.20 and fig. 9.21 shows the system response for a fault at the sending end, on the outer and inner phases respectively. The fault path current shown in fig. 9.20a and fig. 9.21a exhibits the usual high frequency distortion upon de-energising the faulted phase at the receiving end. Following arc transition, it is evident from fig. 9.20b and fig. 9.21b that final arc extinction takes place at approximately 56 msec and 50 msec for outer and inner phase faults respectively. It is of interest to note that for both faults, the secondary arc attempts extinction 10 msec earlier, but an increase in the recovery voltage causes it to restrike again. Higher peaks in the recovery voltage during the dead-time are evident from fig. 9.20b,c and fig. 9.21b,c in comparison to that under the no-load case of fig. 9.4a,b and fig. 9.7b. However, comparable reclosing overvoltages to those when the line is energised from both ends are evident.

9.5 Effect of The Source Parameters

The results presented so far, assume that the source ratio of zero sequence impedance to the positive sequence impedance (Z_{So}/Z_{S1}) is unity, and of 5GVA capacity at both ends. However, in practice a lower Z_{So}/Z_{S1} ratio and/or different source capacities often exist. For systems implementing conventional single-pole switching, it has been shown that the effect of such factors on the arc extinction time is

minimal[25,26]. Fig. 9.22 shows the secondary arc current waveforms following a fault on the inner phase at, the sending end, the receiving end, and on the outer phase at the receiving end when $V_S/V_R = 1\angle 0^o$ and $Z_{So}/Z_{Sl} = 0.5$. A comparison of fig. 9.22a with fig. 9.7a shows, that the decrease of Z_{So}/Z_{Sl} from 1 to 0.5 caused negligible effect on the arc extinction time for the inner phase fault at the sending end. However, from fig. 9.22b and fig. 9.9c, it is evident that the reduction of Z_{So}/Z_{Sl} causes an increase of 19 msec in the arc extinction time for the inner phase fault at the receiving end. For the outer phase fault, a comparison of fig. 9.22c with fig. 9.9a shows a 39 msec shorter arc extinction time when $Z_{So}/Z_{Sl} = 0.5$.

A number of studies were performed at different source capacities. These studies show that the source impedance does not significantly affect the arc extinction time.

9.6 Effect of Neutral Switch Failure

It is obvious that a failure of either neutral switch to operate, will result in a system compensated by conventional 4-legged reactor bank at one end, and a solidly grounded Y-connected reactor bank at the other. Therefore high secondary arc current and recovery voltage are to be expected under such conditions. The 300km transmission system is simulated with 0.75 degree of p.p.s. shunt compensation and under no-load conditions. The neutral reactance at the sending end reactor bank is kept at 400 Ω. Fig. 9.23 shows the secondary arc current and voltage for the outer phase-"a" fault at the sending end. Final arc extinction, as is evident in fig. 9.23a, takes place at approximately 484 msec after transition. The steady-state secondary arc current has a value of approximately 40A (r.m.s.) as seen in fig. 9.23c. This, in conjunction with the high recovery

voltage , shown in fig. 9.23b, accounts for the long arc extinction time. It is of interest to note that the first peak of the recovery voltage is approximately doubled compared to that with operative switches. Accordingly the maximum recovery voltage is quadrupled in this case.

For a fault at the receiving end, fig. 9.24 illustrates the secondary arc current and voltage for the outer and inner phases. From fig. 9.24, it is evident that longer arc extinction time is exhibited by the outer phase fault, than that of the inner phase. Despite the fact that the first peak of the recovery voltage is higher for an inner phase fault compared to that of an outer phase, the maximum value is approximately 70kV less.

9.7 Summary

The results presented in this chapter, prove the applicability of the switched reactor arrangement so far as short arc extinction times are concerned. However, extensive series of simulation studies have shown the sensitivity of the arc behaviour to the neutral reactance value. Practically, the choice of the optimum reactances may be jeopardized by the existence of harmonics, generated by the system and the secondary arc. From the results presented, the following conclusions are reached :-

1. Irrespective of the loading conditions, longer arc extinction times are to be expected for inner phase faults.

2. The minimum arc extinction times are observed for faults at the middle of the line.

3. Longer arc extinction times are exhibited by faults at the neutral switched reactor bank terminal.

4. The source Z_{So}/Z_{Sl} affects the arc extinction time,

depending on the faulted phase and fault position.

5. The highest switching overvoltage occurs at the neutral switched reactor bank terminal.

6. The effect of the pre-fault power transfer on the reactor banks neutral voltage is negligible.

7. The ideal neutral switch current is found to be negligibly affected by the pre-fault system loading.

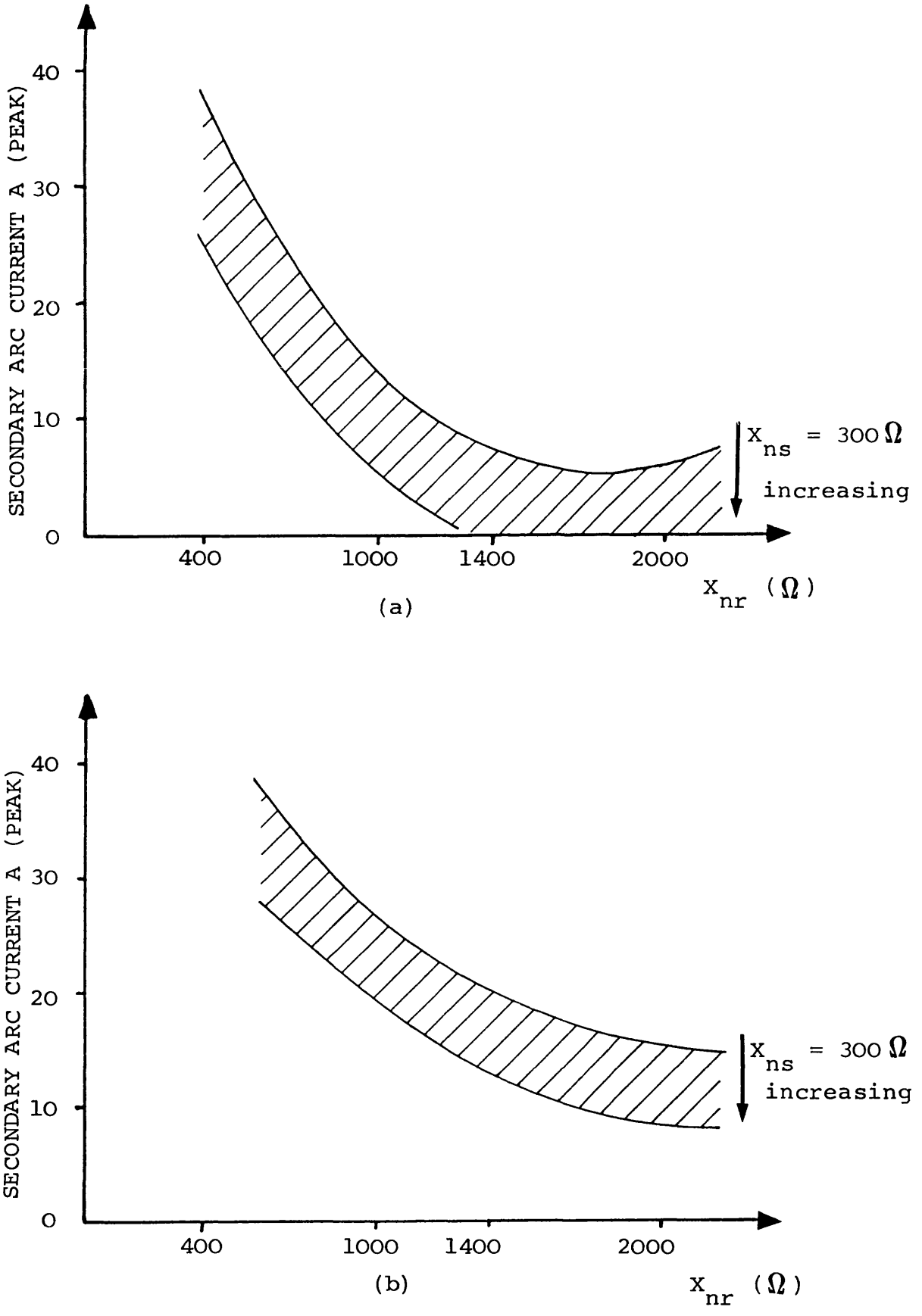

Fig. 9.1 Variation of the secondary arc current with the neutral reactance

(a) Outer phase fault (phase-"a")
(b) Inner phase fault (phase-"c")

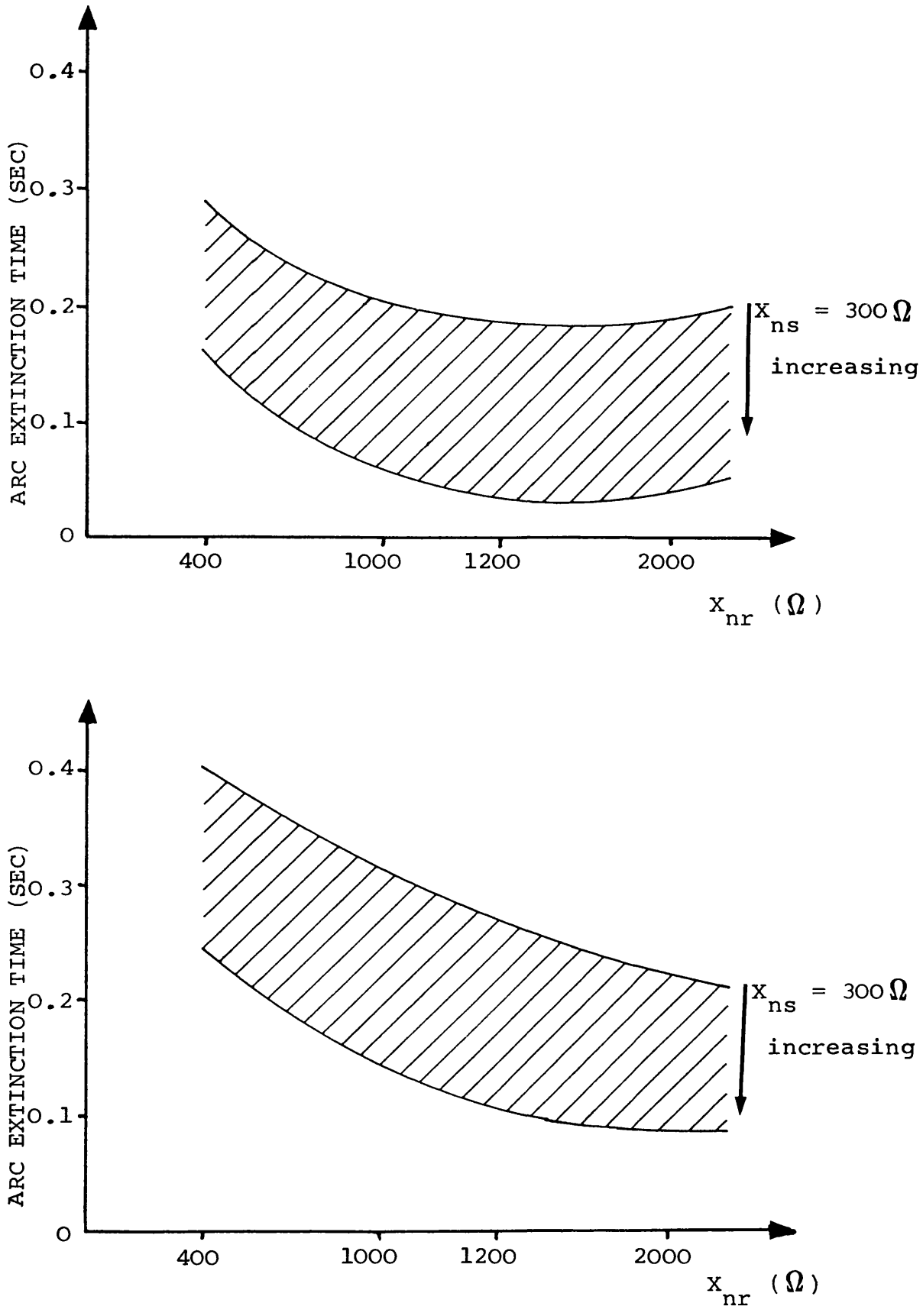

Fig. 9.2 Variation of the arc extinction time with the neutral reactance

(a) Outer phase fault (phase-"a")
(b) Inner phase fault (phase-"c")

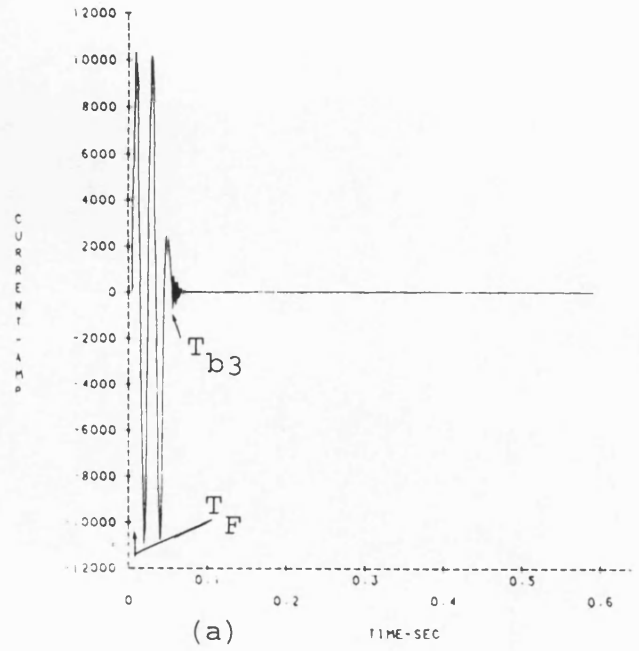

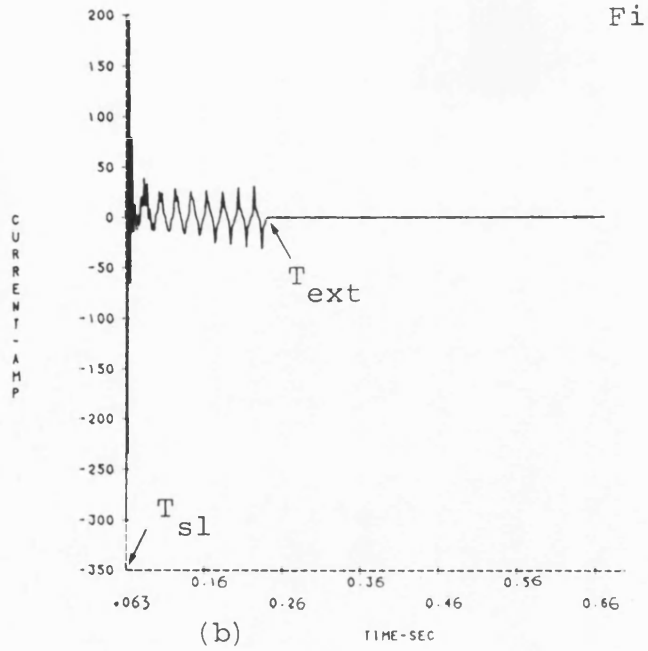

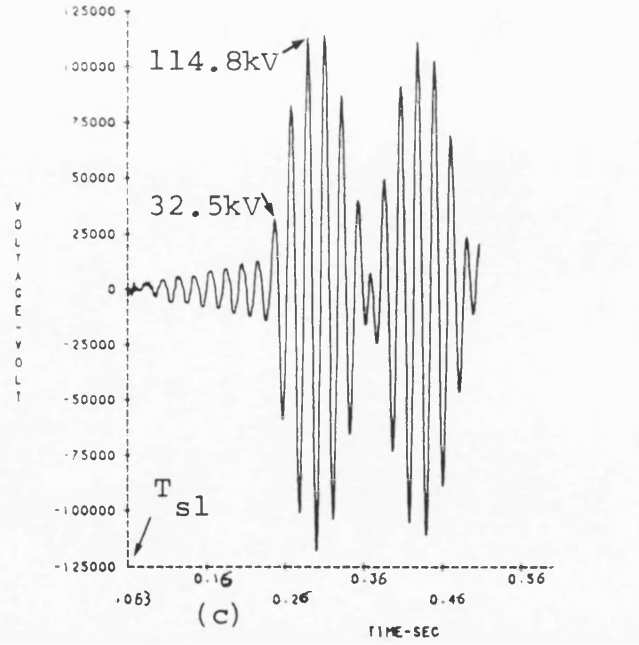

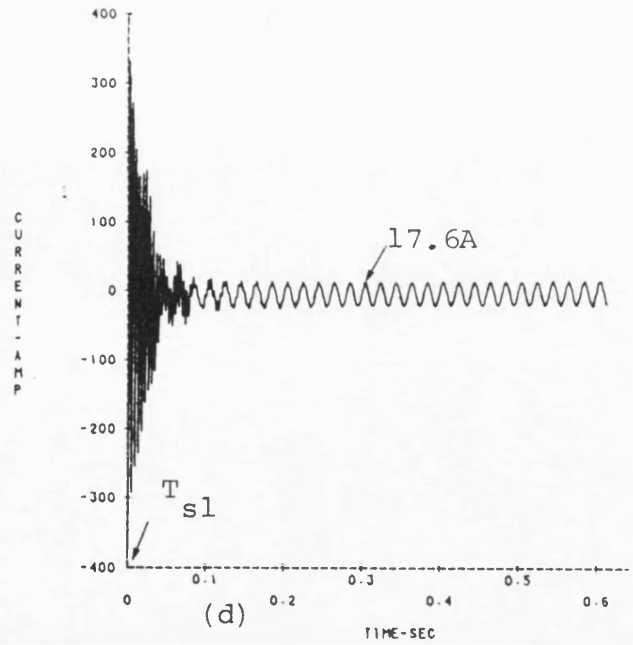

Fig. 9.3 Fault point parameters

"a"-phase to earth fault at the sending end, no-load condition.

L = 300km, $V_s/V_R = 1\angle 0^o$,

s.c.1 = s.c.2 = 5GVA, $h_1 = 0.75$.

T_F = 5 msec,

T_{b2} = 40 msec (a.f.),

T_{b3} = 49.6 msec (a.f.),

T_{s1} = 63.2 msec (a.f.),

T_{ext} = 180.8 msec,

T_{b4} = 495.2 msec (a.f.),

T_{b5} = 501.2 msec (a.f.),

T_{s2} = 551.6 msec (a.f.).

(a) Fault path current
(b) Secondary arc current
(c) Secondary arc voltage
(d) Secondary arc current ($R_F = 0.5\Omega$)

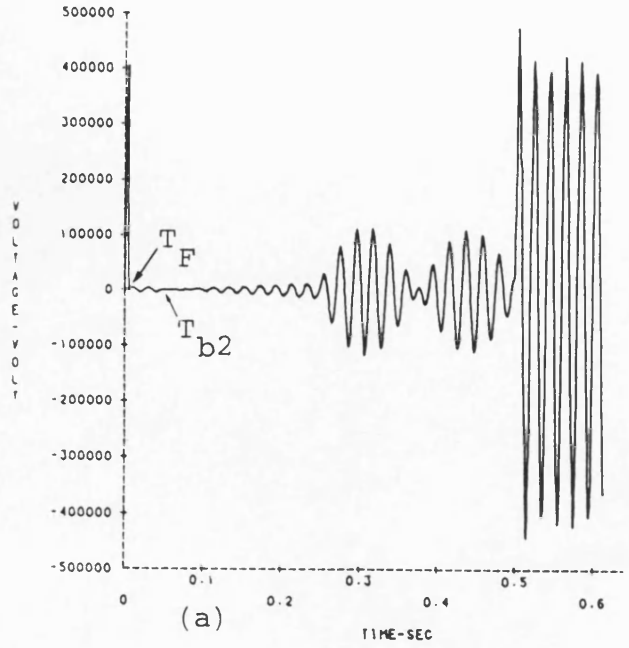

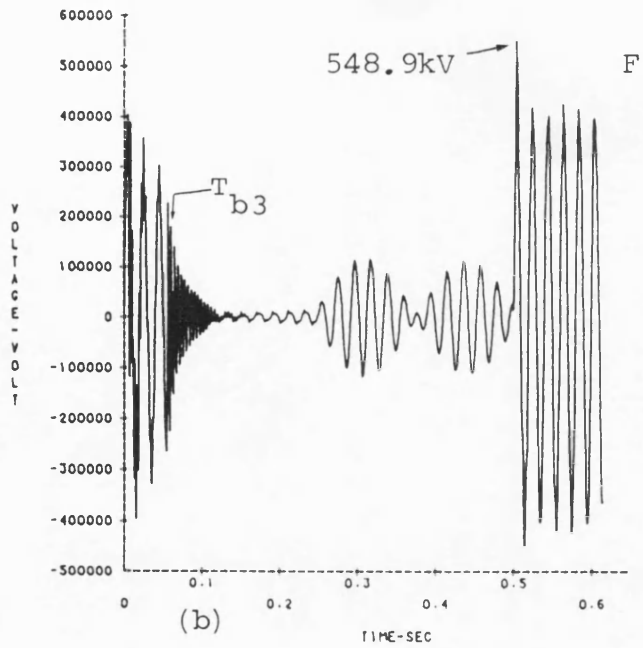

Fig. 9.4 Faulted phase voltage and current

Fault condition, and legend as in fig. 9.3.

(a) "a"-earth voltage at sending end
(b) "a"-earth voltage at receiving end
(c) "a"-phase current at sending end
(d) "a"-phase current at receiving end

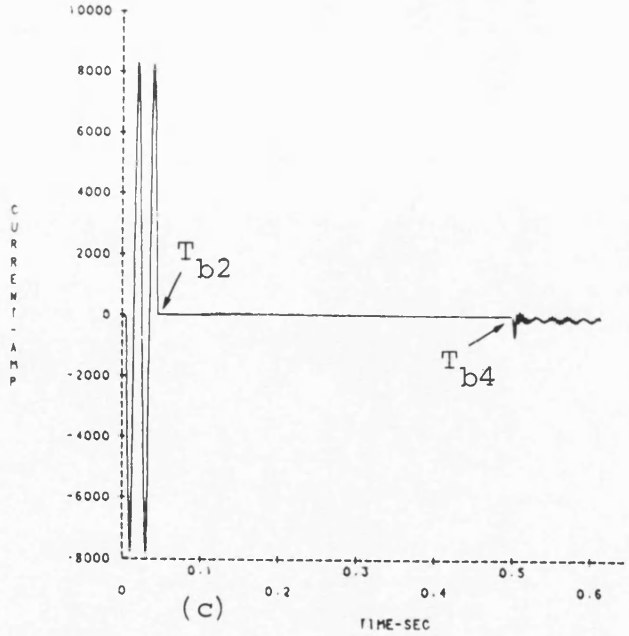

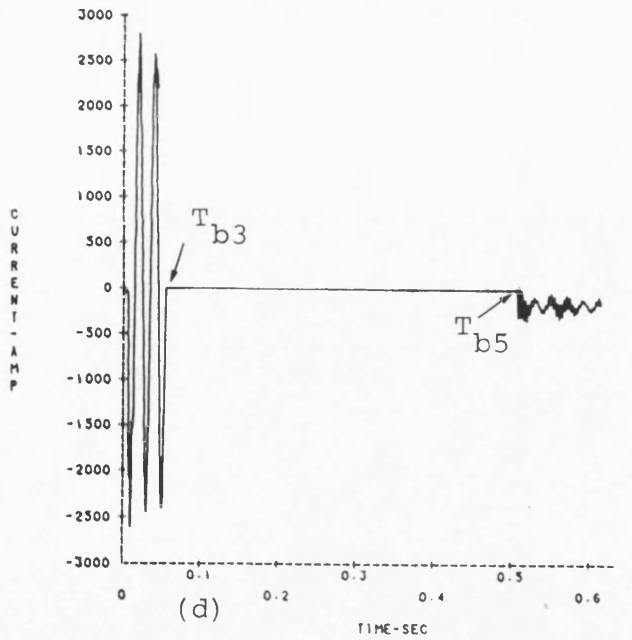

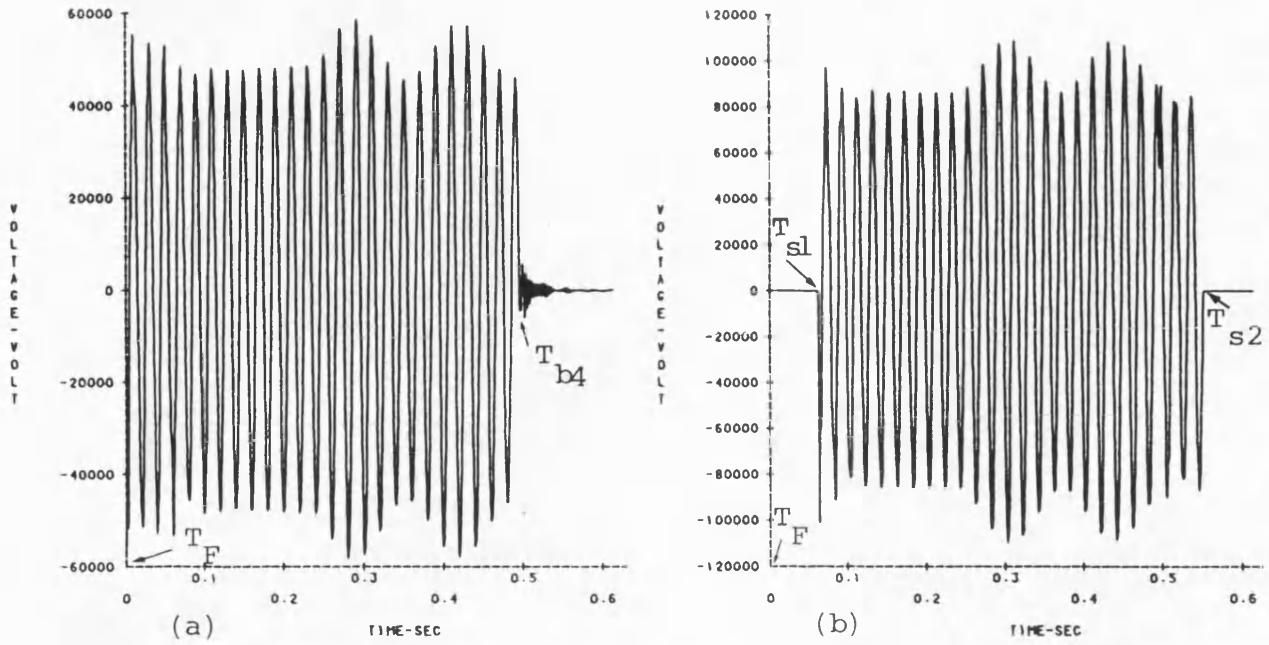

Fig. 9.5 Voltage across the neutral reactance

Fault condition and legend as in fig. 9.3.

(a) Voltage across X_{ns}

(b) Voltage across X_{nr}

Fig. 9.6 Ideal neutral switch current

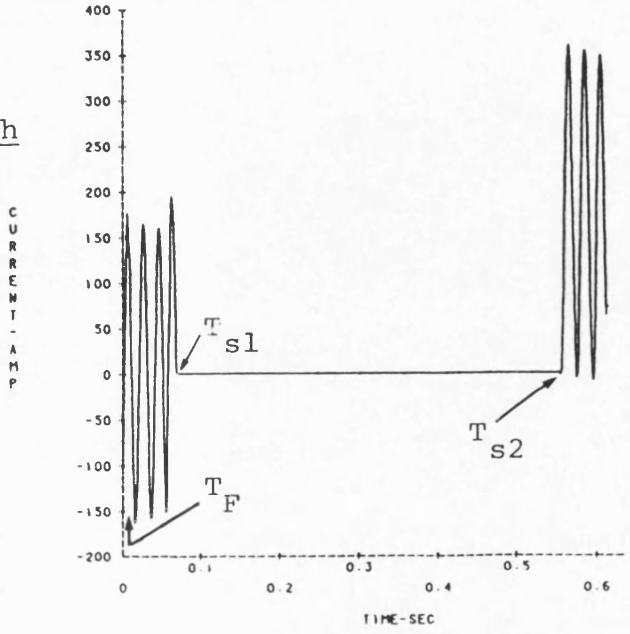

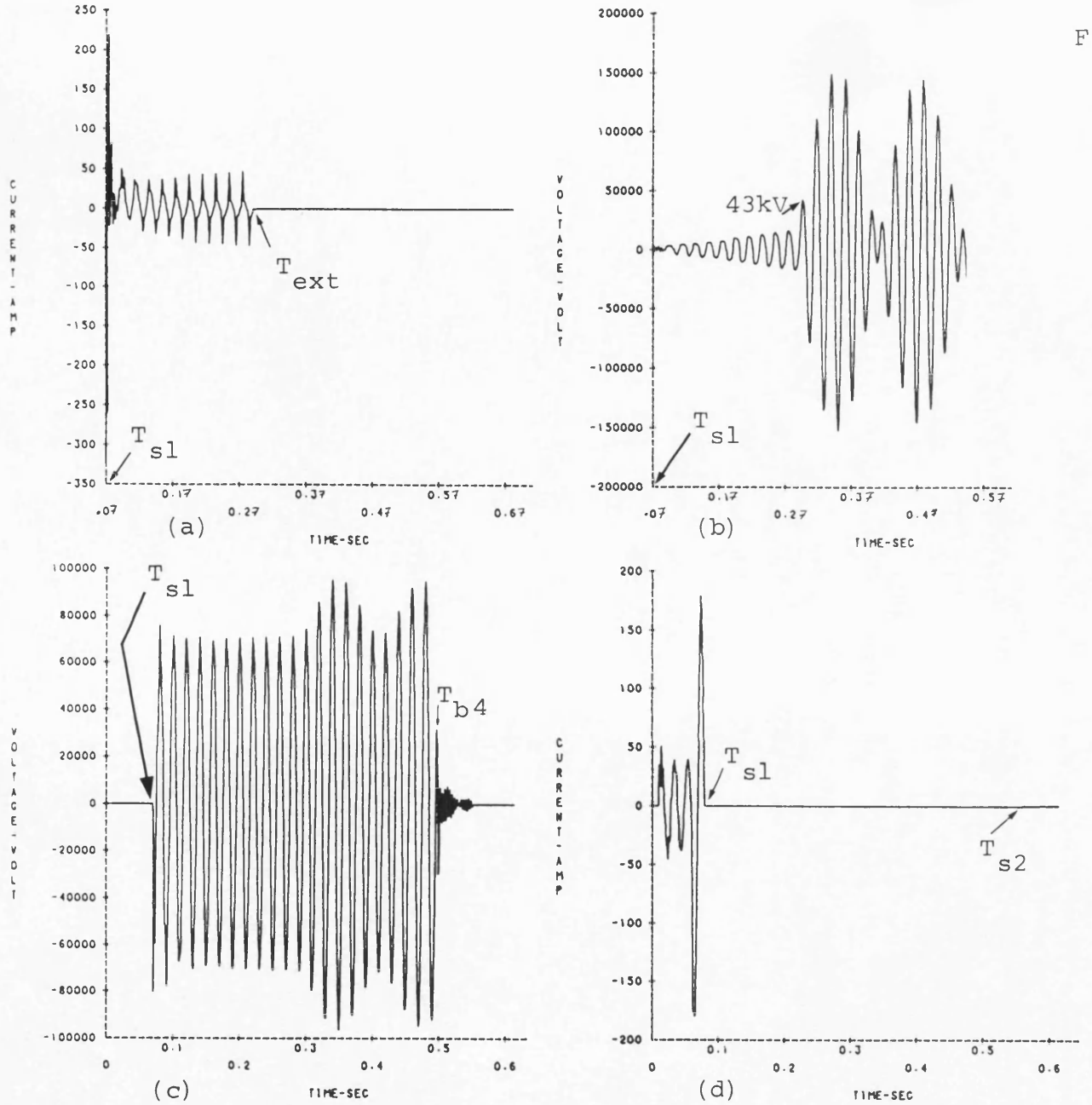

Fig. 9.7 Fault on the inner phase

"c"-phase to earth fault at the sending end, no-load condition.

L = 300km, $V_S/V_R = 1\angle 0^\circ$,
s.c.1 = s.c.2 = 5GVA, $h_1 = 0.75$.

T_{s1} = 70 msec (a.f.),
T_{ext} = 221.6 msec,
T_{b4} = 495.6 msec (a.f.),
T_{s2} = 551.2 msec (a.f.).

(a) Secondary arc current
(b) Secondary arc voltage
(c) Voltage across X_{nr}
(d) The ideal neutral switch current

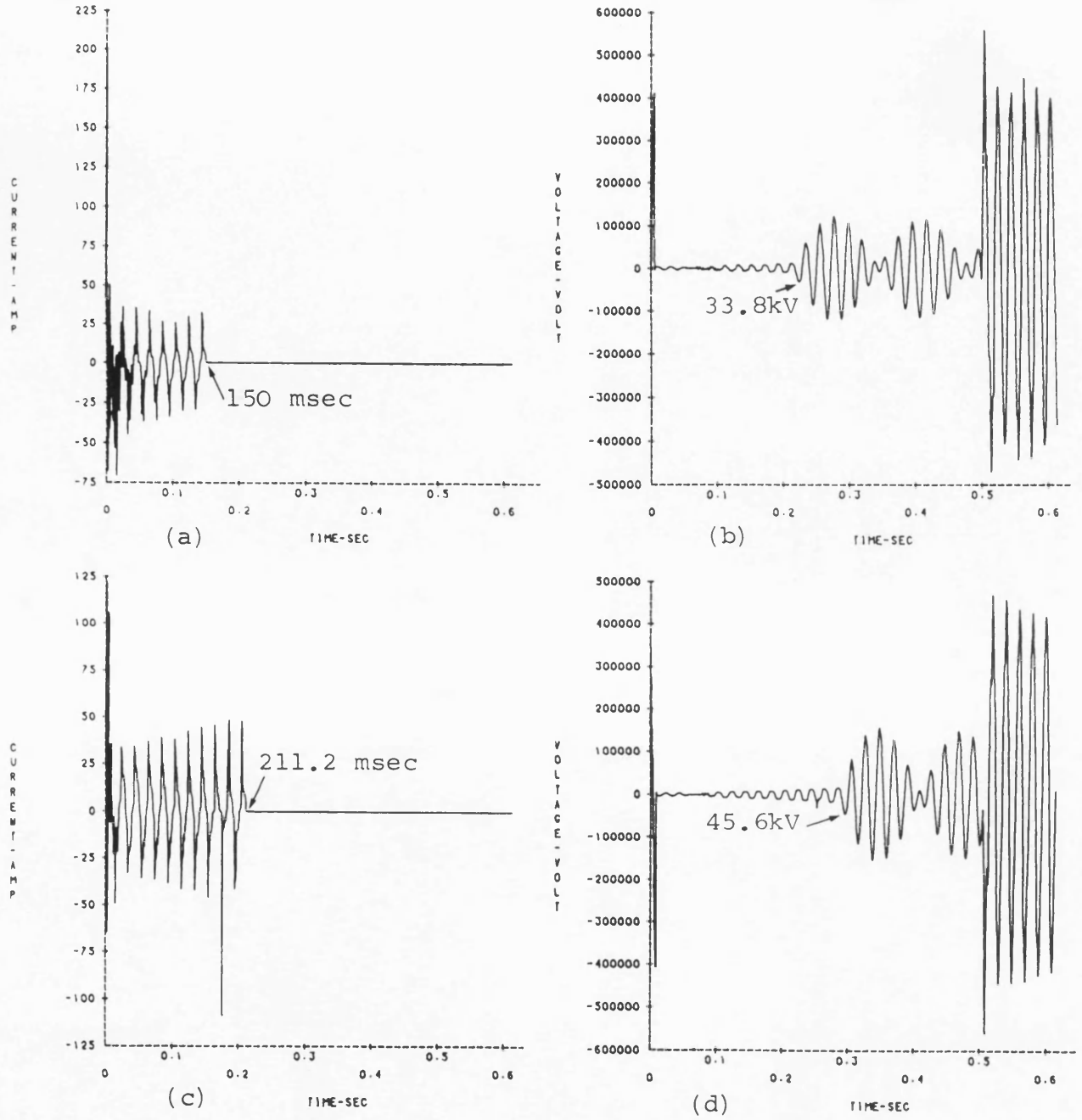

Fig. 9.8 Fault at mid point

No-load condition.

L = 300km, h_1 = 0.75,

s.c.1 = s.c.2 = 5GVA,

$V_S/V_R = 1\angle 0^o$.

Outer phase-"a" to earth fault

(a) Secondary arc current
(b) Fault point voltage to earth

Inner phase-"c" to earth fault

(c) Secondary arc current
(b) Fault point voltage to earth

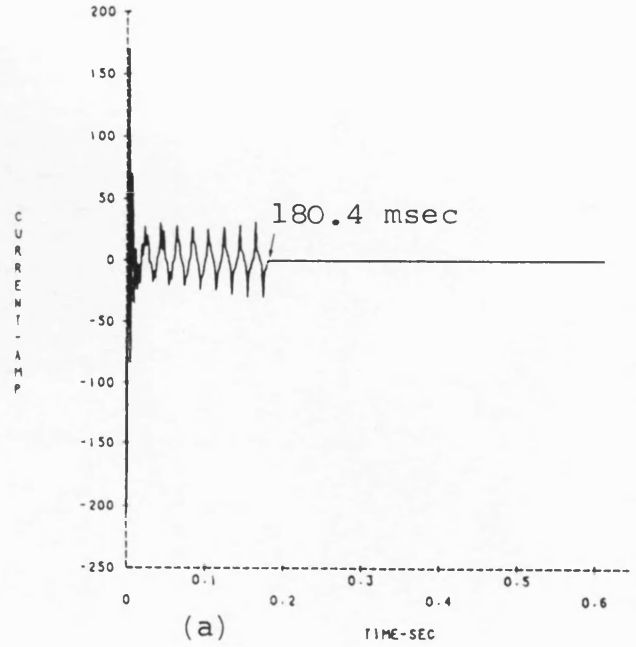

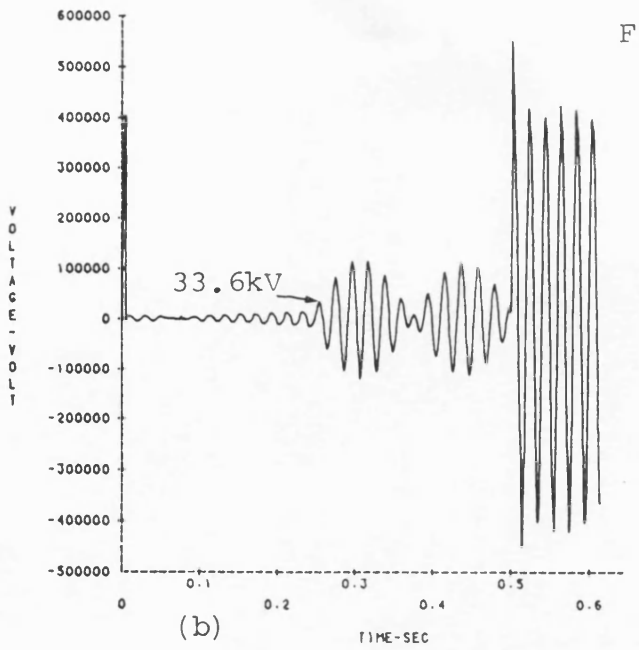

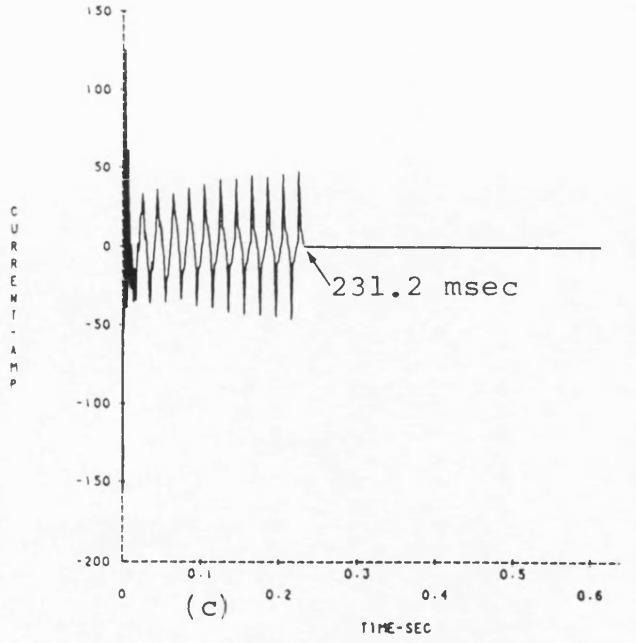

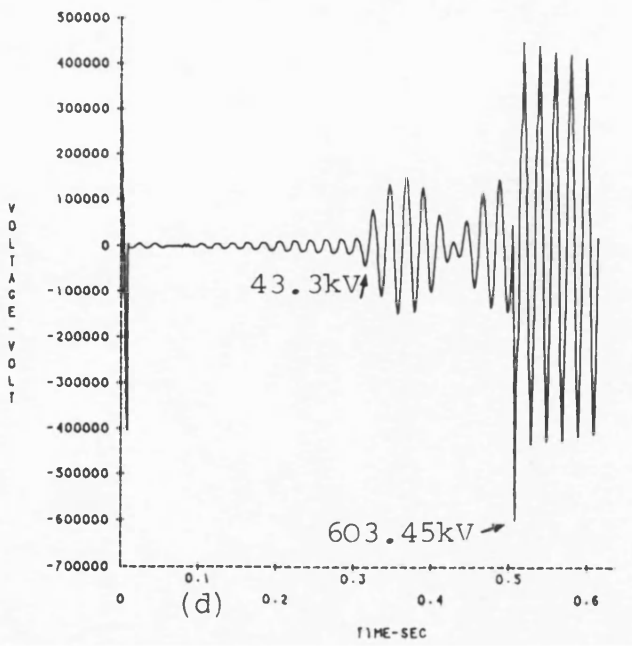

Fig. 9.9 Fault at the switched reactor terminal

No-load condition

L = 300km, h_1 = 0.75,

s.c.1 = s.c.2 = 5GVA,

$V_S/V_R = 1\angle 0^\circ$.

Outer phase-"a" to earth fault

(a) Secondary arc current
(b) Fault point voltage to earth

Inner phase-"c" to earth fault

(c) Secondary arc current
(d) Fault point voltage to earth

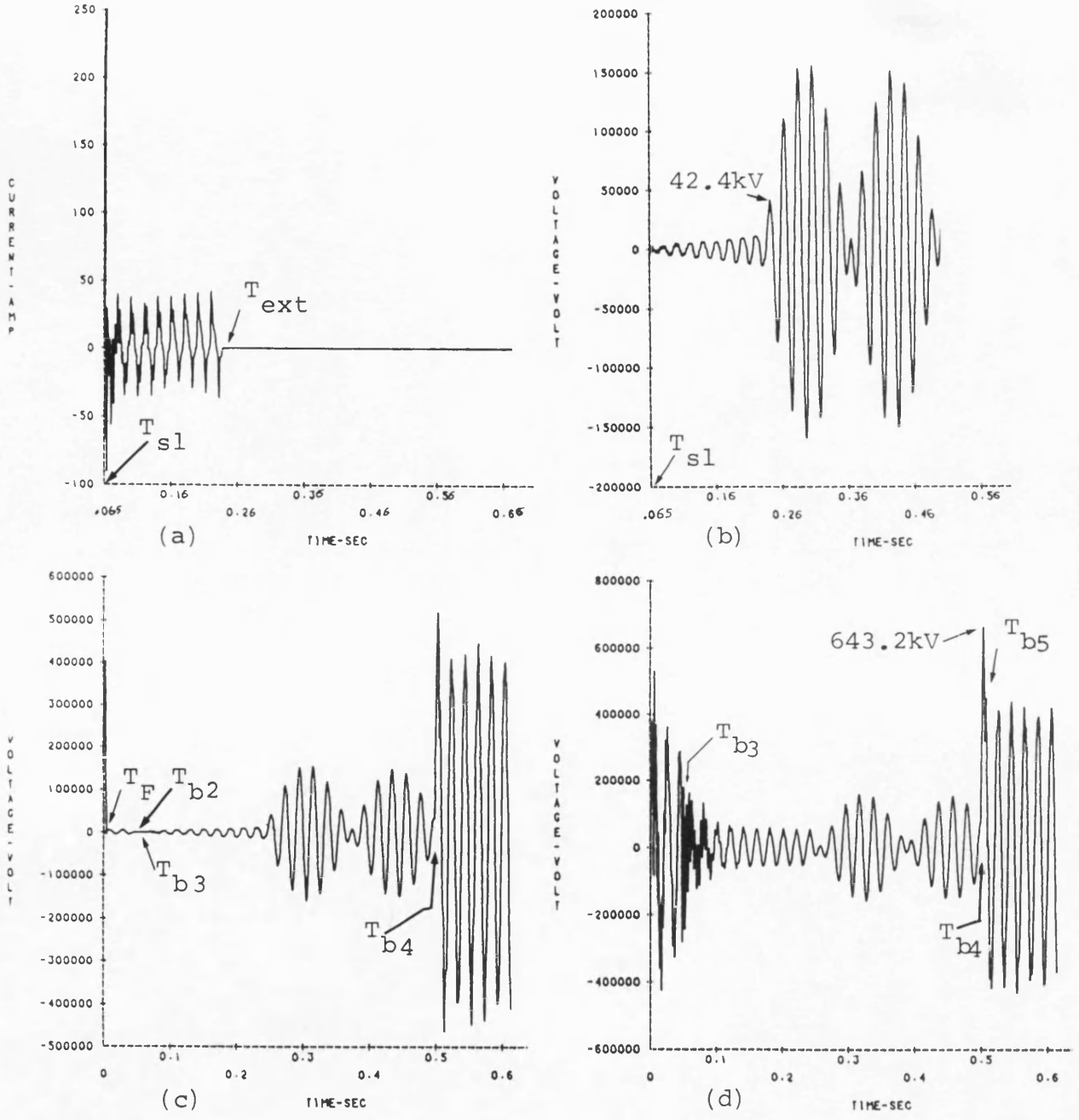

Fig. 9.10 Outer phase fault at the sending end: Power transfer from sending to receiving end

"a"-earth fault.

$L = 300km$, $h_1 = 0.75$,

s.c.1 = s.c.2 = 5GVA,

$V_S/V_R = 1\angle 25.73^o$.

T_{b2} = 39.2msec (a.f.),

T_{b3} = 42.4 msec (a.f.),

T_{s1} = 65.2 msec (a.f.),

T_{ext} = 177.2 msec (a.f.),

T_{b4} = 494.6 msec (a.f.),

T_{b5} = 500.8 msec (a.f.),

T_{s1} = 553.2 msec (a.f.).

(a) Secondary arc current
(b) Secondary arc voltage
(c) "a"-earth voltage at sending end
(d) "a"-earth voltage at receiving end

Fig. 9.10 (continued)

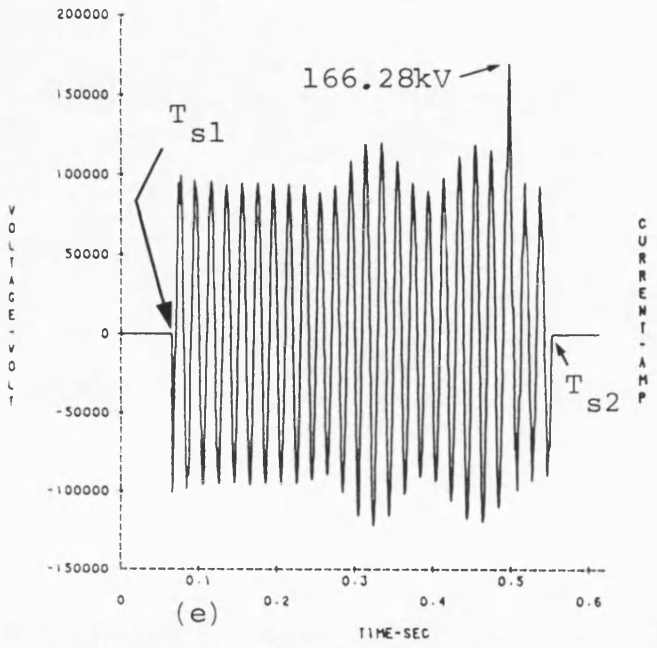

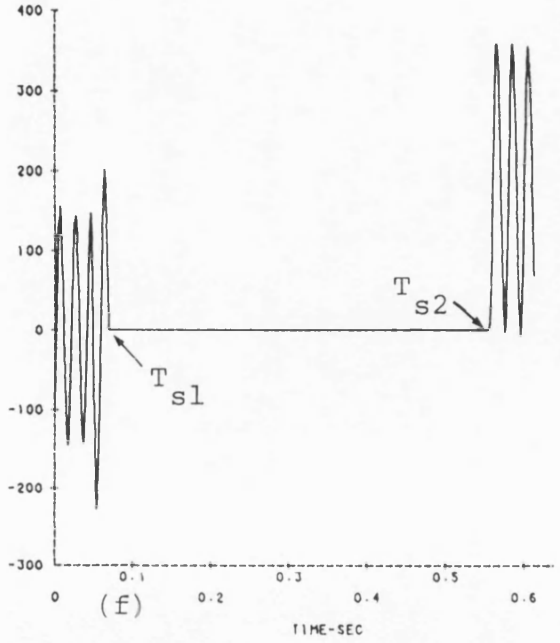

(e) Voltage across X_{nr}

(f) The ideal neutral switch current

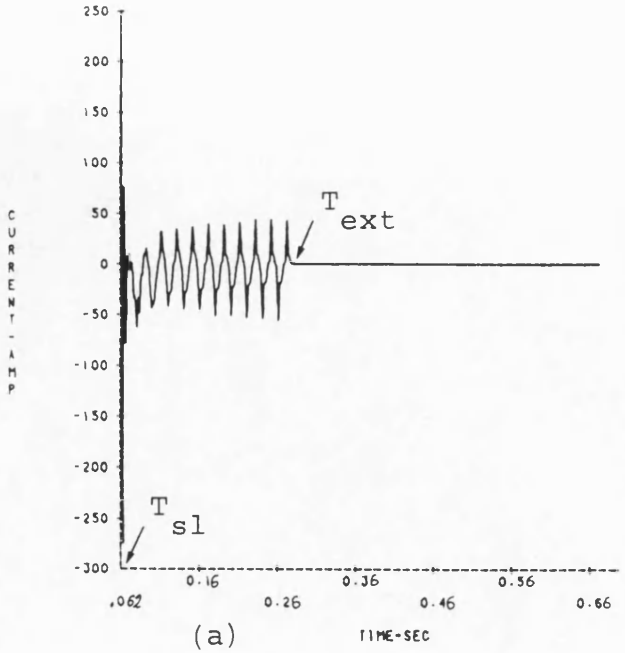

(a)

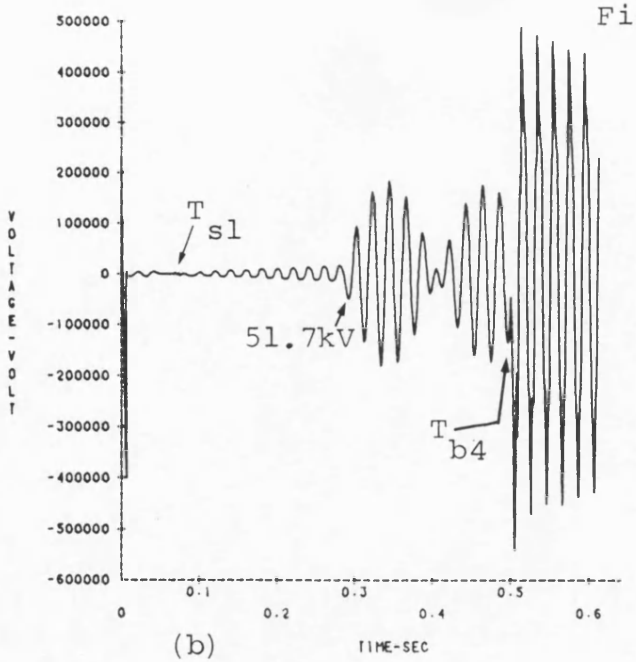

(b)

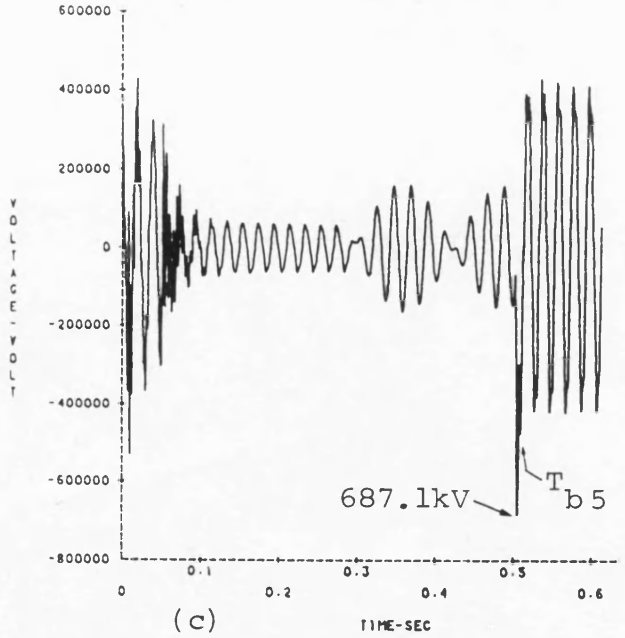

(c)

Fig. 9.11 Inner phase fault at the sending end: Power transfer from sending to receiving end

"c"-earth fault

L = 300km, h_1 = 0.75,

s.c.1 = s.c.2 = 5GVA,

$V_S/V_R = 1\angle 25.73^{o}$.

T_{sl} = 62.4 msec (a.f.),

T_{ext} = 217.6 msec ,

T_{b4} = 494.8 msec (a.f.),

T_{b5} = 500.8 msec (a.f.).

(a) Secondary arc current
(b) "c"-earth voltage at sending end
(c) "c"-earth voltage at receiving end

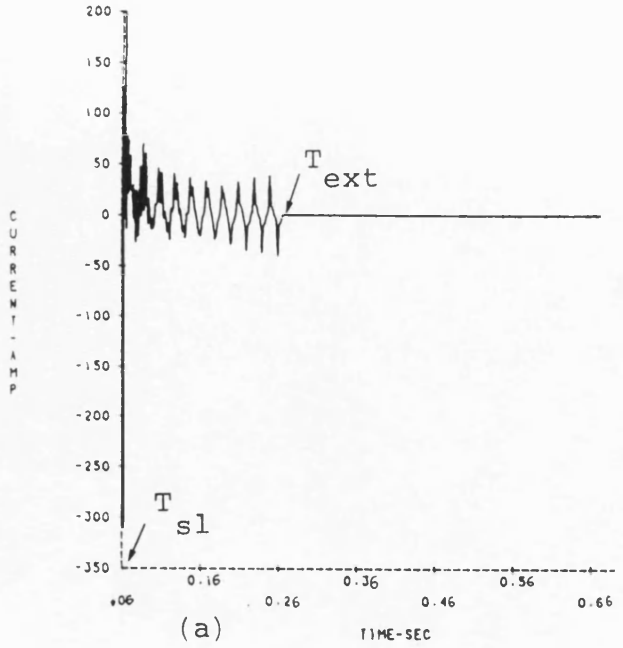

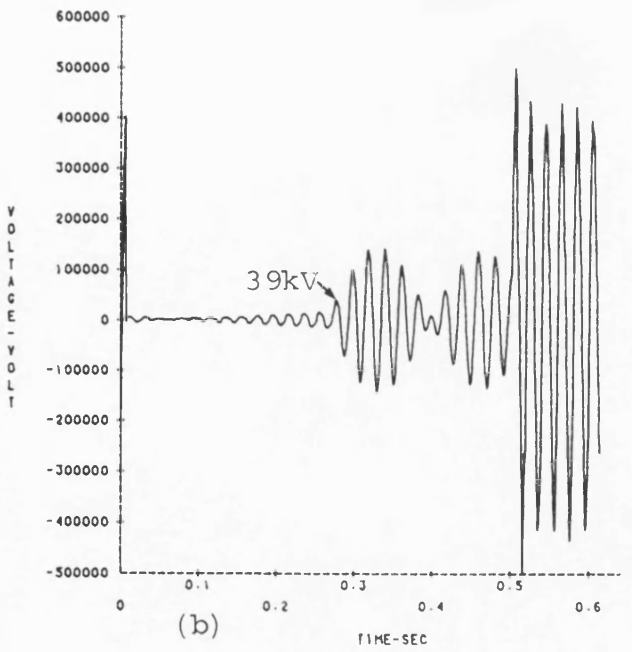

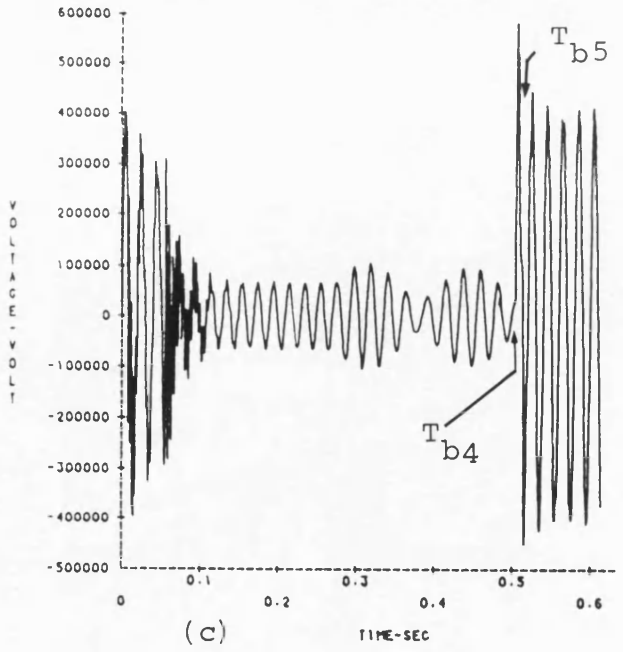

Fig. 9.12 Outer phase fault at sending end: Power transfer from receiving to sending end

"a"-earth fault

$L = 300km$, $h_1 = 0.75$,

s.c.1 = s.c.2 = 5GVA,

$V_S/V_R = 1\angle -25.73^{\circ}$.

$T_{sl} = 61.6$ msec (a.f.),

$T_{ext} = 204.4$ msec ,

$T_{b4} = 496.8$ msec (a.f.),

$T_{b5} = 509.2$ msec (a.f.).

(a) Secondary arc current
(b) "a"-earth voltage at sending end
(c) "a"-earth voltage at receiving end

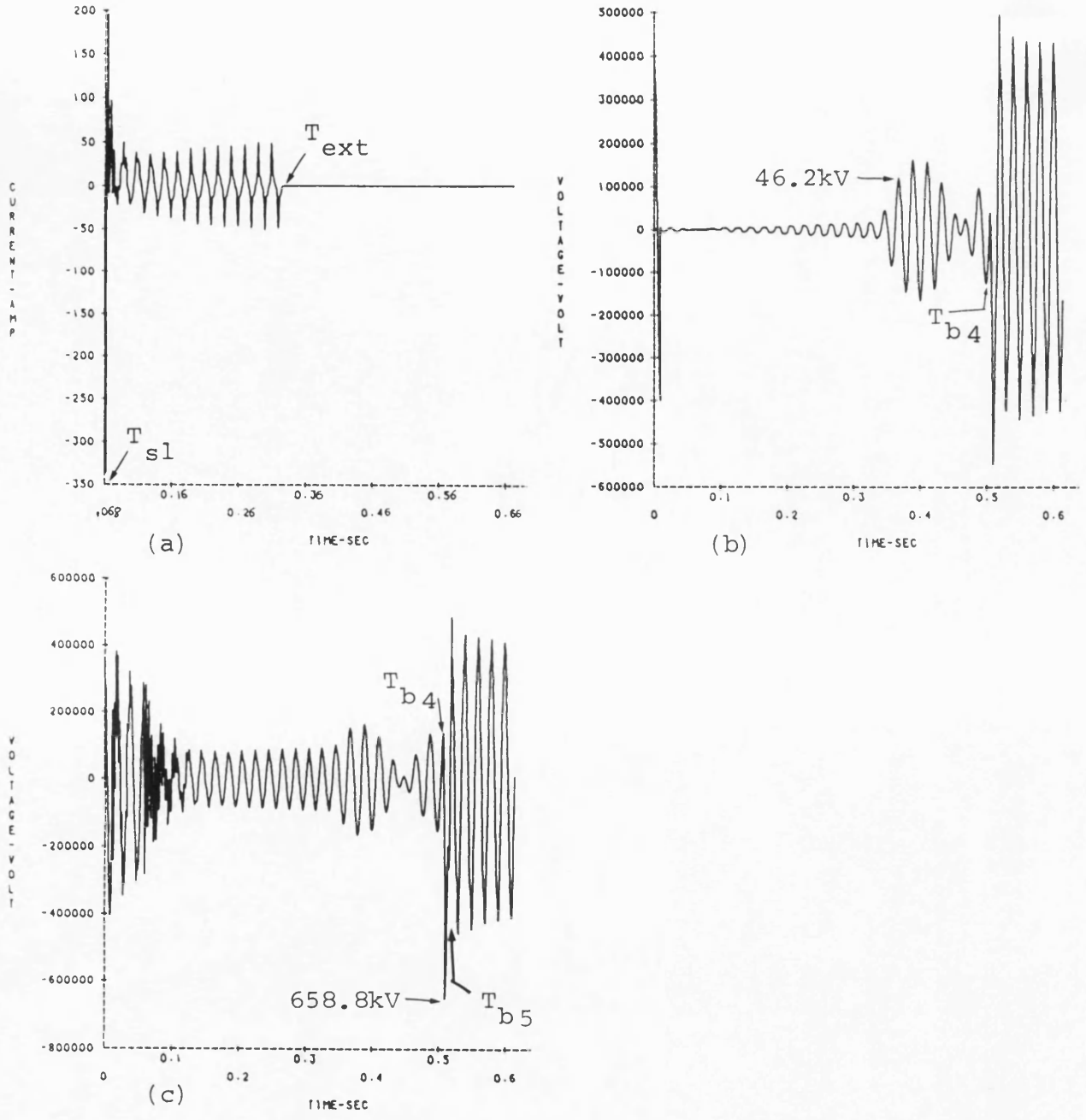

Fig. 9.13 Inner phase fault at the sending end: Power transfer from receiving to sending end

"c"-earth fault

$L = 300km$, $h_1 = 0.75$,

s.c.1 = s.c.2 = 5GVA,

$V_S/V_R = 1\underline{/25.73^{\circ}}$.

$T_{sl} = 68$ msec (a.f.),

$T_{ext} = 264.8$ msec,

$T_{b4} = 496$ msec (a.f.),

$T_{b5} = 508.8$ msec (a.f.).

(a) Secondary arc current
(b) "c"-earth voltage at sending end
(c) "c"-earth voltage at receiving end

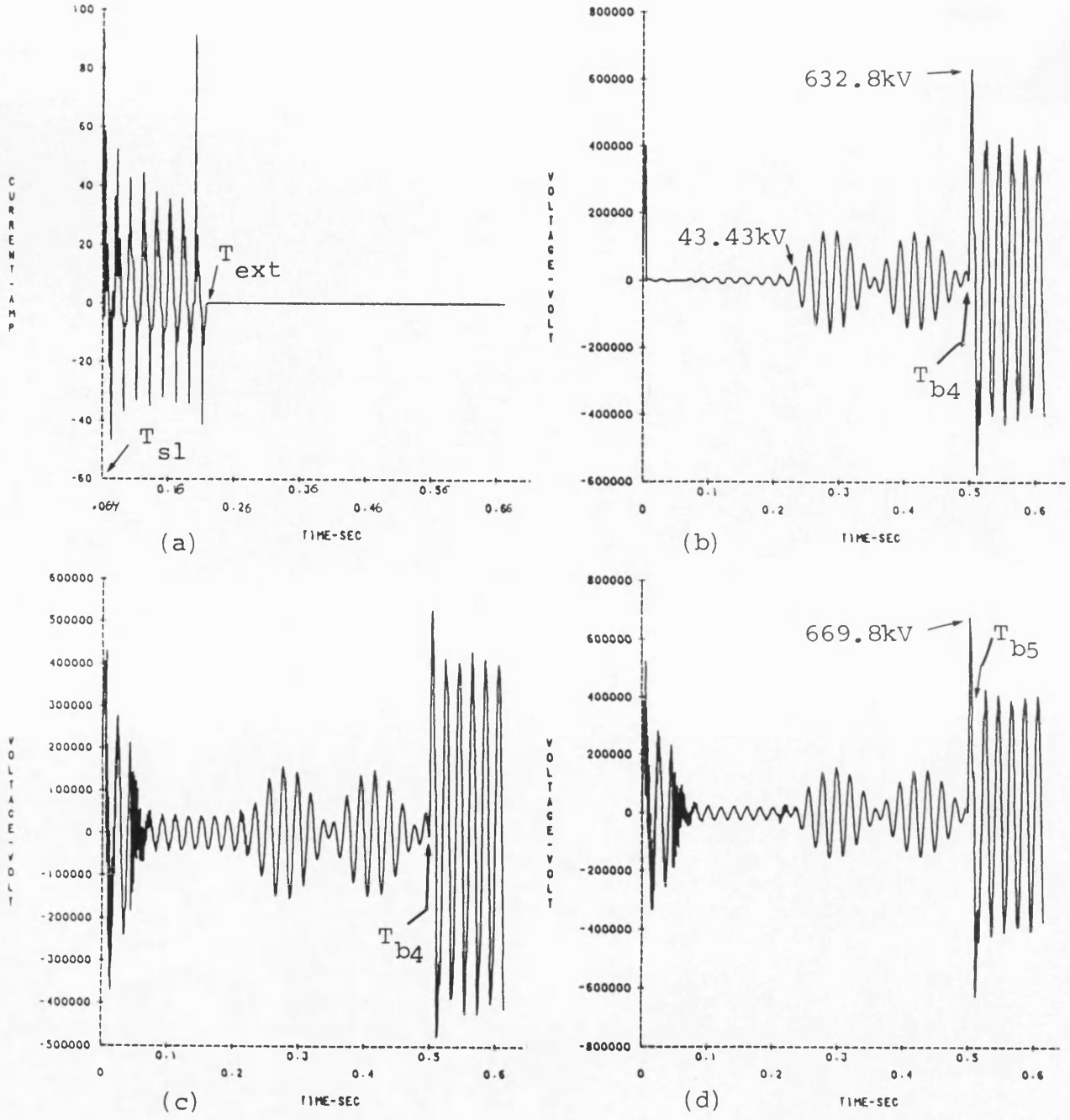

Fig. 9.14 Outer phase fault at mid point: Power transfer from sending to receiving end

"a"-earth fault

$L = 300km$, $h_1 = 0.75$,

$s.c.1 = s.c.2 = 5GVA$,

$V_S/V_R = 1\angle 25.73^{o}$.

$T_{s1} = 64.4$ msec (a.f.),

$T_{ext} = 158.4$ msec,

$T_{b4} = 493.6$ msec (a.f.),

$T_{b5} = 509.6$ msec (a.f.).

(a) Secondary arc current
(b) Fault point voltage to earth
(c) "a"-earth voltage at sending end
(d) "a"-earth voltage at receiving end

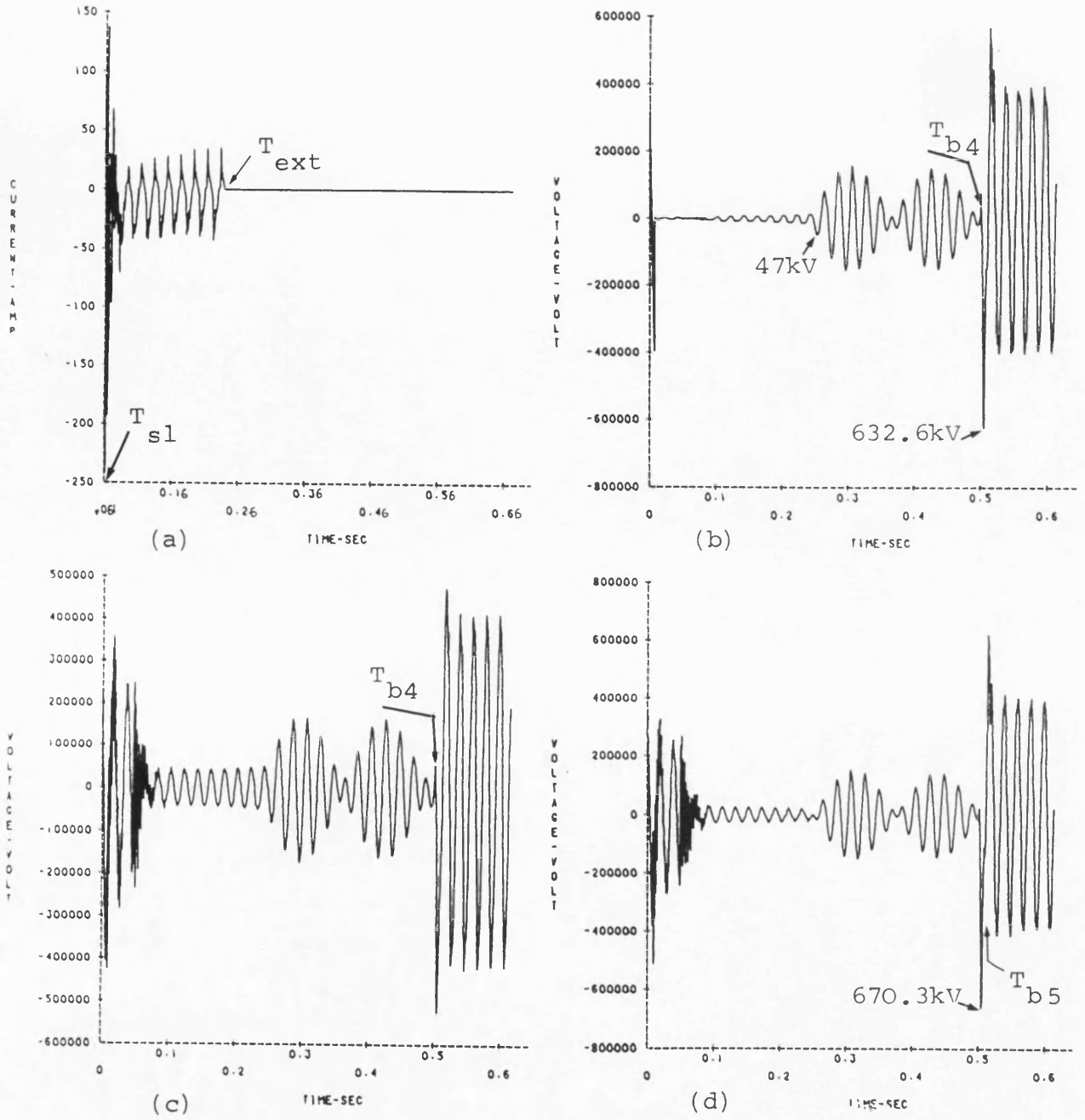

Fig. 9.15 Inner phase fault at mid point: Power transfer from sending to receiving end

"c"-earth fault

L = 300km, h_1 = 0.75,

s.c.1 = s.c.2 = 5GVA,

$V_S/V_R = 1\angle 25.73^{\circ}$.

T_{sl} = 61.2 msec (a.f.),

T_{ext} = 179.2 msec,

T_{b4} = 493.2 msec (a.f.),

T_{b5} = 509.6 msec (a.f.).

(a) Secondary arc current
(b) Fault point voltage to earth
(c) "c"-earth voltage at sending end
(d) "c"-earth voltage at receiving end

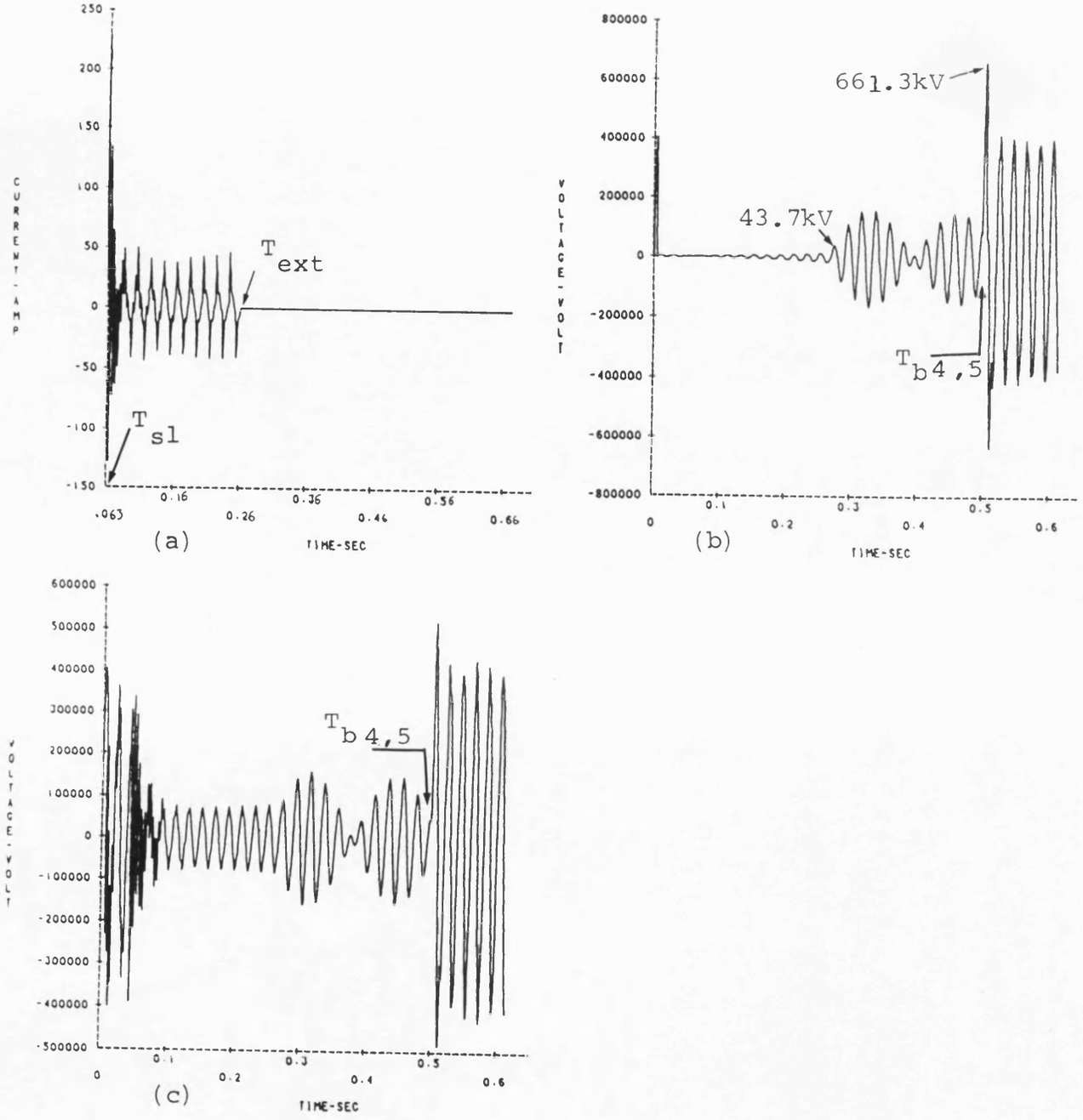

Fig. 9.16 Outer phase fault at the receiving end: Power transfer from sending to receiving end

"a"-earth fault

L = 300km, h_1 = 0.75,

s.c.1 = s.c.2 = 5GVA,

$V_S/V_R = 1\angle 25.73^{\circ}$.

T_{s1} = 63.2 msec (a.f.),

T_{ext} = 200.4 msec ,

T_{b4} = 493.2 msec (a.f.),

T_{b5} = 493.6 msec (a.f.),

(a) Secondary arc current
(b) Fault point voltage to earth
(c) "a"-earth voltage at sending end

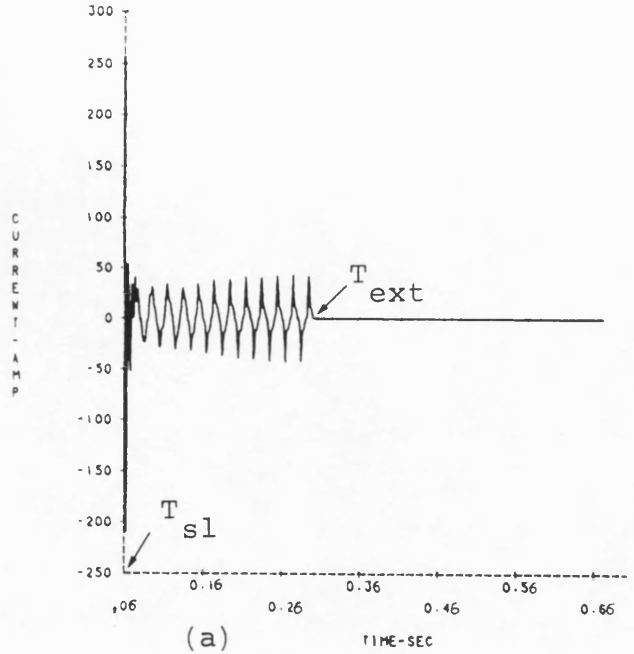

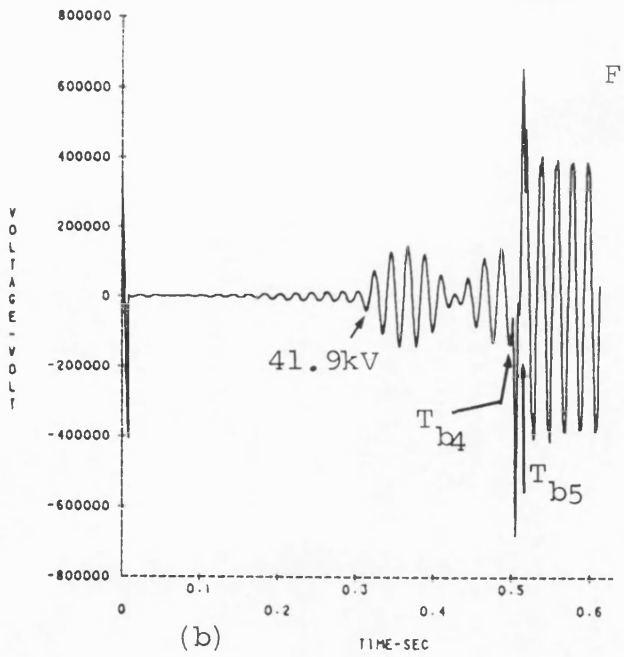

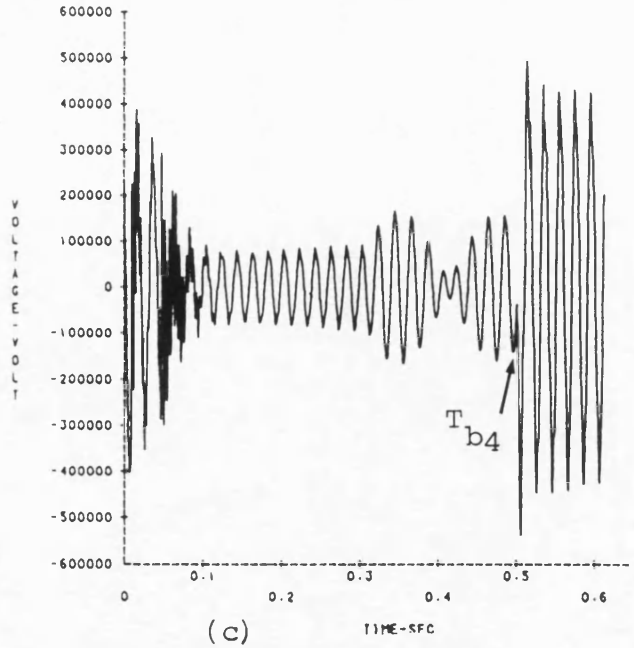

Fig. 9.17 Inner phase fault at the receiving end: Power transfer from sending to receiving end

"c"-earth fault

L = 300km, h_1 = 0.75,

s.c.1 = s.c.2 = 5GVA,

$V_S/V_R = 1/\underline{25.73^o}$.

T_{s1} = 60.4 msec (a.f.),

T_{ext} = 241.2 msec,

T_{b4} = 493.2 msec (a.f.),

T_{b5} = 508.8 msec (a.f.).

(a) Secondary arc current
(b) Fault point voltage to earth
(c) "c"-earth voltage at sending end

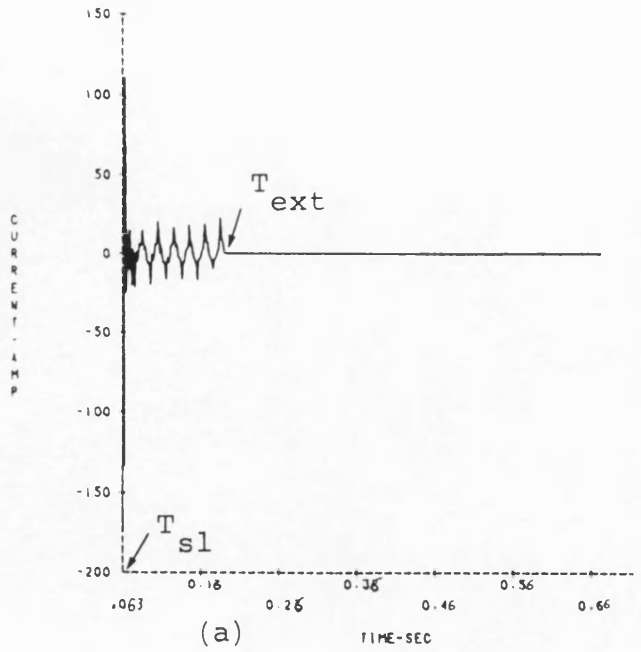

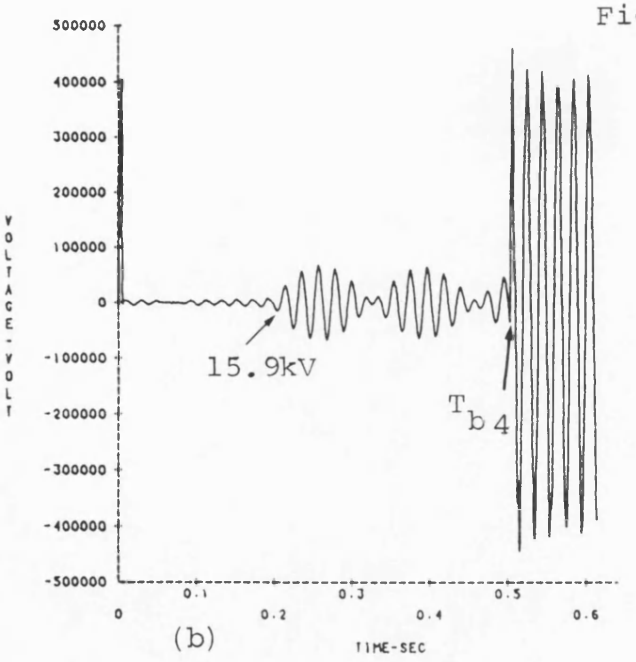

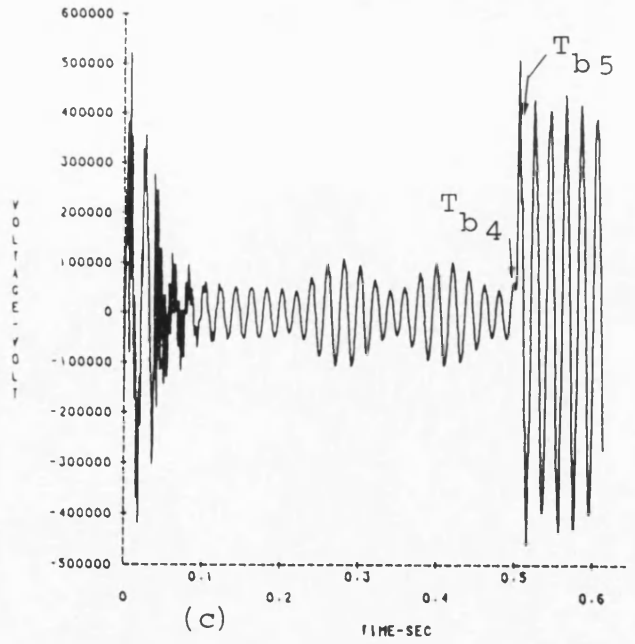

Fig. 9.18 Outer phase fault at the receiving end: Power transfer from receiving to sending end

"a"-earth fault

$L = 300km$, $h_1 = 0.75$,

s.c.1 = s.c.2 = 5GVA,

$V_S/V_R = 1\angle -25.73^{\circ}$.

T_{s1} = 63.2 msec (a.f.),

T_{ext} = 130.8 msec,

T_{b4} = 497.6 msec (a.f.),

T_{b5} = 500.8 msec (a.f.).

(a) Secondary arc current
(b) Fault point voltage to earth
(c) "a"-earth voltage at sending end

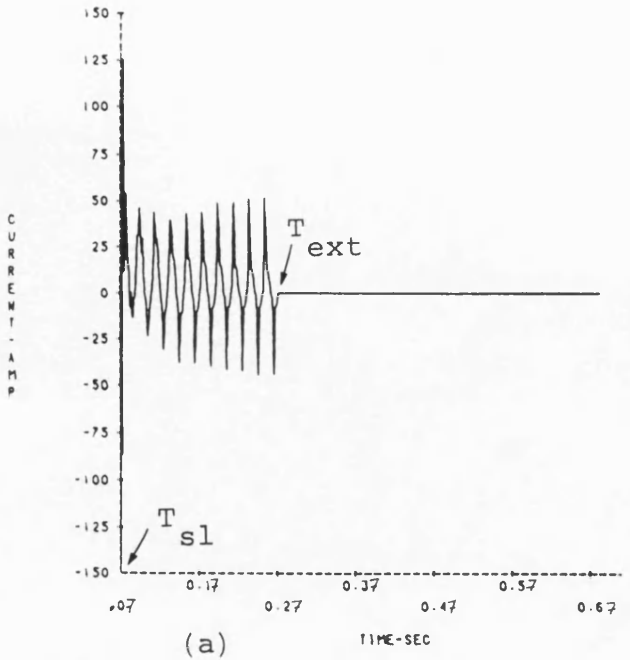

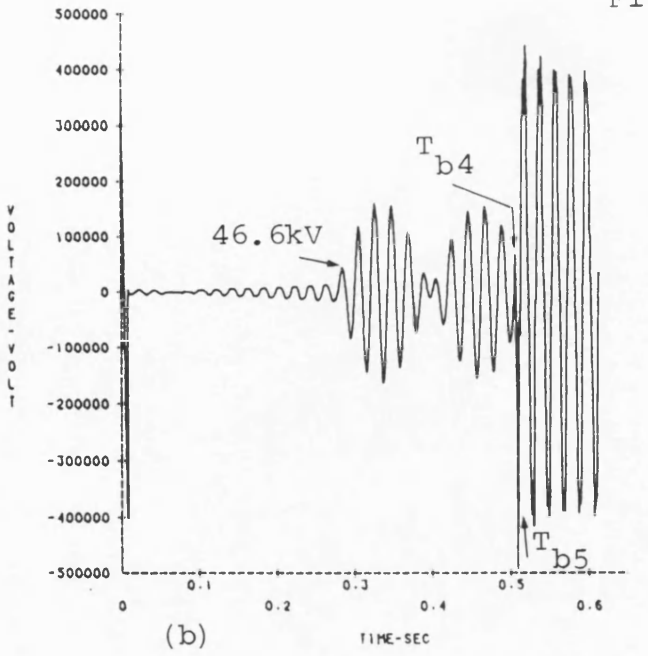

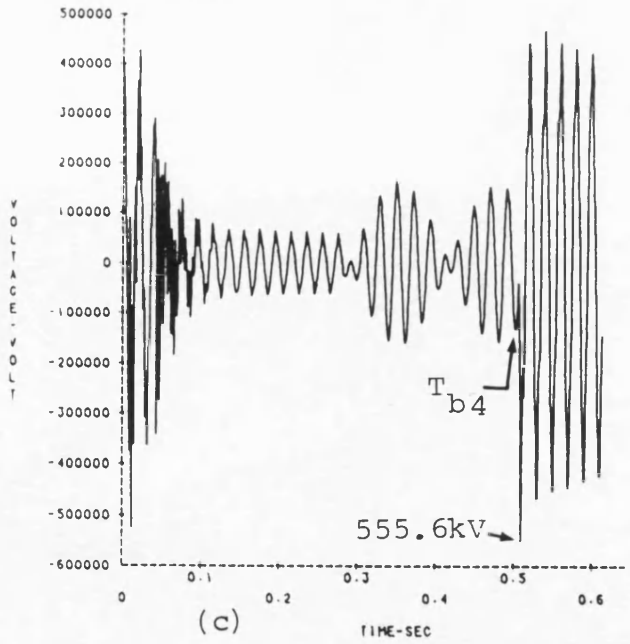

Fig. 9.19 Inner phase fault at the receiving end: Power transfer from receiving to sending end

"c"-earth fault

$L = 300km$, $h_1 = 0.75$,

s.c.1 = s.c.2 = 5GVA,

$V_S/V_R = 1\angle -25.73^{\circ}$.

$T_{s1} = 70$ msec(a.f.),

$T_{ext} = 201.2$ msec,

$T_{b4} = 497.6$ msec (a.f.),

$T_{b5} = 500.8$ msec (a.f.).

(a) Secondary arc current
(b) Fault point voltage to earth
(c) "c"-earth voltage at sending end

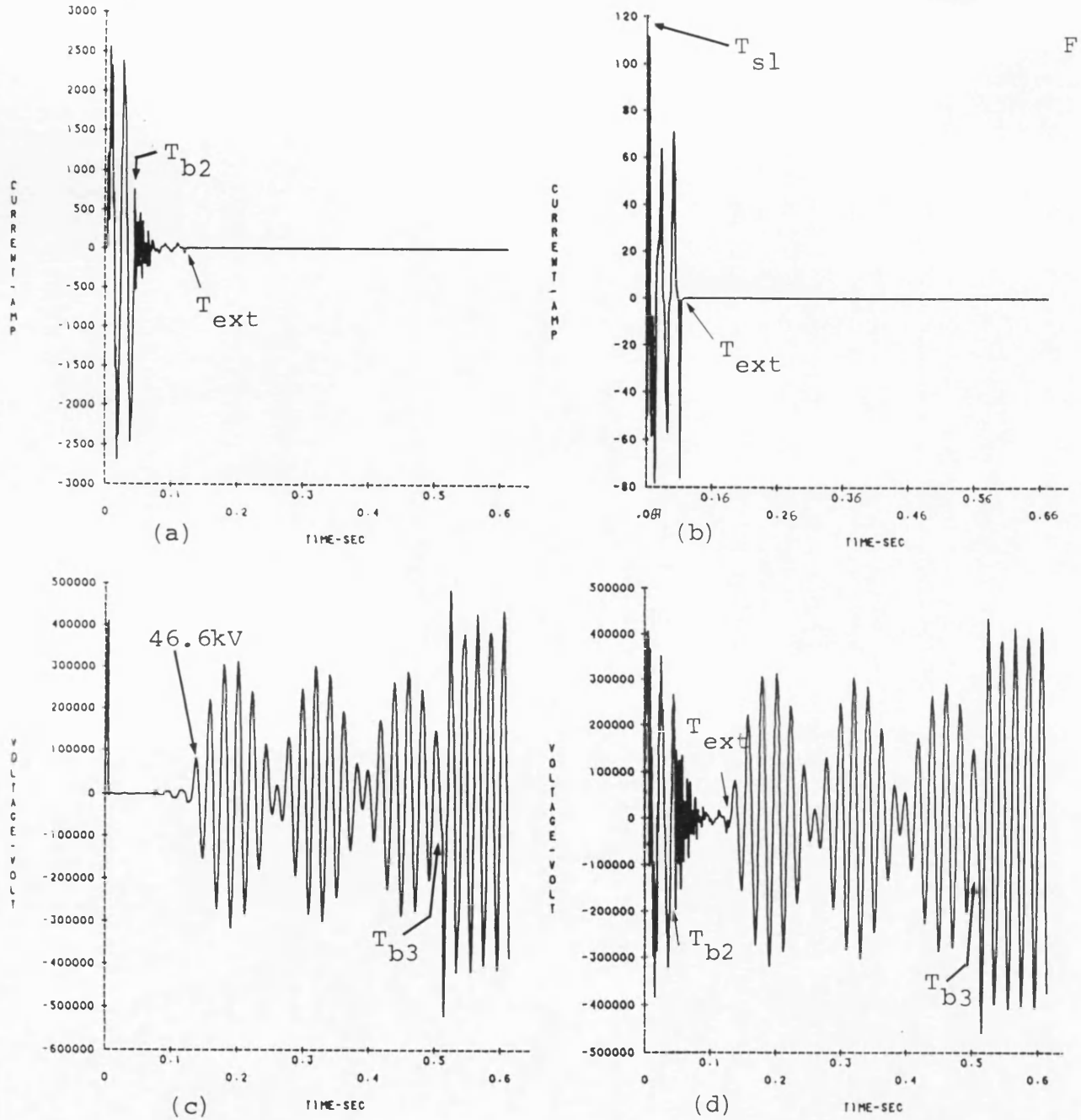

Fig. 9.20 Line energised from receiving end only: Outer phase fault at the sending end

"a"-earth fault

L = 300km, h_1 = 0.75,

s.c.2 = 5GVA .

T_{b2} = 39.6 msec (a.f.),

T_{s1} = 69.6 msec (a.f.),

T_{ext} = 56.8 msec,

T_{b3} = 505.6 msec (a.f.).

(a) Fault path current
(b) Secondary arc current
(c) Fault point voltage to earth
(d) "a"-earth voltage at receiving end

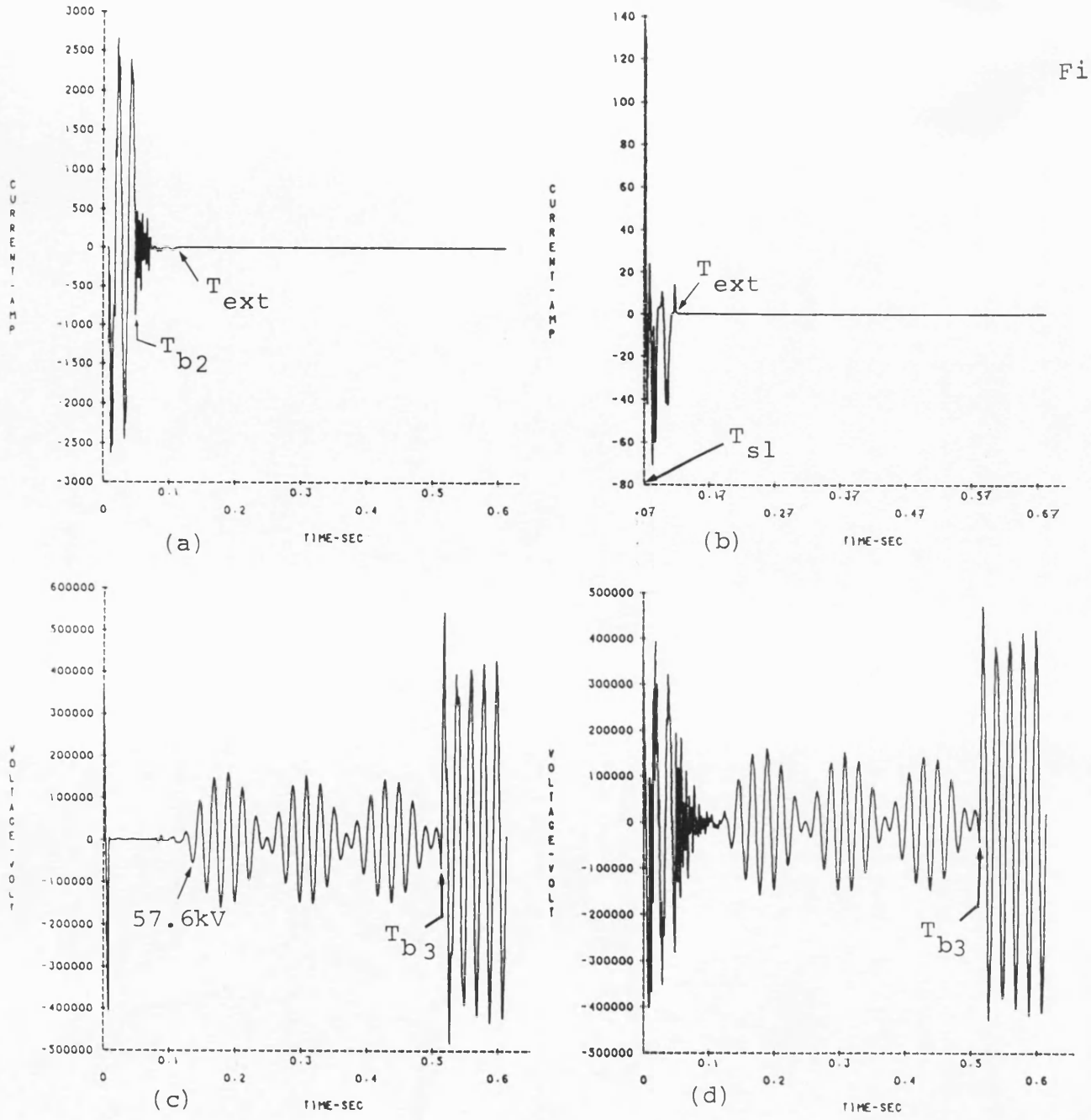

Fig. 9.21 Line energised from receiving end only: Inner phase fault at the sending end

"c"-earth fault

L = 300km, h_1 = 0.75,

s.c.2 = 5GVA.

T_{b2} = 39.6 msec (a.f.),

T_{s1} = 70 msec (a.f.),

T_{ext} = 50.8 msec,

T_{b3} = 504.8 msec (a.f.).

(a) Fault path current
(b) Secondary arc current
(c) Fault point voltage to earth
(d) "c"-earth voltage at receiving end

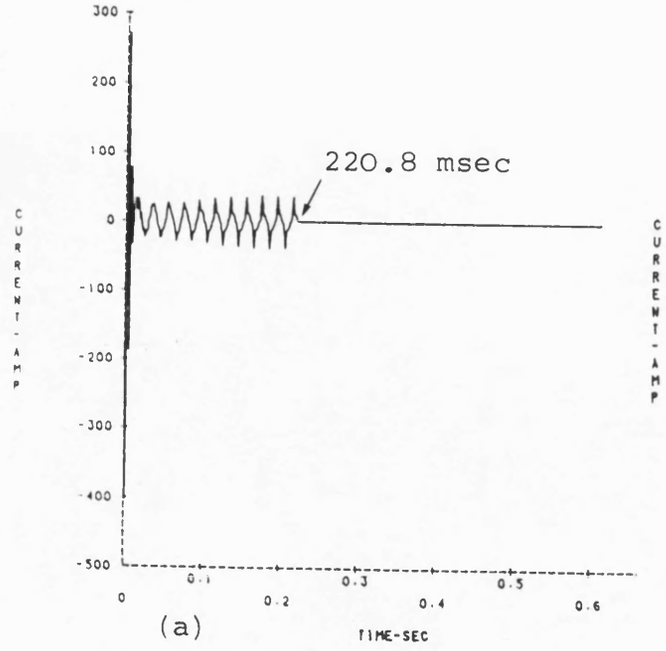

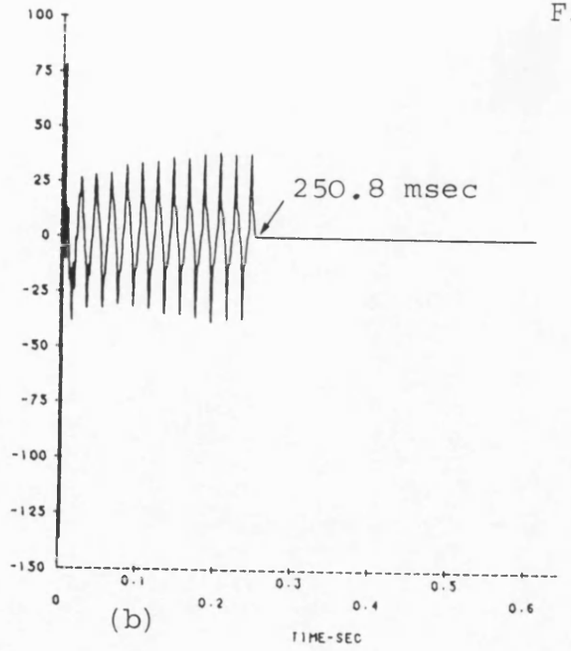

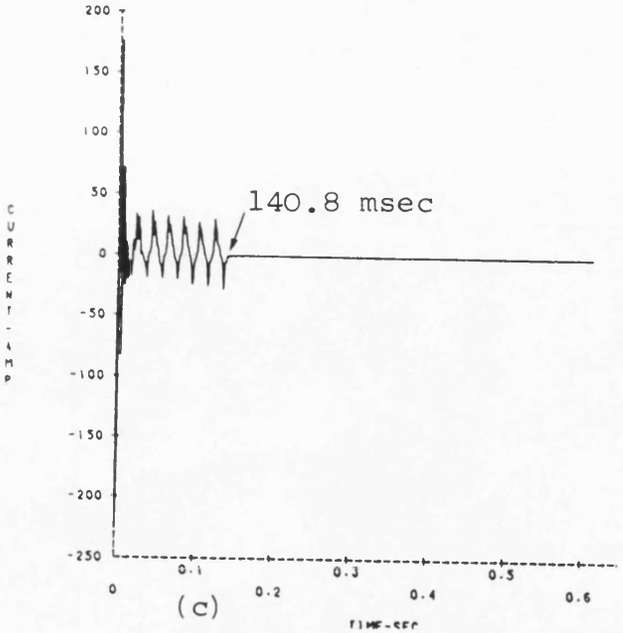

Fig. 9.22 Effect of the source Z_{So}/Z_{Sl} on the secondary arc extinction time

L = 300km, h_1 = 0.75,

s.c.1 = s.c.2 = 5GVA,

$V_S/V_R = 1\angle 0^o$.

(a) Inner phase fault at sending end

(b) Inner phase fault at receiving end

(c) Outer phase fault at receiving end

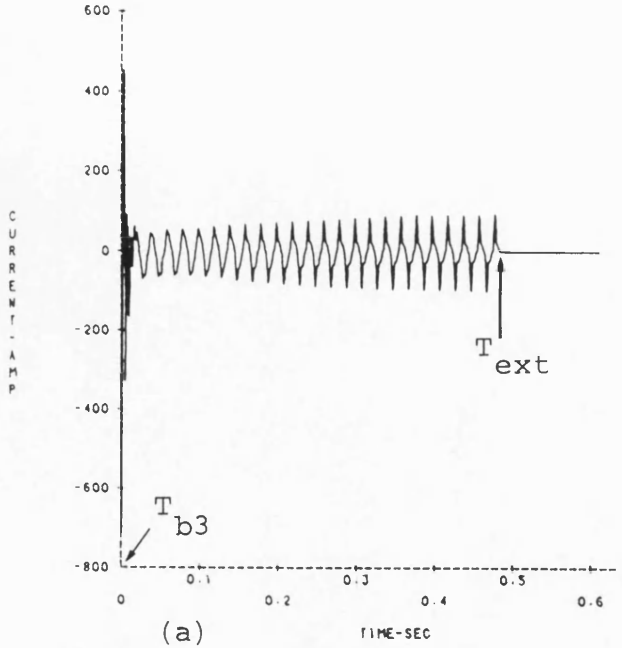

(a)

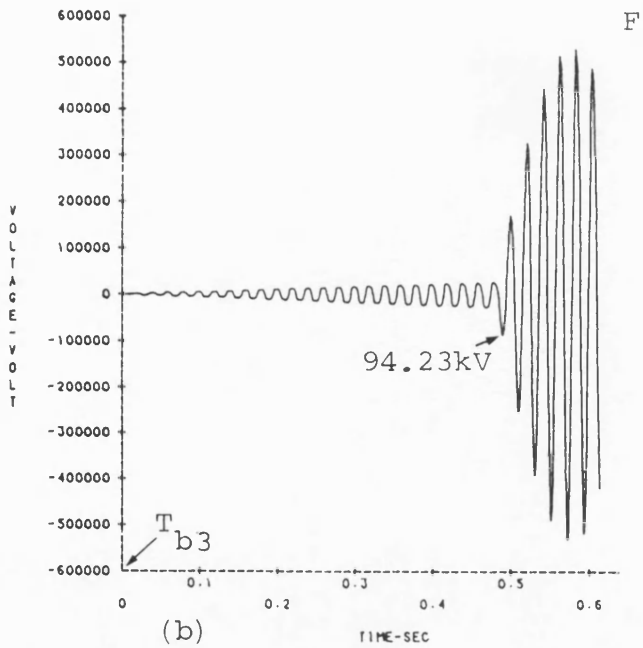

(b)

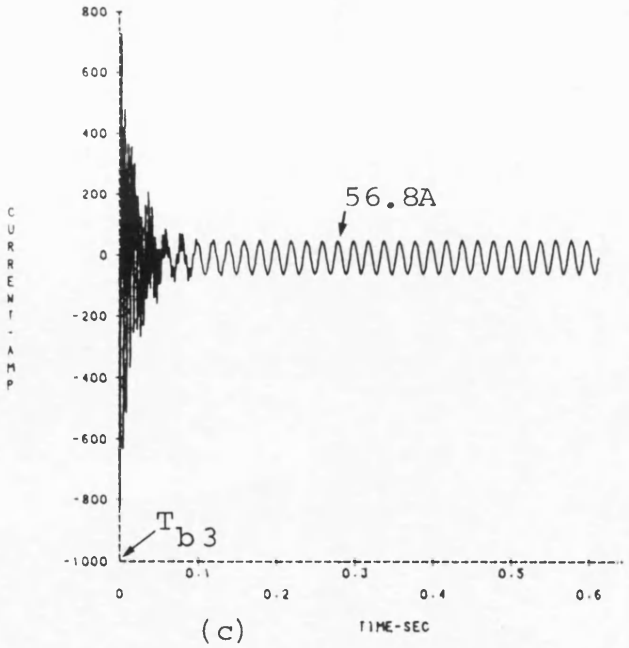

(c)

Fig. 9.23 Effect of neutral switch failure: Outer phase fault at sending end

"a"-earth fault

L = 300km, h_1 = 0.75,

s.c.1 = s.c.2 = 5GVA,

$V_S/V_R = 1\angle 0^\circ$.

T_{b3} = 49.6 msec (a.f.),

T_{ext} = 484.4 msec.

(a) Secondary arc current
(b) Secondary arc voltage
(c) Secondary arc current ($R_F = 0.5\,\Omega$)

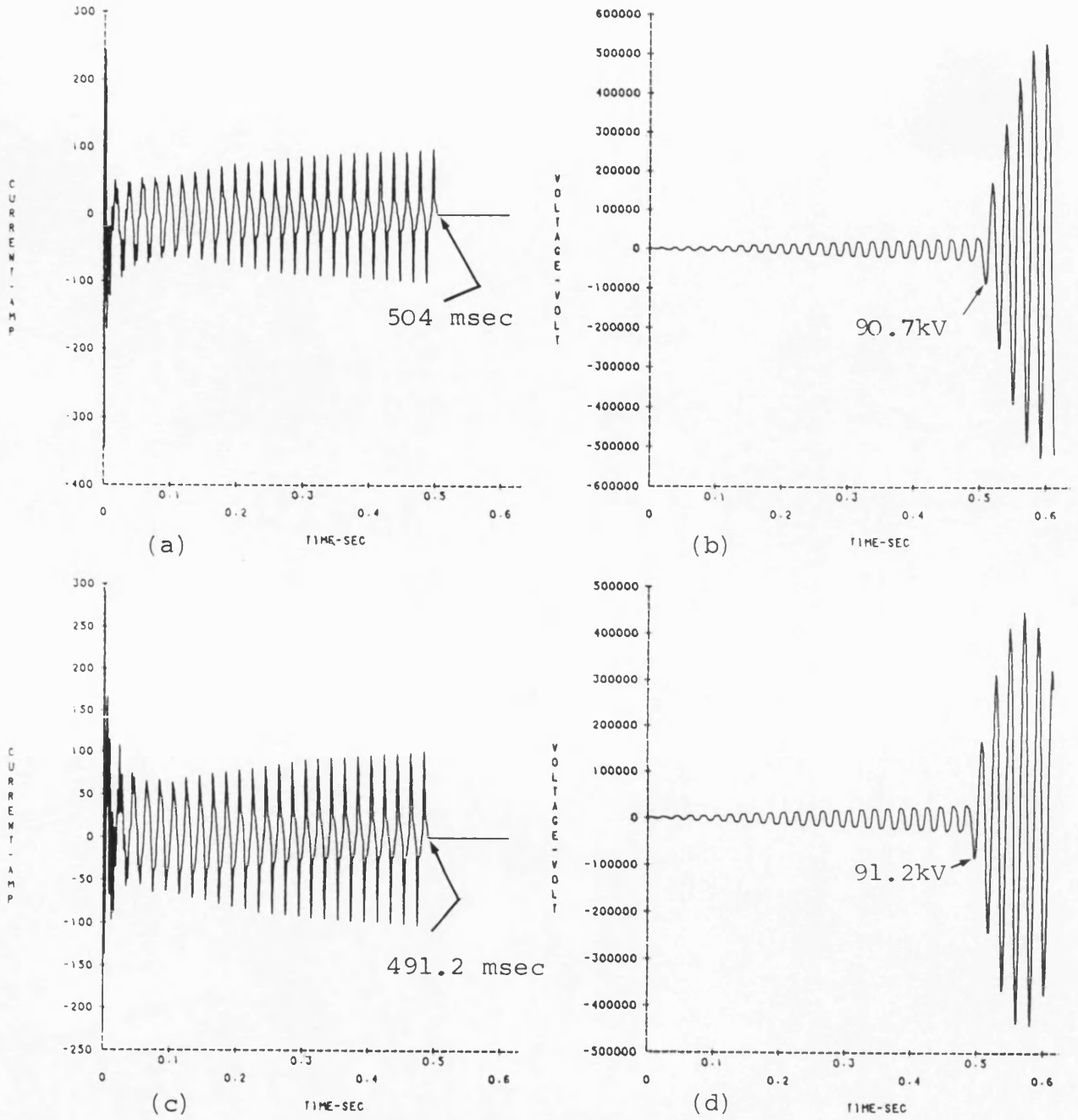

Fig. 9.24 Effect of neutral switch failure: Fault at the receiving end

L = 300km, h_1 = 0.75,

s.c.1 = s.c.2 = 5GVA,

$V_S/V_R = 1\angle 0^o$.

Outer phase fault

(a) Secondary arc current
(b) Secondary arc voltage

Inner phase fault

(c) Secondary arc current
(d) Secondary arc voltage

CHAPTER 10

SYSTEM STUDIES : HSGS's IMPLEMENTATION

10.1 Introduction

Arc extinction by grounding the faulted phase, was proposed as early as 1948[84]. In 1958, Muller et al[29] reported limited number of fault throwing test results concerning arc extinction time after grounding the faulted phase at both ends of a 220kV system. In 1981 , Hasibar et al[30] reported some fault throwing test results of a 500kV, 196km, transposed line transmission system. In the two quoted reports, it was concluded that, grounding the faulted phase at both ends results in a fast arc extinction. However, no comprehensive transient studies have been located in the literature.

The system mathematical formulation, as developed in chapters 2 to 5 is used in obtaining the system transient response. The majority of the studies were performed for a 500kV, 300km untransposed and uncompensated line, with two sources of 5GVA capacity each. The system performance with a transposed line application is studied in section 10.7. The effect of some factors on the arc extinction time are here investigated. These include fault location, line loading, parameters of the terminal station and those of the HSGS.

10.2 Effect of Pre-Fault Loading And Fault Position

For single-pole switching, The HSGS is closed at each end of the faulted phase after circuit breaker tripping. By grounding both ends, two closed loops are formed, where each consists of the HSGS and the secondary arc. The currents in the sound phases induce a voltage in each loop, thus causing circulating currents to be superimposed on the arc current. This fact, in conjunction with the collapse of the faulted phase voltage due to grounding, enhance the secondary arc extinction.

The HSGS's are simulated to close and open at approximately 10 cycles and 20 cycles respectively after fault initiation. Fault locations at, 0, 25%, 50%, and 100% of the line length, from the sending end are studied. Pre-fault power transfer from the sending to receiving end of approximately 1262MW ($V_S/V_R = 1\angle 25.73^o$) is considered.

10.2.1 No-Load Condition

The secondary arc current waveform, assuming constant arc resistance (0.5Ω), following an "a"-phase to earth fault at the sending end, with the HSGS's closed, is shown in fig. 10.1a. It is evident from this figure that the steady-state value of the secondary arc current is approximately 24A (r.m.s). This compares to 50.9A (r.m.s) before the closure of the HSGS's. The total fault path current waveform is illustrated in fig. 10.1b, which shows the arc current subsequent to fault clearance at T_{b2}. The details of the secondary arc current can be appreciated from fig. 10.1c, which shows the final arc extinction at 154 msec after fault clearance, or at approximately 2 msec after the closure of the HSGS's. The effect of grounding the faulted phase is marked on the secondary arc voltage waveform of

fig. 10.1d. In this figure, the sudden collapse of the fault point recovery voltage to approximately 327V, accounts for the fast arc extinction. Fig. 10.1e,f shows the faulted phase terminal voltage throughout the observed interval. In fig. 10.1e, the opening of the HSGS at the sending end first, causes a voltage rise of approximately 6kV. It is evident from fig. 10.1e,f that the faulted phase voltage is offset following the opening of the HSGS at the receiving end. The maximum overvoltage occurs at the receiving end of the line, as seen in fig. 10.1f, and has a value of 1.5 p.u. .

The current through the HSGS at both ends is illustrated in fig. 10.1g,h. From which, it is evident that the currents are approximately equal, and of 25.7A (r.m.s). This is less than the HSGS current reported in reference 30 (approximately 38A (r.m.s.)). Such a difference is mainly attributed to the different line configuration and line transposition of the system of reference 30. Also, from fig. 10.1g,h, it is interesting to note that the current through the receiving end HSGS is doubled as a result of non-simultaneous opening of the HSGS at both ends.

Fig. 10.2 illustrates features of the system response for an "a"-phase to earth fault at 75km from the sending end. In fig. 10.2a, final arc extinction occurs at approximately 7 msec after the closure of the HSGS's. It is worth mentioning that the steady-state secondary arc current after the HSGS closure in this case, is slightly higher (25.2A (r.m.s.)) compared to the previous case. The fault point recovery voltage is approximately 950V (peak), as is evident from fig. 10.2b. Comparable reclosing overvoltage to that of the previous case, is observed also at the receiving end as seen in fig. 10.2c. In comparison to

fig. 10.1h, the receiving end HSGS current in this case, shown in fig. 10.2d, is slightly offset. This is possibly caused by the different closure timing of the HSGS'S in this case.

For an "a"-phase to earth fault at the middle of the line, fig. 10.3 shows the secondary arc current and fault point voltage waveforms. In comparison to the two previous cases, the arc extinction time in this case is slightly longer (approximately 9 msec after closing the HSGS's). However, the fault point voltage is of similar pattern, apart from a maximum 1.3kV is evident after arc extinction. In a case study of a fault at the receiving end of the line, the system response obtained was similar to that of fig. 10.1.

10.2.2 Power transfer from sending to the receiving end

Fig. 10.4 illustrates the secondary arc behaviour and the faulted phase terminal voltage, following an "a"-phase to earth fault at the sending end. A comparison with fig. 10.1 shows that the arc extinction is immediate in this case following the closure of the HSGS's. Therefore, it can be concluded that the effect of the pre-fault power transfer is negligible, in so far as the arc extinction time is concerned. Due to the low HSGS resistance (0.5Ω) considered in this case, fig. 9.4b shows the fault point recovery voltage of 285V (peak), which is essentially the result of $I_{gs} \times R_s$. The effect of the pre-fault power transfer is marked on the terminal voltage waveforms of fig. 10.4c,d. It is of interest to note that the opening of the sending end HSGS ¼ of a cycle earlier than that at the receiving end, in conjunction with the system power flow, causes high frequency distortion at the sending end. This results in a peak voltage of approximately 119kV at the sending end, which upon opening the

receiving end HSGS, exhibits the usual offset voltage feature. The higher voltage to withstand by the first HSGS to open, under load conditions, was also noticed in the results of reference 30. The maximum reclose overvoltage occurs at the receiving end, as seen in fig. 10.4d, and has a value of 1.77 p.u. . The current flowing through the HSGS at the sending and receiving ends are shown in fig. 10.4e and fig. 10.4f respectively. In comparison to fig. 10.1e,f, the HSGS current is offset in this case, which conforms to the field test result results reported in reference 30.

Fig. 10.5 shows several features of the system response for an "a"-phase to earth fault at the middle of the line. It is evident from fig. 10.5a that the final arc extinction takes place at approximately 166 msec after fault clearance, or 6 msec after the closure of the HSGS at both ends. In comparison to the no-load case of fig. 10.3, the fault point recovery voltage is slightly lower in this case. However, the fault point overvoltage upon reclosing the faulted phase, is higher in this case. Fig. 10.5c,d shows the "a"-phase to earth voltage and the HSGS current at the receiving end. No significant difference can be observed in these figures compared to those of a sending end fault, apart from the lower voltage during the first period of secondary arcing in this case.

For an "a"-phase to earth fault at the receiving end, fig. 10.6a shows the immediate arc extinction following the HSGS's closure. In comparison to the sending end fault case of fig. 10.4, minor differences can be observed, particularly in the interval after the HSGS's closure, as can be appreciated from fig. 10.6b,c.

10.3 Effect of Power Transfer Direction

Fig. 10.7a shows the secondary arc current following clearance of an "a"-phase to earth fault at the sending end, when the pre-fault power transfer from the receiving to sending end is approximately 1262MW ($V_S/V_R = 1\angle -25.73^o$). A comparison with fig. 10.4a shows that the arc extinction time is approximately the same in this case. Fig. 10.7b shows a similar response for an "a"-phase to earth fault at the receiving end, which in comparison to fig. 10.6a, shows that the arc extinction time is approximately 2 msec longer in this case. However, these negligible differences in the arc extinction time are mainly caused by the different circuit breaker operating times. Therefore, it can be concluded that power flow direction has negligible effect on the arc extinction time.

10.4 Effect of Source Parameters

The results presented so far, assume equal source capacity of 5GVA at each end of the line. In order to study the effect of the source impedance on the arc extinction time, different combination of source s.c.l. are considered. Relevant results when s.c.1 = 5GVA and s.c.2 = 10GVA are shown in fig. 10.8 for an "a"-phase-to-earth fault at sending end. In fig. 10.8a, it is evident that arc extinction occurs immediately after the closure of the HSGS's. A comparison of fig. 10.8 with fig. 10.1 shows that, the reclosing overvoltage at the fault point is slightly higher, and the HSGS current at the receiving end is offset for about three cycles in this case. Fig. 10.9 shows similar results to those mentioned above, but for a fault at the receiving end. Here again, immediate arc extinction is evident in fig. 10.9a. No significant differences in the system response are observed in comparison to those obtained under the same fault condition,

with both sources of equal capacity of 5GVA. However, in comparison to the sending end fault case (fig. 10.8), the fault point reclosing overvoltage is higher. Moreover, the sending end HSGS current exhibits high frequency distortion in the first half cycle, reaching a peak of 98A.

Fig. 10.10 shows the secondary arc current for a fault at the sending end, and at 75km from the sending end, when both source capacities are 5GVA, and $Z_{So}/Z_{Sl} = 0.5$. Such Z_{So}/Z_{Sl} reduction from 1 to 0.5, caused negligible effect on the arc extinction time, as can be seen from a comparison of fig. 10.10 with fig. 10.1c and fig. 10.2a.

Similar results were obtained for the above cases with pre-fault power transfer of 1262MW in either direction. These showed no significant difference in the arc extinction time, and the general system response.

10.5 Effect of HSGS parameters

The effect of the HSGS resistance (R_s), and its closing time on the arc extinction were investigated for the 300km untransposed line system. The source at each end of the line was considered having 5GVA capacity and of $Z_{So}/Z_{Sl} = 1$. An extensive series of simulation studies for different fault location showed identical variation of the arc extinction time with R_s. An example of this is given in fig. 10.11, for a mid point fault on phase-"a". It is evident from fig. 10.11 that the variation of the arc extinction time is negligible for $R_s = 0.5 - 100\ \Omega$. For higher values of R_s, the arc extinction times increase sharply.

For the same system, the closing time of the HSGS's was varied from 100 to 400 msec after fault initiation (in 50 msec intervals). The effect on the arc extinction time

is found to be negligible, and extinction always takes place within one half cycle after the closure of the HSGS's.

10.6 Using HSGS's in Transposed Line Applications

The 300km line is simulated transposed at 100km intervals. Fig. 10.12 shows the secondary arc current and the faulted phase terminal voltage, for an "a"-phase to earth fault at the sending end. In comparison to the untransposed line case under identical fault conditions of fig. 10.1, the similarity of the response is quite evident. However the arc extinction time is 6 msec longer in this case, which is clearly caused by the delayed closure of the HSGS's. Moreover, slightly higher overvoltages are observed in this case at the receiving end (approximately 1.6 p.u.) as can be appreciated from fig. 10.12b,c in comparison to fig. 10.1e,f. It is worth mentioning that the HSGS current observed in this case, is similar to that with untransposed line application, though of slightly higher magnitude (approximately 5A).

10.7 Summary

Successful single-pole switching depends on rapid arc extinction, which can be provided for by grounding the faulted phase at both ends of the line, hence allowing rapid system restoration. From the results presented in this chapter, the use of HSGS's prove effective in extinguishing the secondary arc, following a single-line-to-earth fault, with transposed and untransposed line applications. For the 300km line considered in the study, the arc extinguishes within one half cycle after the closure of the HSGS's, irrespective of the pre-fault power flow and fault position.

The results of the extensive series of investigations of such system implementation indicated the following :-

1. The HSGS current increases with the system pre-fault power transfer.

2. The source side parameters do not affect the arc extinction time and the HSGS current.

3. The arc extinction time increases steadily with increasing HSGS impedance beyond a certain value.

4. There is negligible effect of the HSGS closing time on the arc extinction process.

5. For the untransposed line applications, system response for an outer and inner phase faults are identical. However, Higher HSGS current was observed for the inner phase faults. This is evidently due to the higher coupling of the inner phase with the two sound outer phases.

6. A slight increase in the arc extinction time was observed for a line of 500km in length, subjected to similar fault conditions to those described in this chapter. However, significant increase (few kA) in the HSGS current was evident with the system loaded.

7. For the 300km untransposed line application, the presented computer results , provided the necessary information to determine some of the performance requirements for the HSGS. Such as, current interrupting capacity of 1kA, and transient recovery voltage withstand of 200kV (p-p).

8. The results obtained, are in good agreement with the practical system fault throwing test results reported in reference 30.

Finally, although the cost of the HSGS is proportional to its current interrupting capacity and operating voltage, its use in heavily loaded and long lines may be favoured from the stability point of view.

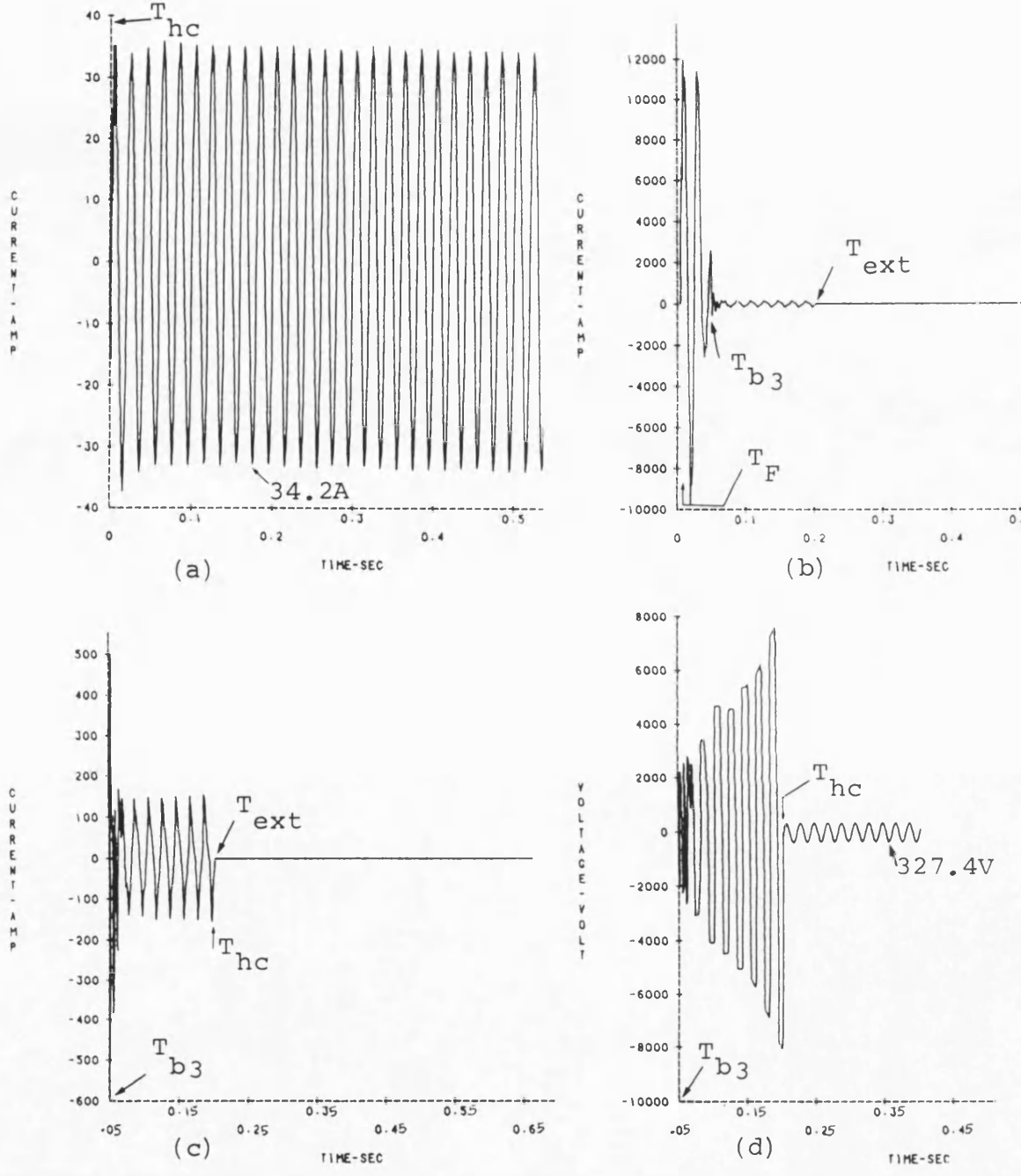

Fig. 10.1 Fault at sending end: No-load condition

"a"-earth fault

$L = 300km$, $R_s = 0.5\Omega$,

s.c.1 = s.c.2 = 5GVA,

$V_S/V_R = 1\angle 0^o$.

T_F = 5 msec,

T_{b2} = 30.4 msec (a.f.),

T_{b3} = 49.6 msec (a.f.),

T_{hc} = 202 msec (a.f.),

T_{ext} = 154 msec,

T_{ho1} = 402.4 msec (a.f.),

T_{ho2} = 412.4 msec (a.f.),

T_{b4} = 495.2 msec (a.f.),

T_{b5} = 501.6 msec (a.f.).

(a) Secondary arc current ($R_F = 0.5\Omega$)
(b) Fault path current
(c) Secondary arc current
(d) Secondary arc voltage

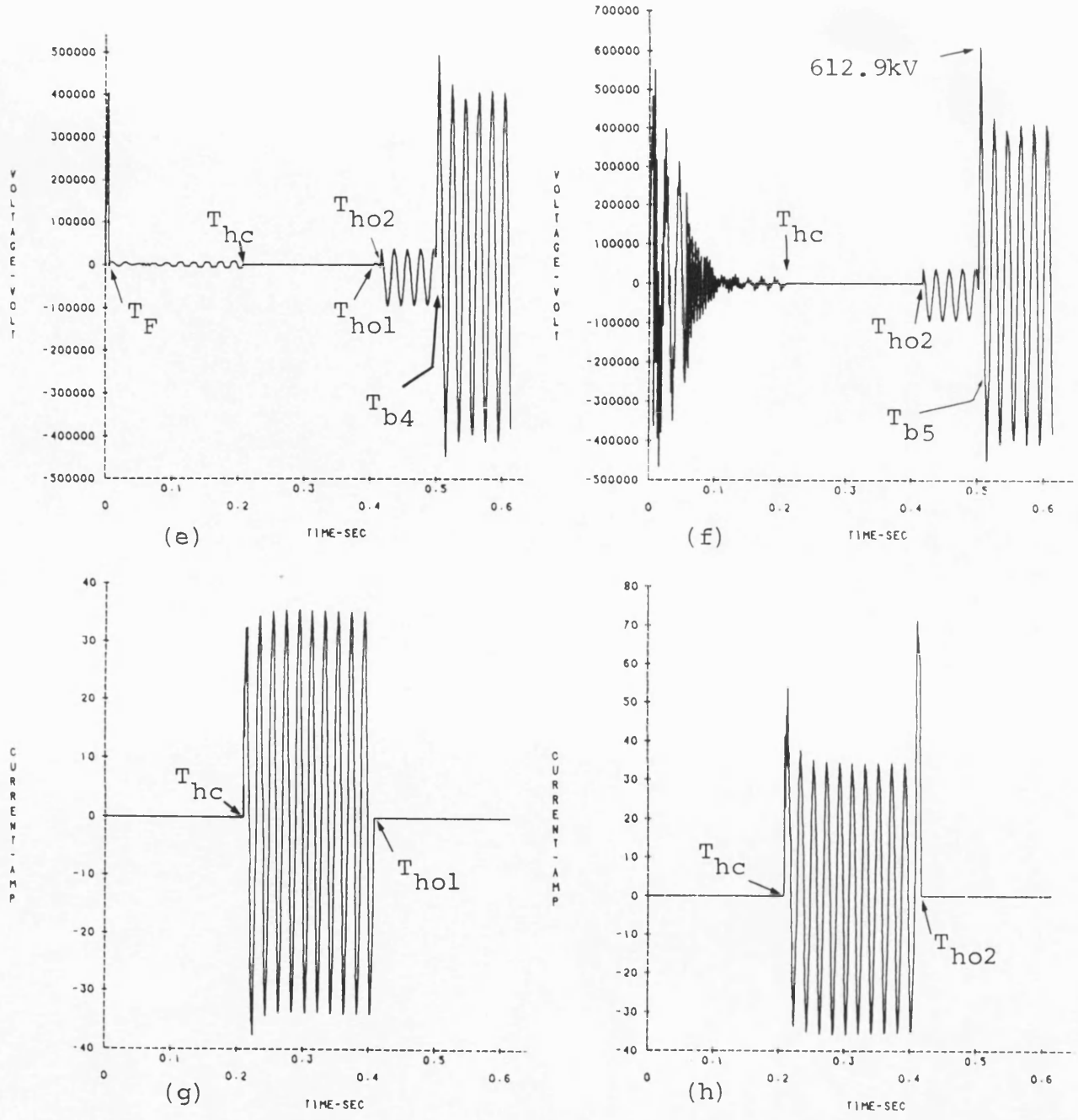

Fig. 10.1 (continued)

(e) Fault point voltage
(f) "a"-earth voltage at receiving end
(g) Sending end HSGS current
(h) Receiving end HSGS current

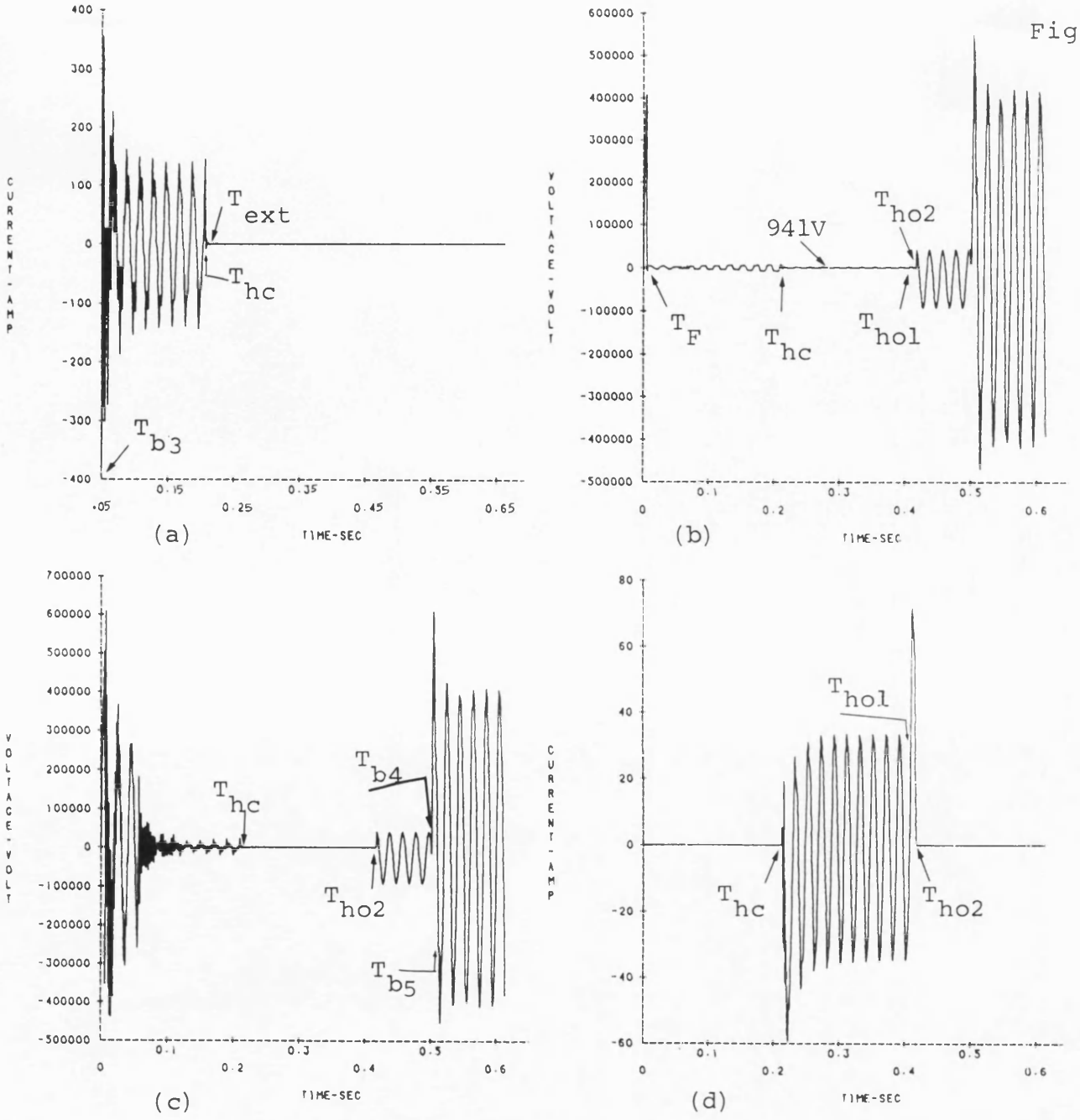

Fig. 10.2 Fault at 75km from sending end: No-load condition

"a"-earth fault

L = 300km, $R_s = 10\,\Omega$,

s.c.1 = s.c.2 = 5GVA,

$V_S/V_R = 1\angle 0^\circ$.

T_F 5 msec,

T_{b2} = 39.6 msec (a.f.),

T_{b3} = 50 msec (a.f.),

T_{hc} = 206.8 msec (a.f.),

T_{ext} = 164 msec,

T_{ho1} = 402.4 msec (a.f.),

T_{ho2} = 412.4 msec (a.f.),

T_{b4} = 495.2 msec (a.f.),

T_{b5} = 501.6 msec (a.f.).

(a) Secondary arc current
(b) Fault point voltage to earth
(c) "a"-earth voltage at receiving end
(d) Receiving end HSGS current

Fig. 10.3 Mid point fault: No-load condition

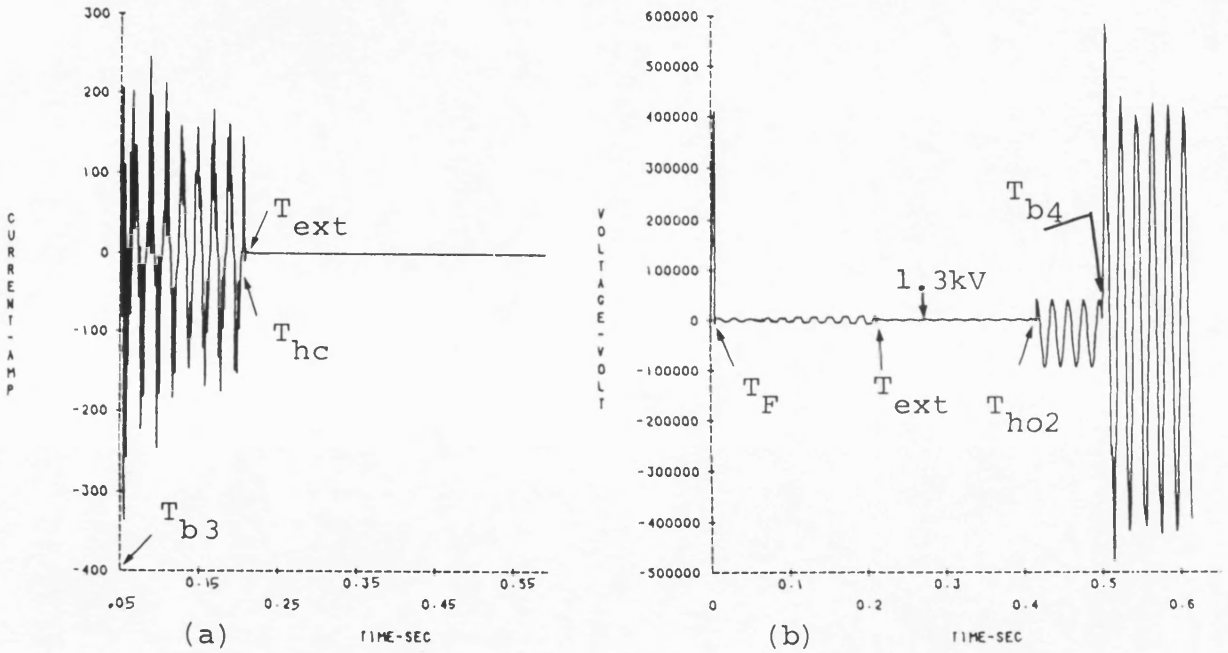

"a"-earth fault

$L = 300km$, $R_s = 10\,\Omega$,

s.c.l. = s.c.2 = 5GVA,

$V_S/V_R = 1\angle 0^o$.

T_F = 5 msec,

T_{b3} = 50 msec (a.f.),

T_{hc} = 206.4 msec (a.f.),

T_{ext} = 165.6 msec ,

T_{ho2} = 412 msec (a.f.),

T_{b4} = 495.2 msec (a.f.).

(a) secondary arc current
(b) Fault point voltage to earth

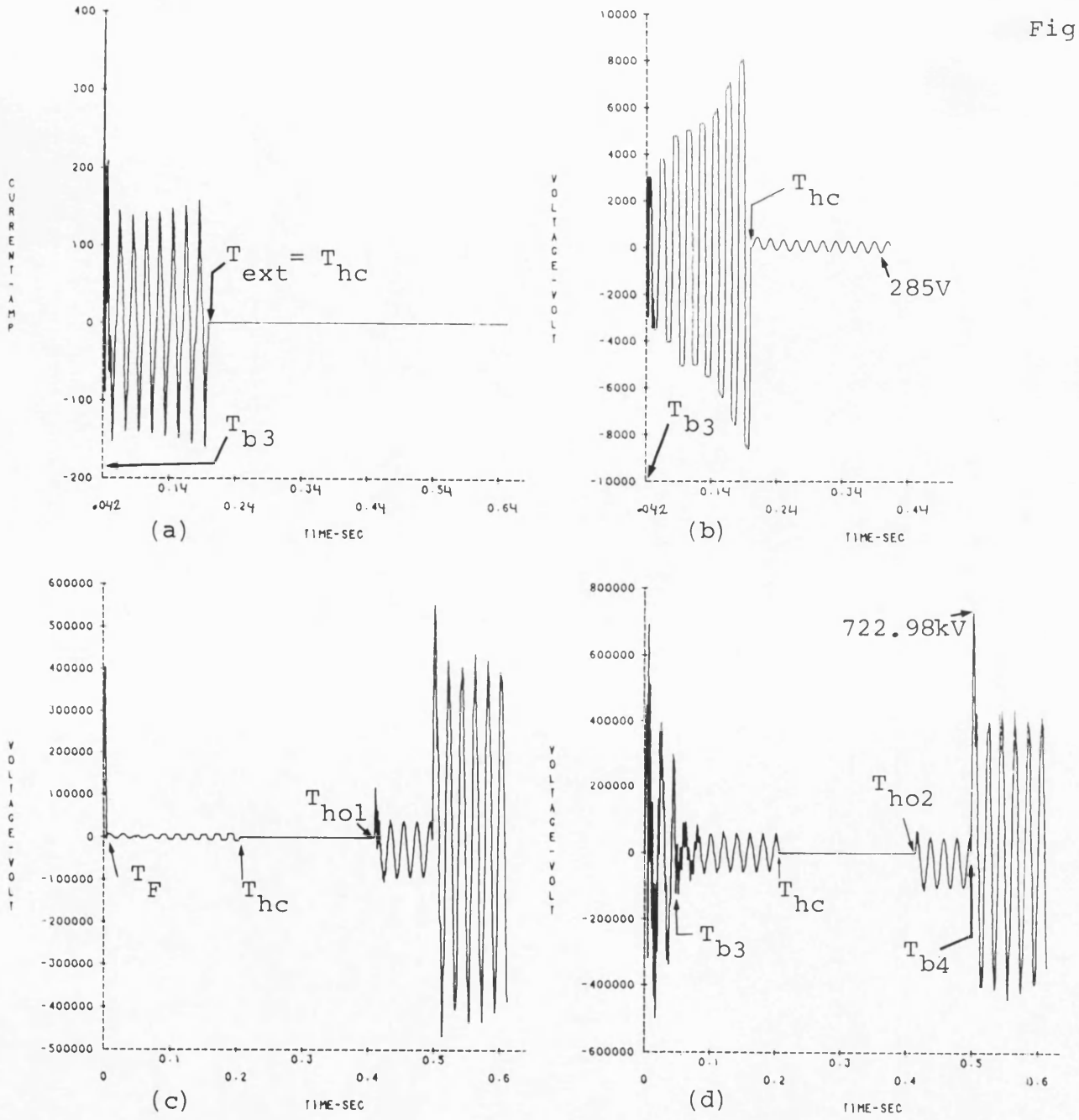

Fig. 10.4 Fault at sending end: Power transfer from sending to receiving end

"a"-earth fault

$L = 300km$, $R_s = 0.5\Omega$,

s.c.1 = s.c.2 = 5GVA,

$V_S/V_R = 1\underline{/25.73^o}$.

T_F = 5 msec,

T_{b3} = 42.4 msec (a.f.),

T_{hc} = 201.6 msec (a.f.),

T_{ext} = 159.2 msec,

T_{hol} = 406.8 msec (a.f.),

T_{ho2} = 411.6 msec (a.f.),

T_{b4} = 494.4 msec (a.f.).

(a) Secondary arc current
(b) Secondary arc voltage
(c) Fault point voltage to earth
(d) "a"-earth voltage at receiving end

Fig. 10.4 (continued)

(e) Sending end HSGS current
(f) Receiving end HSGS current

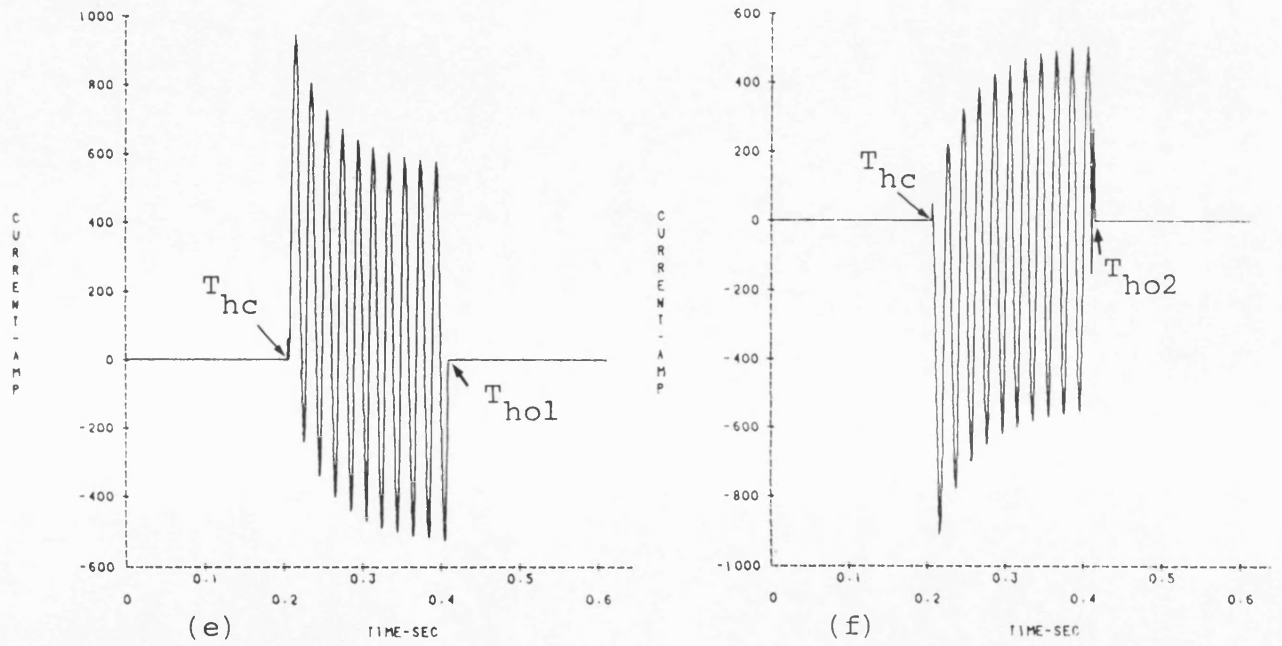

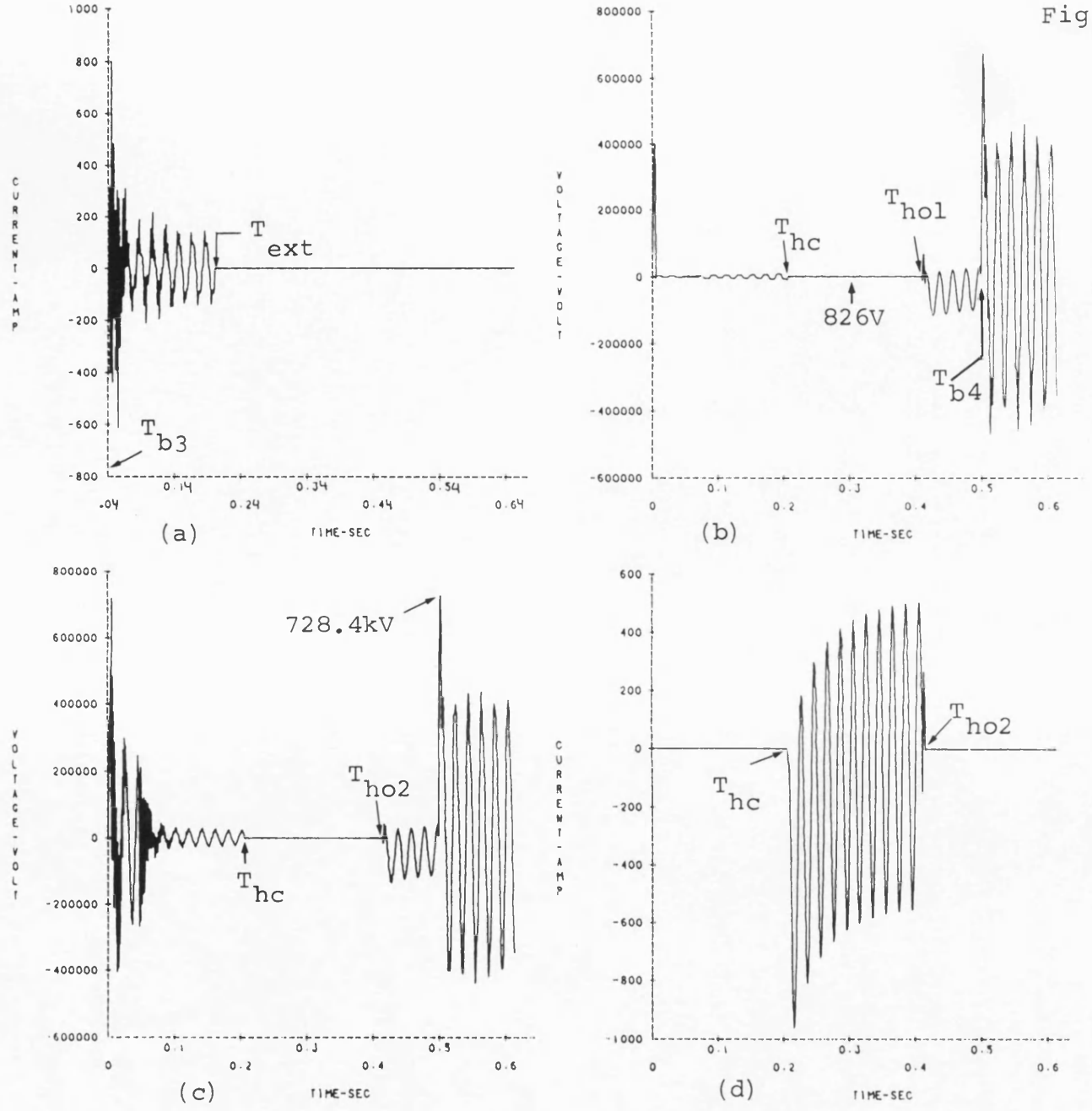

Fig. 10.5 Mid point fault: Power transfer from sending to receiving end

"a"-earth fault

L = 300km, R_s = 0.5Ω,

s.c.1 = s.c.2 = 5GVA,

$V_S/V_R = 1\underline{/25.73^o}$.

T_{b3} = 41.2 msec (a.f.),

T_{hc} = 201.6 msec (a.f.),

T_{ext} = 166.8 msec,

T_{ho1} = 406 msec (a.f.),

T_{ho2} = 410.8 msec (a.f.),

T_{b4} = 493.6 msec (a.f.).

(a) Secondary arc current
(b) Fault point voltage to earth
(c) "a"-earth voltage at receiving end
(d) Receiving end HSGS current

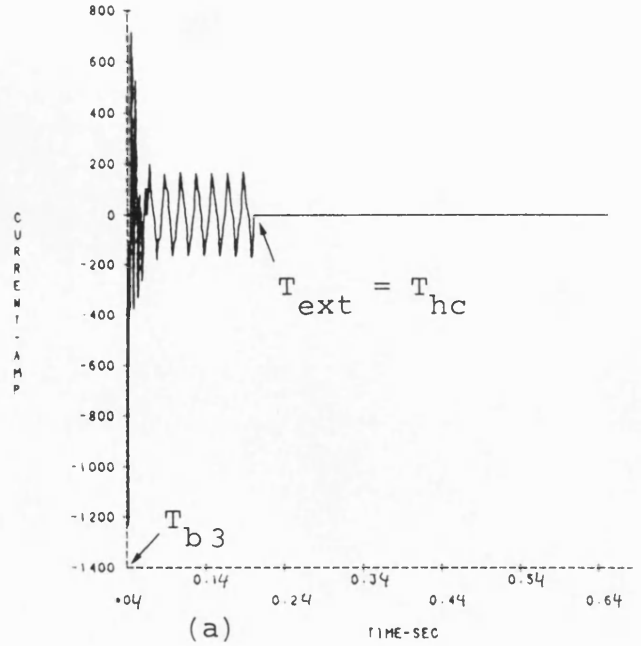

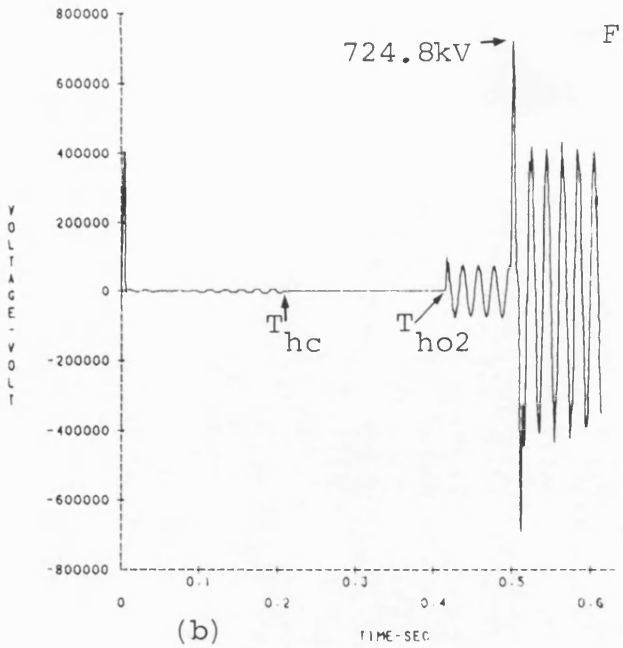

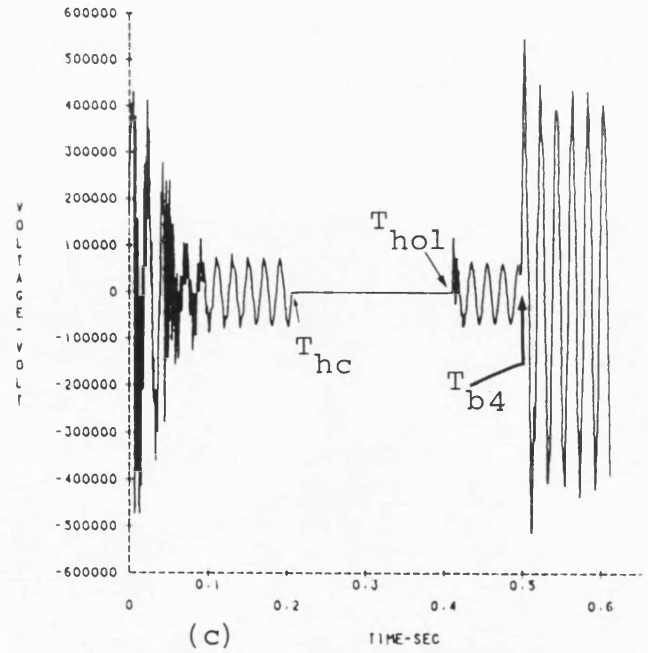

Fig. 10.6 Fault at receiving end: Power transfer from sending to receiving end

"a"-earth fault

$L = 300km$, $R_s = 0.5\,\Omega$,

s.c.1 = s.c.2 = 5GVA,

$V_S/V_R = 1\underline{/25.73^{o}}$.

T_{b3} = 40.4 msec (a.f.),

T_{hc} = 200.8 msec (a.f.),

T_{ext} = 160.4 msec,

T_{hol} = 405.2 msec (a.f.),

T_{ho2} = 411.6 msec (a.f.),

T_{b4} = 493.2 msec (a.f.).

(a) Secondary arc current
(b) Fault point voltage to earth
(c) "a"-earth voltage at sending end

Fig. 10.7 Effect of power transfer direction

"a"-earth fault

$L = 300km$, R_s 0.5Ω,

s.c.1 = s.c.2 = 5GVA,

$V_S/V_R = 1\angle -25.73^{\circ}$.

(a) Secondary arc current (fault at sending end)

(b) Secondary arc current (fault at receiving end)

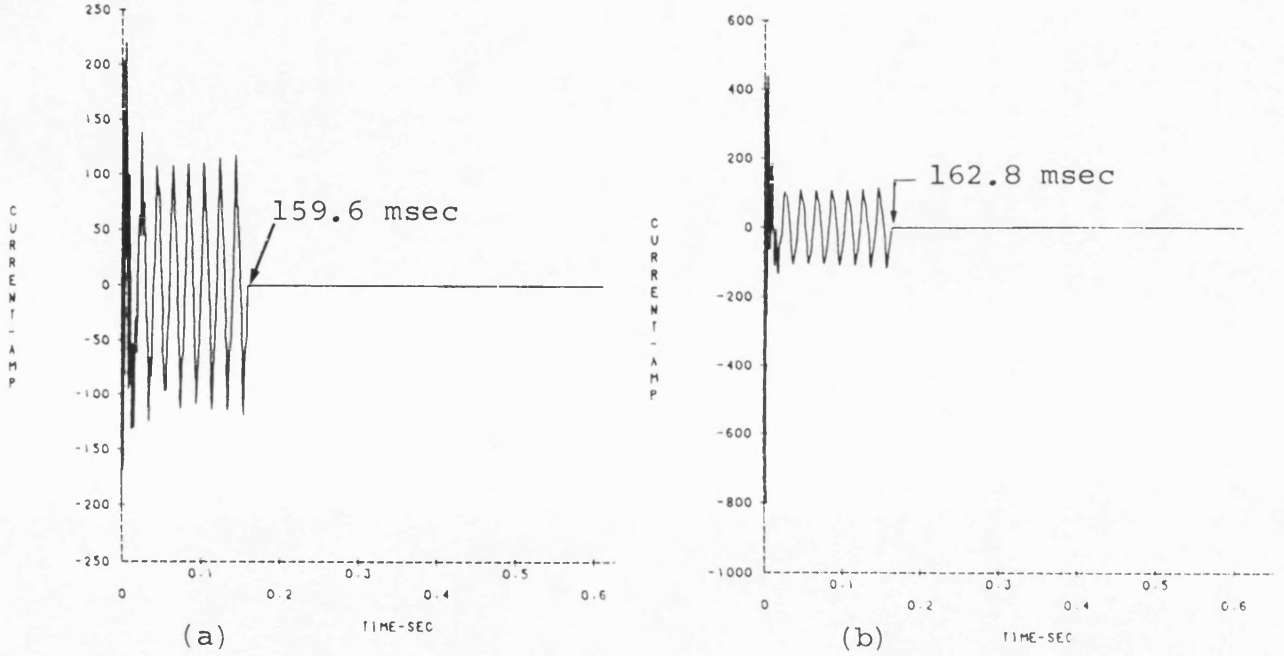

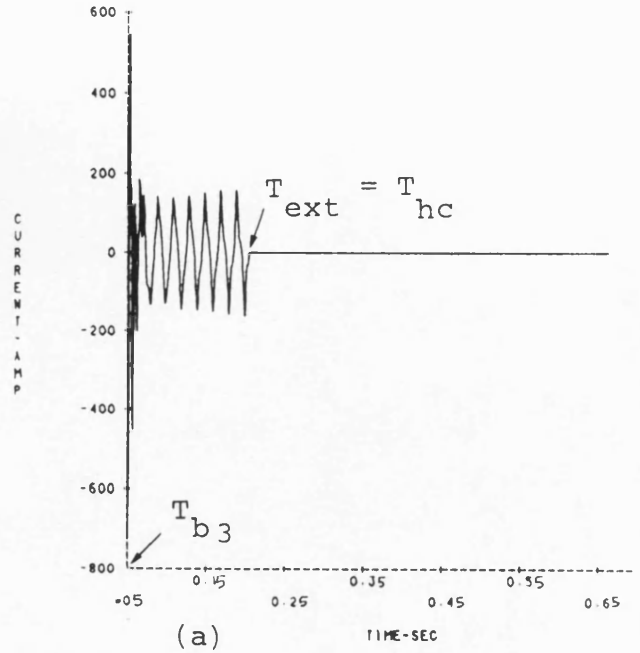

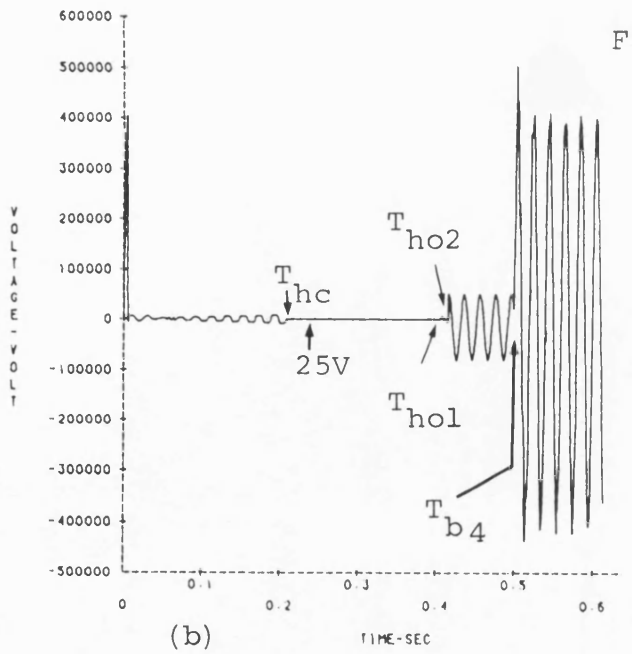

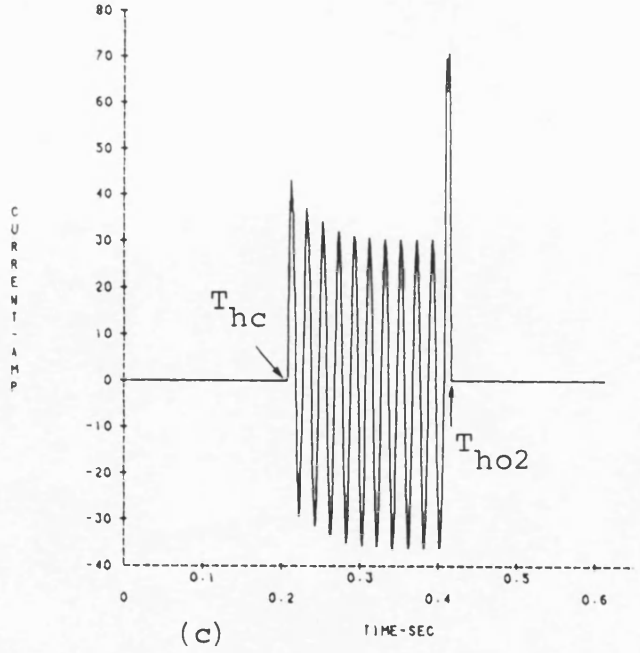

Fig. 10.8 Effect of source capacity: Fault at sending end

"a"-earth fault

L = 300km, R_s = 0.5 Ω,

s.c.1 = 5GVA, s.c.2 = 10GVA,

$V_S/V_R = 1\angle 0^o$.

T_{b3} = 49.6 msec (a.f.),

T_{hc} = 202.8 msec (a.f.),

T_{ext} = 153.2 msec,

T_{ho1} = 402 msec (a.f.),

T_{ho2} = 412 msec (a.f.),

T_{b4} = 495.2 msec (a.f.).

(a) Secondary arc current
(b) Fault point voltage to earth
(c) Receiving end HSGS current

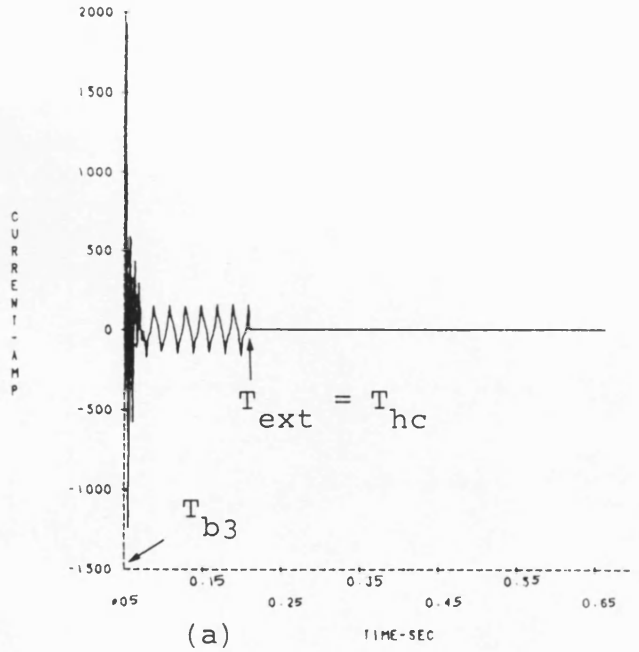

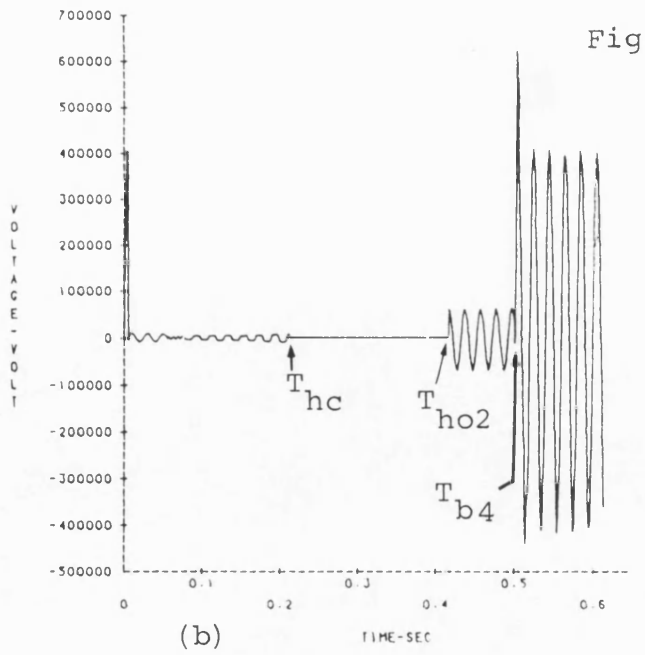

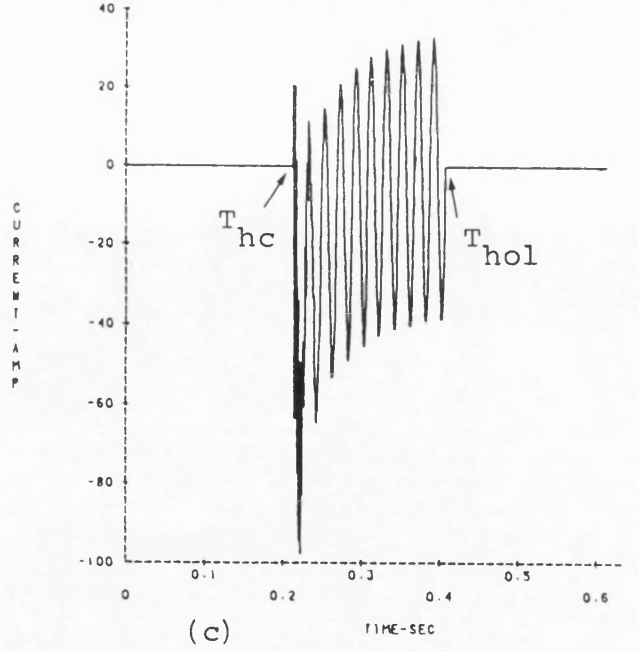

Fig. 10.9 Effect of source capacity: Fault at receiving end

"a"-earth fault

L = 300km, $R_s = 0.5\Omega$,

s.c.1 = 5GVA, s.c.2 = 10GVA,

$V_S/V_R = 1\angle 0^\circ$.

T_{b3} = 50 msec (a.f.),

T_{hc} = 207.2 msec (a.f.),

T_{ext} = 157.2 msec,

T_{ho2} = 412 msec (a.f.),

T_{b4} = 495.2 msec (a.f.).

(a) Secondary arc current
(b) Fault point voltage to earth
(c) Sending end HSGS current

Fig. 10.10 Effect of the source Z_{So}/Z_{Sl} on the secondary arc extinction time

"a"-earth fault

L = 300km, R_s = 0.5 Ω,
s.c.1 = s.c.2 = 5GVA,
$V_S/V_R = 1\angle 0^o$.

(a) Fault at sending end
(b) Fault at receiving end

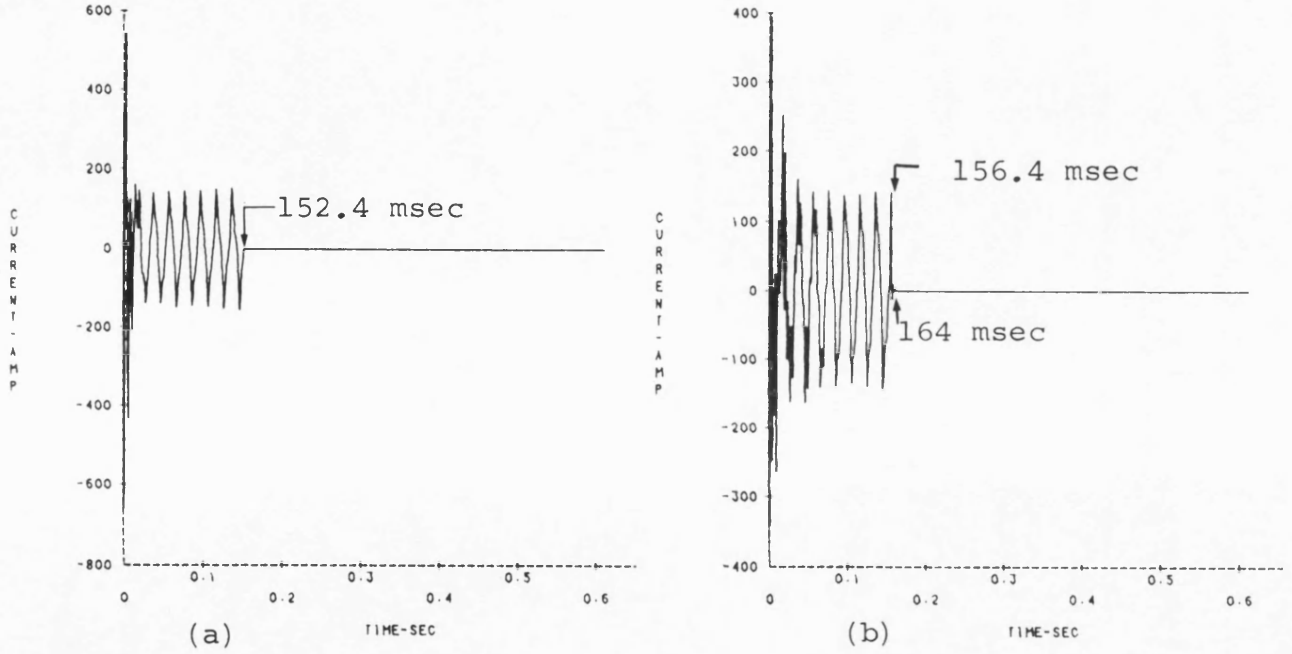

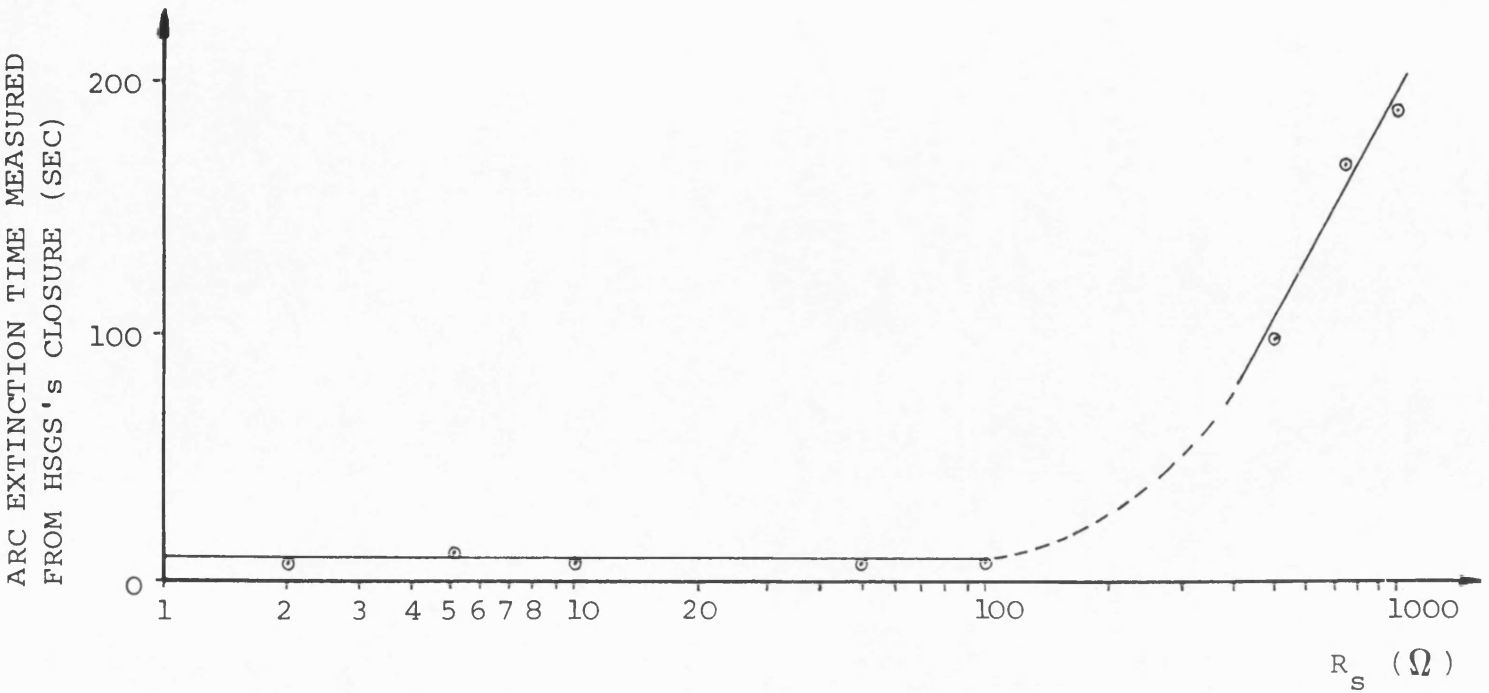

Fig. 10.11 Variation of the arc extinction time with the HSGS resistance (R_s)

Fault on phase-"a", at mid point

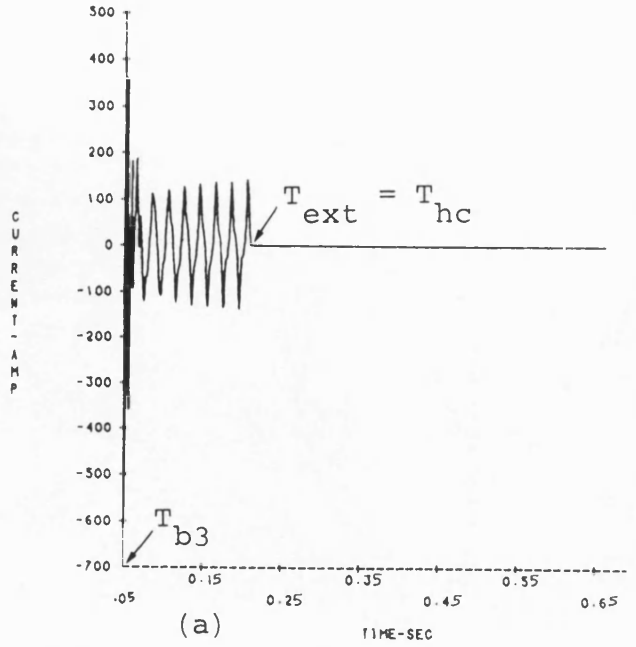

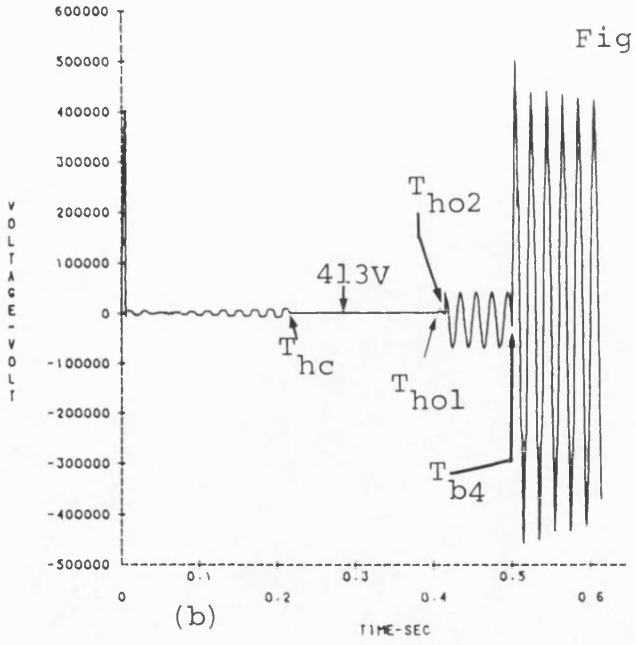

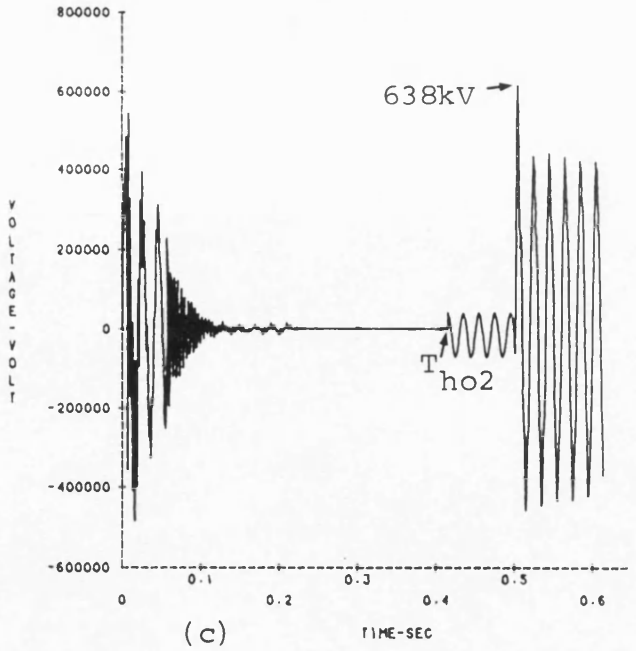

Fig. 10.12 Using HSG's in transposed line application

"a"-phase to earth fault at the sending end.

$L = 300km$, $R_s = 10\Omega$,

s.c.1 = s.c.2 = 5GVA,

$V_S/V_R = 1\angle 0^\circ$.

T_{b3} = 49.6 msec (a.f.),

T_{hc} = 209.6 msec (a.f.),

T_{ext} = 160 msec,

T_{ho1} = 401.6 msec (a.f.),

T_{ho2} = 410.4 msec (a.f.),

T_{b4} = 494.8 msec (a.f.).

(a) Secondary arc current
(b) Fault point voltage to earth
(c) "a"-earth voltage at receiving end

CHAPTER 11

CONCLUSIONS AND FUTURE WORK

11.1 Conclusions

Single-pole switching has long been accepted as a very effective means of retaining system stability, when single-phase faults are being cleared. Furthermore, it could become a necessity to enable better utilization of the transmission capability, in applications where the costs of additional circuits are prohibitive. Detailed simulation techniques, are of obvious importance in relation to the design and assessment of systems employing single-pole switching. In this work, digital methods have been developed to enable better prediction of the faulted system response of EHV transmission systems, subjected to single-phase to earth faults. A variety of different single-pole switching schemes were investigated and assessed, according to their performance, mainly in relation to the secondary arc extinction time, and consequently the overall dead-time. These were, the conventional single-pole switching; the hybrid method of autoreclosure; the neutral switched reactor and the High Speed Grounding Switch implementations. The validation of the developed techniques is enhanced by the similarity of many features of the system response obtained, to those observed during practical field tests.

The developed simulation methods are general, and thereby can be adjusted to accommodate different system

configurations. The system sources can be accordingly chosen, and linked by a transposed or untransposed transmission line. Breakers, HSGS's and the ideal neutral switch opening and closing, can be simulated to occur at any instant and for any sequence. The shunt reactor bank(s), can be either 4-legged or Y-connected with solidly grounded neutral(s), at both or either line end. The fault can be applied anywhere along the line and on any phase. The secondary arc reignition characteristics are defined dynamically according to the peak of the steady-state arc current during each half cycle.

The computer programs have been used to study the effect of different system parameters on the arc exinction time and the system generated overvoltages, thus providing sufficient timing data, line end current, and voltage waveforms. The former can be used in system stability studies, while the latter can be used as data for the system protection equipments. However, the computational results presented in chapters 7 to 10, cover in detail, a variety of different system studies for the above four single-pole switching schemes. The effect of the following parameters, on a 500kV system performance for single-phase to earth faults were considered.

1. The transmission distance and line transposition.
2. The source parameters (Z_{SO}/Z_{S1} and s.c.l.).
3. The shunt reactor bank(s) parameters and connections.
4. The fault location.
5. The pre-fault power transfer and its direction.

However, the effect of particular parameters, according to the specific scheme, along with the general conclusions

drawn for each scheme are given below.

a. Conventional single-pole switching

In chapter 7, emphasis has been placed on investigating in depth, the use of conventional 4-legged reactor bank(s), and the effect of the neutral reactance in the way of minimizing arc extinction times in untransposed line applications. Two systems were considered. The first contains a 300km line, while the second contains a 200km line, both being untransposed. A 300km transposed line transmission system, was also investigated, and results presented for comparison. The conclusions reached are :-

1. For both line lengths considered, significant differences in the arc extinction times were observed in the untransposed line applications, depending on the faulted phase. Generally, higher arc extinction times are associated with faults on the outer phase when the neutral reactance (X_n) is greater than 300 Ω and 200 Ω in the 200km and 300km line systems respectively. However, an opposite trend was observed for lower values of X_n.

2. The arc extinction time dependency on X_n is small for outer phase faults in comparison to inner phase faults.

3. For the 200km line, with faults on the outer phase, the pre-fault power transfer and its direction, was found to cause approximately $\pm$ 10% variations in the arc extinction time from that under no-load conditions. Accordingly, the results indicated lower variations for inner phase faults.

4. Also for the 200km line, the arc extinction time was found to be in the range 0.26 - 0.32 sec for outer

phase faults, providing that the neutral reactance is greater than $400\,\Omega$. Inner phase faults, undergo lower arc extinction times. It follows that a dead-time of 0.5 sec for such line lengths is adequate.

5. For the 300km line, arc extinction times in the range 0.33 - 0.43 sec have been predicted for faults on the outer phase, with $X_n = 625\,\Omega$. However, higher arc extinction times were observed for $625\,\Omega < X_n > 625\,\Omega$.

6. Also for the 300km line, the effect of the pre-fault power transfer on the arc extinction time was found to be insignificant, particularly for faults on the inner phase. However, for outer phase faults, variations of approximately $\pm$ 15% were recorded.

7. The conditions for secondary arc extinction are significantly improved by line transposition, as it considerably reduces the secondary arc current and recovery voltage.

8. The pre-fault power transfer, and its direction significantly affect the arc extinction time in the 300km transposed line application.

9. For the 300km line, the studies revealed that, the use of one 4-legged reactor bank, tuned to compensate the capacitive component of the secondary arc current to - 20A (r.m.s.), allows successful single-pole switching with 0.5 sec dead-time, providing the line is transposed. Such a compensation arrangement in the untransposed line application, is of doubtful use unless higher dead-times are adopted.

10. For both transposed and untransposed line applications, the use of Y-connected reactors with solidly grounded

neutrals, have little effect on the arc extinction time. However, the recovery voltage with such an implementation, was found to increase significantly even if the resonant region is avoided.

11. The results for both line applications, demonstrated the close dependency of the arc extinction time on the level of the steady-state secondary arc current and the recovery voltage features, viz., the first peak, the rate of rise and the maximum value.

12. For the horizontal line configuration considered, the use of conventional 4-legged reactor bank(s) for single-pole switching, is of no significant benefit with line lengths in excess of 200km, unless the line is transposed. Therefore, in untransposed line applications with such lengths, dead-times in excess of 0.5 sec or another single-pole switching scheme should be adopted.

b. The hybrid method of autoreclosure

The effectiveness of the hybrid method of autoreclosure has been assessed, particularly for the 300km, untransposed line application. The performance of systems with transposed line applications, and those employing one Y-connected solidly grounded neutral reactor were also highlighted. In chapter 8, the extensive investigations of the above mentioned systems, provided for the following conclusions :-

1. The de-energisation of the sound phases proved to be effective in ensuring fast arc extinction. This is especially pronounced in long line applications (lengths in excess of 250km) compared to conventional single-pole switching.

2. Generally, for all systems investigated, the secondary arc extinguished in approximately 1 - 2.5 cycles (50Hz base) after de-energising the sound phases.

3. For the untransposed line applications, higher arc extinction times were observed for inner phase faults in comparison to outer phase faults.

4. The pre-fault power transfer and fault location, have little effect on the arc extinction time.

5. The source side parameters have negligible effect on the arc extinction time.

6. For the 300km line, in both transposed and untransposed applications, the de-energisation of the sound phases at approximately 0.4 sec was adequate to allow for successful reclosure at 0.5 sec dead-time.

7. The hybrid method can be used in radial feeders, compensated by one reactor bank. However, the arc extinction times were found to be several milliseconds higher compared to those with the two reactor applications under the same fault condition.

c. The neutral switched reactor implementation

The computational results presented in chapter 9 cover in detail the 300km untransposed line system performance under single-phase to earth faults. The results showed that, short arc extinction times well within the 0.5 sec dead-time, can be achieved with proper choice of the shunt reactor neutral reactances. The findings of chapter 9 compares favourably with the few reported field test results[23,49]. The general conclusions drawn from

the series of studies undertaken, are as follow :

1. With the neutral reactances optimally chosen, the limits of the arc extinction time are 0.05 - 0.3 sec.

2. Faults on the inner phase exhibit extinction times near to the upper limit.

3. Minimum arc extinction times were observed for faults occuring at the middle of the line.

4. In comparison to faults at the conventional reactor bank terminal, faults at the switched reactor bank terminal, exhibit longer arc extinction times.

5. The source side parameters affect the arc extinction time, depending on the faulted phase and the fault location.

6. Generally, the secondary arc extinction time was found to be independent of the steady-state arc current and recovery voltage.

7. The pre-fault power transfer and its direction were found to have a marked effect on the arc extinction time. It was found that the arc extinction time is higher for faults at the power importing terminal.

8. The effect of the pre-fault power transfer on the reactor bank neutral voltages , and the ideal neutral switch current , is negligible.

9. The maximum switching overvoltages occurs at the neutral switched reactor bank terminal.

10. Arc extinction times in excess of 0.48 sec are to be expected in any instance of switch failure.

11. It should be pointed out that, in order to select the optimum neutral reactances, full transient system studies should be performed for the particular system.

d. The High Speed Grounding Switches implementation

Although the cost of the HSGS is reported to have recently increased[3], their use in heavily loaded systems containing long untransposed lines might become a necessity from the stability point of view. Moreover, additional advantage can be gained by employing HSGS's, viz. discharging the line during maintenance or system expansion. Grounding the faulted phase at both line ends, provides the necessary conditions for fast arc extinction. Few field test results of such system implementation have been reported[30], and the findings presented in chapter 10 compare very favourably with them. The following conclusions are reached for the 300km untransposed line application.

1. The secondary arc extinguished within one half cycle (50Hz base) after the closure of the HSGS's, irrespective of the pre-fault power transfer and fault location.

2. The arc extinction time is independent of the HSGS's closing time.

3. The HSGS current increases with the system pre-fault power transfer.

4. No significant variations were observed in the arc extinction time and the HSGS current in relation to the source parameters.

5. For the various fault locations considered in the studies, the inner phase faults were found to cause higher

HSGS currents in comparison to outer phase faults.

6. The HSGS current increases steadily with the transmission distance, especially under loading conditions.

7. For the 300km line, a current interrupting capacity of 1kA, and a transient recovery withstand voltage of 200kV (p-p) have been predicted.

8. The results showed the suitability of the HSGS's scheme, in transposed and untransposed line applications, for successful single-pole switching performance and reclosure in 0.5 sec dead-time.

Finally, although the results obtained and presented throughout this work, showed specific advantages of one single-pole switching technique over the other, it is emphasized that no one technique is a replacement for another. Practically, the decision to employ any particular technique is governed by, the system requirements, the costs and the development stage of the particular power system.

11.2 Future Work

The work presented in this thesis, forms the primary stage in the planning of new or modifying existing EHV transmission systems, envisaged to operate with single-pole switching facilities. This is particularly so in relation to the choice of the scheme to be used, bearing in mind the system requirements and costs. Moreover, it provides ample information about the rating of specific equipments (e.g. reactors, HSGS's, neutral switches, ... etc.), in addition to these required for the system protection design and assessment. Despite the fact that the most apparent area for further work is in field testing the various

schemes, which is practically difficult and expensive, further research in the following directions may be worthy of study.

a. The simulation techniques developed in this work, can be used in assessing the effect of more specific factors on the general system performance, in the same field, such as :

1. The effect of the main breaker operating time and the sequence of switching events on the arcing process and the system overvoltages.

2. The performance of the system with various line constructions and line transposition cycles.

3. The effect of the earth wire(s) presence.

b. Despite the fact that there is often little to be gained from employing single-pole switching in double-circuit line systems, special cases may arise in practice, making it necessary to use single-pole switching. Therefore, extension of the present work to incorporate double-circuit systems would be useful.

c. Simulation of the transformer characteristics along with the saturation characteristics of the shunt reactors, can be of advantage in providing more realistic responses.

d. The simulation techniques presented here, can be extended to incorporate the use of series capacitors, and thereby the effect of the trapped charge ring down on the arcing process can be studied.

e. Although the occurence of L-L faults, not involving ground in EHV systems is rare, investigating the possibility of single-pole switching as a means to clear such faults can be of interest. A brief mentioning of such application

has been reported in a discussion by Sturton in reference 8 with regard to a 230kV system.

f. Transient stability studies, particularly for systems employing the hybrid method of autoreclosure and conventional single-pole switching with long dead-times are areas for future research.

g. The turbine-generator considerations, viz., the turbine blade shocks, the torsional duty of the shaft system, and the generator-rotor body heating due to negative sequence current circulation during the dead-time, are interesting areas worthy of study. Such studies are of importance in setting guidelines and standards for these equipments.

h. Investigating the possibility of using unbalanced 4-legged reactor bank(s), for use in untransposed line applications, is of importance, particularly with conventional single-pole switching.

i. The developed simulation techniques can be used in assessing the performance of very long loaded EHV transmission systems, implementing the idea proposed by Kimbark[8] of sectionalizing the faulted phase, as a measure to aid arc extinction.

j. A very promising area for further work, is the development of hardware for the line protection equipment, enhanced by on-line software support, for detecting the arc final extinction. This can lead to maximum operating system benefits with regard to system stability and supply security, as a result of adaptively reclosing the faulted phase.

k. Although the arc model[25,26,43] used throughout

this work is based on extensive laboratory results, a very challenging area for further research is to develop a long unconstrained arc model, based on energy consumption. Inclusion of the weather parameters, and the probabilistic nature of the arc length variation is of particular relevance.

REFERENCES

1. Trainor, J.J., Hobson, J.E. and Muller, H.N.Jr.: "High speed single-pole reclosing", AIEE Trans., 1942, 61, (2), pp.81-87.

2. Kappenman, J.G., Sweezy, G.A., Koschik, V. and Mustaphi, K.K.:"Staged fault tests with single phase reclosing on the winnipeg-twin cities 500kV interconnection", IEEE Trans,, 1982, PAS-101, No.3, pp.662-673.

3. IEEE Committee Report:"Single-pole switching for stability and reliability", IEEE PES Summer Meeting, paper No. 85 SM 467-6, 1985.

4. Edwards, L., Chadwick, J.W.Jr., Riesch, H.A. and Smith, L.E. :"Single-pole switching on TVA'S paradise-davidson 500kV line, design concepts and staged fault test results", IEEE Trans., 1971, PAS-90, No.6, pp.2436-2450.

5. Gonzalez, A.J., Tylor, C.W., Thorn, D., Kung, G.C. and Raczkowski, C.:"Effects of single- and three-pole switching and high speed reclosing on turbine-generator shafts and blades", IEEE Trans., 1984, PAS-103, No.11, pp.3218-3228.

6. Joyce, J.S., Kulig, T. and Lambrecht, D.:"Torsional fatigue of turbine-generator shafts caused by different electrical system faults and switching operation", IEEE Trans., 1978, PAS-97, No.5, pp.1965-1977.

7. Haun, R.K.:"13-years experience with single-phase reclosing at 345 kV", IEEE Trans., 1978, PAS-97, No.2,pp,520-528.

8. Kimbark, E.W.:"Selective-pole switching of long double-circuit EHV line", IEEE Trans., 1976, PAS-95, No.1, pp.219-230.

9. Hedin, R.A., Hammerquist, F.E. and Alford, R.W.:"Long line effects on single-pole operation of a 500kV transmission line", IEEE PES Winter meeting, paper No. A76 203-0, 1976.

10. Koschik, V.:"Single pole reclosing of a long, extra high voltage transmission line", Trans. of Canadian Elect. Assoc. And Operating Div., 19(1), paper No. 80-A-63,1980.

11. Shipley, R.B., Holley, H.J. and Coleman, D.W.:"Digital analysis of single-pole switching on EHV lines", IEEE Trans., 1968, PAS-87, No.8, pp.1679-1687.

12. Slepian, J.:"Extinction of a long a-c arc", Trans. AIEE, 1930, 49, (2), pp.421-430.

13. Eaton, J.R., Peck, J.K. and Dunham, J.M.:"Experimental studies of arcing faults on a 75kV transmission system", Trans. AIEE, 1931, 50, pp.1469-1479.

14. Terase, H., Sadamoto, K., Abe, K. and Kawaguchi, Y.:" Dielectric strength recovery characteristics after fault arc extinction in 500kV transmission lines", Elect. Engg. in Japan, 1969, 89, (2), pp.29-38.

15. Terase, H., Sadamoto, K., Hashimoto, Y. and Kawaguchi, Y.:" Recovery of heavy circuit arc in a long air gap", Elect. Engg. in Japan, 1968, 88, (7), pp.80-87.

16. Fufunishi, M. Anjo, K., Terase, H., Ozaki, Y., Yano, K. and Kawaguchi, Y.:"Laboratory study on dead time of high speed reclosing of 500kV systems", CIGRE, Paris, paper No. 31-03, 1970.

17. Johnson, I.B., Barthold, L.O., Hagenguth, J.H., Hauspurg, A., Kinghorn, J.H., Naef,O., Phelps, J.D.M., Phillips, V.E., Skeats, W.F., Titus, C.H. and Vose, F.C.:"Fault arc deionization and circuit breaker reclosing on e.h.v. lines-field, laboratory and analytical results", CIGRE, Paris, paper No. 307, 1962.

18. Warrington, A.R.van C.:"Reactance relays negligibly affected by arc impedance", Elect. World, Sept. 1931, pp.502-505.

19. Storm, A.P.:"Long 60-cycle arcs in air", Trans. AIEE, 1946, 65, (3), pp.113-117.

20. Maikopar, A.S.:"The quenching of an open arc", Electrichestvo (USSR), 1960, No. 4, pp.64-69.

21. Cornick, K.J., KO, Y.M. and Pek, B.:"Power system transients caused by arcing faults", IEE Proc., 1981, Vol.128, pt.C, No.1, pp.18-27.

22. Balser, S.B., Eaton, J.R. and Krause, P.C.:"Single-pole switching- Acomparison of computer with field test results", IEEE Trans., 1974, PAS-93, No.1, pp.100-108.

23. Fakheri, A.J., Shuter, T.C., Schneider, J.M. and Shih, C.H. :"Single phase switching tests on the AEP 765kV system-Extinction time for large secondary arc currents", IEEE Trans., 1983, PAS-102, No.8, pp.2775-2783.

24. Al-Rawi, A.M.:"Simulation of secondary arcs in EHV systems employing single-pole autoreclosure", PhD Thesis, University of Bath, 1981.

25. Johns, A.T. and Al-Rawi, A.M.:"Digital simulation of EHV systems under secondary arcing conditions associated with single-pole autoreclosure", IEE Proc., 1982, Vol.129 pt.C, No.2, pp.49-58.

26. Johns, A.T. and Al-Rawi, A.M.:"Developments in the simulation of long distance single-pole switched EHV systems", IEE Proc., 1984, Vol.131, pt.C, No.2, pp.67-77.

27. Haubrich, H.J., Hosemann, G. and Thomas, R.:"Single-phase autoreclosing in EHV systems", CIGRE, Paris, paper No. 31-09, 1974.

28. Lambert, S.R., Koschik, V., Wood,C.E., Worner, G. and Rocamora, R.G.:"Long line single-phase switching Transients and their effect on station equipment", IEEE Trans., 1978, PAS-97, No.3, pp.857-865,

29. Muller, M., Gygax, F., Hahn, C. and Baltensperger, P.:" Protection of e.h.v. systems, taking into account single-phase automatic reclosure on very long line", Brown Boveri Rev., 1958, Vol.45, No.6, pp.243-253.

30. Hasibar, R.M., Legate, A.C., Brunke, J. and Peterson, W.G. :"The application of High-speed grounding switches for single-phase reclosing on 500kV power systems", IEEE Trans., 1981, PAS-100, No.4, pp.1512-1515.

31. Jahn, D., Kottnitz, H.and schulze, H.:"Earth wires as a means of improving single-pole rapid reclosing of long high-voltage lines", CIGRE, Paris, paper No.401, 1964.

32. Peterson, A.H. and Dravid, N.V.:"A method for reducing dead time for single-pole reclosing in e.h.v. transmission", IEEE Trans., 1969, PAS-88, No.4, pp.286-291.

33. Clerici, A., Rukstuhl, G. and Vian, A.:"Influence of shunt reactors on switching surges", IEEE Trans., 1970, PAS-89, No.8, pp.1727-1736.

34. Edlinger, A., Glavitsch, H. and Ritter, A.:"The use of high-voltage reactors for the compensation of e.h.v. transmission lines", CIGRE, Paris, paper No.402,1964.

35. Knudsen, N.:"Single phase switching of transmission lines using reactors for extinction of the secondary arc", CIGRE, Paris, paper No.310, 1962.

36. Kimbark, E.W.:"Suppression of ground-fault arcs on single-pole switched EHV lines by shunt reactors", IEEE Trans., 1964, PAS-83, pp.285-290.

37. Bayless, R.S.:"Single-phase switching scheme protects 500kV line", Trans. & Dist. magazine, 1983, Vol.35, No.1, pp.24-29.

38 Carlsson, L.:"The use of a neutral-point reactor for single-pole reclosing on EHV lines", ASEA Journal, 1976, 49, (4), pp.91-94.

39. Geszti, P.O., Ban, G., Dan, A., Lyskov, Ju.I., Antonova, N.P., Horvath, I., Kisvolcsey, J., Benko,I. and Cisda, S. :"Problems of single-pole reclosing on long EHV transmission lines", CIGRE, Paris, paper No.33-10, 1982.

40. Scherer, H.N.Jr., Belyakov, N.N., Shperling, B.R., Rashkes, V.S., Chadwik, J.W.Jr., and Khoetsian, K.V.:"Single phase switching tests on 765kV and 750kV transmission lines", IEEE Trans., 1985, PAS-104,No.6,pp.1537-1548.

41. Eaton, J.R. and Kozak,E.:"Single-pole switching on reactor compensated lines, optimum operating conditions", IEEE PES Winter Meeting, paper No.C74 075-8, 1974.

42. Carlsson, L., Groza, L., Cristovici, A., Necsulescu, D.S. and Ionescu, A.I.:"Single-pole reclosing on EHV lines", CIGRE, Paris, paper No.31-03, 1974.

43. Johns, A.T. and Ritchie, W.M.:"Application of an improved technique for assessing the performance of single-pole reclosing schemes", IEEE PES Winter Meeting, paper No. 84 WM 217-6, 1984.

44. Balser, S.J. and Krause, P.C.:"Single-pole switching-A study of system transients with transposed and untransposed lines", IEEE Trans., 1974, PAS-93, No.4, pp.1208-1212.

45. Kimbark, E.W.:"Charts of three quantities associated with single-pole switching", IEEE Trans., 1975, PAS-94, No.2, pp.388-394.

46. Shperling, B.R., Fakheri, A. and Ware, B.J.:"Compensation scheme for single-pole switching on untransposed transmission lines", IEEE Trans., 1978, PAS-97, No.4, pp.1421-1429.

47. Shperling, B.R. and Fakheri, A.:"Single-phase switching parameters for untransposed EHV transmission lines", IEEE Trans., 1979, PAS-98, No.2, pp.643-654.

48. Fakheri, A.J., Grazan, J., Shperling, B.R. and Ware, B.J. :"The use of reactor switches in single phase switching" CIGRE, Paris, paper No.13-06, 1980.

49. Shperling, B.R., Fakheri, A, Shin, C.H. and Ware, B.J.:" Analysis of single phase switching field tests on the AEP 765kV system", IEEE Trans., 1981, PAS-100, No.4 pp.1729-1735.

50. Bickford, J.P and Abdel-Rahman, M.H.:"Application of travelling wave methods to the calculation of transient fault currents and voltages in power system networks", IEE Proc., 1980, Vol.127, pt.C, No.3, pp.153-168.

51. Bickford, J.P. and Doepel, P.S.:"Calculation of switching Transients with particular reference to line energisation", Proc. IEE, 1967, Vol.114, No.4, pp.465-477.

52. Johns, A.T. and El-Kateb, M.M.T.:"Developments in techniques for simulating faults in e.h.v. transmission systems", Proc. IEE, 1978, Vol.125, No.3, pp.221-229.

53. Aggarwal, R.K. and Johns, A.T.:"Digital simulation technique for testing line protection relays during 3-phase autoreclosure", IEE Conf. Pub. 185, 1980, pp.250-254.

54. Johns. A.T., El-Nour, M. and Aggarwal, R.K.:"Performance of distance protection of e.h.v. feeders utilising shunt reactor arrangements for arc suppression and voltage control", Proc. IEE, 1980, Vol.127, pt.C, No.5, pp.304-316.

55. Sekine, Y., Ichida, Y., Nakamura, A., Kurihara, I. and Suzuki, H.:"Asymmetrical four legged reactor extinguishing secondary arc current for high-speed reclosing on UHV systems", CIGRE, Paris, paper No.38-03, 1984.

56. Wedephol, L.M. and Mohamed, S.E.T.:"Multiconductor transmission lines. Theory of natural modes and Fourier integral applied to transient analysis", Proc. IEE, 1969, Vol.116, No.9, pp.1553-1563.

57. Johns, A.T. and Aggarwal, R.K.:"Digital simulation of faulted e.h.v. lines with particular reference to very high speed protection", Proc. IEE, 1976, Vol.123, No.4, pp.353-359.

58. Carson, J.R.:"Wave propagation in overhead wires with ground return", Bell System Tech. Journal, 1926, 5, pp.539-554.

59. Johns, A.T.:"Computer simulation studies of new methods of distance protection for e.h.v. lines", Report on Science Research Council Research, Grant B/4534/1, Nov. 1975, Univ. of Bath.

60. Galloway, R.H., Shorrosks, W.B. and Wedepohl, L.M.:" Calculation of electrical parameters for short and long polyphase transmission lines", Proc. IEE, 1964, Vol.111, No.12, pp.2051-2059.

61. Wedepohl, L.M.:"Application of matrix methods to the solution of the travelling-wave phenomena in polyphase systems", Proc. IEE, 1963, Vol.110, No.12, pp.2200-2212.

62. Battisson, M.J., Bickford, J.P., Corcoran, J.C.W., Jackson, R.L., Scott, M. and Ward, R.J.S.:"British investigations on the switching of long EHV transmission lines", CIGRE, Paris, paper No.13-02, 1970.

63. Berglund, R.O., Mittelstadt, W.A., Shelton, M.L., Barkan, P., Bewey, C.G. and Skreiner, K.M.:"One-cycle fault interruption at 500kV: System benefits and breaker design", IEEE Trans., 1974, PAS-93, pp.1240-1251.

64. Hicks, K.L. and Butt, W.H.:"Feasibility and economics of ultra-high speed fault clearing", IEEE Trans., 1980, PAS-99, No.6, pp.2138-2145.

65. Johns, A.T.:"New ultra-high speed directional comparison technique for the protection of e.h.v. transmission lines", Proc. IEE, 1980, 127, pt.C, No.4,pp.228-239.

66. Giuliante, A.T., Stranne, G., Slatem, R.R. and Öhlér, C. :"A directional wave detector relay with enhanced application capabilities for EHV and UHV lines", IEEE Trans., 1983, PAS-102, No.9, pp.2881-2892.

67. Yee, M.T. and Esztergalyos, J.:"Ultra high speed relay for EHV/UHV transmission lines-Installation-Staged fault tests and operational experience", IEEE Trans., 1978, PAS-97, No.5, pp.1814-1825.

68. Chamia, M. and Liberman, S.:"Ultra high speed relay for EHV/UHV transmission lines-Development, Design and application", IEEE Trans., 1978, PAS-97,No.6 pp.2104-2116.

69. Engler, F., Lanz. O.E., Hanggli, M. and Bacchini, G.:" Transient signals and their processing in an ultra high-speed directional relay for EHV/UHV transmission line protection", IEEE Trans., 1985, PAS-104, No.6 pp.1463-1473.

70. Ritchie, W.M., Missan, J.S. and Abu-Elnour, M.H.:"Single pole reclosing on long 220kV transmission lines", Proc. 18th. UPEC, 1983, England.

71. Kimbark, E.W. and legate, A.C.:"Fault surge versus switching surge-A study of transient overvoltages caused by line-to-ground faults", IEEE Trans., 1968, PAS-87, No.9, pp.1762-1769.

72. Cazzan, M., Clerici, A., Margaritidis, P. and Theloudis, J. :"Internal overvoltages on the new Greek 400kV network", CIGRE, Paris, paper No.33-03, 1974.

73. Koschic, V.:"Single pole reclosing of a long EHV transmission line", Trans. of Canadian Elect. Assoc. and Operating Div. 19(1), paper 80-A-63, 1980.

74. Balser, S.J. and Krause, P.C.:"Computer study of electric transients during single-pole switching of a 765kV line", IEEE paper No. CP 72 222-3, 1972.

75. Aggarwal, R.K. and Jöhns, A.T.:"Simulation of electrical transient phenomena associated with single pole autoreclosure of short e.h.v. transmission lines" Proc. 14th. UPEC, 1979, England.

76. Johns,A.T. and Aggarwal, R.K.:"Digital simulation of fault autoreclosure sequences with particular reference to the performance evaluation of protection for EHV transmission lines", Proc. IEE, 1981,128, pt.C, No.4, pp.183-195.

77. Wedepohl, L.M. and Mohamed, S.E.T.:"Transient analysis of multiconductor transmission lines with special reference to nonlinear problems", Proc. IEE, 1970, 117, (5), pp.979-988.

78. Anjo, K., Terase, H. and Kawaguchi, Y.:"Self extinction of arcs created in long air gaps", Elect. Engg. in Japan, 1968, 88, (4), pp.83-93.

79. Gary, C., Hesketh, S. and Moreau, M.:"Tests of self extinction of secondary arcs in case of single-pole switching. Application to 750kV lines", Rev. Gen. de L'Electricite, 1971, 80, (5), pp.406-412.

80. Borgonovo, G., Santagostino, G., Gamelli, G.,Lagostena, L. and Porrino, A.:"Evaluation of the risk of failure due to switching surges in u.h.v. networks", CIGRE, Paris, paper No.33-14, 1978.

81. Bickford, J.P., Mullineux, N. and Reed, J.R.:"Computation of power-system transients", IEE Monograph series 18, 1976.

82. Day, S.J., Mullineux, N. and Reed, J.R.:"Developments in obtaining transient response using Fourier Transforms", Int. J. Elect. Eng. Educ., 1965, 3, pp.501-506.

83. Ametani, A.:"The application of Fast Fourier Transform to electrical transient phenomena", Int. J. Elect. Eng. Educ., 1973, 10, pp.277-287.

84. Amstutz, A.:"Residual currents and voltages with single-pole rapid reclosing", Brown Boveri Rev., 1948, 35, pp.220-226.

APPENDIX 2.1

SOURCE SIMULATION

For the purpose of confirming the digital simulation presented in this thesis, a general source model based upon arbitrarily defined short circuit levels (s.c.l.) at the terminating bus-bars has been used[57,59]. The basic source model is shown in fig. 2.10, and the source side equation in matrix form is :-

$$\bar{E}_S = Z_{SS}\ \bar{I}_S + \bar{V}_S \qquad \text{(A2.1.1)}$$

Where,

$$\bar{E}_S = \left[\bar{E}_{Sa}\ \ \bar{E}_{Sb}\ \ \bar{E}_{Sc}\right]^T,$$

$$Z_{SS} = \begin{bmatrix} Z_{Sl} + Z_{nl} & Z_{nl} & Z_{nl} \\ Z_{nl} & Z_{Sl} + Z_{nl} & Z_{nl} \\ Z_{nl} & Z_{nl} & Z_{Sl} + Z_{nl} \end{bmatrix},$$

$$\bar{I}_S = \left[\bar{I}_{Sa}\ \ \bar{I}_{Sb}\ \ \bar{I}_{Sc}\right]^T, \text{ and}$$

$$\bar{V}_S = \left[\bar{V}_{Sa}\ \ \bar{V}_{Sb}\ \ \bar{V}_{Sc}\right]^T$$

In eqn. A2.1.1, the elements Z_{Sl} and Z_{nl} are calculated as follows,

$$Z_{Sl} = V_L^2 \ / \text{ s.c.l.} \qquad \text{(A2.1.2)}$$

also $$Z_{Sl} = R_{Sl} + jX_{Sl} \qquad \text{(A2.1.3)}$$

Defining the X/R ratio (at power frequency) of the sending and receiving end sources, R_{S1} and X_{S1} in eqn. A2.1.3 can be defined.

The source neutral impedance Z_{n1} is calculated by defining both the p.p.s. and the z.p.s. impedances Z_{S1} and Z_{So} for the circuit of fig. 2.10, where,

$$Z_{So} = Z_{S1} + 3Z_{n1}$$

or $$Z_{n1} = Z_{S1} \left[(Z_{So}/Z_{S1}) - 1 \right] /3 \qquad \text{(A2.1.4)}$$

The z.p.s./p.p.s. impedance ratio is among other source parameters which have to be defined. These parameters are:-

1. Short circuit level (s.c.l.).
2. X/R ratio at power frequency.
3. Z_{So}/Z_{S1} ratio.
4. The system line voltage (V_L).

APPENDIX 2.2

CALCULATION OF THE SHUNT REACTOR IMPEDANCES

The shunt capacitances of a transmission line are usually described by either a capacitance matrix or by a mesh circuit(fig. A2.2.1a). Assuming ideal line transposition, the line inter-phase and phase-to-ground capacitive susceptances of such a line are B_{ch} and B_{cg} respectively. The symmetrical components of these susceptances are found by assuming a set of zero phase sequence (z.p.s.)and positive phase sequence(p.p.s.) voltages applied independently at the terminals(see fig.A2.2.1a) to ground, thus gives[8],

$$B_{co} = B_{cg} \qquad \text{(A2.2.1)}$$

$$B_{cl} = B_{cg} + 3B_{ch} \qquad \text{(A2.2.2)}$$

Fig. A2.2.1b represents the 4-legged shunt reactor in terms of phase quantities. Examination of the circuit of fig. A2.2.1b with z.p.s. and p.p.s. set of currents independently into the terminals gives :

$$X_{Lo} = X_p + 3X_n \qquad \text{(A2.2.3)}$$

$$X_{Ll} = X_p \qquad \text{(A2.2.4)}$$

In terms of the z.p.s. and p.p.s. values of the line capacitive susceptances(B_{co}, B_{cl}), the parameters of the shunt reactor bank when arranged to compensate one half of

any line section of length L are[8] :

$$B_{Lo} = h_o B_{co} L/2 \qquad \text{(A2.2.5)}$$

$$B_{L1} = h_1 B_{c1} L/2 \qquad \text{(A2.2.6)}$$

where h_o and h_1 are the degrees of z.p.s. and p.p.s. shunt compensation respectively.

From eqns. A2.2.1 - A2.2.6, the shunt reactor phase and neutral reactances are :-

$$X_p = 2/h_1 B_{c1} L \qquad \text{(A2.2.7)}$$

$$X_n = 2(h_1 B_{c1} - h_o B_{co})/3h_1 h_o B_{c1} B_{co} L \qquad \text{(A2.2.8)}$$

therefore, the shunt reactor phase and neutral inductances are :-

$$L_p = X_p/\omega_o \qquad \text{(A2.2.9)}$$

$$L_n = X_n/\omega_o \qquad \text{(A2.2.10)}$$

The resistances of the shunt reactor are relatively small, a typical Q-factor of each limb at power frequency (50 or 60Hz) being 250. Therefore, the phase and neutral impedances can be defined :-

$$Z_p = R_p + j\omega L_p \qquad \text{(A2.2.11)}$$

$$Z_n = R_n + j\omega L_n \qquad \text{(A2.2.12)}$$

where $R_p = X_p/Q$, and $R_n = X_n/Q$.

There are a number of factors which determine the degrees of shunt compensation(h_o and h_1), and for a typical compensated line, they generally lie between 0.5 and 1.2[8,36,54]. The line shunt susceptances(B_{co} and B_{c1}) are evaluated in the usual manner, from the average sum of all the self and mutual susceptances per unit length of the line under consideration.

In the developed programs, a 4-legged shunt reactor, a Y-connected with solidly grounded neutral reactor or a combination of them, can be simulated at either or each end of the line.

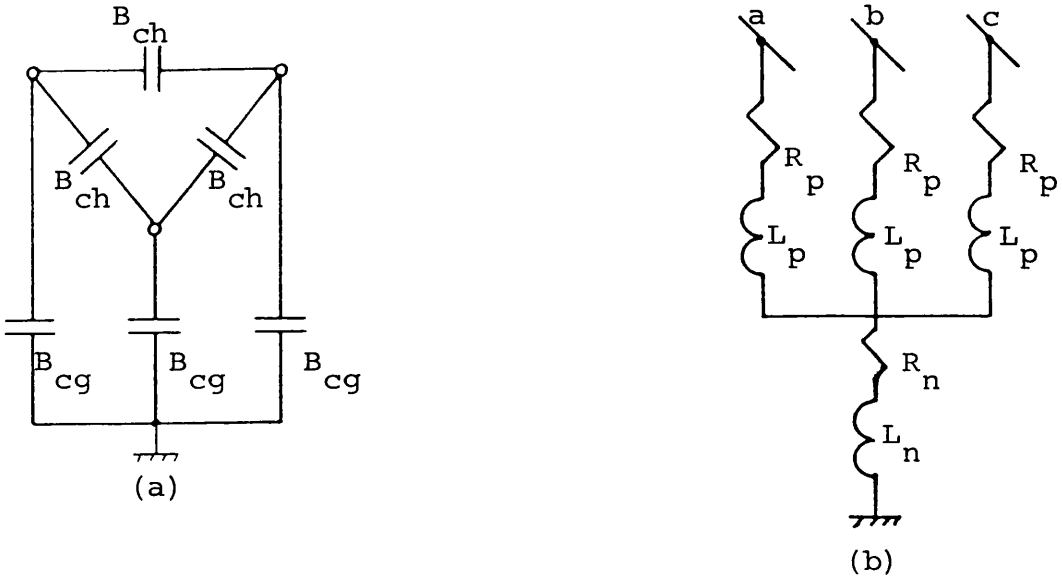

Fig. A2.2.1

(a) Mesh circuit representing the shunt susceptances of balanced single circuit line

(b) Four-legged shunt reactor

APPENDIX 2.3

LINE CALCULATIONS

Any multiconductor transmission line section is defined by its series impedance matrix per unit length $[Z]$ and corresponding shunt admittance matrix $[Y]$. Each element of $[Z]$ varies with frequency and is determined by the conductors type, their physical geometry and the nature of the earth plane[57,60]. Evaluation of the contribution of the conductor physical geometry in $[Z]$ is a simple matter and, the infinite series developed by Carson[58], provides a means by which the effect of the earth plane return path can be incorporated. At power frequencies, and assuming a uniform current distribution in the conductors, the conductor self inductance is calculated in the standard way by the concept of geometric mean radius. At higher frequencies, a typical variation of inductance and resistance with frequency(see fig. A2.3.1) is used to calculate the conductor contribution in $[Z]$ [59]. The $[Y]$ matrix is calculated from the physical geometry of the conductors with the assumption that the air conductance is negligible[60].

The theory of natural modes developed by Wedepohl[61] provides a solution to the system voltage and current equations given by eqns. A2.3.1 and A2.3.2, of the form given by eqns. A2.3.3 and A2.3.4.

$$d2\bar{V} / dX^2 = [Z][Y]\ \bar{V} \qquad \text{(A2.3.1)}$$

$$d2\bar{I} / dX^2 = [Y][Z]\ \bar{I} \qquad \text{(A2.3.2)}$$

$$\bar{V} = Q \exp(-\gamma x)\ Q^{-1}\ \bar{V}_i + Q \exp(\gamma x)\ Q^{-1}\ \bar{V}_r \qquad \text{(A2.3.3)}$$

$$\bar{I} = Y_o\ Q \exp(-\gamma x)\ Q^{-1}\ \bar{V}_i - Y_o\ Q \exp(\gamma x)\ Q^{-1}\ \bar{V}_r \qquad \text{(A2.3.4)}$$

where,

$Y_o = Z^{-1}\ Q \gamma Q^{-1}$

γ = modal propagation constant matrix

Q = voltage eigenvector matrix

$\bar{V}_i, \bar{V}_r$ = incident and reflected voltage Transforms

Equations A2.3.3 and A2.3.4 give the voltage and current vectors at any point distance x from one end of the line. If a section of a multiconductor transmission line is to be represented, then it is possible to formulate the two-port matrix equations using eqns. A2.3.3 and A2.3.4 by replacing x by zero and the length of the line section, L_s, and it can be written :-

$$\begin{bmatrix} \bar{V}_o \\ \bar{I}_o \end{bmatrix} = \begin{bmatrix} Q \cosh \gamma L_s\ Q^{-1} & Q \sinh \gamma L_s\ Q^{-1}\ Z_o \\ Y_o\ Q \sinh \gamma L_s\ Q^{-1} & Y_o\ Q \cosh \gamma L_s\ Q^{-1} Z_o \end{bmatrix} \begin{bmatrix} \bar{V}_{L_s} \\ \bar{I}_{L_s} \end{bmatrix} \qquad \text{(A2.3.5)}$$

where,

$Z_o = Y_o^{-1} = Q\ \gamma^{-1} Q^{-1}\ Z$

$\bar{V}_o, \bar{I}_o$ are the voltage and current vector Transforms at x = zero.

$\bar{V}_{L_s}, \bar{I}_{L_s}$ are the voltage and current vector Transforms at $x = L_s$.

It can be seen that eqn. A2.3.5, gives the transmission line equations in terms of the well known "ABCD" constant matrices, where,

$$A = \cosh(\psi L_s) \quad ; \quad B = \sinh(\psi L_s)\, Z_o$$

$$B = Y_o \sinh(\psi L_s) \quad ; \quad D = Y_o \cosh(\psi L_s)\, Z_o$$

and

$$\psi = Q \gamma Q^{-1}$$

$$\cosh(\psi L_s) = Q \cosh(\gamma L_s)\, Q^{-1}$$

$$\sinh(\psi L_s) = Q \sinh(\gamma L_s)\, Q^{-1}$$

For a single-circuit transmission network, the dimension of any of the matrices given in eqn. A2.3.5 is (3 x 3).

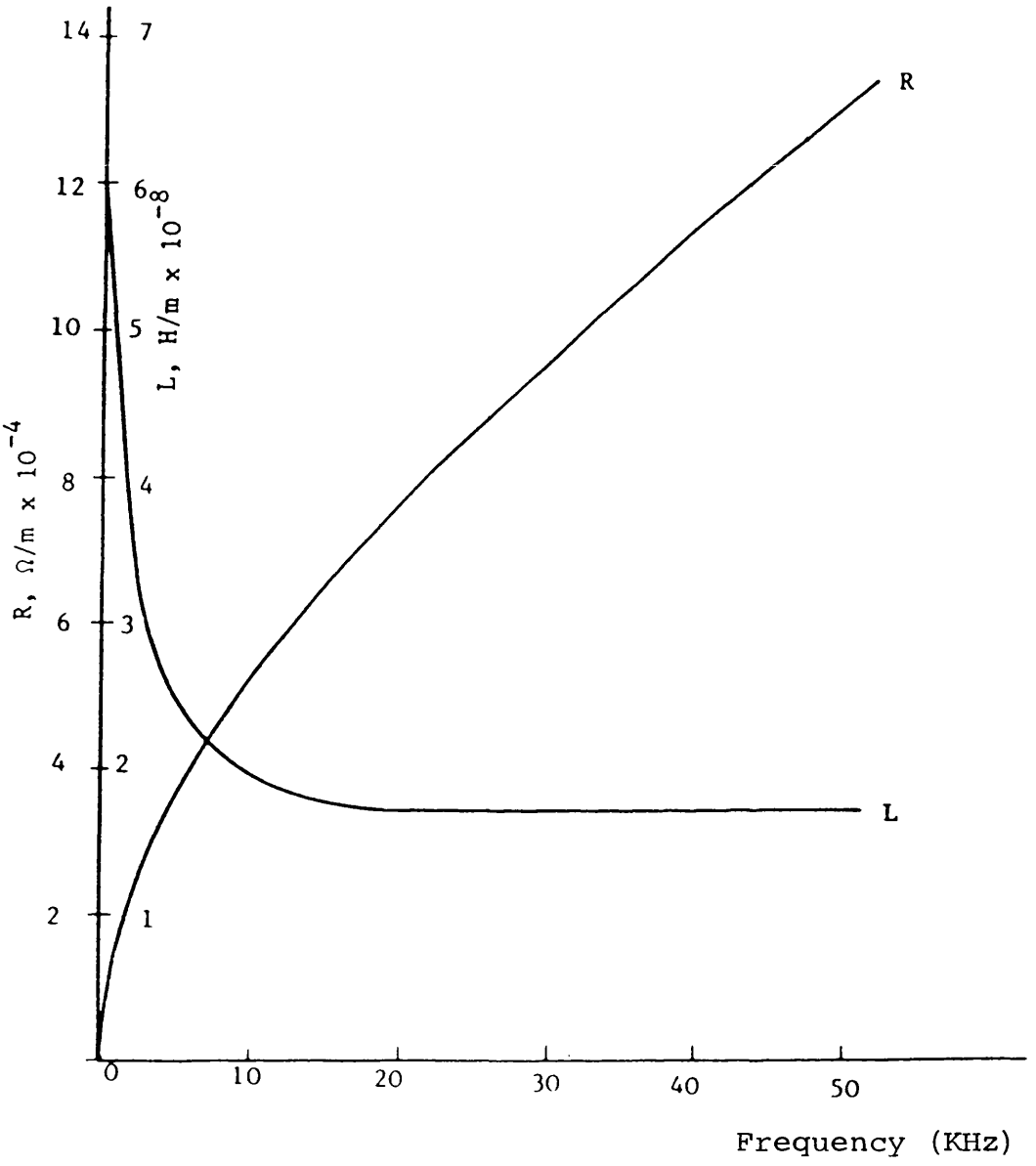

Fig. A2.3.1 Typical variation of conductor inductance(L) and resistance(R) with frequency

APPENDIX 2.4

FAULT SIMULATION

Fig. 2.13 shows the faulted system model in which the fault is simulated by a suddenly applied voltage source at the fault point. It has been shown in reference 57 that this voltage source is equal in magnitude and opposite in polarity to the pre-fault voltage of the faulted phase at the point of fault.

From fig. 2.13, at the fault point, two main equations can be written :-

$$\begin{bmatrix} \bar{E}_{FF} \\ \bar{I}_{FRF} \end{bmatrix} = \begin{bmatrix} A_R & B_R \\ C_R & D_R \end{bmatrix} \begin{bmatrix} \bar{V}_{RF} \\ \bar{I}_{RF} \end{bmatrix} \qquad \text{(A2.4.1)}$$

and

$$\begin{bmatrix} \bar{E}_{FF} \\ \bar{I}_{FSF} \end{bmatrix} = \begin{bmatrix} A_L & B_L \\ C_L & D_L \end{bmatrix} \begin{bmatrix} \bar{V}_{SF} \\ \bar{I}_{SF} \end{bmatrix} \qquad \text{(A2.4.2)}$$

where, $\bar{E}_{FF}$, $\bar{V}_{RF}$, $\bar{V}_{SF}$, $\bar{I}_{FRF}$, $\bar{I}_{RF}$, $\bar{I}_{FSF}$, and $\bar{I}_{SF}$ are the Transforms of the respective voltages and currents shown in fig. 2.13.

(A_R, B_R, C_R, and D_R) are the transfer-function matrices representing the system section linking the fault point

and the receiving end, including the shunt reactor if present.

(A_L, B_L, C_L, and D_L) are the transfer-function matrices representing the system section linking the fault point and the sending end, including the shunt reactor if present.

Applying the superposition principle, with $\bar{V}_{FF}$ is the only voltage source in the circuit of fig. 2.13 gives the following :

$$\bar{V}_{RF} = Z_{SR} \quad \bar{I}_{RF} \tag{A2.4.3}$$

$$\bar{V}_{SF} = Z_{SS} \quad \bar{I}_{SF} \tag{A2.4.4}$$

where, Z_{SR} and Z_{SS} are the receiving and sending end source impedance matrices respectively.

Considering any phase-to-earth fault, at the fault point,

$$\bar{E}_{FF} = \bar{V}_{FF} - Z_F\left[\bar{I}_{FRF} + \bar{I}_{FSF} \right] \tag{A2.4.5}$$

where Z_F is a diagonal (3 x 3) matrix of the required values of the fault resistance (R_F) in each phase.

From eqns. A2.4.1 - A2.4.4, the equation relating $\bar{E}_{FF}$ to $\left[\bar{I}_{FRF} + \bar{I}_{FSF} \right]$ can be easily derived, and is given by eqn. A2.4.6.

$$\bar{E}_{FF} = \left[M_{R1} \quad M_{R2} + M_{S1} \quad M_{S2} \right]^{-1} \left[\bar{I}_{FRF} + \bar{I}_{FSF} \right] \tag{A2.4.6}$$

where,

$$M_{R1} = C_R Z_{SR} + D_R$$

$$M_{R2} = \left[A_R Z_{SR} + B_R \right]^{-1}$$

$$M_{S1} = C_L Z_{SS} + D_L$$

$$M_{S2} = \left[A_L Z_{SS} + B_L \right]^{-1}$$

Finally, substituting eqn. A2.4.6 in eqn. A2.4.5 gives:

$$\bar{V}_{FF} = \left\{ Z_F + \left[M_{R1} M_{R2} + M_{S1} M_{S2} \right]^{-1} \right\} \left[\bar{I}_{FRF} + \bar{I}_{FSF} \right] \qquad \text{(A2.4.7)}$$

Eqn. A2.4.7 , can be written in a general form relating the superimposed voltage Transform $\bar{V}_{FF}$ to the fault path current Transform $(-\left[\bar{I}_{FRF} + \bar{I}_{FSF} \right])$, which is given in eqn. A2.4.8.

$$\bar{V}_{FF} = - Z_{FF} \bar{I}_F \qquad \text{(A2.4.8)}$$

Assuming a line-to-earth fault on phase-"a", $\bar{V}_{FFa}$ is the Fourier Transform of a suddenly applied voltage of the form,

$$V_{FFa} = - V_{FSa} \sin(\omega_o t + \beta) \, h(t) \qquad \text{(A2.4.9)}$$

where,

V_{FSa} = Peak of the fault point pre-fault voltage.

β = Phase displacement between the pre-fault voltage of phase-"a" and the reference voltage.

$h(t)$ = A unit step function.

The currents $\bar{I}_{Fb}$ and $\bar{I}_{Fc}$ are zero as phases "b" and "c"

are sound, hence eqn. A2.4.8 takes the simplified form of eqn. A2.4.10.

$$\bar{V}_{FF} = \left[Z_{FF}(1,1) \quad Z_{FF}(2,1) \quad Z_{FF}(3,1) \right]^T \bar{I}_{Fa} \qquad \text{(A2.4.10)}$$

With reference to eqn. A2.4.8, the voltage Transform $\bar{V}_{FFa}$ is known, so that the superimposed voltages in the sound phases are easily evaluated using eqn. A2.4.5. Finally, the superimposed currents and voltages at the line remote ends are calculated. Using eqns. A2.4.1 and A2.4.3,

$$\bar{I}_{RF} = M_{R2}\ \bar{E}_{FF} \qquad \text{(A2.4.11)}$$

$$\bar{V}_{RF} = Z_{SR}\ M_{R2}\ \bar{E}_{FF} \qquad \text{(A2.4.12)}$$

Likewise, from eqns. A2.4.2 and A2.4.4,

$$\bar{I}_{SF} = M_{S2}\ \bar{E}_{FF} \qquad \text{(A2.4.13)}$$

$$\bar{V}_{SF} = Z_{SS}\ M_{S2}\ \bar{E}_{FF} \qquad \text{(A2.4.14)}$$

For systems compensated by a 4-legged shunt reactor bank(s), the voltage at the neutral point can be calculated as follow:

$$\bar{V}_n = (\bar{V}_{aF} + \bar{V}_{bF} + \bar{V}_{cF}) \left[Z_n / (Z_p + 3Z_n) \right] \qquad \text{(A2.4.15)}$$

where, $\left[\bar{V}_{aF} \quad \bar{V}_{bF} \quad \bar{V}_{cF} \right]^T$ is the voltage Transform vector of the bus-bar to which the 4-legged shunt reactor is connected.

For systems compensated by the neutral switched reactor bank, the ideal neutral switch current is calculated using eqn. A2.4.16 - A2.4.18 for a fault on phase "a", "b", or "c" respectively.

$$\bar{I}_{SWa} = (\bar{V}_{aiF} + \bar{V}_{biF}) / Z_p \qquad \text{(A2.4.16)}$$

$$\bar{I}_{SWb} = (\bar{V}_{aiF} + \bar{V}_{biF} + \bar{V}_{ciF}) / Z_p \qquad \text{(A2.4.17)}$$

$$\bar{I}_{SWc} = (\bar{V}_{biF} + \bar{V}_{ciF}) / Z_p \qquad \text{(A2.4.18)}$$

where the suffix i designate the line end at which the reactor bank is connected(S or R).

The voltage and current Transforms given by eqn. A2.4.10-A2.4.18 are then converted to the time domain via the Inverse Transform[57] and added to the corresponding pre-fault steady-state quantities to obtain the complete fault-transient waveforms.

APPENDIX 3.1

EVALUATION OF THE SYSTEM ADMITTANCE MATRIX- CONVENTIONAL SINGLE-POLE SWITCHING AND THE HYBRID METHOD OF AUTORECLOSURE

With reference to fig. 3.3, the Transforms of the voltage components $\bar{V}_{RK}$ and $\bar{V}_{SK}$ on the line side of the breakers are obtained by noting that,

$$\bar{V}_{RK} = Z_{SR}\ \bar{I}_{RK} - \bar{E}_{RK} \qquad \text{(A3.1.1)}$$

and

$$\bar{V}_{SK} = Z_{SS}\ \bar{I}_{SK} - \bar{E}_{SK} \qquad \text{(A3.1.2)}$$

Also, the line end quantities are related to those at the fault point by,

$$\begin{bmatrix} \bar{V}_{FK} \\ \bar{I}_{FRK} \end{bmatrix} = \begin{bmatrix} A_R & B_R \\ C_R & D_R \end{bmatrix} \begin{bmatrix} \bar{V}_{RK} \\ \bar{I}_{RK} \end{bmatrix} \qquad \text{(A3.1.3)}$$

and

$$\begin{bmatrix} \bar{V}_{FK} \\ \bar{I}_{FSK} \end{bmatrix} = \begin{bmatrix} A_L & B_L \\ C_L & D_L \end{bmatrix} \begin{bmatrix} \bar{V}_{SK} \\ \bar{I}_{SK} \end{bmatrix} \qquad \text{(A3.1.4)}$$

At the fault point,

$$\bar{V}_{FK} = \bar{E}_{FK} - Z_F\ (\bar{I}_{FRK} + \bar{I}_{FSK}) \qquad \text{(A3.1.5)}$$

From eqns. A3.1.1 and A3.1.3,

$$\bar{I}_{FRK} = (C_R Z_{SR} + D_R) \bar{I}_{RK} - C_R \bar{E}_{RK}$$

Likewise, from eqns. A3.1.2 and A3.1.4,

$$\bar{I}_{FSK} = (C_L Z_{SS} + D_L) \bar{I}_{SK} - C_L \bar{E}_{SK}$$

Hence,

$$(\bar{I}_{FRK} + \bar{I}_{FSK}) = M_1 \bar{I}_{RK} + M_2 \bar{I}_{SK} - C_R \bar{E}_{RK} - C_L \bar{E}_{SK} \qquad \text{(A3.1.6)}$$

where,

$$M_1 = C_R Z_{SR} + D_R$$

$$M_2 = C_L Z_{SS} + D_L$$

From eqns. A3.1.1, A3.1.3 and A3.1.5,

$$\bar{I}_{RK} = M_3 \bar{E}_{FK} - M_4 (\bar{I}_{FRK} + \bar{I}_{FSK}) + M_5 \bar{E}_{RK} \qquad \text{(A3.1.7)}$$

where,

$$M_3 = \left[A_R Z_{SR} + B_R \right]^{-1}$$

$$M_4 = M_3 Z_F$$

$$M_5 = M_3 A_R$$

Similarly, from eqns. A3.1.2, A3.1.4 and A3.1.5,

$$\bar{I}_{SK} = M_6 \bar{E}_{FK} - M_7 (\bar{I}_{FRK} + \bar{I}_{FSK}) + M_8 \bar{E}_{SK} \qquad \text{(A3.1.8)}$$

where,

$$M_6 = \left[A_L Z_{SS} + B_L \right]^{-1}$$

$$M_7 = M_6 Z_F$$

$$M_8 = M_6 A_L$$

Now, from eqns. A3.1.6, A3.1.7 and A3.1.8,

$$\bar{I}_{FK} = -(\bar{I}_{FRK} + \bar{I}_{FSK})$$
$$= Y_{11}\,\bar{E}_{FK} + Y_{12}\,\bar{E}_{SK} + Y_{13}\,\bar{E}_{RK} \qquad \text{(A3.1.9)}$$

$$\bar{I}_{SK} = Y_{21}\,\bar{E}_{FK} + Y_{22}\,\bar{E}_{SK} + Y_{23}\,\bar{E}_{RK} \qquad \text{(A3.1.10)}$$

and

$$\bar{I}_{RK} = Y_{31}\,\bar{E}_{FK} + Y_{32}\,\bar{E}_{SK} + Y_{33}\,\bar{E}_{RK} \qquad \text{(A3.1.11)}$$

where,

$$Y_{11} = -M_T\left[M_1\,M_3 + M_2\,M_6\right] \quad ; \quad Y_{12} = -M_T\left[M_2\,M_8 - C_L\right]$$

$$Y_{13} = -M_T\left[M_1\,M_5 - C_R\right] \quad ; \quad M_T = \left[U + M_1\,M_3 + M_2\,M_7\right]^{-1}$$

$$Y_{21} = M_6 + M_7\,Y_{11} \quad ; \quad Y_{22} = M_7\,Y_{12} + M_8$$

$$Y_{23} = M_7\,Y_{13} \quad ; \quad Y_{31} = M_3 + M_4\,Y_{11}$$

$$Y_{32} = M_4\,Y_{12} \quad ; \quad Y_{33} = M_4\,Y_{13} + M_5$$

U is a unity matrix.

Equations A3.1.9 to A3.1.11, can be arranged in the matrix relationship of eqn. A3.1.12 :-

$$\begin{bmatrix} \bar{I}_{FK} \\ \bar{I}_{SK} \\ \bar{I}_{RK} \end{bmatrix} = \begin{bmatrix} Y_{11} & Y_{12} & Y_{13} \\ Y_{21} & Y_{22} & Y_{23} \\ Y_{31} & Y_{32} & Y_{33} \end{bmatrix} \begin{bmatrix} \bar{E}_{FK} \\ \bar{E}_{SK} \\ \bar{E}_{RK} \end{bmatrix} \qquad \text{(A2.1.12)}$$

The 9 x 9 admittance matrix of eqn. A3.1.12 is computed and stored at all spectral frequencies of interest. Eqn. A3.1.12, can be used for fault simulation as well as breakers opening and closing.

APPENDIX 3.2

EVALUATION OF THE SYSTEM ADMITTANCE MATRIX- NEUTRAL SWITCHED REACTOR IMPLEMENTATION

With reference to fig. 3.4, eqns. 3.16 to 3.21 are repeated here as follow :

$$\bar{V}_{Sk} = Z_{SS}\ \bar{I}_{SK} - \bar{E}_{SK} \tag{A3.2.1}$$

$$\bar{V}_{FK} = \bar{E}_{FK} - Z_F\ (\bar{I}_{FRK} + \bar{I}_{FSK}) \tag{A3.2.2}$$

$$\bar{V}_{RK} = Z_{SR}\ \bar{I}_{RK} - \bar{E}_{RK} \tag{A3.2.3}$$

$$\begin{bmatrix} \bar{V}_{RK} \\ \bar{E}_{SWK} \end{bmatrix} = \begin{bmatrix} & I & \end{bmatrix} \begin{bmatrix} \bar{I}_{mK} \\ \bar{I}_{SWK} \end{bmatrix} \tag{A3.2.4}$$

$$\begin{bmatrix} \bar{V}_{FK} \\ \bar{I}_{FSK} \end{bmatrix} = \begin{bmatrix} A_L & B_L \\ C_L & D_L \end{bmatrix} \begin{bmatrix} \bar{V}_{SK} \\ \bar{I}_{SK} \end{bmatrix} \tag{A3.2.5}$$

$$\begin{bmatrix} \bar{V}_{FK} \\ \bar{I}_{FRK} \end{bmatrix} = \begin{bmatrix} A_R & B_R \\ C_R & D_R \end{bmatrix} \begin{bmatrix} \bar{V}_{RK} \\ \bar{I}_{RK} + \bar{I}_{mK} \end{bmatrix} \tag{A3.2.6}$$

From eqns. A3.2.1 and A3.2.5,

$$\bar{I}_{FSK} = M_1\ \bar{I}_{SK} - C_L\ \bar{E}_{SK} \tag{A3.2.7}$$

where,

$$M_1 = C_L\ Z_{SS} + D_L$$

From eqns. A3.2.1, A3.2.2 and A3.2.5,

$$\bar{I}_{SK} = M_2\ \bar{E}_{FK} + M_3\ \bar{E}_{SK} + M_4\ \bar{I}_{FK} \qquad \text{(A3.2.8)}$$

where,

$$M_2 = \left[\ A_L\ Z_{SS} + B_L\right]^{-1} \quad ; \quad M_3 = M_2\ A_L$$

$$M_4 = M_2\ Z_F \quad ; \quad \bar{I}_{FK} = -\ (\bar{I}_{FSK} + \bar{I}_{FRK})$$

From eqn. A3.2.4,

$$\begin{bmatrix} \bar{I}_{mK} \\ \bar{I}_{SWK} \end{bmatrix} = \begin{bmatrix} M_{A1} & M_{A2} \\ M_{A3} & M_{A4} \end{bmatrix} \begin{bmatrix} \bar{V}_{RK} \\ \bar{E}_{SWK} \end{bmatrix} \qquad \text{(A3.2.9)}$$

where,

$$\begin{bmatrix} M_{A1} & M_{A2} \\ M_{A3} & M_{A4} \end{bmatrix} = \left[I\right]^{-1}$$

M_{A1}, is a 3 x 3 matrix, M_{A2} and M_{A3} are a 3 x 1 and 1 x 3 vectors respectively. M_{A4}, is a single element.

From eqns. A3.2.3, and A3.2.9, the following relationships can be written for $\bar{I}_{mK}$ and $\bar{I}_{SWK}$:-

$$\bar{I}_{mK} = M_{A1}\ Z_{SR}\ \bar{I}_{RK} - M_{A1}\ \bar{E}_{RK} + M_{A2}\ \bar{E}_{SWK} \qquad \text{(A3.2.10)}$$

$$\bar{I}_{SWK} = M_5\ \bar{I}_{RK} - M_{A3}\ \bar{E}_{RK} + M_{A4}\ \bar{E}_{SWK} \qquad \text{(A3.2.11)}$$

where,

$$M_5 = M_{A3}\ Z_{SR}$$

Also, from eqns. A3.2.3, A3.2.6 and A3.2.10,

$$\bar{I}_{FRK} = M_6\ \bar{I}_{RK} - M_7\ \bar{E}_{RK} + M_8\ \bar{E}_{SWK} \qquad \text{(A3.2.12)}$$

where, $M_6 = C_R Z_{SR} + D_R + D_R M_{A1} Z_{SR}$

$M_7 = C_R + D_R M_{A1}$; $M_8 = D_R M_{A2}$

and, from eqns. A3.2.2, A3.2.3, A3.2.6 and A3.2.10,

$$\bar{I}_{RK} = M_9 \bar{E}_{FK} + M_{10} \bar{E}_{RK} - M_{11} \bar{E}_{SWK} + M_{12} \bar{I}_{FK} \qquad \text{(A3.2.13)}$$

where,

$$M_9 = \left[A_R Z_{SR} + B_R + B_R M_{A1} Z_{SR}\right]^{-1}$$

$$M_{10} = M_9\left[A_R + B_R M_{A1}\right]$$

$M_{11} = M_9 B_R M_{A2}$; $M_{12} = M_9 Z_F$

From fig. 3.4, at the point of fault, $(\bar{I}_{FSK} + \bar{I}_{FRK})$ represent the fault path current $(\bar{I}_{FK})$ in the opposite direction, hence, from eqns. A3.2.7, A3.2.8, A3.2.12 and A3.2.13,

$$\bar{I}_{FK} = -(\bar{I}_{FSK} + \bar{I}_{FRK})$$
$$= Y_{11} \bar{E}_{FK} + Y_{12} \bar{E}_{SK} + Y_{13} \bar{E}_{RK} + Y_{14} \bar{E}_{SWK} \qquad \text{(A3.2.14)}$$

where,

$Y_{11} = -M_T\left[M_1 M_2 + M_6 M_9\right]$; $Y_{12} = M_T\left[C_L - M_1 M_3\right]$

$Y_{13} = M_T\left[M_7 - M_6 M_{10}\right]$; $Y_{14} = M_T\left[M_6 M_{11} - M_8\right]$

$M_T = \left[U + M_1 M_4 + M_6 M_{12}\right]^{-1}$; U = unit matrix

Substituting eqn. A3.2.14 into eqns. A3.2.8 and A3.2.13, gives the sending and receiving end current Transforms respectively, and are given by :-

$$\bar{I}_{SK} = Y_{21} \bar{E}_{FK} + Y_{22} \bar{E}_{SK} + Y_{32} \bar{E}_{RK} + Y_{24} \bar{E}_{SWK} \qquad \text{(A3.2.15)}$$

where, $Y_{21} = M_2 - M_{14}\, Y_{11}$; $Y_{22} = M_3 + M_4\, Y_{12}$

$Y_{23} = M_4\, Y_{13}$; $Y_{24} = M_4\, Y_{14}$

and,

$$\bar{I}_{RK} = Y_{31}\, \bar{E}_{FK} + Y_{32}\, \bar{E}_{SK} + Y_{33}\, \bar{E}_{RK} + Y_{34}\, \bar{E}_{SWK} \qquad \text{(A3.2.16)}$$

where, $Y_{31} = M_9 - M_{12}\, Y_{11}$; $Y_{32} = M_{12}\, Y_{12}$

$Y_{33} = M_{10} + M_{12}\, Y_{13}$; $Y_{34} = M_{12}\, Y_{14} - M_{11}$

Finally, substituting eqn. A3.2.16 into eqn. A3.2.11 gives,

$$\bar{I}_{SWK} = Y_{41}\, \bar{E}_{FK} + Y_{42}\, \bar{E}_{SK} + Y_{43}\, \bar{E}_{RK} + Y_{44}\, \bar{E}_{SWK} \qquad \text{(A3.2.17)}$$

where, $Y_{41} = M_5\, Y_{31}$; $Y_{42} = M_5\, Y_{32}$

$Y_{43} = M_5\, Y_{33} - M_{A3}$; $Y_{44} = M_5\, Y_{34} + M_{A4}$

Equations A3.2.14 to A3.2.17, can be arranged in the matrix form relationship of eqn. A3.2.18 :-

$$\begin{bmatrix} \bar{I}_{FK} \\ \bar{I}_{SK} \\ \bar{I}_{RK} \\ \bar{I}_{SWK} \end{bmatrix} = \left[\begin{array}{ccc:c} Y_{11} & Y_{12} & Y_{13} & Y_{14} \\ Y_{21} & Y_{22} & Y_{23} & Y_{24} \\ Y_{31} & Y_{32} & Y_{33} & Y_{34} \\ \hdashline Y_{41} & Y_{42} & Y_{43} & Y_{44} \end{array}\right] \begin{bmatrix} \bar{E}_{FK} \\ \bar{E}_{SK} \\ \bar{E}_{RK} \\ \bar{E}_{SWK} \end{bmatrix} \qquad \text{(A3.2.18)}$$

It is important to note that the 10 x 10 admittance matrix in eqn. A3.2.18, is a universal relationship, which can

be computed and stored at all spectral frequencies of interest. Eqn. A3.2.18, can be used for fault simulation as well as breakers and the ideal neutral switch opening and closing.

APPENDIX 3.3

EVALUATION OF THE SYSTEM ADMITTANCE MATRIX-

HSGS's IMPLEMENTATION

With reference to fig. 3.7, the Transform of the voltage component $\bar{V}_{SK}$ on the line side of the breaker at the sending end is given by :-

$$\bar{V}_{SK} = Z_{SS}\ \bar{I}_{SK} - \bar{E}_{SK} \qquad \text{(A3.3.1)}$$

Also, $\bar{V}_{SK}$ is the voltage Transform across the grounding switches at the sending end, and can be written :-

$$\bar{V}_{SK} = Z_g\ \bar{I}_{SgK} + \bar{E}_{SgK} \qquad \text{(A3.3.2)}$$

where,

$$Z_g = \begin{vmatrix} R_s & 0 & 0 \\ 0 & R_s & 0 \\ 0 & 0 & R_s \end{vmatrix}$$

, and R_s is the assumed resistance of the HSGS.

Also, at the sending end,

$$\bar{I}_{S1K} = \bar{I}_{SK} + \bar{I}_{SgK} \qquad \text{(A3.3.3)}$$

Similarly, at the receiving end,

$$\bar{V}_{RK} = Z_{SR}\ \bar{I}_{RK} - \bar{E}_{RK} \qquad \text{(A3.3.4)}$$

$$\bar{V}_{RK} = Z_g\ \bar{I}_{RgK} + \bar{E}_{RgK} \qquad \text{(A3.3.5)}$$

and

$$\bar{I}_{R1K} = \bar{I}_{RK} + \bar{I}_{RgK} \qquad \text{(A3.3.6)}$$

At the point of fault,

$$\bar{V}_{FK} = \bar{E}_{FK} + Z_F \bar{I}_{FK} = \bar{E}_{FK} - Z_F (\bar{I}_{FSK} + \bar{I}_{FRK}) \qquad \text{(A3.3.7)}$$

The fault point quantities are related to those at the sending and receiving end of the line by the two-port matrix relationships A3.3.8 and A3.3.9 respectively.

$$\begin{bmatrix} \bar{V}_{FK} \\ \bar{I}_{FSK} \end{bmatrix} = \begin{bmatrix} A_L & B_L \\ C_L & D_L \end{bmatrix} \begin{bmatrix} \bar{V}_{SK} \\ \bar{I}_{S1K} \end{bmatrix} \qquad \text{(A3.3.8)}$$

$$\begin{bmatrix} \bar{V}_{FK} \\ \bar{I}_{FRK} \end{bmatrix} = \begin{bmatrix} A_R & B_R \\ C_R & D_R \end{bmatrix} \begin{bmatrix} \bar{V}_{RK} \\ \bar{I}_{R1K} \end{bmatrix} \qquad \text{(A3.3.9)}$$

From eqns. A3.3.1 and A3.3.2,

$$\bar{I}_{SK} = Z_{SS}^{-1} (Z_g \bar{I}_{SgK} + \bar{E}_{SgK} + \bar{E}_{SK}) \qquad \text{(A3.3.10)}$$

Substituting eqn. A3.3.10 into eqn. A3.3.3 gives,

$$\bar{I}_{S1K} = M_1 \bar{I}_{SgK} + Z_{SS}^{-1} \bar{E}_{SgK} + Z_{SS}^{-1} \bar{E}_{SK} \qquad \text{(A3.3.11)}$$

where, $M_1 = U + Z_{SS}^{-1} Z_g$, and U = unit matrix.

From eqns. A3.3.2, A3.3.8 and A3.3.11,

$$\bar{I}_{FSK} = M_2 \bar{I}_{SgK} + M_3 \bar{E}_{SgK} + M_4 \bar{E}_{SK} \qquad \text{(A3.3.12)}$$

where, $M_2 = C_L Z_g + D_L M_1$; $M_3 = C_L + D_L Z_{SS}^{-1}$

and $M_4 = D_L Z_{SS}^{-1}$

Also, from eqns. A3.3.2, A3.3.7, A3.3.8 and A3.3.11,

$$\bar{I}_{SgK} = M_5 \bar{E}_{FK} - M_6 \bar{E}_{SK} - M_7 \bar{E}_{SgK} - M_8 (\bar{I}_{FSK} + \bar{I}_{FRK}) \quad \text{(A3.3.13)}$$

where,

$$M_5 = \left[A_L Z_g + B_L M_1\right]^{-1} \quad ; \quad M_6 = M_5 B_L Z_{SS}^{-1}$$

$$M_7 = M_5 (A_L + B_L Z_{SS}^{-1}) \quad ; \quad M_8 = M_5 Z_F$$

Now, from eqns. A3.3.4 and A3.3.5,

$$\bar{I}_{RK} = Z_{SR}^{-1} (Z_g \bar{I}_{RgK} + \bar{E}_{RgK} + \bar{E}_{RK}) \quad \text{(A3.3.14)}$$

Substituting eqn. A3.3.14 into eqn. A3.3.6 gives,

$$\bar{I}_{RlK} = M_9 \bar{I}_{RgK} + Z_{SR}^{-1} \bar{E}_{RgK} + Z_{SR}^{-1} \bar{E}_{RK} \quad \text{(A3.3.15)}$$

where, $M_9 = U + Z_{SR}^{-1} Z_g$

From eqns. A3.3.5 , A3.3.9 and A3.3.15,

$$\bar{I}_{FRK} = M_{10} \bar{I}_{RgK} + M_{11} \bar{E}_{RgK} + M_{12} \bar{E}_{RK} \quad \text{(A3.3.16)}$$

where, $M_{10} = C_R Z_g + D_L M_9$;

$$M_{11} = C_R + D_L Z_{SR}^{-1} \quad ; \quad M_{12} = D_R Z_{SR}^{-1}$$

Also from eqns. A3.3.5, A3.3.7, A3.3.9 and A3.3.15,

$$\bar{I}_{RgK} = M_{13} \bar{E}_{FK} - M_{14} \bar{E}_{RK} - M_{15} \bar{E}_{Rgk} - M_{16} (\bar{I}_{FSK} + \bar{I}_{FRK}) \quad \text{(A3.3.17)}$$

where, $M_{13} = \left[A_R Z_g + B_R M_9\right]^{-1}$; $M_{14} = M_{13} B_R Z_{SR}^{-1}$

$M_{15} = M_{13} (A_R + B_R Z_{SR}^{-1})$; $M_{16} = M_{13} Z_F$

Using eqns. A3.3.12, A3.3.13, A3.3.16 and A3.3.17 to get,

$$\bar{I}_{FK} = - (\bar{I}_{FSK} + \bar{I}_{FRK})$$

$$= Y_{11} \bar{E}_{FK} + Y_{12} \bar{E}_{SK} + Y_{13} \bar{E}_{RK} + Y_{14} \bar{E}_{SgK} + Y_{15} \bar{E}_{RgK} \quad \text{(A3.3.18)}$$

Where,

$Y_{11} = - M_T (M_2 M_5 + M_{10} M_{13})$; $Y_{12} = M_T (M_2 M_6 - M_4)$

$Y_{13} = M_T (M_{10} M_{14} - M_{12})$; $Y_{14} = M_T (M_2 M_7 - M_3)$

$Y_{15} = M_T (M_{10} M_{15} - M_{11})$; $M_T = \left[U + M_2 M_8 + M_{10} M_{16}\right]^{-1}$

Substituting eqn. A3.3.18 into eqn. A3.3.13 gives,

$$\bar{I}_{SgK} = Y_{41} \bar{E}_{FK} + Y_{42} \bar{E}_{SK} + Y_{43} \bar{E}_{RK} + Y_{44} \bar{E}_{SgK} + Y_{45} \bar{E}_{RgK} \quad \text{(A3.3.19)}$$

where, $Y_{41} = M_5 - M_8 Y_{11}$; $Y_{42} = M_8 Y_{12} - M_6$

$Y_{43} = M_8 Y_{13}$; $Y_{44} = M_8 Y_{14} - M_7$; $Y_{45} = M_8 Y_{15}$

Substituting eqn. A3.3.18 into eqn. A3.3.17 gives,

$$\bar{I}_{Rgk} = Y_{51} \bar{E}_{FK} + Y_{52} \bar{E}_{SK} + Y_{53} \bar{E}_{RK} + Y_{54} \bar{E}_{SgK} + Y_{55} \bar{E}_{RgK} \quad \text{(A3.3.20)}$$

where, $Y_{51} = M_{13} - M_{16} Y_{11}$; $Y_{52} = M_{16} Y_{12}$

$Y_{53} = M_{16} Y_{13} - M_{14}$; $Y_{54} = M_{16} Y_{14}$

$Y_{55} = M_{16} Y_{15} - M_{15}$

From eqn. A3.3.10 and eqn. A3.3.19,

$$\bar{I}_{SK} = Y_{21}\,\bar{E}_{FK} + Y_{22}\,\bar{E}_{SK} + Y_{23}\,\bar{E}_{RK} + Y_{24}\,\bar{E}_{SgK} + Y_{25}\,\bar{E}_{RgK} \qquad \text{(A3.3.21)}$$

where, $Y_{21} = Z_{SS}^{-1}\,Z_g\,Y_{41}$; $Y_{22} = Z_{SS}^{-1}\,(U + Z_g\,Y_{42})$

$Y_{23} = Z_{SS}^{-1}\,Z_g\,Y_{43}$; $Y_{24} = Z_{SS}^{-1}\,(U + Z_g\,Y_{44})$

$Y_{25} = Z_{SS}^{-1}\,Z_g\,Y_{45}$

Also, from eqn. A3.3.14 and eqn. A3.3.20,

$$\bar{I}_{RK} = Y_{31}\,\bar{E}_{FK} + Y_{32}\,\bar{E}_{SK} + Y_{33}\,\bar{E}_{RK} + Y_{34}\,\bar{E}_{SgK} + Y_{35}\,\bar{E}_{RgK} \qquad \text{(A3.3.22)}$$

where, $Y_{31} = Z_{SR}^{-1}\,Z_g\,Y_{51}$; $Y_{32} = Z_{SR}^{-1}\,Z_g\,Y_{52}$

$Y_{33} = Z_{SR}^{-1}\,(U + Z_g\,Y_{53})$; $Y_{34} = Z_{SR}^{-1}\,Z_g\,Y_{54}$

$Y_{35} = Z_{SR}^{-1}\,(U + Z_g\,Y_{55})$

Equations A3.3.18 to A3.3.22 can be arranged in the matrix relationship of eqn. A3.3.23 :-

$$\begin{bmatrix} \bar{I}_{FK} \\ \bar{I}_{SK} \\ \bar{I}_{RK} \\ \bar{I}_{SgK} \\ \bar{I}_{RgK} \end{bmatrix} = \begin{bmatrix} Y_{11} & Y_{12} & Y_{13} & Y_{14} & Y_{15} \\ Y_{21} & Y_{22} & Y_{23} & Y_{24} & Y_{25} \\ Y_{31} & Y_{32} & Y_{33} & Y_{34} & Y_{35} \\ Y_{41} & Y_{42} & Y_{43} & Y_{44} & Y_{45} \\ Y_{51} & Y_{52} & Y_{53} & Y_{54} & Y_{55} \end{bmatrix} \begin{bmatrix} \bar{E}_{FK} \\ \bar{E}_{SK} \\ \bar{E}_{RK} \\ \bar{E}_{SgK} \\ \bar{E}_{RgK} \end{bmatrix} \qquad \text{(A3.3.23)}$$

The 15 x 15 admittance matrix in eqn. A3.3.23 is a universal one, which can be computed and stored at all spectral frequencies of interest. Eqn. A3.3.23 can be used for fault inception as well as breaker and HSGS opening and closing.